The chemical syntheses and physico-chemical characterization of polymer conjugates of antimalarial compounds.

By

Sindisiwe Mvango

(17405832)

Submitted in partial fulfillment of the requirements for the

PhD Degree in Chemistry

in the Faculty of Natural & Agricultural Sciences

University of Pretoria

2021

Supervisor: Professor Lynne Pilcher

Co-supervisor: Dr Mohammed Balogun

Summary

Title: The chemical syntheses and physico-chemical characterization of polymer conjugates of antimalarial compound.

By:

Sindisiwe Mvango

Supervisor:

Prof Lynne A. Pilcher

Co-supervisor:

Dr Mohammed O. Balogun

Department:

Department of Chemistry

Degree:

PhD

Malaria is a well-known infectious disease that is still the leading cause of illness and death in many countries mostly in the sub-Saharan Africa. The most vulnerable groups are children who have not developed immunity and pregnant women whose immunity has decreased due to pregnancy. The negative consequences of malaria to individuals and the economies of countries where the disease is endemic are enormous: Many lives are lost each year because of the disease, there is also disruption to education and learning stemming from absence from school. Many manhours are lost annually as workers are incapacitated by the infection or as they have to care for someone suffering from the disease. Yet, malaria remains a neglected disease with respect to modern advancement in prevention, diagnosis and treatment. The most widely used preventative is anti-mosquito bed nets preventing transmission by infected insects, while physical observation of the causative parasite in a blood smear under a light microscope is the most conclusive diagnosis of infection. Chemotherapeutic options are currently limited to only a small arsenal of drugs, which are at risk of being further depleted by a developing drug resistance crisis. The use of combination therapy to manage drug resistance is also not a permanent solution, as resistance is also reported for the widely used fast acting artemisinin drugs. New antimalarial drugs that are in the pipeline target multiple stages on the malaria cycle, but still these suffer from low solubility resulting in

high doses that increase the risk of toxicity. Nanomedicine has significantly improved modern cancer drugs by development of novel drug delivery systems under the polymer-therapeutics platform. In many cases, significant success has been achieved for anticancer drugs and unfortunately, the efforts have not been extended to malaria. In this project, we report on the use of polymer therapeutics technology for the delivery of anti-malaria drugs.

The primary objective of this doctoral thesis was to explore the chemistry of developing polymer therapeutics of antimalarial drugs. It recognizes that success in synthesizing effective anticancer polymer therapeutics does not automatically imply that there can be a linear translation to malaria therapeutics. The synthesis of every new chemical entity or polymer therapeutic must be rationally considered and the resulting macromolecular "drug" must be extensively characterized before performance or activity testing can be initiated.

In Chapter 1, a review of the literature is presented to make the case for the application of nanomedicine technology to malaria chemotherapy. A general introduction to malaria, challenges with its chemotherapy and development of new antimalarial drugs is discussed. This is followed by highlighting the advantages offered by nanomedicine, "polymer-therapeutics" to be specific, in resolving these challenges. The carbodiimide chemistry chosen to synthesize these polymer-drug conjugates are compared to traditional synthetic methods. Finally, the significance and clinical perspective on the use of polymer-drug conjugation for malaria is outlined.

Chapter 2 presents a basic introduction into the physico-chemical analytical techniques used in the thesis to investigate the newly synthesized polymeric entities. The field of polymer therapeutics employs analytical techniques from multiple scientific disciplines for characterization of organic synthetic intermediates and polymer drug conjugates.

Chapter 3 is the first of three chapters presenting the research undertaken in this doctoral project. It explores the synthesis of polymer conjugates of natural compounds that are used or are being investigated for the treatment of malaria. With over 80% of the global population relying on herbal medicines as their primary health option, natural compounds cannot be excluded from modern pharmaceutical technologies. Herbal medicines encounter the same biological barriers to maximizing their pharmacological potentials as do conventional synthetic chemical drugs. Herbal medicines are also exposed to the body's drug metabolism and distribution system, which could result in suboptimal exposure and undesirable side effects. As with any other chemical substance, they possess an inherent dose-related toxicity, which is often naively and mistakenly underestimated because of their natural origins. Many antimalarials either are natural compounds or have been derived from natural molecules. In Chapter 3, the plant-derived pentacyclic

triterpenoid betulinic acid and the semi-synthetic sesquiterpene lactone dihydroartemisinin are conjugated to the polymers polyethylene glycol and chitosan.

Chapter 4 reports on the efforts to synthesize polymer conjugates of the drugs that make up the World Health Organization's artemisinin-based triple combination for malaria: DHA – normally in the form of artemether lumefantrine and primaquine. In the officially recommended regimen, artemether is prescribed with lumefantrine for falciparum malaria but artemether, a methyl ether derivative of dihydroartemisinin, has no functional group suitable for reversible conjugation. Dihydroartemisinin, which is the active metabolite of artemether, is used instead as it possesses a hydroxyl group for conjugation. This chapter investigates the syntheses of polymer-drug conjugates in which these drugs are covalently linked to multivalent polymers that provide the opportunity for increased aqueous solubility and better drug loading than divalent polyethylene glycol. The main objective of the research reported in this chapter was to explore the synthesis of water-soluble polymer therapeutics that could be intravenously administered for the treatment of severe malaria.

Chapter 5 reports on the investigation of linker chemistry, a crucial aspect of polymer conjugates. The chemical linker between the drug and the polymer is the most important component of the polymer therapeutics architecture contributing to the release kinetics and therefore the observed therapeutic effect. In chapters 3 and 4, the drugs were linked either directly to the polymer or via the homo-bifunctional linker succinic acid. In Chapter 5, the hetero-bifunctional amino acid glycine was explored as a linker for lumefantrine. Because of the compatibility of the carboxylic acid and amino group of glycine, selectivity in reaction was required. The chapter reports on the efforts to selectively protect and activate the functional groups of the amino acid. The findings reported in this final experimental chapter emphasizes the difficulty of direct extrapolation or translation of the established anticancer polymer therapeutics' chemistry to antimalarial therapeutics.

This doctoral research emphasizes the chemistry of synthesizing the antimalarial polymer therapeutics and their physico-chemical properties. The findings will inform and guide the development of novel antimalarial polymer therapeutics. The biological activities of the conjugates were not explored except for basic cytotoxicity tests using normal and cancer cell lines. Some of the conjugates have been tested for antimalarial activities as parts of other research projects.

Declaration

I declare that the thesis/dissertation, which I hereby submit for the degree PhD (Chemistry) at the University of Pretoria, is my own work and has not previously been submitted by me for a degree at this or any other tertiary institution.

Signature..... .....

Date.....13/12/2021.....

Plagiarism Declaration

1. I understand what plagiarism is and am aware of the University's policy in this regard.

2. I declare that this ……Thesis…… (E.g. essay, report, project, assignment, dissertation, thesis, etc.) is my own original work. Where other people's work has been used (either from a printed source, Internet or any other source), this has been properly acknowledged and referenced in accordance with departmental requirements.

3. I have not used work previously produced by another student or any other person to hand in as my own.

4. I have not allowed, and will not allow, anyone to copy my work with the intention of passing it off as his or her own work.

SIGNATURE..... .....

Acknowledgements

First and foremost, I would like to thank my Heavenly Father, God and the almighty for all the blessing and gift of LIFE and through Christ, all things are possible. I dedicate this dissertation to my beautiful two angels, my parents and my pillars of strength who were there when I started this journey. To you Mr Tembani Mvango and Mrs Noluthando Noluvuyo Mvango, thank you for everything and rest in peace my angels.

My heartfelt and sincere gratitude goes to my two supervisors Dr Mohammed Balogun and Prof Lynne Pilcher for their supervision, guidance and encouragement throughout this program. I am grateful, thank you very much.

This research would have not been possible without the financial support from NRF/CSIR PDP program. This work is based on the research supported in part by the National Research Foundation of South Africa (Grant 105942). My project would have never been so exciting and successful with the useful support and advice I got from my collogues and mentors at the CSIR. Thank you very much to you guys for the laughs, hugs, support and science talks/debates.

I would also like to thank people I collaborated with in this work, Dr Pascaline Fru, Nompumelelo Mthimkhulu (Wits), Dr Zamani Cele (CSIR), William Matshe (CSIR), Thenesia Govender and Nokubongwa Dlamini. Thank you for your hard work.

I would like to have a special thanks to Dr Lesego Tshweu (CSIR), Dr Selepe (UP), thank you for everything. Also to my friend Zipporah Madikane, thanks for being a shoulder to cry on. To my flatmate, Nwabisa “Lolo” Takata, thank you so much for everything, you witnessed my cries, laughs, weakness and strengths throughout this journey, “enkosi ntombi”.

Lastly, I would like to thank my entire family- To you my sisters (Simbongile and Bathandwa), I hope I’ve made you proud. To Onothando (my daughter), mommy did this for you and I love you so much. You were my strength throughout this journey. “Ndithi kuni nonke enkosi!”. To you Mr Isaac Maila Masigo, thank you for everything, God bless you.

Table of contents

List of Figures

List of Schemes

List of Tables

Abbreviations

°C	Degree Celsius
µm	Micrometer
^{1}H	Proton
ACT	Artemisinin-based combination therapy
ART	Artesunate
BA	Betulinic acid
CS	Chitosan
Đ	Polydispersity index
DCM	Dichloromethane
DHA	Dihydroartemisinin
DIC	Diisopropyl carbodiimide
DLS	Dynamic light scattering
DMAP	4-(Dimethylamino)-pyridine
DMF	Dimethyl formamide
DP	Degree of polymerization
DSC	Differential scanning calorimetry
EDC	1-Ethyl-3-(3-dimethylaminopropyl)carbodiimide hydrochloride
EPR	Enhanced permeability and retention
FDA	Food and Drug Administration
FT-IR	Fourier transmission-infra red
g/mL	Gram per mill
G6PD	Glucose-6-phosphate dehydrogenase
Gly	Glycine

hr	Hour(s)
H_2O	Water
HPLC	High performance liquid chromatography
I.V.	Intravenously
kDa	Kilo Dalton
Lum	Lumefantrine
m	Multiplet
mg	Milligram(s)
mg/mL	Milligram per milliliter
MHz	Megahertz
min	Minute(s)
mL	Milliliter
Mm	Millimolar
mmol	Millimole
Mn	weight size distribution
Mol%	Mole percentage
mol. eq.	Molar equivalent
MW	Molecular weight
MWCO	Molecular weight cut-off
nm	Nanometer
NMR	Nuclear magnetic resonance
p(NAM-stat-AA)	Poly(N-acryloylmorpholine) macromonomers copolymerized acrylic acid
PBS	Phosphate buffer saline
PDI	Polydispersity index
PEG	Polyethylene glycol
PGA	Polyglutamic acid
ppm	Parts per million

PQ	Primaquine
PXRD	Powder x-ray diffraction
r.t.	Room temperature
RBCs	Red blood cells
R_f	Retention factor
s	Second(s)
s	Singlet
SEM	Scanning electron microscopy
$SOCl_2$	Thionyl Chloride
Suc	Succinic
t	Triplet
TEM	Transmission electron microscope
TGA	Thermal gravimetric analysis
TLC	Thin layer chromatography
UV	Ultraviolet
WHO	World Health Organization
Wt%	Weight percentage
µg/mL	Microgram per mill
µM	Micromolar

Chapter one includes sections from the submitted manuscript, before publication. Titled: Nanomedicines for malaria chemotherapy: encapsulation vs. polymer therapeutics. The bibliographic details for the published manuscript are:

Mvango, S., Matshe, W.M., Balogun, A.O., Pilcher, L.A. and Balogun, M.O., 2018. Nanomedicines for malaria chemotherapy: encapsulation vs. polymer therapeutics. Pharmaceutical research, 35(12), p.237.

Chapter One:
Nanomedicines for malaria chemotherapy-polymer therapeutics

1.1 Introduction

Malaria is an infectious disease known to virtually every inhabitant of the Earth's tropical regions like sub-Saharan Africa. It exacts an enormous economic and social impact in the hardest hit countries. It mainly affects children under the age of five years old (Griffin, Ferguson and Ghani, 2014). The incapacitating symptoms of the disease are unmistakable, whether to the expert observation of the medical professional or an ordinary adult. However, the disease is much less recognized in the generally malaria-free and sub-tropical temperate countries (Walker, Nadjm and Whitty, 2010). This has in part contributed to a lack of significant technological advancement in the clinical management of the disease. Much of the malaria chemotherapy still relies on classes of drugs that have been in use for several centuries. Diagnosis is still primarily by microscopic visualization of the parasite in infected red blood cells (RBCs) (World Health Organization, 2015). Prevention is almost entirely dependent on the use of physical barriers like bed nets (Hill, Lines and Rowland, 2006). While drug toxicity and poor pharmacological potentials have been addressed or ameliorated with various nanomedicine drug delivery systems in diseases like cancer, no clinically significant success story has been reported for malaria. With reports of resistance rising against our latest and most powerful antimalarial treatment—the artemisinin-based combination therapy (ACT)—there is an imperative need for clinically successful antimalarial nanomedicines.

1.2 Scope of the thesis

According to the World Health Organization (WHO), the total number of mortalities in 2019 was estimated to be 409 000 and children under the age of five years accounted for 67 % of all malaria deaths worldwide. The WHO African region accounted for about 94 % of malaria cases and related deaths (World Health Organization, 2020). This is an increase from the 228 million cases of 2018 which means there is still an enormous burden caused by the disease, especially in the African continent (World Health Organization, 2019). In 2018, WHO delivered approximately 214 million artemisinin-based combination regimens, 98 % of which were in the WHO African region. The WHO-recommended first line treatment has recently demonstrated challenges with resistance. The WHO (2019) reported partial artemisinin resistance for *Plasmodium falciparum* parasite in Great Mekong Sub-region and Southern China. Since the emergence of resistance in these countries, WHO has introduced several

initiatives to fight artemisinin resistance and also continues to monitor the situation. Despite the emergence of artemisinin resistance, treatment efficacy remains high for *P. falciparum* and no resistance has been reported towards lumefantrine (World Health Organization, 2019; 2020). However, meeting the call for reduction of malaria incidence and mortality by 90 % by 2030 (World Health Organization, 2020) will be difficult to achieve without new and accelerated malaria chemotherapy. In the past few years, high-throughput screening has identified several chemotypes that can be developed towards antimalarial drugs. Efficacy, toxic side effects, pharmacokinetic compatibility and susceptibility to natural drug resistance mechanism of the parasite are still major parameters that hinder success of these new drugs and their progress from clinical trials to the market. This thesis explored the use of nanomedicine to address challenges related to conventional antimalarial chemotherapy.

1.3 Historical malaria

Malaria, or at least a disease with symptoms closely similar to it, has been around for over five millennia. From the ancient Chinese, Greek, Indian and Roman civilizations medical experts have described and recorded almost identical symptoms of the disease. Some of these early experts rightly linked the disease to either insect bites or swampy marshlands. Extracts of medicinal plants were the earliest effective treatment and indeed many still rely on these natural potions for 'curing' the disease. For example, the Chinese used the Qinghao plant (*Artemisia annua*) to 'treat' the fever and the medieval Europeans learnt that the Peruvian bark from the *Cinchona* tree could be used to the same effect (Arrow, Panosian and Gelband, 2004).

The spectacular discoveries made in eighteenth and nineteenth century related to malaria parasite and transmission inevitably meant that the twentieth century would see widespread malaria control efforts. The chemical, dichloro-diphenyl-trichloroethane (DDT), which had been synthesized in 1874 merely as a doctoral thesis, became central to the malaria vector control efforts after its insecticidal property was recognized in 1939. By the time the detrimental environmental effects of DDT were recognized it had ensured that much of the United States and many other countries had been ridden of the mosquito vector that spread the disease (Zucker, 1996). The twentieth century also saw the first synthetic anti-malaria chemotherapeutic agent, chloroquine, approved for use after the Second World War. It was less toxic and more efficient than the naturally derived quinine (Bloland, 2001; Butler, Khan and Ferguson, 2010).

In 1955 the World Health Organization (WHO) began a bold and ambitious plan to eradicate malaria globally. This effort was successful in eliminating malaria from countries in temperate regions. It failed in tropical countries where the campaign was either not sustained until total elimination was achieved or the program was never implemented. Unfortunately, sub-Saharan Africa was in the latter group and today the continent bears more than 90 % of malaria incidence and mortality. This overwhelming burden is in spite of a new and relatively successful concerted Roll Back Malaria effort by the WHO (Bhatt et al. 2015) and the disease is currently the organization's top priority tropical infectious disease.

1.3.1 Biology and pathophysiology of malaria

Malaria is caused by protozoans of the genus *Plasmodium*. Currently, five *Plasmodium* species cause the disease in humans. *Plasmodium falciparum* is responsible for the most clinically morbid form of malaria and was accountable for over 99.7 % of malaria cases in 2018 with 405 000 reported cases of mortalities worldwide (World Health Organization 2019). Outside Africa *P. vivax* is the most prevalent species (Battle et al. 2015), *P. ovale* (Collins and Jeffery, 2005) and *P. malariae* (Collins and Jeffery, 2007) are even less common. *P. knowlesi* is a zoonotic species that is primarily a simian parasite (Barber et al. 2017).

The complicated life cycle of the *Plasmodium* parasite occurs in two hosts—the mosquito and the human. Only the female *Anopheles* mosquitoes are able to transmit the parasite because they require regular blood meals to develop their eggs; the males only feed on sugary fluids. The *Anopheles* genus has about 400 known species of which 30-40 transmit malaria. To put these figures into perspective, there are 41 mosquito genera grouping 3500 species (Tuteja, 2007).

The human segment of the *Plasmodium* life cycle has three stages, which are of significance to the characteristics of the disease (**Figure 1.1**). The infectious sporozoites from the salivary gland of the *Anopheles* mosquito are injected into the human host. These reach the liver, which is the first pre-erythrocytic or exo-erythrocytic stage. The parasite grow and multiply in this stage forming schizonts and infect the RBCs. This depends on the *Plasmodium* species, a fraction of the parasites which do not mature immediately into schizonts remains dormant in the liver as hypnozoites. This is observed only in *P. vivax* and *P. ovale* and it is manifested in some patients as a relapse weeks or months after 'successful' treatment of the disease even though there is no re-exposure to the transmitting mosquito (Collins and Jeffery, 2007).

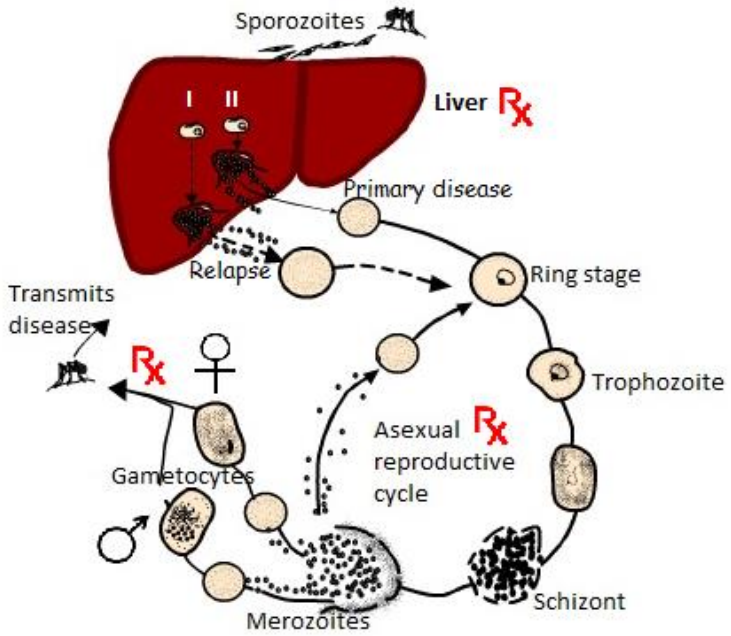

Figure 1. 1: A schematic of the human segment of the Plasmodium spp. life cycle. Rx indicates stages targeted by antimalarial chemotherapy. Hypnozoites of P. vivax and P. ovale take the (I) life cycle path while all species causing immediate illness takes the (II) path.

The schizonts, mature into merozoites and invade the RBCs when they are released into the blood from the liver rapture. The second stage is the erythrocytic asexual stage in which the parasite lives within RBCs (Tilley, Dixon and Kirk, 2011). This occurs in all *Plasmodium* species and these replicate asexually. This results in high parasite burden and destroying of each RBC they infect causing clinical symptoms of the disease (fever, chills, anemia, muscular aches and rigors). After further morphological changes and multiplication in the RBCs the parasite, now known as merozoite, emerges with lysis of the host cell. There could be more than 10^{12} parasites circulating in a single patient at this stage. RBC lysis occurs with a circadian consistency that is accompanied by fever and chills. Most antimalarial drugs are most effective against this stage of the parasite.

A divergence also occurs in the erythrocytic stage with a fraction of the parasites differentiating into mature cells called trophozoites. Mature trophozoites further develop into gametocytes to initiate the third intra-human stage contributory to the malaria disease characteristics. *Plasmodium* gametocytes are the transmissible forms of the parasite. All forms of the parasite have this stage and it completes the human-mosquito circuit when the gametocytes are picked up by the insect during a feeding session. *P. falciparum* gametocytes may take up to two weeks to appear in the blood while those of *P. vivax* appear just a few days after infection. A few

drugs are able to target the gametocytes and inhibit transmission [*vide infra*] (Suemizu et al. 2015; Baker, 2010).

1.4 Malaria chemotherapy

Malaria treatment has existed for centuries in traditional folk medicines and many of the most effective 'modern' drugs are derived from this traditional knowledge (Burns, 2008; Butler, Khan and Ferguson, 2010). Chemotherapy of malaria is directed towards three objectives: to cure infection, prevent the development of resistance to the drugs and reduce the risk of further transmission. The multi-stage complicated life cycle of the *Plasmodium* parasite offers multiple sites for chemotherapeutic vulnerability (Chenette, 2017) (**Figure 1.1**).

The major antimalarial drugs used to treat various forms of the disease can be grouped into several chemical and functional classes. Of these, four chemical classes—aryl amino alcohols, 4-aminoquinolines, 8-aminoquinolines, and artemisinins—are notable for their historical and clinical impact (**Table 1.1**). Drugs under each class share a common pharmacophore. This chapter, discusses three of the four classes, as these are more relevant to the work conducted. For more detail please refer to the published review paper (Mvango et al. 2018).

Table 1.1: Classification and structures of common antimalarials and their pharmacophores.

Chemical group	Structure of pharmacophore	Related compounds[a1]
Aryl amino alcohols	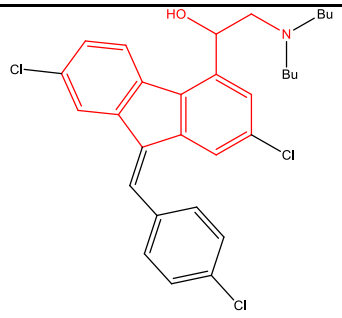 **Lumefantrine**	• Desbutyllumefantrine

[1a]The related compounds are either lesser known antimalarials, experimental drugs, or metabolites with significant antimalarial properties

<table>
<tr><td>4-
aminoquinoline</td><td colspan="2"> 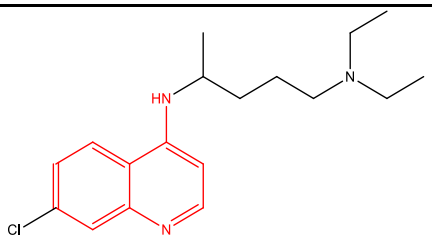
Chloroquine</td><td>Hydroxychloroquine
Amodiaquine</td></tr>
<tr><td>8-
aminoquinoline</td><td colspan="2"> 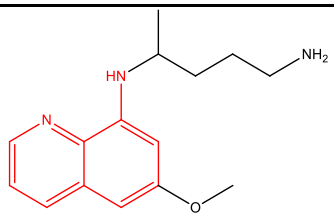
Primaquine</td><td>Pamaquine</td></tr>
<tr><td>Artemisinins</td><td> 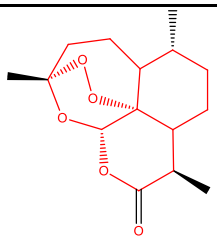
Artemisinin

 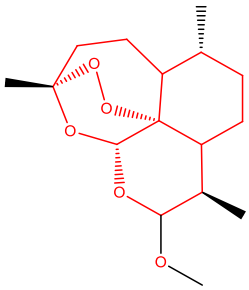
Artemether</td><td> 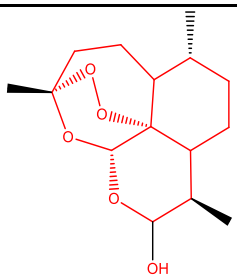
Dihydroartemisinin

 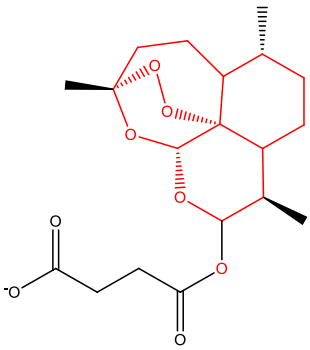
Artesunate</td><td>Artemisone
Artelinic acid</td></tr>
</table>

	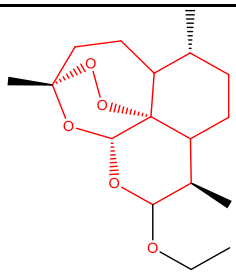 **Arteether**		

.

1.4.1 The aryl amino alcohols

The aryl amino alcohol class of antimalarials which are currently in clinical use include quinine, lumefantrine, mefloquine, and halofantrine. Quinine is the oldest, pure antimalarial compound while lumefantrine is currently the most prescribed member of this class. Mefloquine is the first choice prophylactic for travellers to high risk malaria areas. Many new compounds being researched as antimalarial drugs are based on the aryl amino alcohol pharmacophore (Quiliano et al. 2016). Due to Lumefantrine being the most prescribed long acting drug in combination with artemisinin based drugs, this work focus on this drug under aryl amino alcohols.

Lumefantrine

Lumefantrine is an aryl amino alcohol and the most widely administered. Treatment courses go into the hundreds of millions. It is never prescribed alone but as a fixed combination with artemether (World Health Organization, 2015). This combination regimen has staved off any confirmed report of resistance to lumefantrine. Its plasma half-life of 4-6 days ensures complete parasite clearance as artemether only has a half-life of a couple of hours. The seventh-day plasma concentration of lumefantrine is indicative of the combination therapy outcome. A plasma concentration higher than 500 µg/mL is consistent with a successful treatment while below 200 µg/mL is often a sign of an unsuccessful treatment as this could result in recurrent malaria (Price et al. 2006, Tchaparian et al. 2016).

Lumefantrine is used to treat multidrug resistant and cerebral malaria. It acts against the blood schizonts and gametocytes by forming complexes in the parasite's food vacuole which interfere with heme polymerisation (Warhurst et al. 2001).

The characteristics of lumefantrine which impact majorly on its performance as a drug are its very low aqueous insolubility (3.1 x 10^{-5} mg/mL) and very high lipophilicity (logP: 8-9). The drug must be taken along with a fatty meal so as to achieve significant gastrointestinal absorption. This simple dietary requirement is problematic as malaria patients have low appetite, nausea and vomiting. Also, due to poverty, which is rampant in malaria-endemic regions, it is difficult for most patients to have access to the appropriate meal for the six-dose regimen of the combination treatment (Van Vugt et al. 1999).

The primary known liver metabolite of lumefantrine is desbutyllumefantrine. It occurs at about 0.1 % of the plasma concentration of the parent drug but has an anti-parasite potency of about seven times that of lumefantrine in laboratory-adapted *P. falciparum* strains (Wong et al. 2011). It has been suggested that it could potentially be an antimalarial drug in combination with an artemisinin.

1.4.2 The 8-aminoquinolines

The 8-aminoquinolines are structurally related to the 4-aminoquinolines of which chloroquine is a member. They are renowned for activity against hepatic infections and also for blocking gametocyte transmission. Until recently, primaquine was the only approved member of this group and it has been so for over 60 years. However, in 2018 the Food and Drug Administration in the United States granted licenses for tafenoquine as the radical cure of *P.vivax* malaria (Chamignon et al. 2016; Mccarthy and Price, 2018).

Primaquine

Primaquine is the most notable 8-aminoquinoline antimalarial compound. It is primarily used as a chemo-preventative drug to avoid relapse of *P. vivax* and *P. ovale* infection because of its ability to target the liver hypnozoites (White, 2011). It also targets mature gametocytes of *P. falciparum*, reducing the risk of transmission (Lanners, 1991). Its mode of action and why it is able to act against different stages of the parasite's life cycle is unclear. It has been suggested that this might involve the generation of radical oxygen species that damage the parasite's mitochondria and interfere with the electron transport chain needed for respiration (Baird and Hoffman, 2004). Primaquine has been reported to improve the treatment of chloroquine-resistant plasmodia with chloroquine (Gonzalez-Ceron et al. 2016; Awab et al. 2017).

Oral administration of primaquine results in rapid liver metabolism into the inactive carboxyprimaquine—the major plasma metabolite (Constantino et al. 1999). Primaquine

reaches peak plasma concentration at 1-3 h and a half-life of 4-9 h (Mihaly et al. 1985). It is well tolerated by and safe for most patients who are good candidates to receive it (Baird and Hoffman, 2004).

The most significant toxicity of primaquine and other 8-aminoquinolines is hemolysis in patients with Glucose-6-phosphate dehydrogenase (G6PD) deficiency. G6PD deficiency is an inherent X-linked enzymatic defect that affects about 400 million people around the world (Bancone et al. 2016). WHO therefore recommends, that in low transmission areas, a single dose of 0.25 mg/kg with ACT must be given to patients with *P. falciparum* malaria and this excludes pregnant women, infants under six months and breast feeding women. With this dose, testing of G6DP deficiency is not required (World Health Organization, 2015). Although resistance to primaquine is of less clinical significance than other antimalarial drugs, it is difficult to definitively ascribe failure of treatment singly to either parasite resistance, relapse or re-infection (Thomas et al. 2016).

1.4.3 The artermisinins

This class of antimalarial drugs is also referred to as peroxides because of the presence of an endoperoxide in the pharmacophore (Meshnick, Taylor and Kamchonwongpaisan, 1996; Pandey et al. 1999). Artemisinin is the parent compound of this group of sesquiterpene endoperoxide drugs originally isolated from the herb *Artemisia annua* in 1972 (Chaturvedi et al. 2010). The medicinal use of this herb in treating malaria has been known in traditional Chinese medicine for several centuries. At the beginning of the 21st century the WHO recommended artemisinin-based combination therapies (ACTs) as frontline treatment for multidrug resistant *P. falciparum* (Bosman and Mendis, 2007). Today, five ACTs form the cornerstone of antimalarial chemotherapy (World Health Organization, 2015) and they have been pivotal to recent successes achieved in the fight against the disease (Kolaczinski et al. 2007; World Health Organization, 2017). Mortality is down 60 % while morbidity has fallen about 40 % since the adoption of these drugs.

The artemisinins are currently the most powerful and effective antimalarial therapeutic agents in clinical use. They have the highest parasitemia clearance rate, achieving two of the three treatment objectives—prevention of clinical morbidity and transmission. Artemisinin, the parent compound, is mainly used for complicated malaria (Mishra et al. 2017). Instead, the derivatives artemether, arteether, dihydroartemisinin and artesunate are used to treat

uncomplicated, severe, complicated and multidrug resistant cases of the disease. They act rapidly against the asexual erythrocytic stage and inhibit the development of the gametocytes.

As with many other antimalarial drugs, their exact mode of action is not understood but it is believed that they are activated by interaction with heme (Meshnick, 2002; Wang et al. 2015). Artesunate inhibits the *P. falciparum* antigen EXP1, a membrane glutathione S-transferase that degrades the iron-bound heme cytotoxin hematin (Lisewski et al. 2014). Several reviews and original research articles have been published on the contentious issue of the mode of action of artemisinins (Meshnick, 2002; Krishna, Uhlemann and Haynes, 2004; Golenser et al. 2006; Gopalakrishnan and Kumar, 2015). It is however almost universally accepted that the endoperoxide bridge is crucial to the antimalarial activities of these compounds (Pandey et al. 1999).

Apart from the short plasma half-life and high recrudescence rate — when used in monotherapy — artemisinin and most of its derivatives are poorly soluble in water and oil. Artesunate is the only water-soluble (9.480×10^{-6} at T = 278.15 K) artemisinin derivative currently approved for clinical use (Xu et al. 2019). It is a highly effective antimalarial drug, which has made significant impact on the treatment of severe malaria, providing rapid regain of consciousness and is recommended preferentially to quinine for these cases. It has lower toxicity than the hydrophobic analogues. Artesunate is the salt form of artesunic acid, which in turn is derived from the succinoylation of dihydroartemisinin. A 5 % sodium bicarbonate solution is used to dissolve the acid. This preparation is very unstable as the sodium artesunate has a half-life in solution of less than 15 minutes.

Research is still limited on the metabolism of artemisinins. The major metabolite so far reported of cytochrome P450 enzyme metabolism of artemether, arteether and artesunate in the liver is dihydroartemisinin (Lee and Hufford, 1990; Medhi et al. 2009). Dihydroartemisinin is further metabolized to α-dihydroartemisinin-β-glucoronide. Artemisinin undergoes a different metabolic pathway to four metabolites: 9,10-dihydrodeoxyartemisinin, deoxyartemisinin, deoxydihydroartemisinin and crystal-7. Unlike dihydroartemisinin, none of these metabolites are active as they have lost the endoperoxide bridge (Navaratnam et al. 2000). This is a strong supportive indication of the indispensability of this functionality to antimalarial activity and reason artemisinin is a less effective antimalarial compared to its derivative.

Oral artemisinins are rapidly absorbed and metabolized after administration and reach a maximum plasma concentration after 2 - 3 h (Navaratnam et al. 2000; Meshnick, 2002; Krishna, Uhlemann and Haynes, 2004). This rapid disappearance may be the reason why

resistance is slow and recrudescence is common. The WHO has therefore recommended that these drugs be used only in combination therapy and as first line treatment of uncomplicated *P. falciparum* (World Health Organization, 2015).

Depending on the route of administration artemisinins, especially the highly lipophilic artemether and arteether, have been shown to be neurotoxic in laboratory animal models at high doses (Brewer et al. 1994; Petras et al. 1997; Bhattacharjee and Karle, 1999). This toxicity has not been observed in humans; in fact, the artemisinins have a remarkably low toxicity profile in humans.

Today, artemisinins based drugs are used in combination therapy (WHO, 2001; Bosman and Mendis, 2007; World Health Organization, 2015) (**Table 1.2**). In the context of malaria, combination therapy "*is the simultaneous use of two or more blood schizontocidal drugs with independent modes of action and different biochemical targets in the parasite*" (WHO, 2001). This definition excludes drug combinations with only one blood schizontocide or fixed-dose combinations that act synergistically and the individual drug components cannot be given alone.

Table 1.2: Antimalarial therapy combination drugs (Mishra et al. 2017; World Health Organization, 2015; WHO, 2001).

Major artemisinin-based combinations	**Other artemisinin based combinations**
• Artemether + lumefantrine • Artesunate + mefloquine • Artesunate + sulfadoxine-pyrimethamine • Artesunate + amodiaquine • Dihydroartemisinin + piperaquine	• Artesunate + pyronaridine • Artemisinin + piperaquine • Artemisinin + napththoquine • Piperaquine-dihydroartemisinin-trimethoprim + primaquine Chlorproguanil-dapsone + artesunate

The most significant advantage of antimalarial drug combination is the delay or even prevention of parasite resistance to the chemotherapy. Drug combinations are able to do this because of the synergistic or additive modes of action of the individual components, optimum compatibility in their half-lives and the ability to block transmission of drug resistant strains, i.e. gametocytocidal activity (Nosten and Brasseur, 2002).

1.4.4 Development of new antimalarials

New medicines for malaria are slow in coming through even though improvements are being seen (Anthony et al. 2012; Wells, Van Huijsduijnen, and Van Voorhis, 2015). As there was a slow discovery of new antimalarial drugs between the 1980s and early 2000 (**Figure 1.2**) it was only in 2012-2015 that new drug discoveries were recorded (Wells, Van Huijsduijnen, and Van Voorhis, 2015).

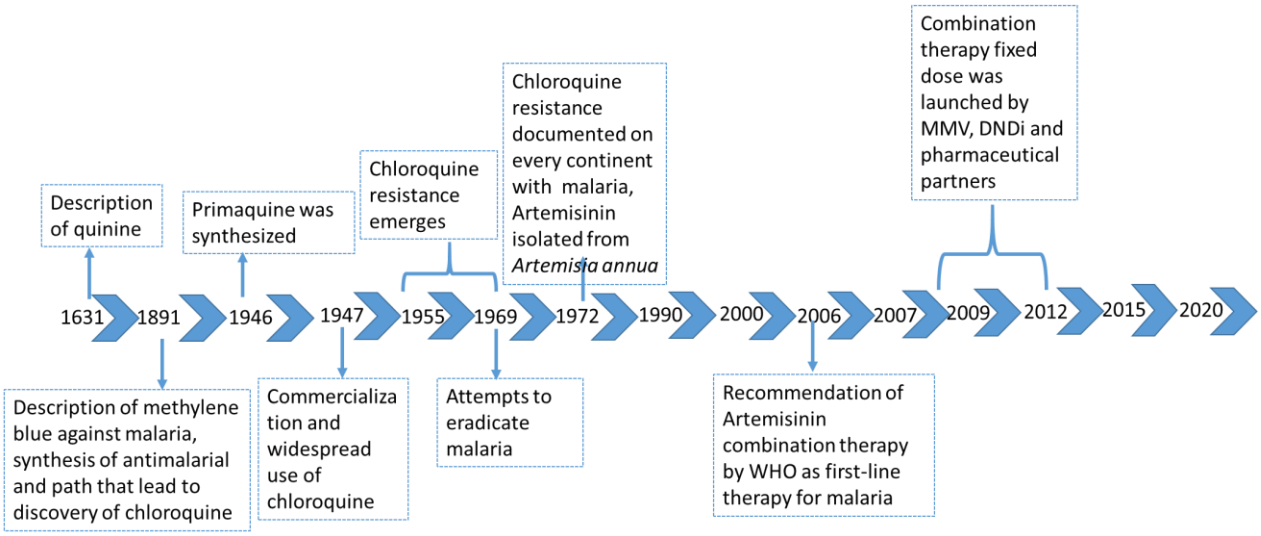

Figure 1.2: Historical events on the discovery of antimalarial.

Among the newly developed antimalarial drugs, there is a group of drugs that were developed with structural functionality resembling the endoperoxide bridge of the artemisinins. The first registered drug that had the peroxide was zonide (OZ277) (**Table 1.3**). (Dong et al. 2017; Charman et al. 2011)**.** It is a 1,2 trioxolane also known as arterolane and has potency similar to artesunate *in vitro* with increased activity in the *P. berghei* mouse model. Arterolane has longer half-life than DHA in human volunteers (Clark et al. 2017)**.** This compound showed 70% efficacy after seven days of treatment and was approved for use in India in 2012 in combination with piperaquine as a three day cure (Flannery, Chatterjee, and Winzeler 2014; Clark et al. 2017). While, this shows promise, there is still a room for improvement.

Table 1.3: Properties of potential antimalarial drugs in development and in clinical trials.

Name	**Structure**	**Key features**
Arterolane OZ277	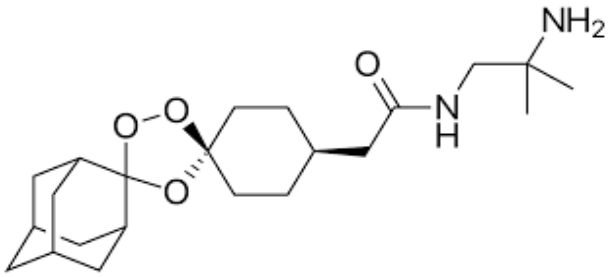	Rapidly acting oral antimalarial
Artefenomel OZ439	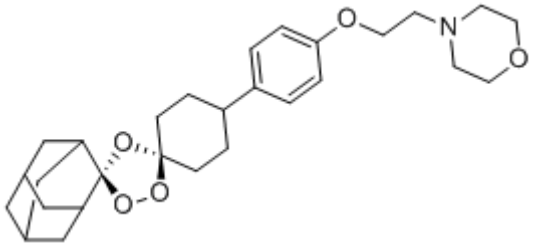	Fast killing of parasite
Artemisone	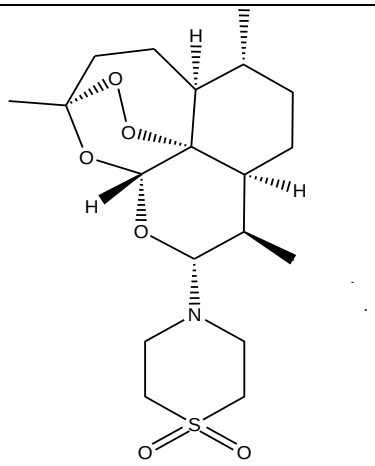	Efficacies of artemisone against the malaria parasite are substantially greater than those of the current artemisinin
Artelinic acid	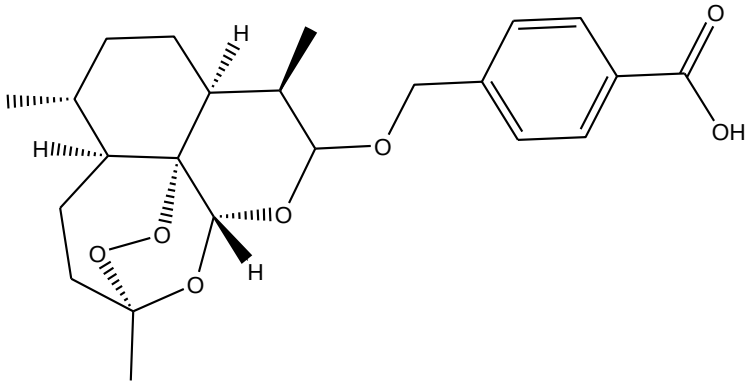	Artelinic acid has a lower rate of neurotoxicity than the related artemisinin derivatives arteether and artemether.

DSM 256	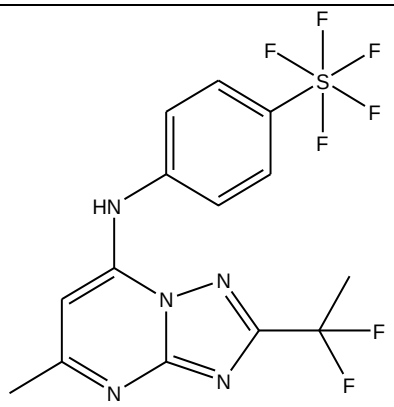	Novel mechanism of action
Cipargamin	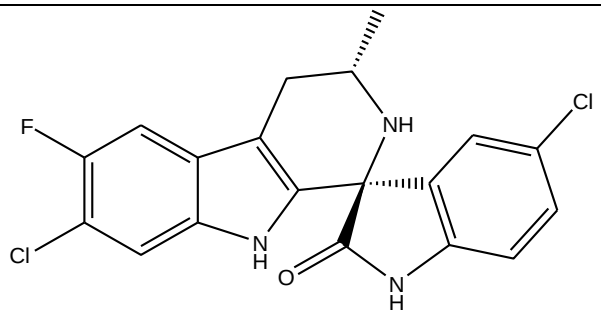	Potential for transmission blocking
MMV390048	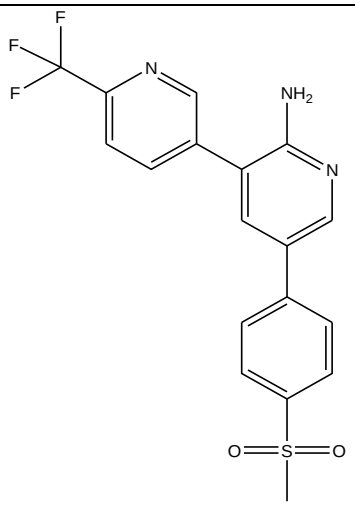	Long half-life in human

Another drug developed to mimic artemisinins is ozonide OZ439 also known as artefenomel (**Table 1.3**). It is fast-acting, potent, has a longer pharmacological activity and has improved bioavailability compared to arterolane (Flannery, Chatterjee and Winzeler, 2014). Artefenomel is now in phase IIb clinical trials in combination with ferroquine as a potential shorter treatment regimen or even a single-dose cure for malaria (Medicines for Malaria Venture 2020; Clark et al. 2017). Artefenomel is more stable in blood than arterolane due to the modification in its chemical structure (Clark et al. 2017). There is a new lead compound containing 1,2,4,5-tetraoxanes known as RKA182 (Flannery, Chatterjee and Winzeler, 2014). It has shown excellent *in vivo* activity, prolonged mouse survival and it is also fast-acting (Barnett and Guy, 2014).

This newly developed class of ozonide antimalarials were developed to address the high cost of artemisinins that were extracted from plants in the early 2000s (Clark et al. 2017). Now the issue related to these compounds is how they will differentiate themselves from the inherent artemisinin resistance (Wells, Van Huijsduijnen and Van Voorhis, 2015) (Flannery, Chatterjee and Winzeler, 2014).

Other synthetic derivatives of artemisinin have been made to circumvent issues of possible toxicity and stability. Haynes et al. 2006, reported the synthesis of artemisone, a 10-alkylamino derivative (**Table 1.3**), with an improved logP of 2.49 compared to artemether's logP of 3.98. Artemisone also showed significantly less neurotoxicity than other artemisinins in fetal rat brain stem cells assays. Artelinic acid was synthesized to resist rapid *in vivo* degradation (Vishwakarma et al. 1992). In spite of these attractive properties, neither these nor any new artemisinins have made it to clinical development (Wells, Van Huijsduijnen, and Van Voorhis, 2015).

The other group of antimalarials was developed by first identifying a molecular target, followed by performing experiments that boost confidence in the role of that target in human disease. Then, an inhibitor is found through screening combined with three-dimensional structure elucidation (Wells, Van Huijsduijnen, and Van Voorhis, 2015). One of the antimalarial compounds found through this process is DSM265 and is in phase IIb clinical trials (Medicines for Malaria Venture, 2020). DSM265 inhibits plasmodial dihydroorotate dehydrogenase and has both blood stage and liver stage activities (Mccarthy et al. 2017; Phillips et al. 2017). Human phase Ia/Ib studies showed that DSM265 has prolonged half-life, suggesting it as a good combination partner for a single-dose treatment of uncomplicated malaria (Mccarthy et al. 2017).

The major breakthrough in drug discovery in the past years come from phenotypic screening, with some on the compounds being in clinical trials. One of the compounds that has advanced to phase IIb clinical trials is spiroindolone KAE609 also known as cipargamin (Wells, Van Huijsduijnen, and Van Voorhis, 2015; Medicines for Malaria Venture, 2020). This compound is highly potent and provides parasite clearance in patients more than peroxides (Phillips et al. 2017). KAE609 has the ability to inhibit gametocyte and oocyst development in mosquitoes (Spillman and Kirk, 2015).

A significant recent highlight is the MMV390048, an aminopyridine which was developed by a team led by Kelly Chibale of the University of Cape Town, South Africa (Paquet et al. 2017). MMV390048 represents a novel class of antimalarial drugs capable of blocking the three human life stages of the *Plasmodium* parasite and has no cross resistance with current drugs (Younis et al. 2012). This compound inhibits the asexual liver and blood stage as well as the sexual gametocyte stage. It has good exposure in animal model, which means that it can be used in a single-dose combination therapy (Phillips et al. 2017). Many other compounds have been investigated but very few have made it significantly far enough in development to hold promise of actually reaching the clinic (Wells, Van Huijsduijnen, and Van Voorhis, 2015). Even those compounds that show potential as powerful antimalarial agents still face the past traditional hurdles. Over 70% of newly discovered drug candidates suffer from solubility issues, which enforce high doses to achieve a therapeutic effect that increase the risk of toxicity and patient non-compliance. With the historical resilience of the *Plasmodium* parasite and *Anopheles* vector as a reference, coupled with our poor understanding of their resistance mechanisms (Olliaro, 2001), resistance to the current antimalarial drugs is on the cards (Wongsrichanalai et al. 2002; Dondorp et al. 2009; Ashley et al. 2014; Tun et al. 2015) and the only question is how much time would it take for them to be ineffective.

1.5 Nanotechnology

Nanotechnology offers an opportunity to save the current chemotherapy (Santos-Magalhães and Mosqueira, 2010; Singh, 2012; Aditya et al. 2013), reclaim some of the drugs lost to resistance (Huh and Kwon, 2011) and strengthen what might be developed next (Mishra et al. 2017; Paquet et al. 2017). It is very expensive to develop new pharmaceutical compounds, even if it is just to solve a physico-chemical problem with an existing compound. Even worse is that the new compound might not provide the same therapeutic benefits as the original drug. Hence, delivery systems offer a cheaper and less research and development-intensive alternative.

There are different types of techniques that are used to improve or modulate the pharmacokinetics and pharmacological potential of drugs. A widely used technique is encapsulation to physically entrap the drug. Encapsulation of liposomes, dendrimers and nanostructured lipid carriers have limited potential for malaria treatment. Liposomes, for example require temperature-controlled storage and must possess specific fluidity for fusion

with RBC plasma membrane. This chapter looks into the use of polymer-drug conjugation as a potential delivery system for antimalarials.

1.5.1 Polymer therapeutics

In 1975 the German polymer chemist Helmut Ringsdorf described a model for a "pharmacologically active polymer" (Ringsdorf, 1975). A polymer-based delivery system in which a low molecular weight, water-insoluble bioactive agent or drug is covalently conjugated to a hydrophilic polymeric carrier was envisaged (**Figure 1.3**). He predicted that the system would have several significant advantages over small drugs such as increased solubility and reduced toxicity. This macromolecular conjugated construct would affect the cellular pharmacokinetics of the drug such that its therapeutic potential is enhanced. Conjugation to a polymer can prevent uptake of the drug through the conventional route, which is susceptible to small-molecule efflux-mediated resistance. Cellular uptake would occupy endocytosis (Duncan, 2003; Vicent and Duncan, 2006).

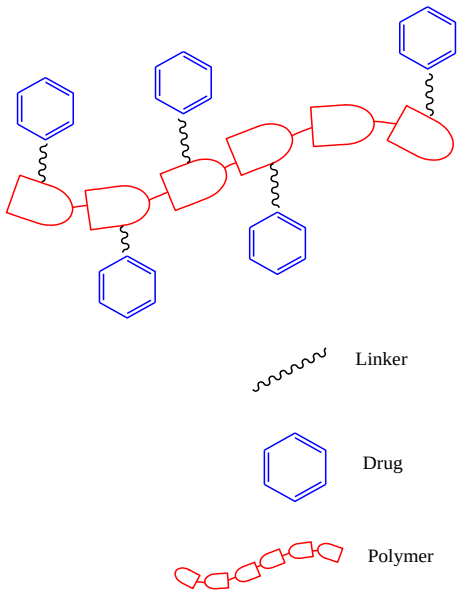

Figure 1.3: A presentation of chemical conjugation of drugs.

Ringsdorf's pharmacologically active polymer included a chemically stable but physiologically labile covalent linker between the drug and polymer, which is responsive to a specific pre-determined intracellular trigger such as enzymolysis or pH-dependent hydrolysis. Many conjugates are made with an ester or amide linkages but some constructs have linkers

that are recognized by specific enzymes that may be upregulated in diseased tissues (Duncan et al. 1987; Lee et al. 2013; Zhong, Shao and Li, 2013).

Antibodies have been investigated as targeting ligands (McCarron et al. 2005; Ross and Wolfe, 2016) but so have small molecules like the amino sugars galactosamine (Seymour et al. 1991) and mannosamine (Nan et al. 2001, 2004) and peptides (Eldar-Boock et al. 2011). One of such actively targeted conjugates made it to clinical trials (Duncan et al. 1986; Seymour et al. 2002). Targeted conjugates are taken up by receptor-mediated endocytosis (Vicent and Duncan, 2006) but this has not always been shown to present a distinct advantage over non-targeted conjugates (Nicoletti, Seifert and Gilbert, 2009) and might actually be dysfunctional in certain disease states (Duncan and Vicent, 2013). Today, polymer therapeutics is a collective term used to describe any polymeric drug, polymer-drug conjugates, polymer-protein conjugates and polymeric micelles where the drug is covalently bonded to the carrier polymer (Duncan, 2003). This work focuses on polymer-drug conjugates, with the attention paid to the polymer, the drugs and physiological labile linkers.

1.6 Polymer therapeutics combination therapy for malaria treatment

The WHO recommends artemisinin based combination therapy (ACTs) for the treatment of uncomplicated malaria caused by *P. falciparum* (World Health Organization, 2015). Combination is a general term normally used in therapeutics as the simultaneous administration of two or more pharmacologically active agents (Shenfield, 1984; Godman et al. 2020). In malaria, the simultaneous use of drugs that target blood schizontocidal with independent modes of action are used in combination to prevent or delay development of drug resistance. An ideal antimalarial combination therapy must possess the following characteristics (Nosten and Brasseur, 2002):

1. One of the drugs must be fast acting drug.
2. The drugs must have different modes of action.
3. The treatment must be active against at least two stages of the malaria life cycle.
4. The combination must possess a good tolerance and toxicity.
5. Treatment should not exceed three days to ensure patient adherence to dosage regimens.
6. The drugs must have no adverse pharmacological interactions.

7. The treatment must be affordable.

All of these points are extremely important when one design combination therapies for malaria. Currently, artemisinin-based combination therapy mentioned in **Table 1.2** is one of the approaches that is currently used to treat malaria.

The term combination therapy is normally used to describe administration of co-formulated active ingredients in one tablet (World Health Organization, 2015). In polymer therapeutics, there are four types of combination therapies. **Type I**, is when a low molecular weight drug is co-administered with a polymer-drug conjugate carrying one drug as illustrated in **Figure 1.4**. **Type II**, is when two different polymer drug conjugates each carrying a single drug are co-administered. While **Type III**, one polymer is carrying more than one drug. The fourth type **(Type IV)**, encompasses combination of polymer-drug conjugate carrying a single drug with a polymer-enzyme conjugate or combination of liposome with a polymer phospholipase conjugate (Greco and Vicent, 2009).

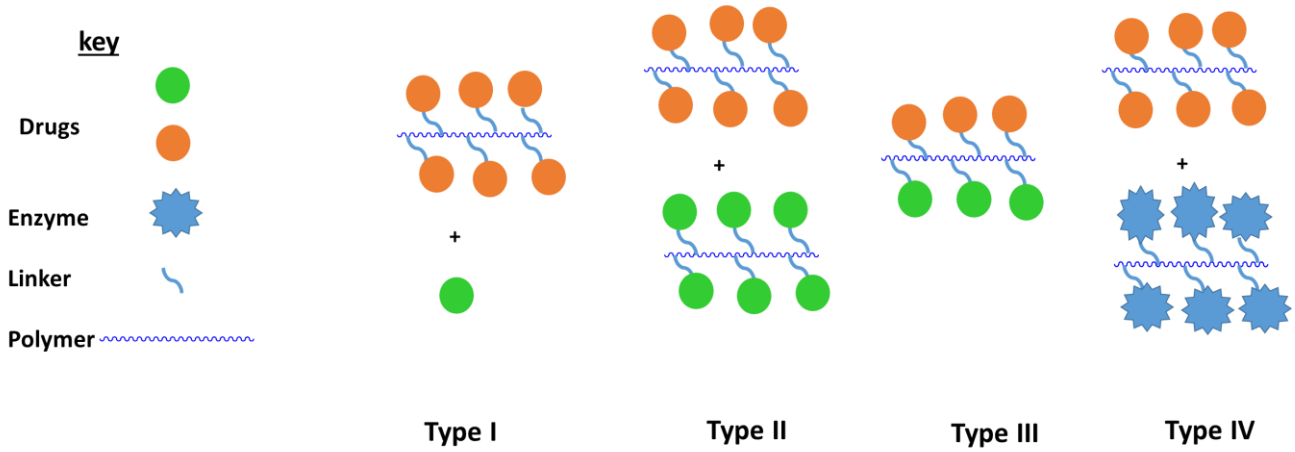

Figure 1.4: Representation of different types of polymer-drug conjugate combination therapy.

In this work, the design of combination therapy for malaria will adhere to the points listed above, especially points 1-4. In designing such chemotherapy, it is important that one considers the route of administration for each drug, drug loading, vehicle structure and drug release mechanism. In the case of malaria which requires a combination therapy to target different sites of pharmacokinetic activity, it is more appropriate for the drug to be able to accumulate independently at different sites of infection. In this thesis the preparation of individual polymer conjugates was investigated for type II combination therapy.

1.7 Selection of polymers

Polymers are large molecules formed from repeating units of small chemical units called monomers (Ebewele, 2000). Polymers have been used in the pharmaceutical industry as backbone of pharmaceutical drug delivery systems. They have been utilized as stabilizers, taste-masking agents and proactive agents. Recent advances in research has now seen the use of polymers to control the rate of drug release from formulations (Priya et al. 2016; Gandhi, Deshmane, and Biyani, 2012).

The physiological characteristics of a drug carrier (i.e. polymer or macromolecules) in the development of a delivery system is important. One needs to keep in mind the mode of action of the drug, the biological pathway and the route of administration when choosing the type of polymer. For a polymer to be used as a carrier for a drug it must have the following properties (Gandhi, Deshmane, and Biyani 2012; Pillai, Paul, and Sharma, 2009):

- The polymer must be soluble and easy to synthesize and the molecular weight distribution must be narrow.
- It should have functional groups that allow for the conjugation and also allow controlled drug release once it has reached the targeted site.
- The polymer should also have the ability to target specific cell types through physico-chemical properties or the incorporation of a specific target ligand.
- The polymer should be biodegradable and easily eliminated from the body.
- The polymer should also be biocompatible with the biological environment and not be toxic or antigenic.

There are two types of polymers one can chose from, (i) synthetic polymers and (ii) natural polymers. These two types differ in their biodegradability and their ability to be structurally modified. Natural polymers have biodegradable bonds, while synthetic polymers that are not biodegradable are used mainly because of their narrow molecular weight distribution. Synthetic polymers are mostly used as drug carriers because their functional groups can be easily modified, while natural polymers have a limited number of functional groups to attach the drugs. Polymers that are used for conjugation should provide good polymer-drug linkage (Gandhi, Deshmane and Biyani, 2012) and should contain one of the functional groups listed in **Table 1.4**.

Table 1.4: Functional groups needed in polymers or drugs for conjugation.

Functioanl group name	Chemical Structure
Carboxylic acid	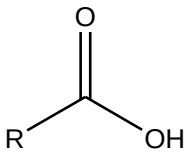
Amines	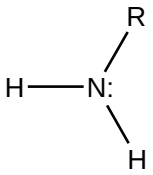
Sulfhydryl	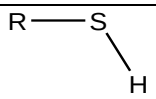
Hydroxyl	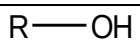
Aldehydes	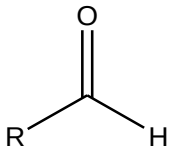
Organic phosphate	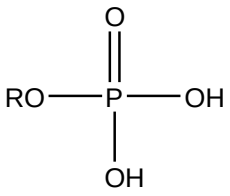

These functional groups allow the attachment of drugs and targeting moieties. The bonds formed should be hydrolysable. The rate of hydrolysis will vary according to type and specific structural features, for example, amide bonds are reported to have low uncatalysed hydrolysis but this may be increased by the introduction of specific groups close to the amide bond. The resulting bond linkage between the polymer and the drug should also be relatively stable to prevent premature drug release outside of the targeted cellular location.

1.8 Antimalarial polymer therapeutics

Nanomedicines have had a remarkable impact on the chemotherapeutic management of diseases like cancer where many of the drug agents used for treatment have significant

pharmacological inadequacies and toxicities (Venditto and Jr., 2014). They have reduced toxicity, increased efficacy, extended drug release, exposure, improved stability and bioavailability. Nanomedicines have even reversed drug resistance (Assanhou et al. 2015). This impact is yet to be seen in malaria and indeed in most infectious diseases (Islan et al. 2017) but the therapeutic and pharmacological potential offered by nanomedicines in infectious diseases are increasingly being recognized (Dube et al. 2013; Dube and Ebrahim, 2017). In this section of the thesis, we discuss polymer-drug conjugation for antimalarial drugs and the pharmacological improvements.

1.8.1 Poly (ethylene) glycol

Poly (ethylene) glycol (PEG) is a polymer made of repeating units of ethylene oxide and is mostly used in drug delivery due to its unique physico-chemical properties (Li et al. 2013; Banerjee et al. 2012). PEG is soluble in organic and inorganic solvents, amphiphilic and has low polydispersity in molecular weight (Li et al. 2013, Kolate et al. 2014). The most common form of PEG is a linear polyether terminated with hydroxyl groups (**Figure 1.5**) (Roberts, Bentley and Harris, 2002). The linear polymer has an inherently low drug loading as it only has two sites available for conjugation. Therefore, other types of PEG (multi-arm, fork and branched shaped) have been used to overcome the limitation of low drug loading of linear PEG (Marasini, Haque, and Kaminskas, 2017; Kolate et al. 2014). The immunogenicity, antigenicity, toxicity and rapid clearance of pegylated delivery system has been debated (Armstrong et al. 2007; Sherman et al. 2012; Knop et al. 2010), for example Sherman et al. 2012, reported that monofunctional activated PEG-OH might decrease the loss of affinity of antibodies that have high affinity for methoxy groups as affinity was lost when mPEG was used. The FDA still continues to approve mPEG containing biopharmaceuticals with the most recent being pegylated Nyvepria that was approved in 2020 and is used to reduce the chance of infection due to low white blood cell count in people with certain types of cancer (Hossain et al. 2020). There is also a recommendation that patients should be screened and monitored for pre-existing anti-PEG and development of anti-PEG for any PEG containing agent (Armstrong et al. 2007) and other researchers reported that anti-PEG antibodies is not of concern (Schellekens, Hennink, and Brinks 2013).

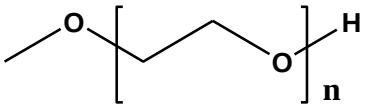

Figure 1.5: Chemical structure of poly(ethylene) glycol.

1.8.1.1 PEG- malaria drug conjugates

Multi-arm PEG conjugates of dihydroartemisinin of different molecular weights were synthesized by Dai et al. (2014). They showed remarkable stability at physiologically significant pHs of 6.1, 7.4 and 8.1 at 37 °C. At pH 7.4 as much as 50 % of the conjugates were still intact after incubation for over 24 h. Although these experiments were conducted to show the improvements in the circulating half-lives offered by polymeric conjugation, they also serve as a positive outcome for overcoming the very low stability of artesunate in solution.

1.8.2 Chitosan

Chitosan (CS) shown in **Figure 1.6**, is a polysaccharide that is made of a copolymer of glucosamine and *N*-acetylglucosamine that is derived from Chitin (Illum et al. 2001; Dutta, Dutta, and Tripathi 2004 ; Dash et al. 2011). Chitin is the most abundant natural polysaccharide derived from the exoskeletons or shells of living organisms such as prawns, lobsters, crabs and crustaceans (Illum et al. 2001; Pillai, Paul, and Sharma, 2009). Chitosan is obtained via the deacetylation of chitin under alkaline conditions or through enzymatic hydrolysis (Rinaudo, 2006). Chitosan is insoluble under alkaline conditions and at neutral pH but forms salts with organic and inorganic acids such as hydrochloric acid, acetic acid and lactic acid. In the presence of acid, the amino (NH_2) functional groups become protonated (NH_3^+) which results in a positively charged aqueous soluble polysaccharide (Illum et al. 2001, Pillai, Paul, and Sharma, 2009). The degree of deacetylation and molecular weight affects the solubility of the chitosan at neutral pH and physiological conditions (Dash et al. 2011). Chitosan has found a variety of applications in the pharmaceutical industry due to its non-toxicity, biodegradable, biocompatible and low immunogenicity (Pillai, Paul, and Sharma 2009; Kean and Thanou, 2010). Thus, it has been approved for dietary applications in Japan, Italy and Finland. It is also approved by FDA for wound dressing (Dash et al. 2011).

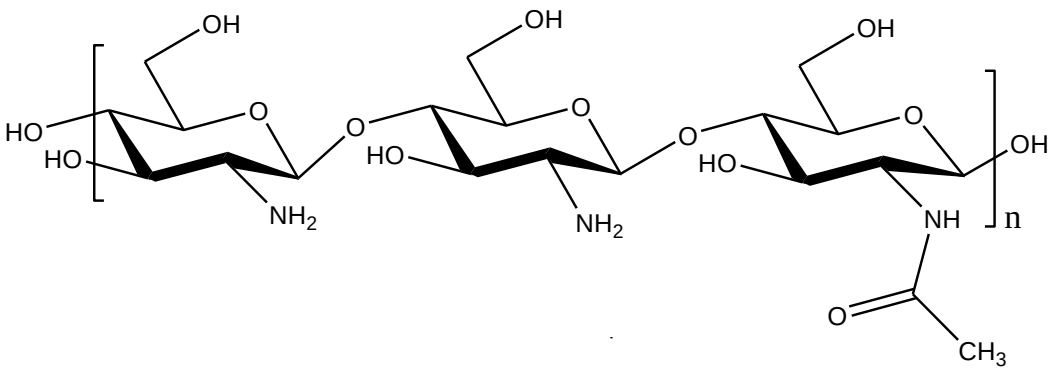

Figure 1.6: Chemical structure of chitosan.

1.8.2.1 Chitosan- malaria drug conjugates

Tripathy et al. (2012), synthesized chitosan-tripolyphosphate (TPP)-conjugated chloroquine as a delivery system, to reduce *Plasmodium berghei* in infected Swiss Mice. Results showed potential elimination of parasite and protection of the lymphocytes, serum and red blood cells against *P. beghei* infection at the dose of 250 mg/kg.

Xiao et al. (2013), synthesized water-soluble C-10 phenoxy artemisinin chitosan conjugate. Artemisinin was converted to dihydroartemisinin which was further converted to artesunate by conjugating dihydroarteminin to succinic anhydride. The artesunate was conjugated to chitosan (MW 1800 Da). The solubility of the conjugate was evaluated and compared to commercially available artemisinin. The results showed that the conjugate had improved solubility compared to artemisinin from 0.084 g/dL to 3.123 g/dL.

1.8.3 Polyglutamic acid

Polyglutamic acid (PGA) is a polyamide made up of glutamic acid units. It exists in two forms α-PGA or γ-PGA, depending on the attachment of the carboxy group (**Figure 1.7)** (Bajaj and Singhal 2011; Candela and Fouet 2006). γ-PGA is a natural polymer that is made by *Bacillus subtilis* grown from soybeans (Candela and Fouet, 2006). It can be prepared on large scale by chemical synthesis, peptide synthesis, biotransformation or microbial fermentation, the latter being the most cost effective method (Luo et al. 2016). While, α-PGA is synthesized chemically by nucleophile initiated polymerization of the γ-protected *N*-carboxyanhydride of L-glutamic acid. α-PGA has been widely used for medical application and for sustained drug delivery, as it is not susceptible to proteases and thus provides sustained delivery of the

conjugate within the body. The limitation of using α-PGA is the cost, pure γ-PGA can be obtained at less cost in large quantities without many chemical steps compared to α-PGA (Ogunleye et al. 2015). Due to PGA being water-soluble in the presence of inorganic salts (K^+, Na^+ or Ca^{2+}); biodegradable and non-toxic (Chettri, Bhutia and Tamang, 2016), PGA can be used as a drug carrier, animal feed additive and bitterness-relieving agent (Luo et al. 2016).

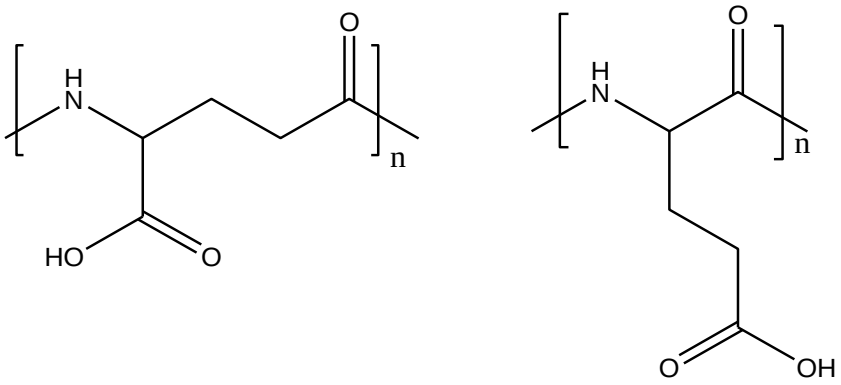

γ-PGA α-PGA

Figure 1.7: Chemical representation of γ-PGA and α-PGA.

1.8.3.1 PGA-malaria drug conjugates

Tomiya et al. (2013) conjugated primaquine to γ-PGA using trivalent glyco-ligand as a targeting moiety to deliver γ-PGA to the liver hepatocytes. Binding, uptake and catabolism of the conjugate was investigated using rat hepatocytes. The results demonstrated that the conjugate was almost completely degraded over 24 h. There was approximately 250 ng per million cells of the conjugate that could bond to one million rat hepatocytes at 0 °C. The binding experiment at 0 °C are carried out to demonstrate at such temperature there is no particle internalization and that these are energy dependent process.

1.9 The use of linkers for polymer-drug conjugation

Another aspect included in the definition of polymer-drug conjugate is a physiologically labile but chemically stable covalent linker between the drug and polymer. A linker is defined as a multifunctional molecule that is used to connect a drug to a polymer (Ross and Wolfe, 2016). The drug circulates as a polymer-conjugate and its release can be triggered by either endogenous stimuli such as pH or enzymes (Feng and Tong, 2016). There are three important aspects to the use of linkers, these include functional groups that allow conjugation, mechanism

of drug release and the physical properties of the linker (Ross and Wolfe, 2016; Lu et al. 2016). Linkers reduce crowding as they serve as a spacer between the drug and the polymer (Chang et al. 2016; Lu et al. 2016). Linkers may also provide efficient conjugation, prevent premature drug release and may enhance release of the drug at the active site. Teicher and Chari (2011) explained that they could be used to influence the circulation half-life and safety of conjugates by minimizing the release of the drug molecule in circulation and optimizing the delivery of the conjugate to the target site. Linkers are classified as cleavable and non-cleavable.

Non-cleavable linkers

Non-cleavable linkers are defined as molecules that have no in-built chemical triggers to cleave the linker, most popular being thioether linkers. Thioethers have been used in antibody-drug conjugates (ADCs) and the release of the drug from the ADCs requires complete hydrolysis of the polypeptide backbone of the antibody in cell lysosomes after internalization (Feng and Tong, 2016; Erickson et al. 2006; McCombs and Owen, 2015). One example, is the trastuzumab emtansine (T-DM1) which is an antibody-drug conjugate that consists of anti-HERS2 antibody trastuzumab linked via nonreducible thioether linker to maytansinoid antitubulin agent. The thioether is stable as it resists chemical or enzymatic cleavage. When compared to a disulphide linker, the T-DM1 showed better antitumor efficacy than the disulphide conjugate (Erickson et al. 2012).

Cleavable linkers

Cleavable linkers are stimulus sensitive linkers that are cleaved by endogeneous stimuli (pH, redox state and enzyme-activated) and exogenous stimuli (magnetic field, temperature, light and ultrasound) (Feng and Tong, 2016 ; Chang et al. 2016). Exogenous linkers mostly find use in cancer therapy. This work will discuss endogeneous linkers.

In the polymer-drug conjugation field of nanomedicine , pH-labile linkers commonly used rely on hydrazone, orthoether, acetal, imine, vinyl ether functional groups (Chang et al. 2016; Leriche, Chisholm and Wagner, 2012). Linkers that rely on hydrazone formation are the most widely used pH-sensitive linkers but they suffer from premature degradation with a half-live between 48-72 h in plasma (Lee et al. 2006;Feng and Tong, 2016).

Another category of cleavable linkers is spacers that can be degraded by natural enzymes such as esterases, proteases and glycosidases. These enzymes are localised or are more abundant in

certain tissues and are able to recognize the structure of an ester, the sequence of peptide or pattern of carbohydrate in order to degrade the linker (Chang et al. 2016; Feng and Tong, 2016).

Redox-sensitive linkers, also known as reducible linkers, use the difference in redox potential between intracellular and extracellular environments (Feng and Tong, 2016). These have functional groups, such as the disulfide group, with a different reduction potential in the intracellular compartment versus plasma. This type of linker is appropriate for cancer chemotherapy as tumor cells have a high concentration of Glutathione (GSH) that easily reduced disulfides (Chang et al. 2016).

One needs to consider several things when designing polymer-drug conjugate that contains a linker. It must withstand mild synthesis conditions to protect the therapeutic activity of the drug molecule; must be stable during synthesis and after internal administration; it should undergo cleavage mediated by specific stimuli for controlled drug release. The linker must also be biocompatible and safe for clinical use (Chang et al. 2016). The mechanism of drug release is an important consideration in a linker selection. While, cleavable linkers are dependent on physiological stimuli such as pH, the design of the polymer-drug linked conjugate must be well thought to suit the specific pharmacological conditions of that specific disease.

1.10 Carbodiimide crosslinking chemistry

Polymers are normally covalently linked to small molecule drugs via ester, amide bonds or to protein and peptides via thioester, thioether and disulfide bonds (Sagita, Syahdi and Arrahman, 2018). Conventional synthetic methods such as the Fischer esterification methodology requiring a strong acid catalyst or conversion of carboxylic acids to acid chlorides and anhydrides for reaction with alcohols and amines are either not efficient or use reagents that may degrade the drug or polymer. These complicate purification and the toxicity of reagents and byproducts can also be problematic. Carbodiimide chemistry has become the preferred methodology as it enables the use of mild reagents to achieve efficient coupling of large, complex carboxylic acid containing substrates to alcohols, including sterically hindered secondary and tertiary alcohols (Hermanson, 2008 ;Morales-serna, 2011; Tsakos et al. 2015).

Carbodiimides (RN=C=NR') are unsaturated compounds with an allene structure (Nakajima et al. 1995). These were first synthesized from thioureas and they been widely used in organic synthesis, biotechnology mostly in peptide synthesis and modification of proteins and polysaccharides (Nakajima et al. 1995). There are different types of carbodiimide reagents, water soluble and water insoluble carbodiimide. The water soluble reagents are 1-ethyl-3-(3-

dimethylaminopropyl)carbodiimide hydrochloride (EDAC) and 1-cyclohexyl-3-(2-morpholinoethyl)carbodiimide (CMC). The water insoluble reagents comprise of dicyclohexyl carbodiimide (DCC) and diisopropyl carbodiimide (DIC). The commonly used reagent for bioconjugation is EDAC as it can be used in water and it also produces a water soluble isourea by-product that can be easily removed by dialysis (Hermanson 2008, Everaerts et al. 2008). EDAC is normally used with *N*-hydroxysulfosuccinimide sodium salt or *N*-hydroxysuccinimide to increase the solubility and stability of the active intermediate. The resultant intermediate is a good electrophile that can be attacked by moderate to good nucleophiles (**Scheme 1.1**) such as amino, hydroxyl and thiol groups to form a stable amide, ester or thiol ester respectively (Hermanson, 2008). During these reactions one needs to consider that the water is also a nucleophile that competes with alcohols, thus it is important to carry esterification reactions in dry conditions using organic solvents (Hermanson, 2008).

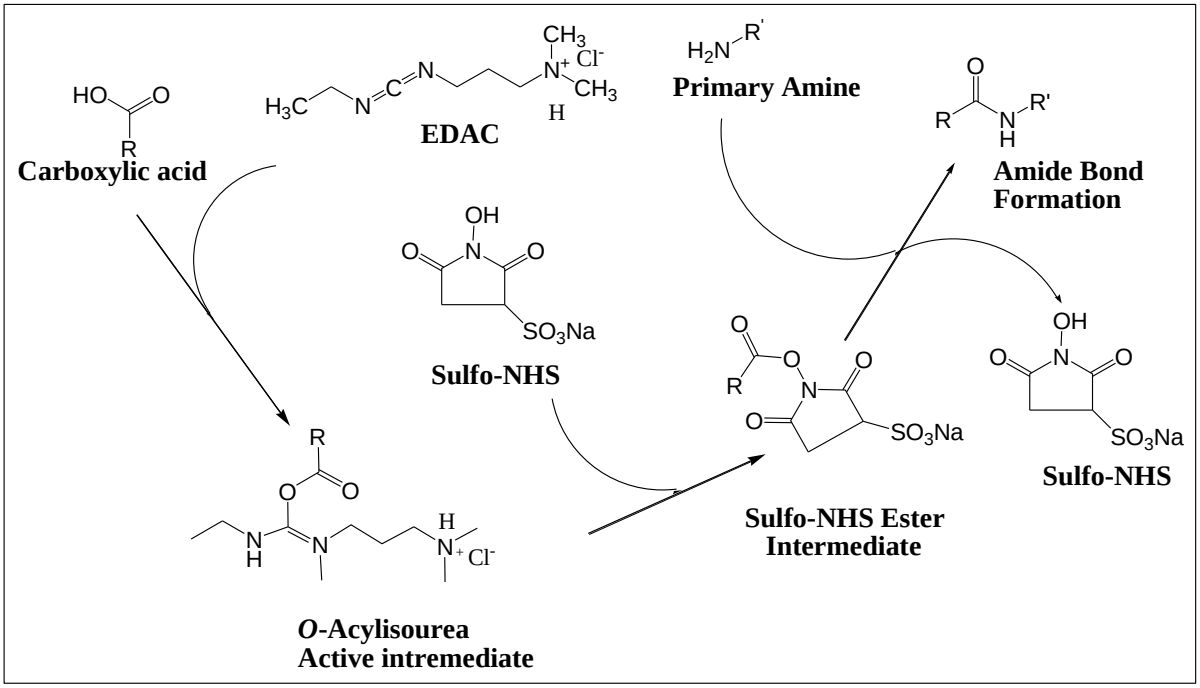

Scheme 1.1: Chemical synthesis of amide bond using EDAC as coupling reagent.

1.11 Significance and clinical perspective of this work

If this technology is to have a significant clinical impact in malaria, the development of polymer-combination drug conjugates of antimalarial drugs is essential as the WHO has strictly prohibited monotherapy (World Health Organization, 2015). Polymer therapeutics for combination therapy is still in its early stages even in the treatment of cancer (Greco and Vicent, 2009; Duncan and Vicent, 2013). The adoption of combination therapy as the accepted treatment strategy means that multiple drugs must be administered in a fixed ratio and there

must be a synergism in their delivery. This is more efficiently accomplished by conjugating both drugs to a single carrier in an appropriate ratio. Malaria has not yet benefited from such new technological developments. Therefore, this work is significant as it reports on the state-of-the-art technology (polymer-drug conjugation) for malaria and it indicates the advantages and challenges thus guiding future studies and development.

1.12 Hypothesis

Polymer drug conjugation having found extensive application in cancer chemotherapy, can be used in malaria chemotherapy to improve the physico-chemical properties and enhance the *in vivo* properties of anti-malarial drugs.

1.13 Aims

1. Synthesize plant-derived polymer conjugates that have antimalarial properties.
    - Analyze their physicochemical properties using spectroscopic, microscopic, chromatographic techniques and thermal analysis.
    - Analyze their *In vitro* properties before and after conjugation.
2. Synthesize polymer-drug conjugate for malaria combination therapy using multivalent polymers.
    - Comparison of the physico-chemical properties of multivalent polymer to a single attachment polymer (p(NAM-stat-AA)-DHA compare to PEG-DHA conjugate).
    - Analysis of the cytotoxicity of polymer-drug conjugates.
3. Conjugation of lumefantrine to glycine linker.
    - Exploration of different methods to conjugate glycine to lumefantrine.
    - Characterization of the synthesized linked lumefantrine.

Chapter Two:
The physico-chemical characterization of polymer-drug conjugates and other specialized techniques

2.1 Introduction

Polymer-drug conjugates are complex chemical entities that are used mainly *in vivo* and *in vitro* applications. Thus, careful physico-chemical characterization is required as composition uncertainties can cause regulatory concerns. The understanding of the critical physical and chemical properties of the polymer-drug conjugates in respect to the proposed use is crucial as residual solvent, impurities and toxicity can affect for biological activity and pharmacokinetics of the new entity. It is therefore necessary to identify and use reliable robust techniques that are relevant to the purpose to which the conjugates will be put to used (Sagita et al. 2018; Nino-Pariente, J. Nebot and J. Vicent, 2016). It is also important to note that it is not only chemical composition that could affect toxicity, biodistribution and efficacy but also the physico-chemical properties of the polymer (e.g. molecular weight, polydispersity index (PDI), size; architecture of the polymer shape, charge distribution and hydrophilic-hydrophobicity) have to be considered (Gaspar and Duncan, 2009). This chapter discusses the spectroscopic, thermal, microscopic and chromatographic techniques that are normally used to characterize polymer-drug conjugates. Their application and limitations related to polymer-drug conjugates will be discussed.

2.2 Significance of the review

Gaspar and Duncan (2009) suggested that many polymer-drug conjugated products fail in clinical trials because of the neglect of the fundamental science surrounding the understanding of the architectural control of the molecules, their behavior in vivo administration and how the host will respond. Therefore, before synthesis of polymer-drug conjugate one needs to consider the route of administration (important for choice of polymer used) and the characterization of the conjugates once they are synthesized. The new chemical entity's behavior is dependent on the physico-chemical properties of the new entities. This is why it is important to consider the chemical analytical techniques used to analyze these properties before questioning the biological models used. The purpose of this review is to highlight several techniques that are used to analyze polymer-drug conjugates. In the absence of standardized universal protocol for characterization of conjugates, these different techniques can be exploited to better understand the physico-chemical properties of the new chemical entities.

2.3 Spectroscopic techniques

2.3.1 Nuclear Magnetic Resonance (NMR) analysis of polymer drug conjugates

Nuclear magnetic resonance (NMR) spectroscopy in polymer therapeutics is used as a characterization tool to determine the content and purity of the sample as well as the molecular structure. Proton NMR (^{1}H NMR) spectroscopy is the most used NMR technique in conjugated polymer-drug analysis. This is because ^{1}H is the most common nuclei investigated, this method is also fast, reproducible and relatively simple technique for confirmation of covalent bonding between a drug and polymer (Nino-Pariente, J. Nebot and J. Vicent, 2016).

^{1}H NMR is commonly used in polymer-drug conjugate structure determination by analyzing chemical shift, intensity and shape of the signals. For example, in the analysis of the drug paclitaxel after conjugating to acetylene-functionalized polylactide (PLA) and poly(ethylene glycol) (PEG), formation of an ester bond could be identified by the shift in the ^{1}H NMR spectra of the drug (paclitaxel) from 4.78 ppm to 5.46 ppm (Yu et al. 2013). Confirmation of conjugation could also be seen by appearance and disappearance of NMR proton peaks. The formation of an amide bond was identified by Saneja et al. (2017) through appearance of a signal at 7.59 ppm. While, Bernaczek et al. (2019) identified the formation of an amide bond by disappearance of the broad free carboxylic group peak between 11.75 to 12.75 ppm and the appearance of new broad peak at 7.50 ppm due to formation of the amide bond –CO-NH-. Successful conjugation of drugs to polymers can also be shown using other NMR measurements, like nuclear relaxation time (T_1) and diffusion ordered spectroscopy (DOSY).

Nuclear relaxation time is a measure that provides information about the structure and dynamic information about molecules (Bakhmutov, 2004; Freeman, 2014; Freeman, Hill and Tomlinsont, 2014). There are three principal mechanisms of spin-lattice relaxation for a nuclei of spin ½. Dipole-dipole interactions (most dominant in solution), chemical shift anisotropy and spin-rotational interaction (Bakhmutov, 2004). Intermolecular interactions between the drug (daunorubicin) and polymer (butylcyanoacrylate) were investigated using T_1 (Ivanova et al. (2011). The results showed successful incorporation of the drug into the polymer matrix by the drug having increased spin-lattice of its protons in the conjugate compared to a free drug and a physical mixture of the drug and polymer. This is due to limited molecular mobility of the bound drug that interact directly with the polymer chains via hydrogen bonding or dipole-charge interactions.

Polymer-drug interactions can also be confirmed using diffusion NMR spectroscopy (DOSY), for example two different types of drug inclusions were discovered when daunorubin was conjugated to a polymer (Ivanova et al. 2011). The diffusion coefficients of the free drug, polymer and physical mixture were similar and this showed a lack of intermolecular interaction between these molecules. While in the loaded polymer it showed two different diffusion coefficients. These results predicted two types of mobilization of the drug to the polymer; physical entrapment or adsorption and T_1 predicted dipole-charge interactions meaning there is no direct chemical bonding between the drug molecule and polymer matrix.

^{1}H NMR spectra can also be used to calculate the percentage molar content of a linked drug. This is done by integrating signals of anomeric proton of the polymer as internal reference and compared to that of the drug within the conjugate. One unit of the polymer monomer contains one anomeric proton, then the ratio of the anomeric proton to the drug is observed and used in **Equation 2.1.** (Wannachaiyasit, Chanvorachote and Nimmannit, 2008).

$$\text{mol \% of linked drug} = \frac{x}{5y} \text{ x } 100 \qquad \textbf{Equation 2.1}$$

where x is the sum of the integrated area of the proton of the drug and y is the integrated area of anomeric proton of the polymer.

The limitation of the use of NMR spectroscopy to characterize polymer-drug conjugates arises when there is an overlap of the drug peaks with the polymeric peaks (Bernaczek et al. 2019). This sometimes can be overcome by using ^{13}C NMR spectrum, as it could be easy to identify the carbonyl stretch due to amido linkage Sun et al. (2017); but the limitation for using ^{13}C is long experiment caused by low abundance of ^{13}C. Also a peak overlap can make it difficult to obtain drug loading, as it is determined from ratio of integrated peaks. Therefore other spectroscopic techniques like Ultraviolet–visible (UV-VIS) spectroscopy are used.

2.3.2 Ultraviolet–visible (UV-VIS) spectroscopy

UV-VIS spectroscopy is an analytical technique, which is used to quantify the molar concentration of an ultraviolet or visible light absorbing substance in solution. Drug loading can be determined by calibrating the absorbance at a λ_{max} of serial dilutions of the free drug in a suitable solvent against the drug concentrations in the dilutions. The drug loadings are reported as molar percentages or weight percentages (Dai et al. 2014). The calibration curve method can also be used to quantify the amount of drug released *In vitro* studies (Aderibigbe

et al. 2019). UV-VIS spectroscopy can also be utilized to determine solubility of the conjugate compared to a free drug (Lee et al. 2009). A standard curve is generated with a series of the drug at different concentrations with the absorbance recoreded a specific wavelength. The polymer drug conjugate is dissolved in water and UV-VIS absorbance is recorded at the wavelength (nm) of the drug and the concentration of drug in the polymer is calculated using the standard curve. The other property that can be determined by UV-VIS spectroscopy is stability of the drug after conjugation. This is done monitoring the absorption of the drug and changes are used to calculate polymer-drug binding constant. This may be achievable by using the plot 1/ ($A-A_0$) vs (1/polymer concentration), where A represents the recorded absorbance of the complexes at different polymer concentration and A_0 is the initial absorbance of the free drug at specific wavelength. The double reciprocal plot is linear and gives the overall binding constant for each (Chanphai, Konka, and Tajmir-Riahi, 2017)

UV-VIS spectroscopy has found widespread application as an accurate method for determining drug loading however, it has serious limitation in requiring the analyte drug to have a chromophore (Merckx, 2014).

2.3.3 Fourier transmission infrared (FT-IR) spectroscopy

Fourier transmission infrared (FT-IR) spectroscopy is a fast, simple technique that does not require sample preparation that is used to confirm polymer-drug conjugation. FT-IR spectroscopy is an important technique that can also be used in polymer-drug conjugation for the determination of various functional groups (hydroxyl, amine, and carboxylic acid) and formation of bonds like esters and amides being the most commonly used functional groups in polymer-drug conjugation. Kim et al. (2015) confirmed the formation of ester bond when polyethylene glycol was conjugated to ginsenoside by presence of intense carbonyl (C=O) bond at 1735 cm^{-1}. Saneja et al. (2017) also showed clear conjugation and formation of amide bond when betulinic acid was conjugated to polyethylene glycol – amine by appearance of the absorption peaks at 1711 and 1645 cm^{-1}. The formation of an amide bond can be easily identified from three diagnostic peaks: amide I, which is due to the carbonyl (C=O) stretching at 1600-1700 cm^{-1}, amide II (1300-1580 cm^{-1}) and amide III (1300- 1450 cm^{-1}) which are due to N-H bending and C-N stretching respectively as represented in **Figure 2.1** (Mallamace et al. 2015).

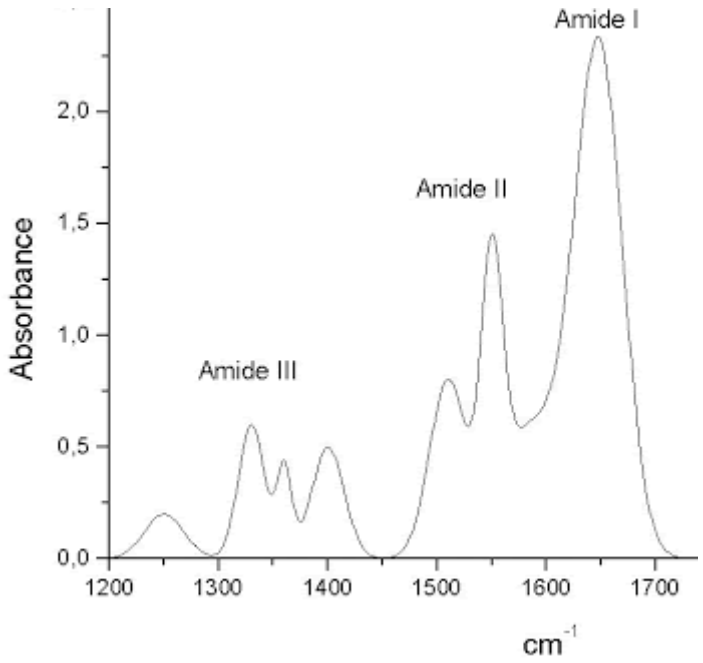

Figure 2.1: FT-IR spectrum showing formation of amide bond (Mallamace et al. 2015).

FT-IR spectroscopy is a non-disruptive, inexpensive technique that requires a small sample to do analysis, but unfortunately due to overlapping of diagnostic peaks, specificity and interpretability may be compromised (Khan et al. 2018). Carbon dioxide (CO_2, at 2400 cm^{-1}) and water (H_2O at 3800 and 1600 cm^{-1}) are always found in the spectra. Most instruments have a system to purge the atmosphere but because of the atmospheric variations a background spectrum is required every 30 minutes and everytime a new set of parameters is entered. Samples can be prepared using KBr and NaCl pellets as they are invisible in infrared to avoid the interference of atmospheric CO_2 and H_2O (Hsu, 1998). FT-IR spectroscopy alone is not sufficient to confirm the formation of ester bonds as it is not easy to tell the difference between carboxylic acid or ester functional groups as the shifts in wavenumber or appearance of a new peak is not easily identified (Thompson et al. 2008, Kim et al. 2015). Hence, it is important to also use it complementary to other techniques.

2.4 Thermal analysis

2.4.1 Differential Scanning Calorimetry (DSC)

Differential scanning calorimetry (DSC) is a tool for investigating the structural or thermal transitions in materials, including polymers (Lukas and LeMaire, 2009). Thermal characteristics include transition temperature, melting and boiling point as well as glass

transition temperature and crystallization temperature **Figure 2.2**. For example, a conjugate can demostrate a complete change of the profile after conjugation with the drug. An endotherm could have multiple crystalization peaks and these reflect the presence of different regions of crystallinity due to varying side chains of a polymer-drug conjugate. A polymer with uniform side chain functionalization would show one melting endotherm and thus one melting endotherm can also be observed for polymer-drug conjugates (Thompson et al. 2008). As seen from the previous example, one can also gather information about the crystallinity, amorphous or combination of crystallinity and amorphous state of the polymer-drug conjugate (Lukas and LeMaire, 2009). If a molecule is amorphous that means it is arranged in a random fashion. While, the molecules of a crystalline material are arranged in a repeatable and predictable pattern.

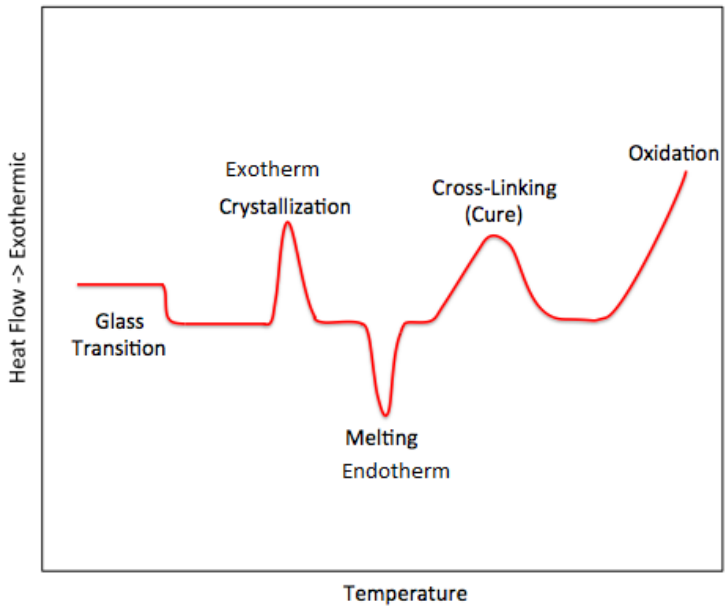

Figure 2.2: DSC curve showing the shapes associated with particular phase transitions (Lukas and LeMaire, 2009).

Glass transition temperature (T_g) values of polymer-drug conjugates can also be determined by DSC and these could be compared to the pure drug and polymer. High T_g value is a generally favoured property, as compounds with high T_g show reduced recrystallization at a given temperature (Knapik-Kowalczuk et al. 2020). A high T_g in polymer-drug conjugate can be caused by drug pendant groups' present within a macromolecule. Oledzka et al. (2015) and Qian et al. (2019) explained that the T_g of polymer-drug conjugates is not clear when measured by conventional DSC using a simple heat and cool scan due to the rigidity of the polymer

backbone and semicrystallinity. This is due to rigid backbone and the semicrystalline nature of conjugated polymers. As a result Oledzka et al. (2015) used modulated DSC to measure T_g values.

DSC can also be used to determine the melting point, which could tell information about the covalent linkange of the drug to the polymer. For example, Thompson et al. (2008) demostrated that a synthesized conjugate had reduced melting point compared to free polymer. This was explained to be due to the presence of the drug which resulted in the weakening of the interaction forces (hydrogen bonding) of the polymer backbone resulting in less heat energy needed to break the bonds. DSC sometimes is used in complemetary with thermogravimetric analysis (TGA).

2.4.2 Thermogravimetric Analysis (TGA)

TGA can be used in polymer-drug conjugation to give information about the bonding components within a sample, the thermal stability, moisture and also the volatile content (Xu et al. 2005; Feist, 2015). TGA works by measuring the rate of change in weight of a sample or absolute amount as a function of time or temperature (Xu et al. 2005). This was demonstrated by Kumar et al. (2012) in a chitosan-thymine conjugate. The conjugate showed weight loss at 98 °C due to evaporation of water and moisture content in the polysaccharide. The other weight loss was shown between 180 to 284 °C attributed to lower grafting of acid in a polymer conjugate. The TGA results showed the loss of thermal stability of the chitosan-thymine conjugate relative to the chitosan polymer and also showed that the introduction of the drug to the polymer increased the degree of crystallinity of the conjugate relative to the polymer.

TGA can be used in complement with DSC, as when one observes an endothermic or exothermic peaks in DSC. TGA will help determine whether the change is physical or chemical in nature. Physical change occurs when there is no mass change and chemical change results in a change in mass (Xu et al. 2005). Margaritis and Manocha (2010) used both DSC and TGA to evaluate the stability of a polyglutamic acid-doxorubin complex. The stability was tested from 25-600 °C, the authors observed that the drug did not decompose to a vapour state and its decomposition residue was collected as a char in the crucible. It was the polymer that experienced thermal degradation at 210 °C and about 60 % of the polymer was decomposed as the temperature reached 600 °C. The polymer-drug complex showed about 60 % remained undecomposed in the same temperature range suggesting that the drug is strongly associated to the polymer. Thus, the observed weight loss in the complex is due to the polymer. The TGA

analysis was also interpreted to reflect the heterogeneous nature of the interaction between the drug and polymer, the drug was observed to have participated in the complexation by interacting with hydrophobic domains of the polymer-backbone.

For both thermal analyses, small samples are required that cannot be recovered. Also, if the decomposition or reactive event occurs within the same temperature region as the phase transition like melting point, accurate data cannot be obtained.

2.5 Microscopic techniques

2.5.1 Scanning Electron Microscopy (SEM)

Scanning electron microscope (SEM) is a technique that scans the surface of a sample to obtain information about its shape and morphology as a topographic 3D image (Nino-Pariente, J. Nebot and J. Vicent, 2016). It is a non-destructive method, that has spatial resolution of ~50 to 100 nm that restrict sample size that can be analyzed to ~ 200 nm. SEM uses a focused beam of high-energy electrons; the interaction between the electrons and the surface of the sample results in the deflection of the electrons (Ping-Chang Lin, Stephen Lin, Wang, 2014). This results in the signal that contains the information about the sample topography, crystalline structure, morphology and orientation of the material. Data is collected over a selected area of the sample and 3D image is generated (**Figure 2.3**) (Goodhew, Peter J, 2000; Manaia et al. 2017).

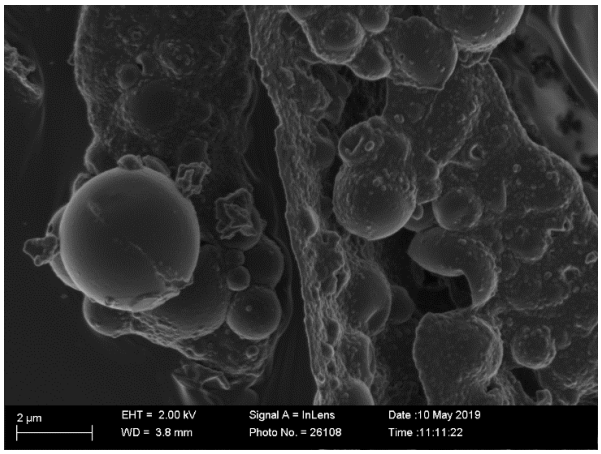

Figure 2.3: SEM image of polymer-conjugate shown in 3D (unpublished data).

SEM can be used to show a change in morphology of the polymer, drug and polymer-drug conjugates. Kumar et al. (2012) showed that the polymer (chitosan) exhibited nonporous, smooth membrane phase consisting of dome shaped orifices, crystallites and microfibrils.

While, the chitosan-thymine conjugate morphology was rough with rod like structures compared to chitosan, the rod-like structures enhance the surface area for better proliferation. In some cases, a mixture of morphologies (plate-shape, rod-shape, spherical-shape and globular shaped, flake-like, plate-like and block shaped) were observed (Alven et al. 2019; Aderibigbe et al. 2019). This was mostly observed in cases where two or more drugs were incorporated in a polymer.

SEM requires special sample preparation and the measurements are not relevant for polymer-drug conjugates because this technique is restricted by material that can sufficiently deflect the electron beam (Nino-Pariente, J. Nebot and J. Vicent, 2016). Moreover, SEM does not provide the size of the polymer-drug conjugate in solution as a solid is used to analyze SEM. The analyses due to the intended application should be in solution to mimic the physiological conditions. Another microscopic technique used to analyze the size and morphology of the particles is transmission electron microscopy (TEM).

2.5.2 Transmission Electron Microscopy (TEM)

TEM uses transmitted electron to form the image, this is through transmission of electrons through a thin sample. Unlike SEM that produces 3D images, TEM provides the visualization of the internal structures of the specimens by producing 2D images from a 3D object as illustrated in **Figure 2.4 (a)-(b)**. As mentioned before, TEM images also provide information about the shape, size and distribution of the particles (Goodhew, Peter J. 2000; Williams, David B. 2009; Manaia et al. 2017). TEM can measure nanomaterial at a wide range from nanometer to micrometer (from <1 nm) but its main restriction is laborious sample preparation which can limit the resolution (Ping-Chang Lin, Stephen Lin, Wang, 2014) . TEM samples need to be thin and they must be placed in a vacuum inside the instrument due to electrons having limited range transiting matter. Also it is able to detect nanoparticles with sufficient combination of size and electron density. Due to this electrically non-conductive samples must be coated or stained with conductive material to facilitate imaging. A negative stain of phosphotungstic acid (PTA) is the most commonly used to analyze polymer-drug conjugates. As the polymer and drug consist of light elements whose elastic interaction with energetic electrons are relatively weak, it is difficult to generate image contrast that generates the image in **Figure 2.4(a)** (Kim et al. 2015). PTA is an electron dense compound that interacts with the electrons beam of the TEM.

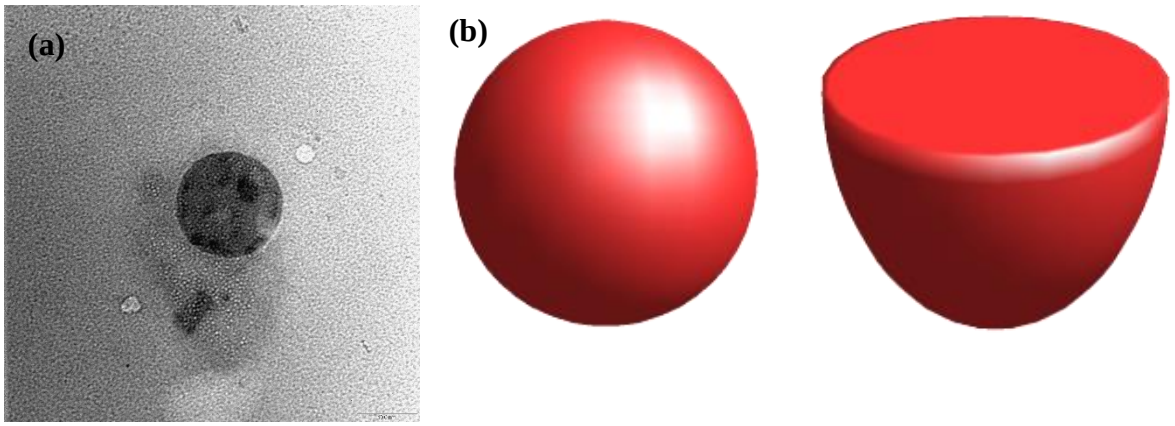

Figure 2.4: (a) TEM image showing a part in 2D (unpublished data) and (b) shows 3D illustration.

The size of a particle is an important parameter that can be used to predict the biological pathway of the conjugate as particle size ranged from 10-30 nm are desired for kidney clearance. While, sizes between 100 to 200 nm can be cleared through the reticuloendothelial system. Also sizes between 10-100 nm promote enhanced permeability and retention (EPR) effect and high bioavalability (Yu et al. 2013). TEM can also be used to see what happens to the size of the conjugate as you increase the number of chains of polymer conjugated to a drug (Bernaczek et al. 2019).

2.6 Chromatographic techniques

Chromatography techniques are used for separation of molecules in a mixture in solution or as a suspension through a medium in which the molecules move at different rates (Coskun 2016). There are different types of chromatography, thin-layer chromatography, gas chromatography, column chromatography and paper chromatography. The most frequently used in polymer therapeutics is high perfomance liquid chromatography (HPLC) which is used to separate complex mixtures into single components and to identify them using mass spectrometry (MS) (Kilz and Pasch, 2006). Therefore, this part of the review will discuss the chromatographic techniques that are mostly used in polymer therapeutics.

2.6.1 High Performance Liquid chromatography (HPLC)

HPLC is an analytical technique that is used to separate, purify, quantify and identify components within a mixture (Banger, Par, and Sigouin, 1997). The mixture is separated under high pressure, then UV-VIS spectroscopy or mass spectrometry are used to detect and identify the fractions collected.

HPLC is used for different analysis in polymer-drug conjugates ranging from drug loading to drug release and solubility studies. Saneja et al. (2017) used HPLC with a UV detector and on a C18 column study the solubility and in vitro stability of pegylated-betulinic acid. While, Forte et al. (2016) also used HPLC with a UV detector to analyze the ex vivo drug release in a naproxen–polymer conjugates using 2-naphthoic acid as internal standard. Similar to the UV-VIS spectroscopy, the use of UV-VIS detectors can limit analysis of drugs without a chromophore. Analysis of polymers is also challenging due to polymer dispersity, chemical heterogeneity and poor solubility in chromatographic solvents (Uliyanchenko, van der Wal, and Schoenmakers, 2012). Due to this, another mode of chromatography is used and that is Gel permeation chromatography (GPC).

2.6.2 Gel permeation chromatography (GPC)

GPC is a type of liquid chromatography, the difference between a GPC and HPLC is the principle of how molecules separate. Unlike HPLC that separates molecules based on their hydrophilicity or hydrophobicity, GPC separates molecules based on their size. Another difference is in the type of column used, GPC uses a column packed with very small, round, porous particles that are insoluble cross-linked polymers or inorganic material. During GPC analysis, molecules of different size, travel at different rates through the column and are collected in separate fractions as they are eluted as shown in the chromatogram below (**Figure 2.5**) with the bigger size eluted first (Sagita, Syahdi and Arrahman, 2018). By comparing eluents of a representative standard of a known molecular weight, an estimation of the relative molar mass and polydispersity can be obtained. Therefore, GPC can be used to study molecular weight (Mw) of the conjugate and weight size distribution (Mn) (Thompson et al. 2008; Hanton and Liu, 2000). The GPC can also be used to obtain molar mass dispersity (Đ) by using a ratio Mw/Mn. This describes how far away the encountered distribution is from a uniform distribution (Gavin, 2016; Lavignac et al. 2009). GPC can also be used to do polymer degradation kinetics studies (Margaritis and Manocha, 2010).

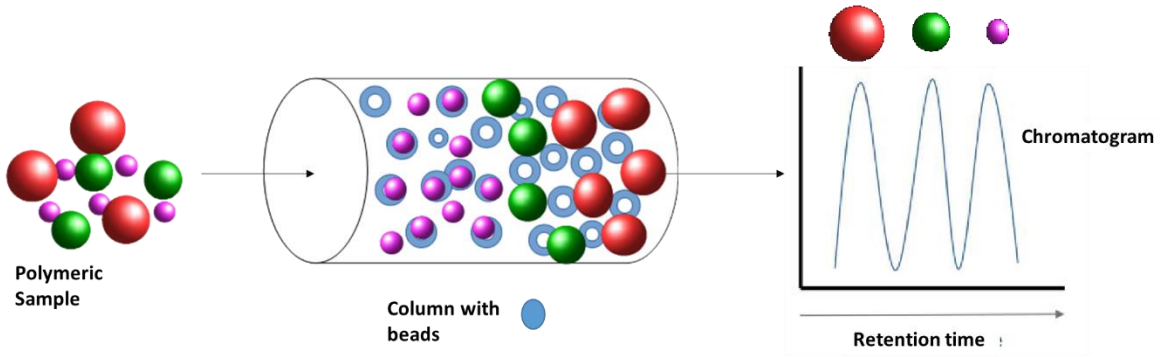

Figure 2.5: The chromatographic method in GPC instrument.

Even though GPC is becoming a widely used technique mainly in polymer synthesis, choosing a suitable column can be a challenge as some columns can retain the sample and therefore do not display a chromatogram (Merckx, 2014). This means that a laboratory needs to be equipped with a variety of columns.

2.6.3 Mass spectrometry (MS)

Mass spectrometry is coupled to liquid chromatography due to its sensitive and highly specific nature of the mass detector compared to other chromatography detectors. The coupling of liquid chromatography with mass spectrometry was developed for trace quantitative analysis (Pitt, 2009).

Mass spectrometry works by converting the analyte molecules to a charged (ionized) state. The technique therefore, analyses the ions and any fragment ions that are produced during the ionization process reporting them on their mass to charge ratio (m/z). Mass spectrometer does not measure the molecular mass directly but rather the mass to charge ratio (m/z) of the ions formed from the molecules (Parasuraman et al. 2014). Thus for small molecules with ions either ±1 formal charge, the mass of the ion is the same as the m/z ratio but this is not the case for macromolecules like polymers (Sargent 2013). Polymers are suitable to be analyzed by soft ionization techniques like Electrospray ionization (ESI) and matrix-assisted laser desorption/ionization mass spectroscopy (MALDI-MS). The disadvantage of using ESI is the limited mass range, preventing macromolecules with molar mass above 2000-3000 g/mol to be ionized without fragmentation. This led to the introduction of matrix-assisted laser desorption ionization time-of-flight mass spectrometry (MALDI-TOF MS) that allows analysis of the macromolecules like polymers with less ionization due to its soft ionization capabilities (Kilz and Pasch, 2006).

MALDI uses low-mass organic compounds called the matrix to ensure successful ionization of the sample. The matrix is added to the sample to act as a scaffold by which ionization can occur and supplies protons that allow ionization. MALDI is normally coupled with a time of flight (TOF) analyzer as it has unlimited mass range which is advantageous as MALDI produces charged molecular ions that have high mass to charge ratio (Clark et al. 2013). MALDI-TOF MS it is more sensitive than other ionization techniques but unfortunately it encounters difficulties in detecting low molecular weight compounds (< 500 Da) (Clark et al. 2013; Hosseini, Samira 2016; Lo, Fall, and Samb-ba, 2017). This is due to matrix ion interference in the low mass range (m/z <1000) resulting in low detection sensitivities and poor reproducibility (van Kampen et al. 2011; Tang et al. 2016; Zhang et al. 2010).

In polymer therapeutics, MALDI-TOF MS has been used to show conjugation by an increase in mass values. It can also be used to indicate how many molecules of the drugs are conjugated to a polymer (Forte et al. 2016; Saneja et al. 2017). Saneja et al. (2017) showed successful conjugation PEGylated betulinic acid by a shift in the peaks of the PEG to higher masses upon conjugating with betulinic acid (BA). For example, PEG peaks at 2168.5, 2080.4 and 1992.4 shifted to 2606.8, 2518.7 and 2430.7 in the PEGylated BA, which confirmed that one molecule of BA (456 Da) was bound to one molecule of PEG.

2.7 Other techniques

2.7.1 Powder X-Ray Diffraction (PXRD)

Powder x-ray diffraction (PXRD) is a tool used to analyze solid materials that have been ground to a powder. It does this by identifying the lattice parameters, phase identity, phase purity, crystallinity, preferred crystal orientations (texture), chemical nature of the compound and crystal structure also percentage phase composition (Scintag, 1999; Dong and Boyd, 2011). XRD can also be used to differentiate between the single crystal and polycrystalline materials. This technique works by shining a beam of x-ray light into the sample, these x-rays interacts with the sample and the beam is diffracted or scattered by the surface atoms in the path of the x-ray. The monochromatic beam of x-rays is scattered at specific angles from each set of lattice planes in a sample. The scattered x-rays constructively interfere resulting in a diffraction pattern from the material under investigation. The interference of the scattered light must fulfil Bragg's law for this technique to be used to determine various characteristics of the crystal or polycrystalline materials. The peak intensities are determined by the distribution of atoms within the lattice causing a characteristic x-ray diffraction pattern, which is a fingerprint of

periodic atomic arrangements in a given material. Sharp diffraction peaks are observed for crystalline material and broad peaks are for amorphous material (Manaia et al. 2017; Dong and Boyd, 2011). In the pharmaceutical industry XRD is used to evaluate the crystal nature of the drug and drug-carriers (Aderibigbe et al. 2019; Kumar et al. 2012). Amorphous material is important in pharmaceuticals as it determines the solid-state physical and chemical properties of many pharmaceutical dosage forms (Vranic, 2004). Amorphous formulation are appealing due to their improved solubility as the strength of intermolecular forces holding the molecules together and energetic barrier to solvation are reduced (Schittny, Huwyler and Puchkov, 2020). XRD can be used complementary to DSC analysis as both can determine the crystal nature of polymer-drug conjugates.

2.7.2 Dynamic Light Scattering (DLS)

It is also important to determine the size of the new entities in solution, to do this dynamic light scattering (DLS) is used. DLS hypothetically predicts the diameter of hard spheres that diffuse with the same speed as the particle being measured. The particles size diameter measured using DLS is bigger than the size measured using TEM (Kang et al. 2015; Sun et al. 2017), due to the solvating layer that forms around the particles as they move dynamically in solution (**Figure 2.6**). Furthermore, as TEM images are acquired after solvent evaporation this results in shrinkage of the particles (Kang et al. 2015; Sun et al. 2017). For TEM, size analysis is used to visualise the morphology and DLS is used to understand behaviour of the conjugates within a biological system. According to Aderibigbe et al. (2019) particle size has been reported to give information about the particles in solution which influences their bioavailability, dissolution and immunotoxicity, as particle size ranging from 100-300 nm have been reported to adsorb to cellular membrane followed by internalization.

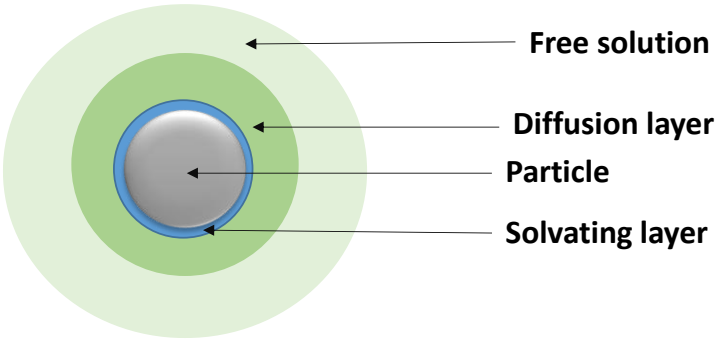

Figure 2.6: Showing the difference between DLS size and TEM image size (Drelish, 2014).

The DLS size is recorded with polydispersity index (PDI) which is generated based on the width of a hypothetical Gaussian distribution as a measure of the degree of heterogeneity in the sample (Maguire et al. 2018; Danaei et al. 2018). It is used to tell how uniform a sample is in size. PDI greater than 0.4 indicates that the sample is polydisperse meaning multiple size distribution. A high PDI illustrates an inhomogeneity in aggregate size that could be caused by poor experimental control.

DLS sizing does not measure the actual size, also size is affected by sample preparation and any solid particles dispersed in a liquid phase can distort the measurement resulting in a bigger measured size of the material. Some materials that are soluble in buffer or biological fluids aggregate in water, thus affecting the measured size of the particle. It is thus crucial to measure DLS in biological fluids or simulated fluids under physiological conditions to mimic the in vivo behavior (Covered, 2013).

The charge of the particles is determined by measuring zeta potential, this is used to determine the electronic state of the nanoparticle surface and data obtained can be used to predict the stability. It is reported by Manaia et al. (2017) that a zeta potential greater than +30 mV or lower than -30 mV indicates that the particles are stable while values between -30 and +30 may indicate instability of the particle. Instability could be due to aggregation, coagulation and flocculation of the material. Kumar et al. (2015) used zeta potential to determine the stability of particles based on the electrostatic repulsion. The synthesized particles had a zeta potential greater than ± 21 mV. The authors discussed that the high electric charge on the surface of the particles can cause strong repellent forces among the nanoparticles to prevent aggregation which indicate stability. Zeta potential can also be used to determine the potential interaction of a polymer-drug conjugate with a biological system. Aderibigbe et al. (2019) reported that

the charge on the surface of the conjugates affects their cellular uptake. For oral delivery, a positive charged surface of the conjugate has the potential of enhancing the cellular uptake and thus improving the cell uptake by endocytosis or indirect penetration, due to electrostatic interaction between the cell surface and conjugate. Negatively charged conjugates are cleared faster with higher reticuloendothelial uptake than neutral or positively charged conjugates (Forest and Pourchez, 2017; Jeon, 2018).

2.8 Specialized purification techniques for polymer-drug conjugates

The quality of the conjugate and quantification of free unconjugated drug is another important aspect of analysis of polymer-drug conjugates. This is important as it raises safety issues and differential toxicity. These residual amounts of unconjugated material may remain in the final product due to incomplete purification. It is therefore important to use relevant purification methods for polymer-drug conjugates and the next section explains these techniques in detail.

Due to the application of polymer-drug conjugates in vivo and in vitro studies, pure conjugates are therefore required. Ideally, the conjugate must not contain any impurities or free drug to avoid false positive or negative results *in vitro* and *in vivo*. There are different techniques used to remove impurities and unreacted drug. These include precipitation, dialysis and desalting columns and these are discussed in detail below.

2.8.1 Precipitation

Precipitation is widely used in the synthesis of molecules, for polymer-drug purification. The technique normally uses the principle of using a solvent that poorly dissolves the polymer and dissolves the drug. The polymer must be precipitated, while leaving the free-drug in supernatant after centrifugation as shown by **Figure 2.7 (a)** (Sagita, Syahdi and Arrahman, 2018).

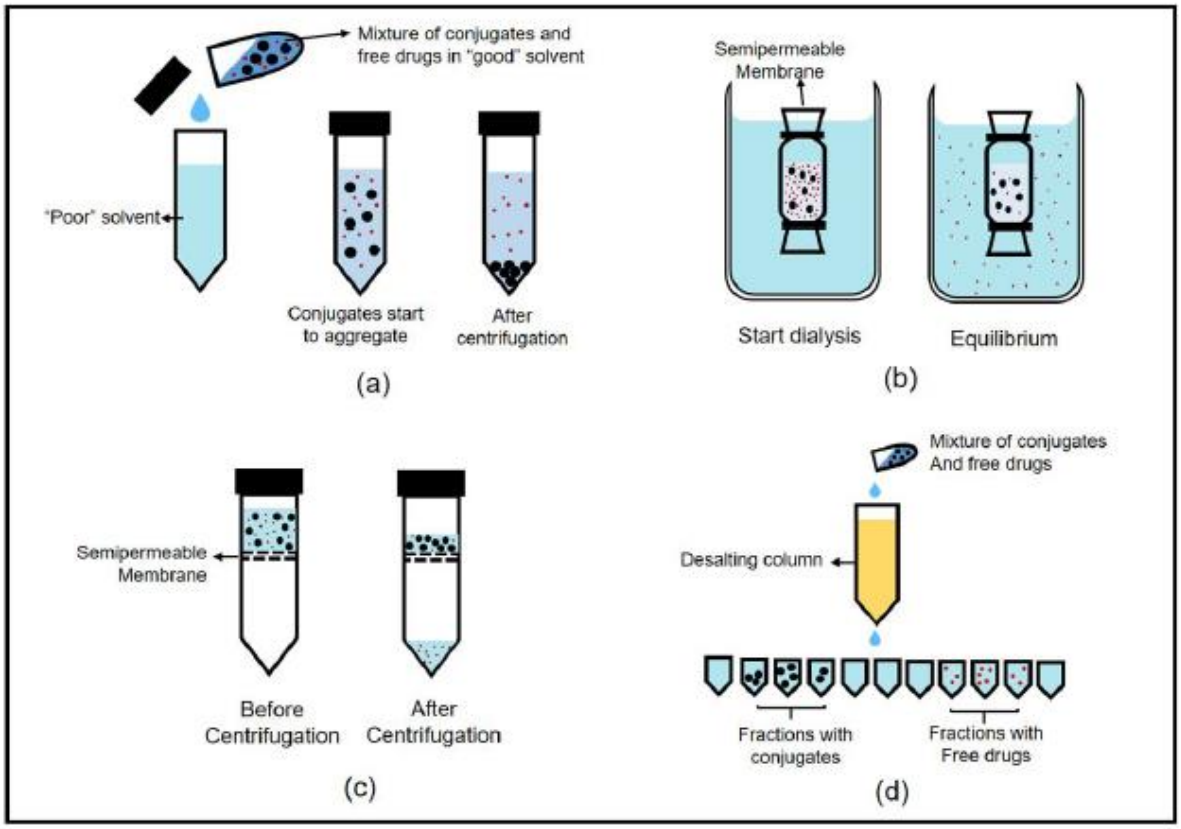

Figure 2.7: Purification of polymer-drug using (a) Precipitation, (b)-(c) dialysis and (d) desalting column (Sagita, Syahdi and Arrahman, 2018).

2.8.2 Dialysis

There are two types of dialysis and both involve semi-permeable membranes with a certain molecular weight cut off (MWCO). The first method (**Figure 2.7 (b)**) is a gradient-based diffusion dialysis method. The principle is basically retention of molecules larger than the MWCO in the donor compartment, while all molecules smaller than MWCO pass through the membrane into acceptor compartment. This is an equilibrium method, and when equilibrium is reached there is no diffusion of molecules from one compartment to the other because of the concentration in gradient. Therefore, the solvent in acceptor compartment must be regularly changed to maintain the concentration gradient and allow diffusion of small molecules.

The second method is a gradient diffusion method that involves the use of centrifugation. The solution of the impure conjugate is place at the top part of the tube, through centrifugation the solvent and molecules smaller than MWCO will be collected at the bottom and the centrifugation is repeated several times through addition of solvent the pure conjugate will remain at the top as illustrated in **Figure 2.7 (c).**

2.8.3 Desalting column

Desalting columns are similar to size exclusion chromatography (i.e. GPC), which separates based on the molecular size **(Figure 2.7 d)**. The solution of polymer-drug conjugate is passed through the column and the fractions are collected, either free-drug or polymer or conjugate and each sample is analysed using spectroscopic techniques to identify the pure fraction as shown in (Sagita, Syahdi and Arrahman, 2018).

The purification of polymer-drug conjugate can also be done by using a combination of the methods described. Cesar et al. (2018) used a mixture of precipitation and dialysis to purify the polymer-drug conjugate. The product was precipitated using acetone and then put into a membrane bag (14 kDa) carried out into water for about 24 h. Oledzka et al. (2015) also used precipitation with cold diethyl ether and then with dialysis membrane (MWCO = 500) for 24 h to remove excess reactants from synthesized polymer-drug conjugate.

2.9 Challenges on characterization of polymer-drug conjugates

The most important property of polymer-drug conjugates is the average number of drug molecules that are conjugated to each polymer unit as this determines the amount of drug that can be delivered to the biological site. This plays a crucial role in the safety and efficacy of the drug. Different methods have been used to measure this property including spectroscopic techniques. Unfortunately overlap in the spectrum may hinder confirmation of conjugation and also calculations of drug loading. Drug loading is important for determing the dose that should be given of the conjugate for therapeutic effect and UV-VIS spectroscopy is the most used technique for calculation of drug loading but the drug must be chromophoric for the analysis to be conducted. Uncertainties in drug loading due to the challenges highlighted may affect therapeutic effects of the conjugate as it would not be clear how much to administer from the percentage drug loading calculated.

To measure the size of nanomaterial, different techniques have been developed that operate under different principles. Microscopic techniques like scanning electron microscope (SEM) give an accurate measurement of dehydrated particle size, but these do not measure the particle size in solution – the environment in which the drug-conjugate must function. Therefore, techniques like dynamic light scattering are used to measure size in solution including the solvation shell in the calculation of particle size and relying on the assumption that the particle has a spherical shape.

As it is critical that a detailed characterization is conducted like any other pharmaceutical agent to be able to fully understand its properties and performance. Even though these techniques are used for analysis of polymer-drug conjugates one needs to keep in mind that each technique has its own advantages and disadvantages. The use of these techniques will lead to one getting an estimation on the behavior of the conjugates in physiological conditions and thus conclude if the conjugate will be effective or not once used in biological systems.

Some of the content of chapter three has been published and citation given below:

Mvango, S., Mthimkhulu, N., Fru, P.N., Pilcher, L.A. and Balogun, M.O., 2020, November. Physico-chemical characterization of polyethylene glycol-conjugated betulinic acid. In AIP Conference Proceedings (Vol. 2289, No. 1, p. 020039). AIP Publishing LLC.

Chapter Three:
Synthesis and physico-chemical characterization of polymer-drug conjugates from plant-derived medicinal compounds

3.1 Introduction

Medicinal plants have been used for millennia as a source of therapeutic agents and today plant-derived natural products or their derivatives are used widely. It has been estimated that 80% of the world's population rely on traditional medicines and more than 40% of the drugs on the market originate from natural products (Atanasov, Waltenberger and Pferschy-wenzig, 2016; Fernandes et al. 2017). This includes the use of plant extracts and their active compounds. Due to their natural origins, these chemicals are considered to have a very wide window of safety and a high toxicity threshold (Moreira et al. 2014; Mensah et al. 2019). Even in orthodox, science-based clinical medicine, many of the regulator-approved drugs are directly of plant origin even though synthetic routes of production or derivatization might have been discovered. This notwithstanding, they present similar pharmacological challenges to purely synthetic drugs. These include systemic toxicity, aqueous solubility challenges, pharmacokinetic inadequacies etc. It has been proposed that application of drug delivery technologies, like polymer-drug conjugation, might help address these challenges with plant-derived drugs (Devi, Jain and Valli, 2010).

The use of nature-derived compounds has been extensively studied for cancer chemotherapy. Unfortunately, most of these compounds are lipophilic and do not dissolve well in the blood stream. These compounds also have low bioavailability and large quantities of the compounds have to be administered in order to achieve their maximum therapeutic effects. These large doses can lead to toxicity and low patient compliance (Stegemann et al. 2007; Watkins et al. 2015). Nanomedicine methods such as conjugation have been utilized to improve these disadvantages. For example, the first commercially available anticancer nanoparticle drug delivery system approved by FDA in 1995 was Doxil, a circulating sustained-release liposome nanoformulation of doxorubicin. It was approved for the treatment of AIDS-related Kaposi's sarcoma and later used for ovarian cancer and multiple myeloma (Ventola, 2012). Polymer-drug conjugation has also been used to conjugate paclitaxel to polyglutamic acid (PGA) through the 2' position to form an ester. The conjugate had 37 wt% of covalently bound drug content. The conjugate, known as Opaxio®, is under clinical trials for treatment of ovarian cancer. It enhanced the solubility of the drug, doing away with the use of toxic solvents like

Cremphor EL. The conjugate has a prolonged elimination time. Furthermore, the drug conjugated to the polymer is pharmacological inactive which leads to less systematic exposure of the patients to the drug (Merckx, 2014; Markovsky et al. 2012).

Terpenoids, a large and structurally diverse group of plant secondary metabolites with medicinal properties (Zhou et al. 2017), are found in concoctions of herbal extracts as traditional or alternative medicines. This chapter focusses on the investigation of polymer conjugates of two representative natural molecules of the terpenoid family: betulinic acid (BA) and dihydroartemisinin (DHA). BA is a triterpenoid that is being investigated for its antiretroviral, antimalarial, anticancer, antioxidant, anti-obesity, antimicrobial and anti-inflammatory properties. A 1997 patent of Lee, KH et al. of the University of Chapel Hill, USA, claims that BA and its derivatives have potent anti-HIV activity (Lee et al. 1997). It has an aqueous solubility of only 0.2 mg/L and poor gastrointestinal absorption that results in poor bioavailability. There have been attempts to improve on these properties by encapsulation (Harwansh, Mukherjee and Biswas, 2017) and even conjugation to polyethylene glycol (PEG) (Dai et al. 2015; Saneja et al. 2017). However, there is no full report on the polymer conjugate syntheses or physicochemical characterization of the macromolecular product. These data are crucial as conjugation via covalent bonds results in entirely new chemical entities with predictable physical properties like aqueous solubility (influenced by the much larger molecular weight hydrophilic polymer) and other less predictable properties that require deliberate application of advanced analytical techniques.

In this chapter, the conjugation of BA to PEG and chitosan is reported along with detailed characterization. PEG was considered as one of its attributes is long plasma circulation time (Teng et al. 2020; Yang et al. 2020). This is favoured for the development antimalarial conjugates as the erythrocytic plasmodium parasites are released in a circadian manner. It would therefore be important that an antimalarial polymer therapeutic should persist in the blood for as long as necessary to the blood of the parasites. Another advantage of long plasma circulation is that the probability of the conjugated therapeutic being delivered to the brain is increased significantly. Therapeutic agents do not readily pass the brain endothelium to enter the parenchyma. Previous reports suggest that surface modification of polymer nanoparticles (NPs) can improve their ability to cross the blood-brain barrier (Saucier-Sawyer, 2015). This is important for the development of antimalarial polymer therapeutics for the treatment of cerebral malaria, a severe complication of the disease where parasite-filled red blood cells (RBCs) occlude small blood vessels to the brain.

Chitosan is widely favoured in drug delivery systems for enhancing and facilitating the gastrointestinal adhesion of the drug-laden particulate to the mucosa wall. It is uncommon to target the oral route for the administration of polymer-drug conjugates, primarily because of the pH sensitivity of most of the linkers used. However, this is the preferred route for the administration of antimalarials for uncomplicated malaria. Lee and co-workers reported two instances of using chitosan for the oral delivery of docetaxel and insulin (Lee et al. 2009; Lee, Lee and Jon, 2010). In this work, we investigated the chemistry of synthesizing chitosan conjugates.

DHA is both a synthetic derivative of the natural sesquiterpene lactone artemisinin and an endogenous metabolite of the semisynthetic drugs artemether and artesunate. DHA, along with these precursors and derivatives, is a potent approved antimalarial drug and is also being investigated for use as an anticancer compound (Slade et al. 2009; Das, 2015). The synthetic route for linking DHA to PEG to increase its water solubility has been investigated by Dai et al. (2014). Chitosan conjugated to DHA was also synthesized by Xiao et al. (2013) but no full detailed physio-chemical characterization was given.

This work further investigates the chemical (NMR and FTIR) and physical (DLS, electron microscopy, TGA, DSC and XRD) characterization and, as with BA, the *in vitro* cytotoxicity of the conjugate is reported.

The aims of this chapter are therefore to synthesize polymer conjugates of the nature-derived compounds BA and DHA and interrogate their physico-chemical properties by extensive characterization and analytical techniques. In *vitro* biological assays of the cytotoxicity of the conjugates relative to the free drug are also reported.

3.2 Results and discussion

PEG is a well-established polymer in drug delivery and is FDA approved, as it is biocompatible, largely non-immunogenic, non-antigenic and highly water soluble (Veronese and Pasut, 2005; Li et al. 2013). PEG-drug conjugates show decreased degradation by metabolic enzymes, reduced immunogenicity, and increased circulation in the body (Veronese and Pasut, 2005; Verhoef and Anchordoquy, 2013). FDA has approved PEG for human oral, intravenous and dermal pharmaceutical applications (Li et al. 2013). The route of administration is critical for diseases such as malaria, which is primarily an infection of RBCs. For fast relief and severe malaria cases, intravenous administration would be preferred.

Therefore, in this work PEG-drug conjugates will be developed for potential intravenous delivery of the polymer-drug conjugates.

3.2.1 Synthesis of PEG-BA conjugate

The conjugation of PEG-amine to BA through an amide bond to form PEG-BA was carried out via a two-step reaction as illustrated in **Scheme 3.1**. The carboxylic acid of BA was activated using EDC/NHS as coupling reagents. The nucleophilic attack of the BA on the carbodiimide forms an activated complex with BA. To minimize the risk of the formation of a dimer of BA through an ester bond, a drop of water was added to the reaction solution. This destabilizes of the BA-EDC complex. NHS rapidly reacts with the BA-EDC complex to form the more stable BA-NHS ester (BA-succinimide). After 2 h, the BA-succinimide is added dropwise to a solution of PEG amine and left for 24 h.

The PEG-BA conjugate was purified by precipitation from a THF solution of the crude product using cold diethyl ether, this was done to remove the by-products and unreacted BA that remained in solution. A process of re-dissolution in THF and ether precipitation was repeated several times to wash the conjugate. After the washing cycles, the PEG-BA conjugate was dissolved in water and dried by lyophilization to obtain the pure product as a yellowish waxy substance.

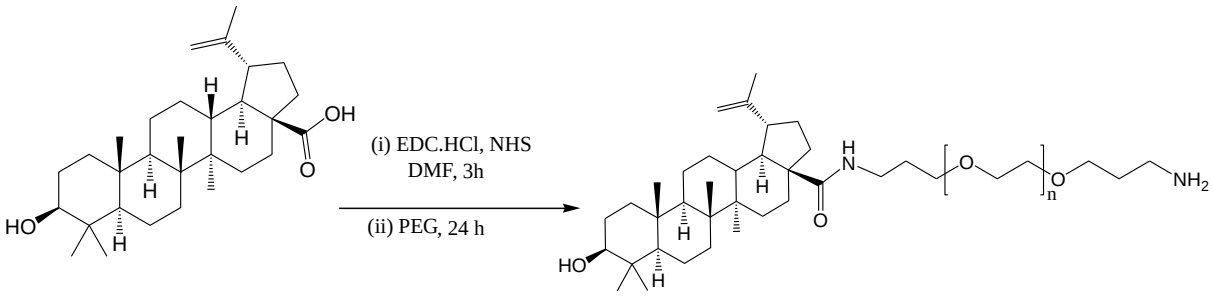

Scheme 3.1: Synthesis of PEG-BA conjugate.

3.2.1.1 NMR and FT-IR spectroscopy analysis

The successful synthesis of the conjugate was confirmed by ^{1}H NMR and FT-IR spectroscopy shown in **Figure 3.1** and **Figure 3.2** respectively. A ^{1}H NMR spectrum (400 MHz in deuterated pyridine) of BA **Figure 3.1 (i)** ((**a**) exhibited proton peaks from 0.79 ppm to 2.69 ppm due to the terpenoid protons and also distinctive alkenyl terminal (-CH_2) protons at 4.90 ppm and 4.74 ppm. The characteristic methylene protons of the PEG backbone (-O-CH_2-CH_2-) were observed at 3.4-3.6 ppm as a multiplet (**Figure 3.1(i) (b**)). The PEG-BA conjugate in **Figure**

3.1(i) (b) in pyridine-d_5 showed signals of both BA and PEG, with the appearance of the amide peak signal at 6.83 ppm and conjugation was further confirmed by the slight shift downfield by the alkene protons labelled 6 on spectra and also the shift of other drug protons from 2.2 ppm to 1.9 ppm as shown in **Figure 3.1(i)**. This is also noticed when D_2O is used as shown in **Figure 3.2 (ii)** where the methylene proton of the PEG is shifted downfield upon conjugation. It is important to note that even though monofunctionalization of the polymer is shown in **Scheme 3.1**, there is a possibility of bifunctional polymer, where BA is found on both NH_2 ends.

A notable observation is that in D_2O some characteristic peaks of the PEG-BA conjugate were not visible as seen in **Figure 3.1 (ii).** The most important of these was the loss of the alkene protons between 4.7-4.9 ppm. This phenomenon was interrogated by proposing two possible explanations. The first explanation (EXP-I) is that the signal loss could be due to the aggregation of the conjugate into a micellar assembly in D_2O with the BA encapsulated within a hydrophilic PEG corona (**Scheme 3.2 (a))**. This is structurally a conventional micellar construct with the hydrophobic BA forming the core-shell or the PEG extending into the D_2O forming a hydrophilic corona. The second explanation (EXP-II) is that each PEG-BA molecule adopts a globular confirmation with the hydrophilic PEG encapsulating the BA head by wrapping around it (**Scheme 3.2 (b))** Running BA alone in D_2O was not an option as it is insoluble in water.

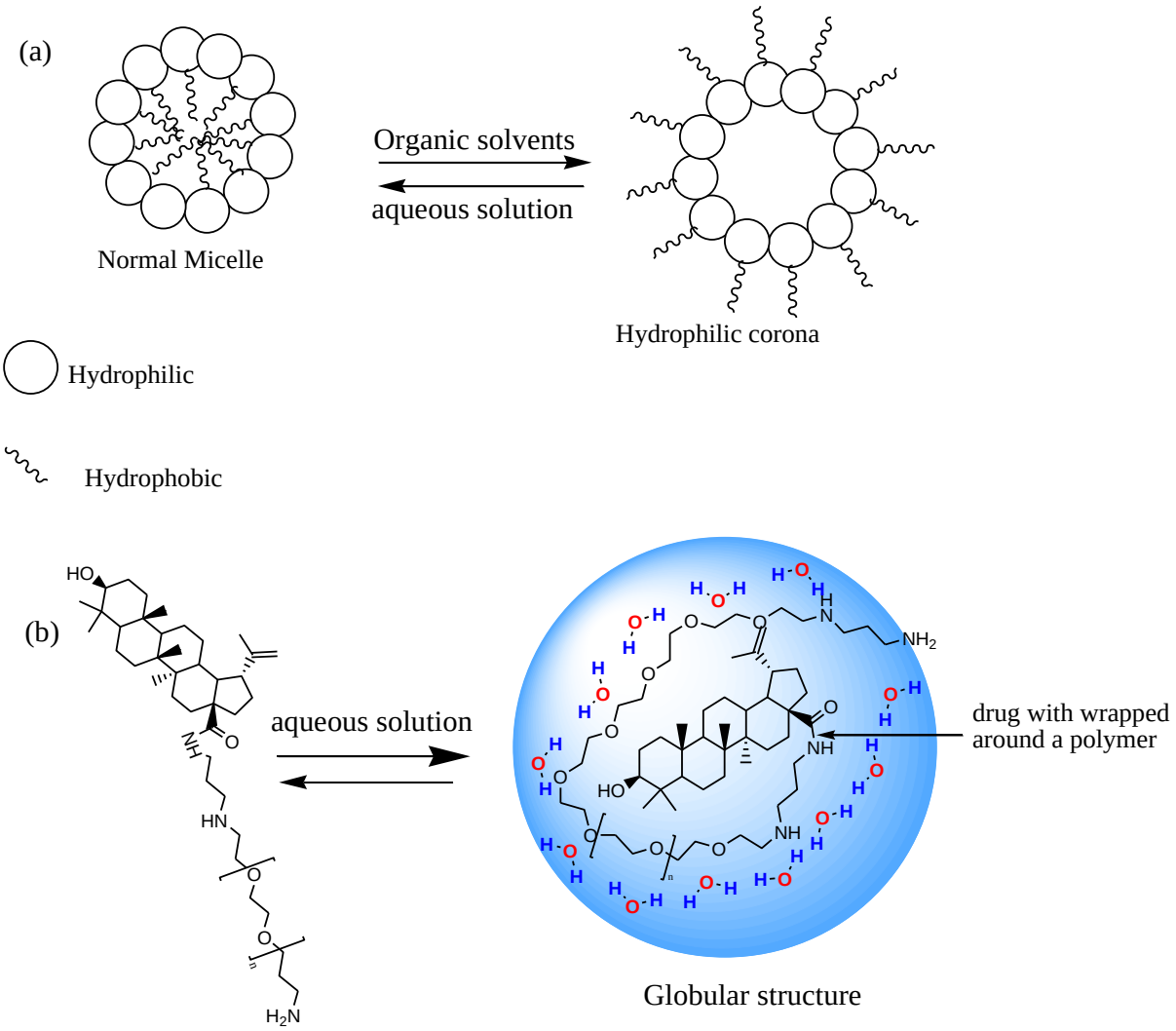

Scheme 3.2: Illustration of (a) EXP-I and (b) EXP-II for PEG-BA conjugate in an aqueous solvent.

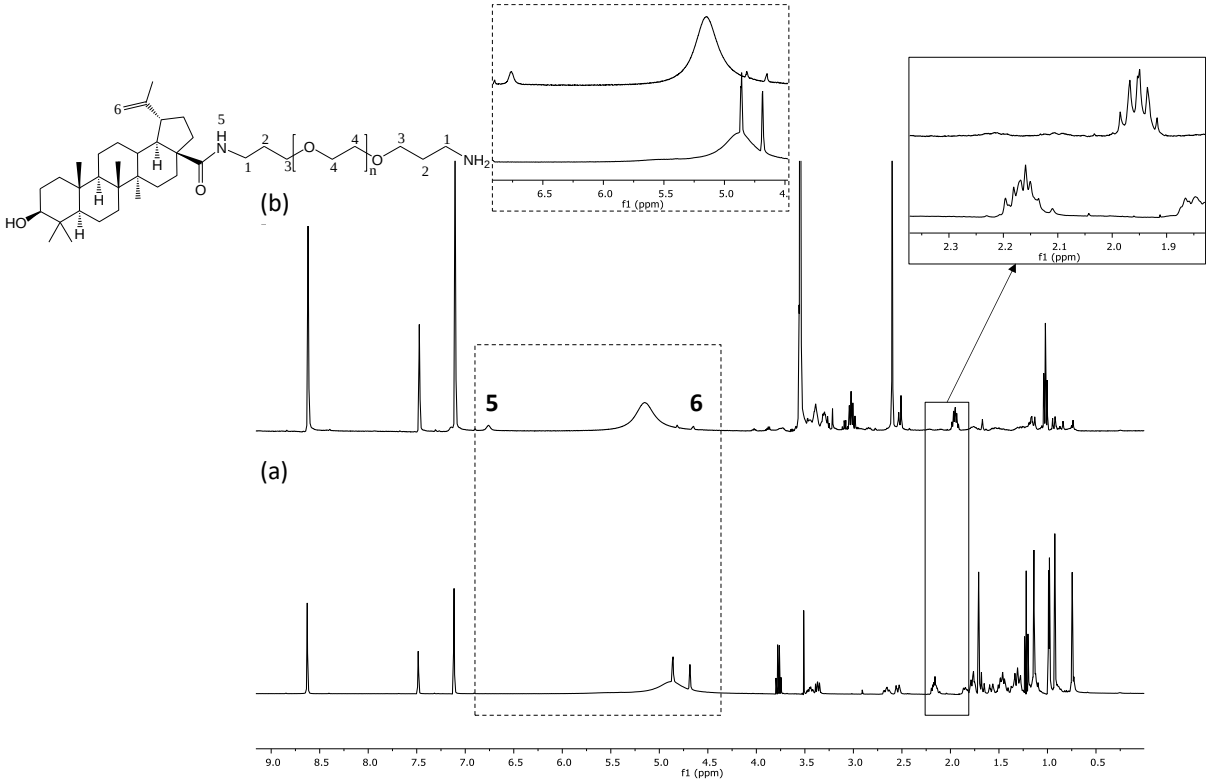

Figure 3.1 (i): ^{1}H NMR (400 MHz in pyridine-d_5) spectra of (a) betulinic acid (BA) and (b) PEG-BA conjugate.

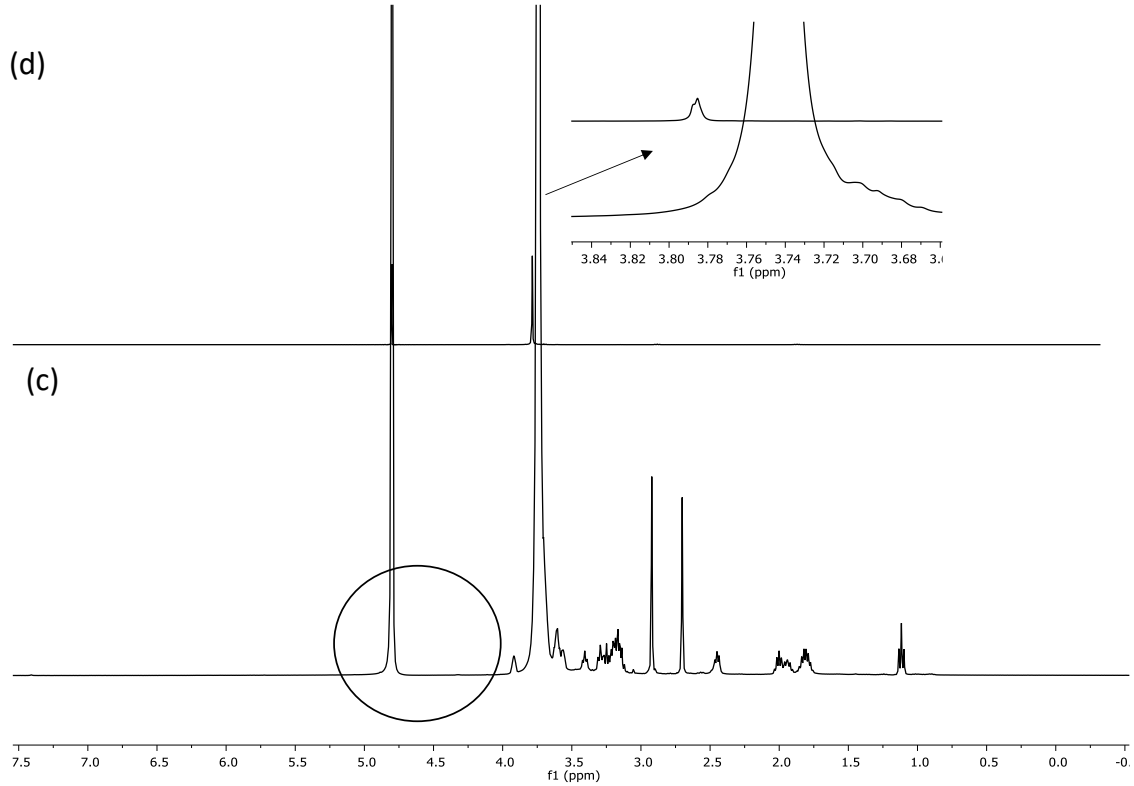

Figure 3.2 (ii): ^{1}H NMR (400 MHz in D_2O) spectra of (c) PEG-BA conjugate and (d) PEG.

EXP-II was tested as it required less resources to conduct. If the assumption that the signal loss was due to the folding of PEG around BA in water, then signals should be visible in organic solvents where the structure of the conjugate would be more extended. The NMR experiment was repeated in pyridine-d_5. The multiplet protons of BA from 0.76 ppm to 2.69 ppm due to terpenoid were observed, with the distinctive alkenyl terminal (-CH_2) protons at 4.90 ppm and 4.74 ppm. These results would fit with this second explanation. However, they do not exclude the possibility of EXP-I. Further experiments would be required to confirm the reason for the lack of terpenoid peaks in D_2O.

The PEG used in this work is divalent (has two attachment points), thus ^{1}H NMR was used to determine drug functionalization of BA to PEG. The intensity and the ratio of the integrated peaks of BA (alkenyl terminal protons) and PEG (methylene protons) were compared (**Figure 1A appendix**). This was calculated by multiplying the normalised integral value of repeating units obtained from ^{1}H NMR spectrum of PEG-BA conjugate with normalised integral values of end-group of PEG. Therefore, the drug functionalization of the conjugate was determined to be 9 mol%.

FT-IR spectroscopy (**Figure 3.2**) was also used to support the conclusion that the conjugation was successful. The hydroxyl group of BA **(a)** was observed as a characteristic broad peak around 3100 cm^{-1} while the carboxyl group was observed at 1683.8 cm^{-1}. The peak at 2939.3 cm^{-1} and 1448.2 cm^{-1} imply both asymmetric and symmetric C-H stretching vibration due to the methyl and methylene groups. The PEG **(b)** showed characteristic peak at 1100 cm^{-1} due to the (C-O-C) unit of the PEG backbone, also with the appearance of the (C-H) stretching at 2884.9 cm^{-1} due to the repeating units of the ethylene group. Also with the appearance of the (C-H) stretching at 2884.9 cm^{-1} due to the repeating units of the ethylene group. New peaks indicating successful conjugation were observed for the PEG-BA (**c**) by three distinctive peaks at 1711.7 cm^{-1}, 1554.9 cm^{-1} and 1651.1 cm^{-1} due to carbonyl (C=O) stretching of the newly formed amide bond, N-H bending and C-N stretching respectively.

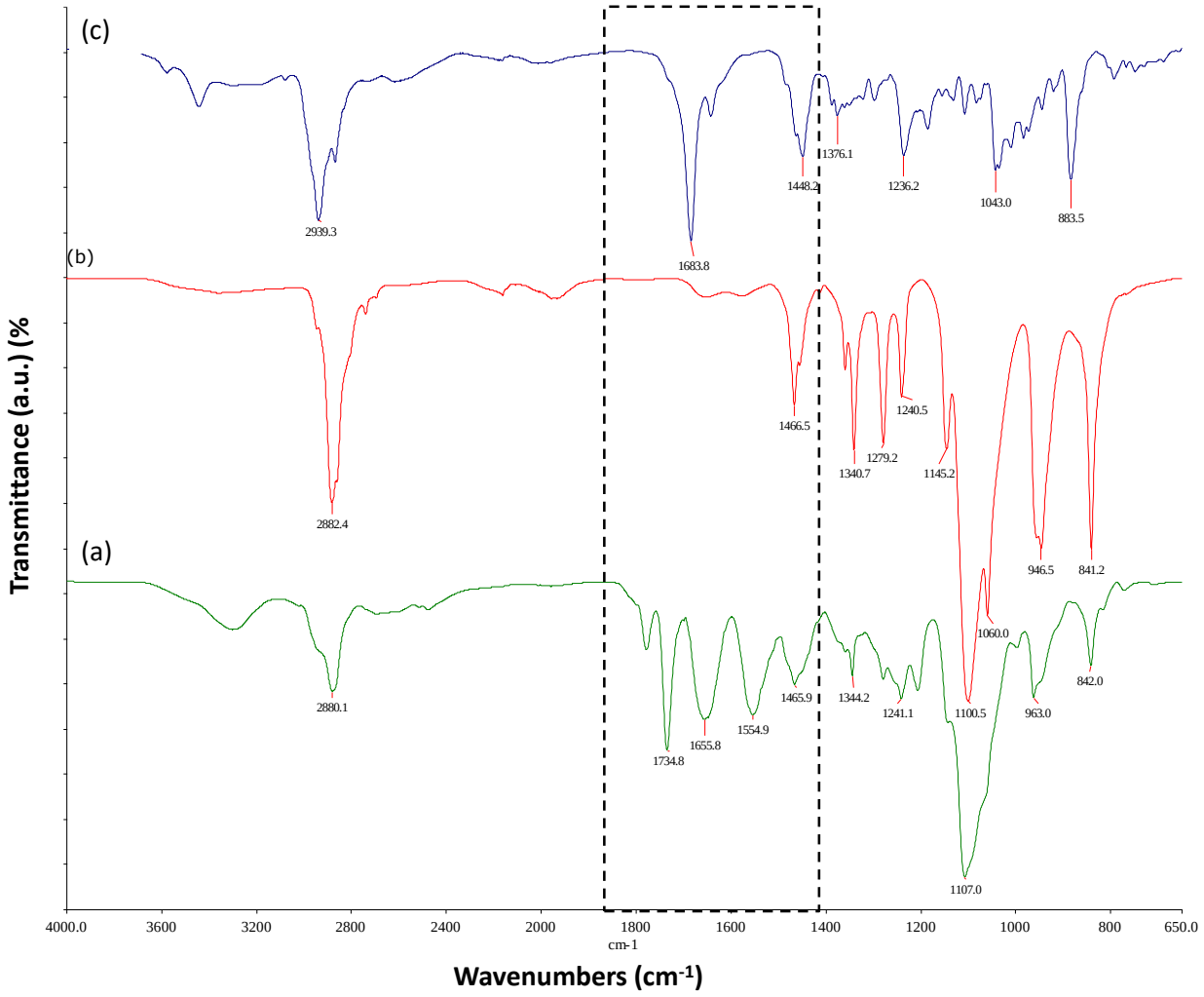

Figure 3.3: FT-IR spectra of (a) BA (b) PEG and (c) PEG-BA conjugate.

3.2.1.2 Shape and Particle Size Distribution

The shape and size of the PEG-BA conjugate was studied using TEM (**Figure 3.3**). TEM micrographs reveal spherical nanoparticles with an average diameter of 59.58±2.36 nm (**Figure 3.4 (b)**). A spherical morphology of the conjugate in the aqueous medium correlates with both hypotheses discussed above. The bright white spots observed in the TEM images are due to the negatively charged phosphotungstic acid stain used to aid visualization of the uncharged conjugate.

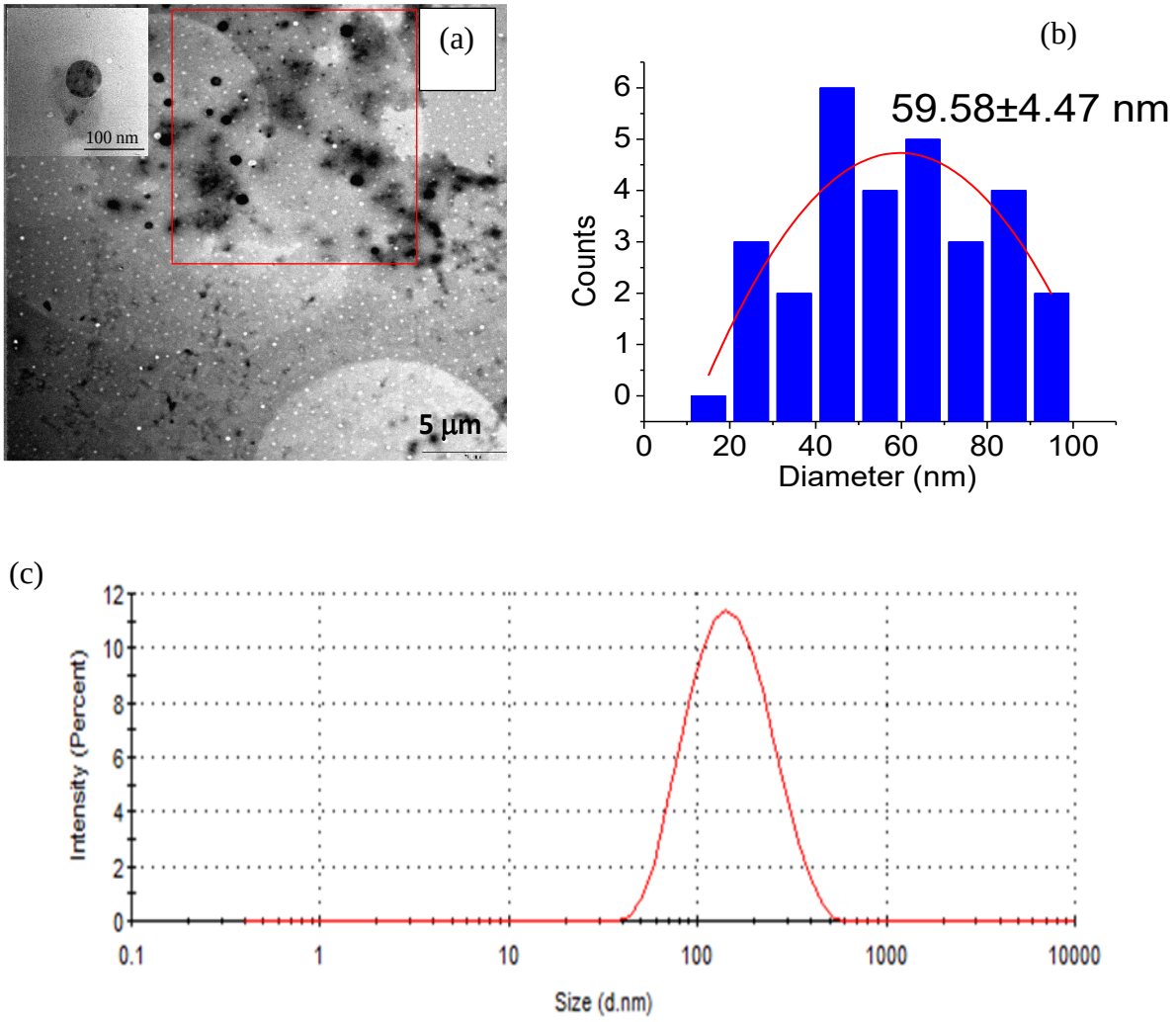

Figure 3.4: (a) TEM image and (b) Particle size distribution histogram and (c) hydrodynamic size of PEG-BA conjugate.

The size of the particles was further analysed using dynamic light scattering (DLS). **Figure 3.3 (c)** and **Table 3.1** show the mean particle size distribution, poly-dispersity index (PDI) and zeta potential of the synthesized conjugate. The results show unimodal narrow size distribution with hydrodynamic size of 125.7±2.30 nm with a PDI of 0.225±0.007. A PDI value close to 1 indicates a broad size distribution (Danaei et al. 2018). TEM measured dimension is smaller than DLS size because the latter is affected by solvent (solvating layer) and shape of the particles (Wen-hsuan Tsai, Kun-hua, Yu Yi-cheng huang, 2018). The DLS size less than 130 nm is good for reticuloendothelial system clearance (Yu et al. 2013) but size optimization will be needed for the passive targeting of the infected red-blood cells, via the so called new permeability pathways (NPPs).

The zeta potential is a key factor to consider when evaluating the stability of a colloidal dispersion and interaction with cells as positively charged particles have greatest efficiency in cell-membrane penetration and cellular internalization (Dai et al. 2015). The net surface charge of the conjugates was investigated by dispersing the conjugates in PBS pH 7.40. The results show that the conjugate had net surface charge of -1.29±0.501 indicating a trend to aggregation during storage, as particles with zeta potential values above ± 30 mV are regarded as stable (Manaia et al. 2017). The instability is not a problem as parenterally injected nanoparticles acquire a protein biocorona when absorbed by biological fluids (Berardi and Baldelli, 2019; Lundqvist et al. 2017).

Table 3.1: The TEM and hydrodynamic size and zeta potential of PEG-BA conjugate.

Parameters tested	PEG-BA
Particle size distribution	125.7±2.30 (d.nm)
PDI	0.225±0.007
Zeta potential	-1.29±0.50 (mV)
TEM size	59.58±2.36 (nm)

3.2.1.3 Solid material characterization

The physical characterization of the dry solid conjugate is best achieved with SEM, PXRD, TGA and DSC. They provide data on the crystallinity of the PEG-BA conjugate, i.e. the arrangement of the macromolecular conjugate, which is a determinant of its solubility.

Under the SEM, the PEG-BA appeared as irregular and amorphous spherical particles that were in stark contrast to rod-like crystals of BA but more approximately like PEG in **Figure 3.4**. This was not a surprise as lower crystallinity correlates with greater aqueous solubility (S. Murdande, M. Pikal, R. Shanker, 2009). The SEM observations are complemented by the physical change in data obtained from PXRD.

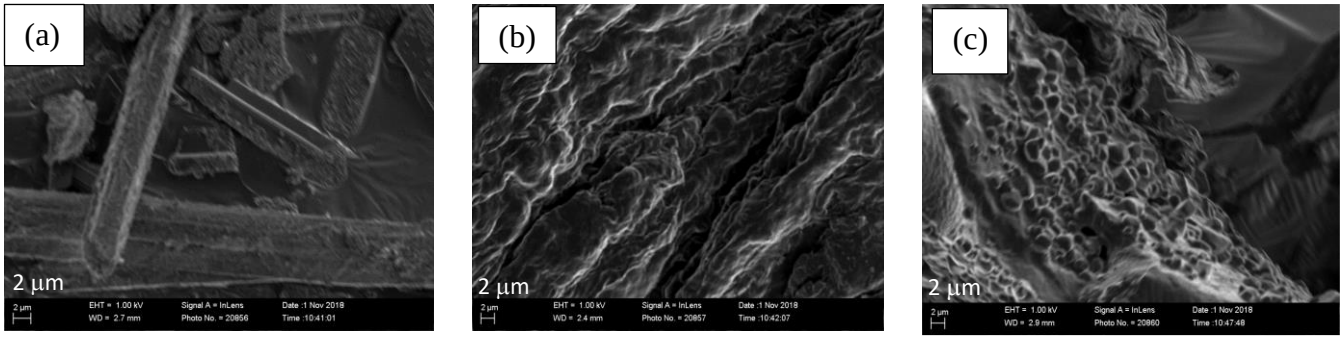

Figure 3.5: SEM images of (a) BA, (b) PE and (c) PEG-BA conjugate.

Figure 3.5 (a) showed a crystalline nature of the drug (BA) as observed also with the SEM microscopic images. The PEG **(b)** exhibited two peaks at 2θ = 19.3° and 23.4°, indicating that the polymer is also crystalline in nature (Ahmad et al. 2011; Tzitzios et al. 2008). PEG-BA **(c)** showed peaks of the PEG with the appearance of new peaks at 2θ = 32.5° and 47.1° indicate by star, also by disappearance of the peak at at 2θ = 15° seen both in the PEG and BA. These changes indicated a slight physical change or distortion in the structure as the diffraction pattern still resembles that of pure PEG with appearance of new peaks (star).

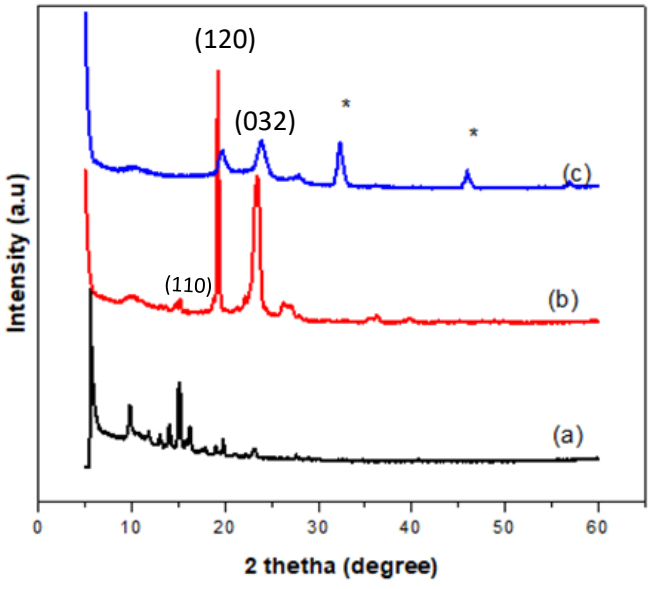

Figure 3.6: X-ray diffraction of (a) BA, (b) PEG and (c) PEG-BA conjugate.

To further evaluate the interaction of the polymer with the drug, TGA analysis was conducted and is shown in **Figure 3.6**, where (a) PEG-amine, (b) BA and (c) PEG-BA conjugate were three thermograms were recorded for each sample. BA underwent sublimation at temperatures between 290 to 393 °C with weight loss of 80 % (Şoica et al. 2012; Hussein-Al-Ali et al. 2014). PEG underwent rapid decomposition from 259 to 381 °C indicated by a weight loss of about 88.0 % due to the decomposition of the C-O and C-C bonds forming the backbone of the polymer (Nagarajan et al. 2009; Kwon et al. 2006). The PEG-BA conjugate showed decomposition in several stages. The initial weight loss of 8 % is due to moisture content possed by the conjugate. High moisture content provides a degradation environment that also facilitate also microbiological contamination during storage. The second degradation occurred between 200 to 248 °C with a weight loss of 9 %, this could be due to the decomposition of the drug from the polymer, degradation of the amide bond formed during conjugation. The major decomposition happened between 310 to 438 °C with weight loss of 67.4 %, this degradration could be due to the thermal decomposition of the polymer backbone (C-O, C-C). TGA thermogram of the conjugate reflects a heterogeneous decomposition pattern of the conjugate showing that there was an interaction between BA and PEG-amine (Azmeera et al. 2012; Malik et al. 2020; Margaritis and Manocha, 2010). This interaction could be due to the carboxylic and amino group of the drug and polymer respectively.

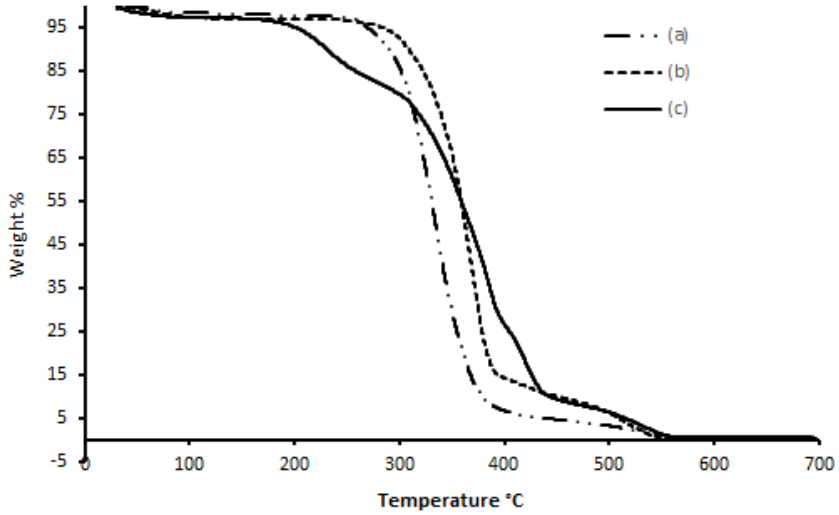

Figure 3.6: TGA thermogram of (a) PEG-amine (b) BA and (c) PEG-BA conjugate.

Differential scanning calorimetry (DSC) was conducted to investigate thermal transitions in polymers of material upon chemical change and in this case conjugation. DSC thermogram in Figure 3.7 (a) showed PEG-amine endotherm at 52.24 °C (Dabbagh et al. 2015; Gerasimov et al. 2014), while BA showed endotherm peak at 319.11 °C due to the decomposition of the compound (Fontanay et al. 2012). It was observed that upon conjugation, there was a small change in the profile of the drug and polymer. The change was indicated by a shift in the endothermic peaks of PEG-amine and BA and this presumably confirms a physical interaction upon conjugating BA to the polymer and a similar phenomenon was reported by Danafar et al. (2017) for the doxorubicin poly (ethylene glycol)-poly caprolactone (DOX-PEG-PCL).

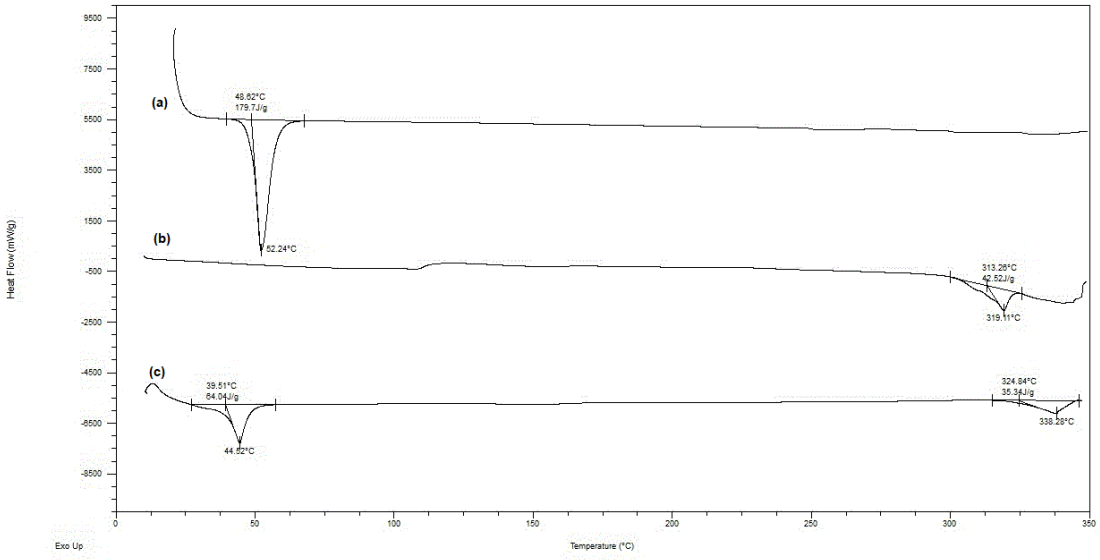

Figure 3.7: DSC thermogram of (a) PEG-amine (b) BA and (c) PEG-BA conjugate.

To conjugate DHA to the amino group of PEG-amine, a hetero-bifunctional linker is required to create compatible hydrolysable bonds to the polymer and drug. In this work, succinic acid is used as a linker (**Figure 3.8**). It is a dicarboxylic acid well-favoured as a linker for its safety and ease of use. It occurs as an endogenous intermediate of cellular metabolic pathways.

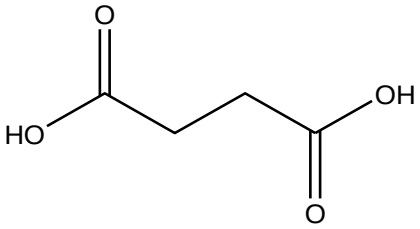

Figure 3.7: Structure of succinic acid.

3.2.2 Synthesis of DHA-Suc

The reaction of DHA with succinic anhydride (**Scheme 3.3**) in a 1:3 molar equivalent ratio resulted in the formation of a DHA-hemisuccinic acid in the presence of imidazole as a base. This synthetic method had been reported by Sharma and Kumar (2008). They had reported completion of the reaction under N_2 gas after 3 h but this could not be reproduced here. Instead, the reaction was only complete after 24 h at 35 °C (**Table 3.2**).

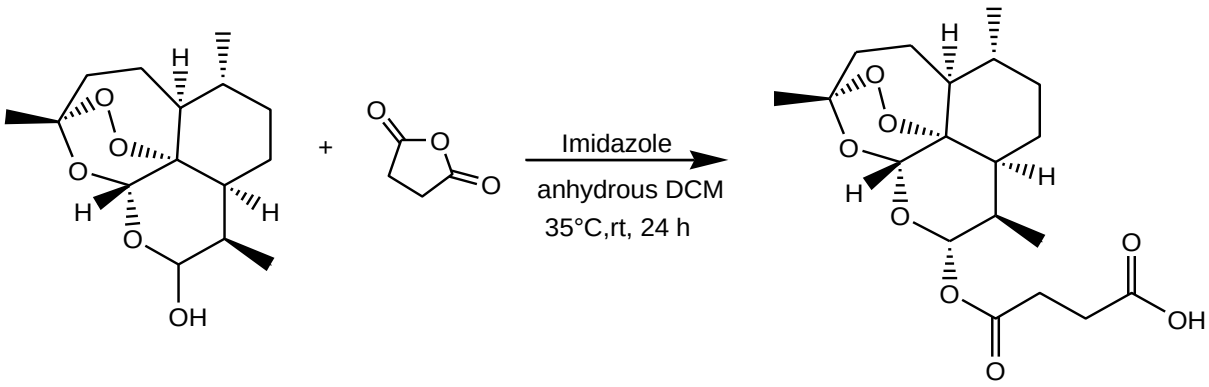

Scheme 3.3: Synthesis route for DHA-Suc.

Table 3.2: Comparison between methods used to synthesise DHA-Suc.

Conditions	**Patent synthesis** (Sharma and Kumar; 2008)	**Successful synthesis**
Solvent	DCM	Anhydrous DCM
Ratio	Not specified	1:3
Base	Imidazole	Imidazole
Reaction time	25-210 minutes	24 h
Temperature	20-35 °C	30 °C
Purification method	Crystallization	Column purification

It must be noted that upon formation of DHA-Suc in DCM, the reaction solution became cloudy from the original colourless solution (**Figure 3.9**). As DCM is a not a very polar solvent, whereas the carboxylic acid group in DHA-Suc increases the polarity of the solute thus poor solubility resulting in the crystallization of DHA-Suc in the solvent. The crude DHA-Suc was purified by silica column chromatography (Hexane: EtOAc, 1:3) and the pure product obtained as a fine crystalline powder (1.33 g; 49.2 % yield) as seen ^{1}H NMR and ^{13}C NMR spectra below. Successful synthesis was also indicated using TLC (hexane/EtOAc, 1:3) analysis shown in **Figure 3.9,** DHA showed one spot for the DHA (R_f = 0.65) and tailed spot for DHA-Suc (R_f = 0.37). DHA-Suc showed lower retention factor compared to the DHA due to the increased polarity from the carboxylic acid group.

			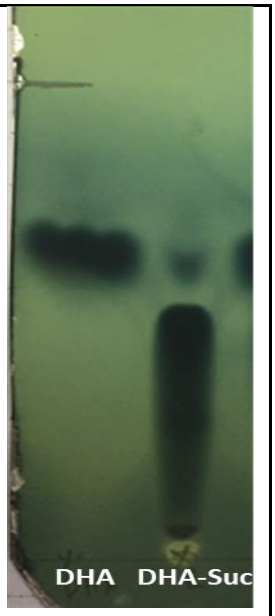
Clear DHA solution in DCM.	Reaction after 24 h forming cloudy solution of DHA-Suc in DCM.	DHA-Suc final product after column purification.	TLC hexane:ethyl acetate (1:3). Stained with phosphomolybdic acid.

Figure 3.8: Pictures showing the change in colour of solution upon formation of DHA-Suc and TLC analysis.

3.2.2.1 NMR and FT-IR spectroscopy, thermal analysis and mass spectroscopy of DHA-Suc

The product was first purified on a deactivated silica column with trimethylamine as a base. The base interacts with the silanol group on the silica and it was used to neutralise the column to avoid the hydrolysis of the ester. This resulted in a round spot instead of a tailed spot with lower R_f values (0.26). This could mean that the addition of a base to the free acid of the DHA-Suc resulted in the formation of a salt, thus the low R_f values. The pure DHA-Suc was obtained using flash silica chromatography but the column had to be completed within 90 min to avoid hydrolysis. The formation of the ester bond was confirmed using ^{1}H NMR spectroscopy (400 MHz, DMSO-d_6) in **Figure 3.10**.

The ^{1}H NMR spectra of DHA and DHA-Suc are shown in **Figure 3.10(a)-(b),** DHA showed the protons of hydroxyl group (-OH) at 2.77 ppm as a singlet. Also the presence of the two interconverting lactol hemiacetal epimers at 4.75 ppm and 5.60 ppm due to the alpha (α) and beta (β) epimers (Cabri et al. 2011; Presser, Feichtinger and Buzzi, 2017). Upon formation of ester bond only a doublet appears at 5.68-5.69 ppm due to formation of ester bond favouring the α-configuration due to steric hindrance of the axial ester group. It could also be due to the higher stability and thermodynamically favouring the α-configuration (Presser, Feichtinger and Buzzi, 2017). A new peak was observed further downfield (12.2 ppm) in the typical carboxylic acids OH regions. Therefore, to confirm that this signal was indeed from the proton of the carboxylic acid, a D_2O exchange was carried out as seen in **Figure 3.10(c)**. In D_2O, carboxylic acids exchange their proton with deuterium resulting in no proton on the ^{1}H NMR spectra and also the peak appearing at 3.3 ppm is a water peak as DMSO absorbs water. The esterification reaction was further confirmed by the appearance of the carbon peak at 174.08 ppm on the ^{13}C spectra in **Figure 3.11**.

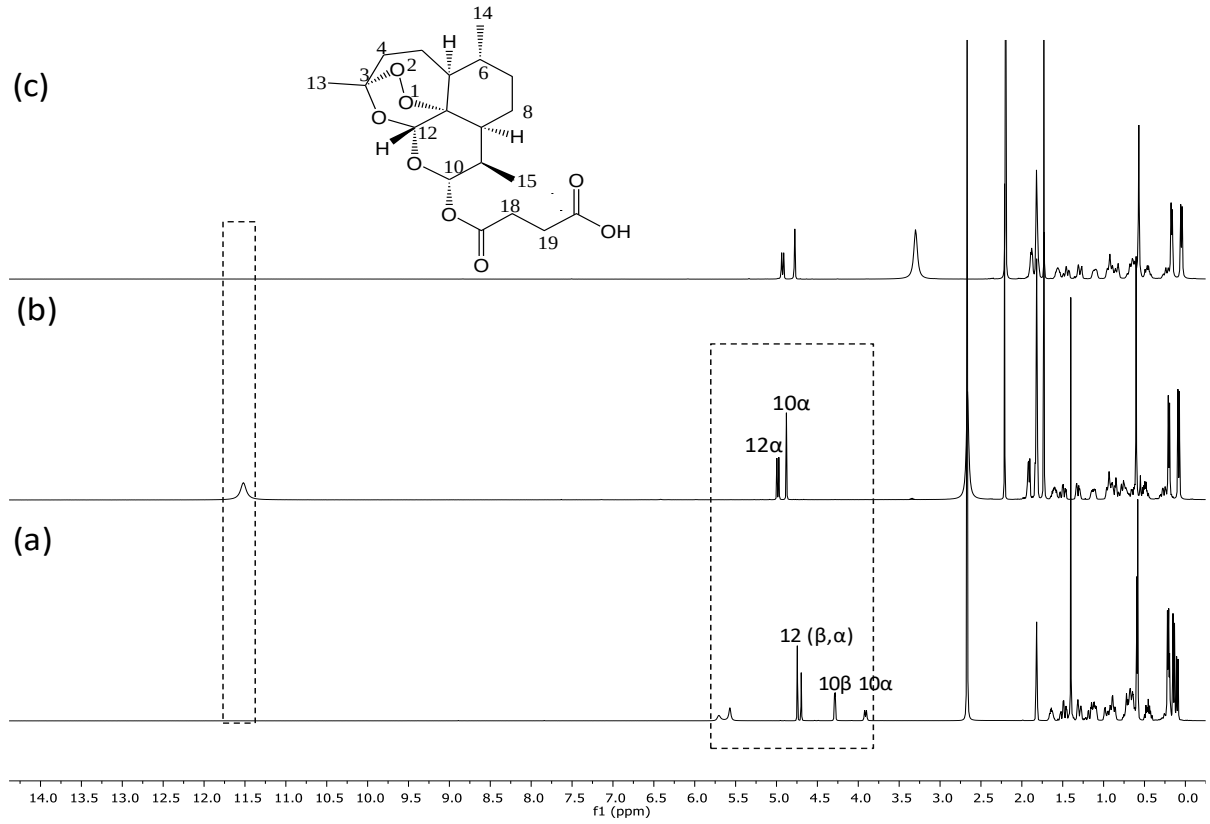

Figure 3.10: ^{1}H NMR (400 MHz) spectra of (a) DHA, (b) DHA-Suc in DMSO-d_6 (c) DHA-Suc in DMSO-d_6+ D_2O.

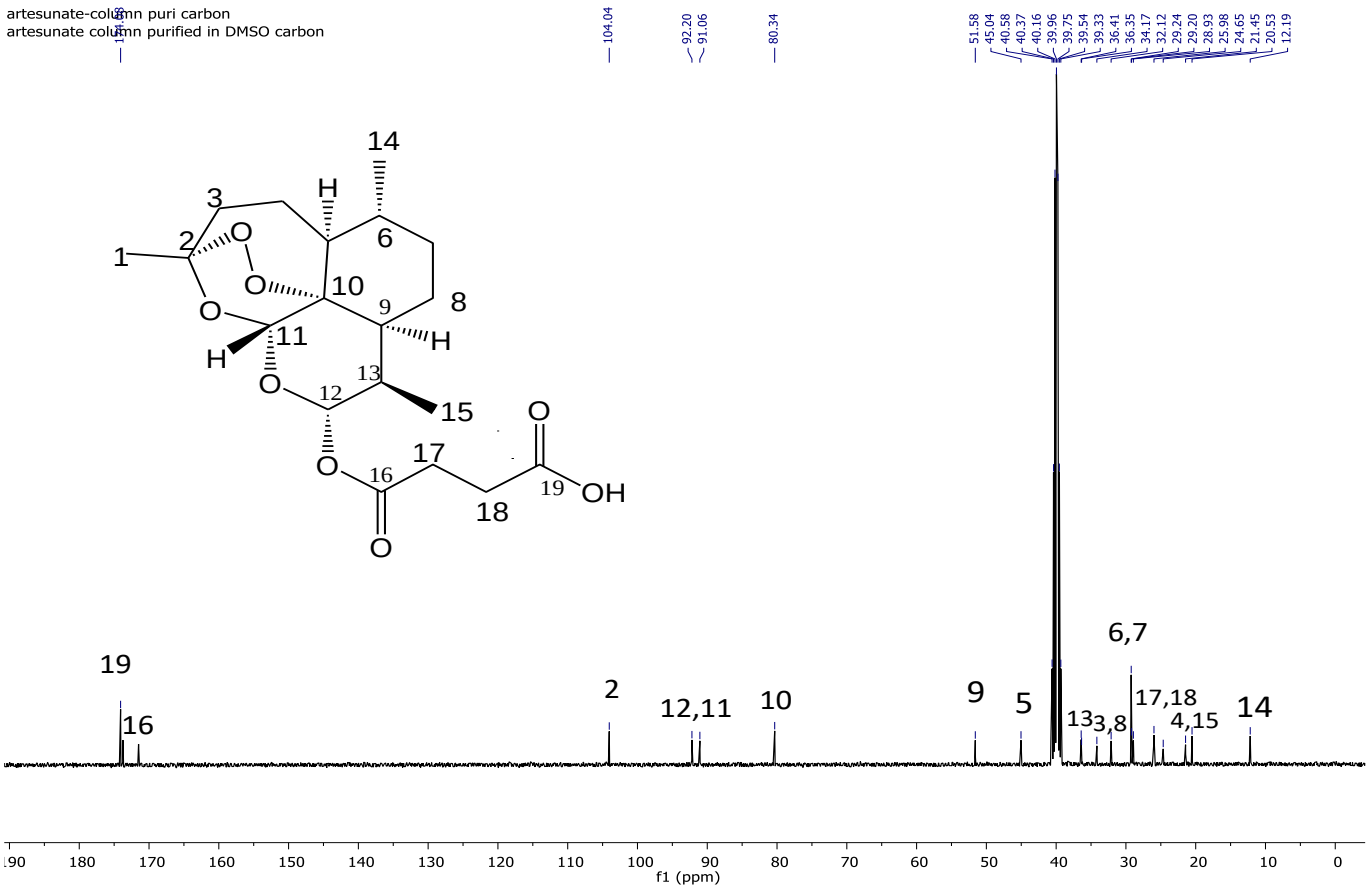

Figure 3.11: ^{13} C NMR (101 MHz in DMSO-d_6) spectrum of DHA-Suc.

FT-IR spectra of DHA and DHA-Suc were analyzed (**Figure 3.12**). The hydroxyl group of the DHA was observed as a sharp peak at 3372.6 cm^{-1}. For DHA-Suc, new peaks were observed at 1688.2 cm^{-1} and 1754.1 cm^{-1} due to carbonyl (-C=O) functional groups of the carboxylic and ester bonds. The TGA thermogram depicted in **Figure 3.13** showed decomposition of DHA between 113 °C and 240 °C due to decomposition of the compound with a weight loss of 84%. DHA-Suc is more stable with decomposition threshold of 140 °C, this was followed by loss of volatile components of about 15 % to the second decomposition threshold at 155 °C. DSC (**Figure 3.13**) was used to evaluate changes in thermodynamic properties that occur when the material supplied heat energy. The DSC thermogram of DHA **(a)** showed two exothermic peaks at 158.74 °C and 173.06 °C which are due to decomposition of the peroxidase and these results are similar to the ones published by Ansari, Iqbal and Sunderland (2009). These exothermic peaks also indicate the crystalline nature of the drug. The synthesized DHA-Suc (b) exhibited a melting endotherm at 136.46 °C, which was followed by a decomposition exotherm at 162.88 °C. The results showed different thermograms for both compounds. This

indicates that DHA was transformed into a new crystalline form, DHA-Suc. **Figure 3.9:** FT-IR spectra of (a) DHA and (b) DHA-Suc.

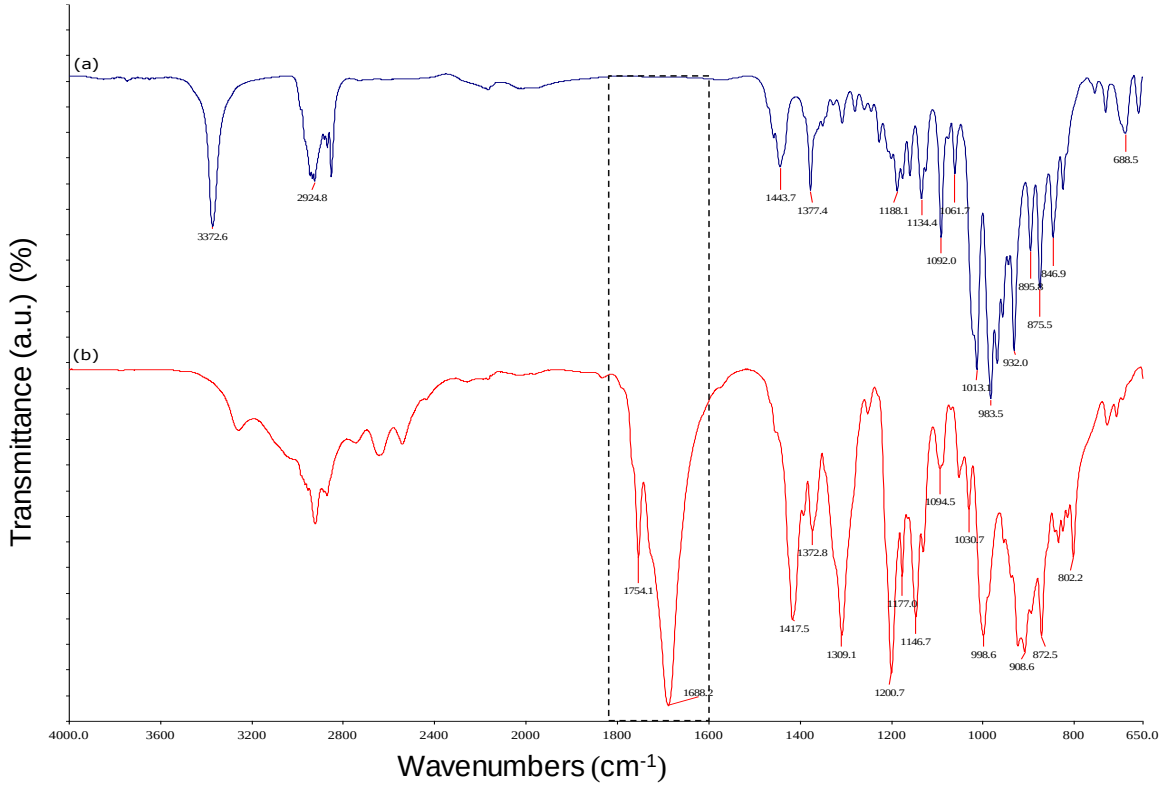

Figure 3.10: FT-IR spectra of (a) DHA and (b) DHA-Suc.

3.2.3 Stability of DHA at different pH conditions.

DHA-Suc also known as artesunic acid is administered as sodium salt artesunate intravenously or intramuscular. This is for the treatment of severe malaria caused by *P. falciparum.* Clinically, artesunate is prepared by dissolving the artesunic acid in sodium bicarbonate. Due to the instability of artesunate in aqueous solution, WHO recommends that the reconstitute solution must be used within an hour of preparation (Ntuku et al. 2016; WHO, 2013). Artesunate is hydrolyzed to DHA in the gastro-intestinal lumen before first pass metabolism in the gut wall and liver (Haydar, 2011). The rate of hydrolysis by esterase to DHA is pH depended. Haydar (2011) did full studies on degradation of artesunate at different pH conditions. Therefore, in this work the stability of DHA was investigated with pH values ranging from highly acidic to neutral pH to mimic gastrointestinal (pH 2.0-6.8) and blood (pH 7.4). This is for oral administration using chitosan and intravenous administration using PEG respectively. DHA mass spectrum were obtained and the predominated peaks were observed

at *m/z* 284.2, which is the parent ion $[M+H]^+$), *m/z* 267.2, 231.3, 221.3, 163.3 are other fragments observed with DHA (**Figure 3.14**).

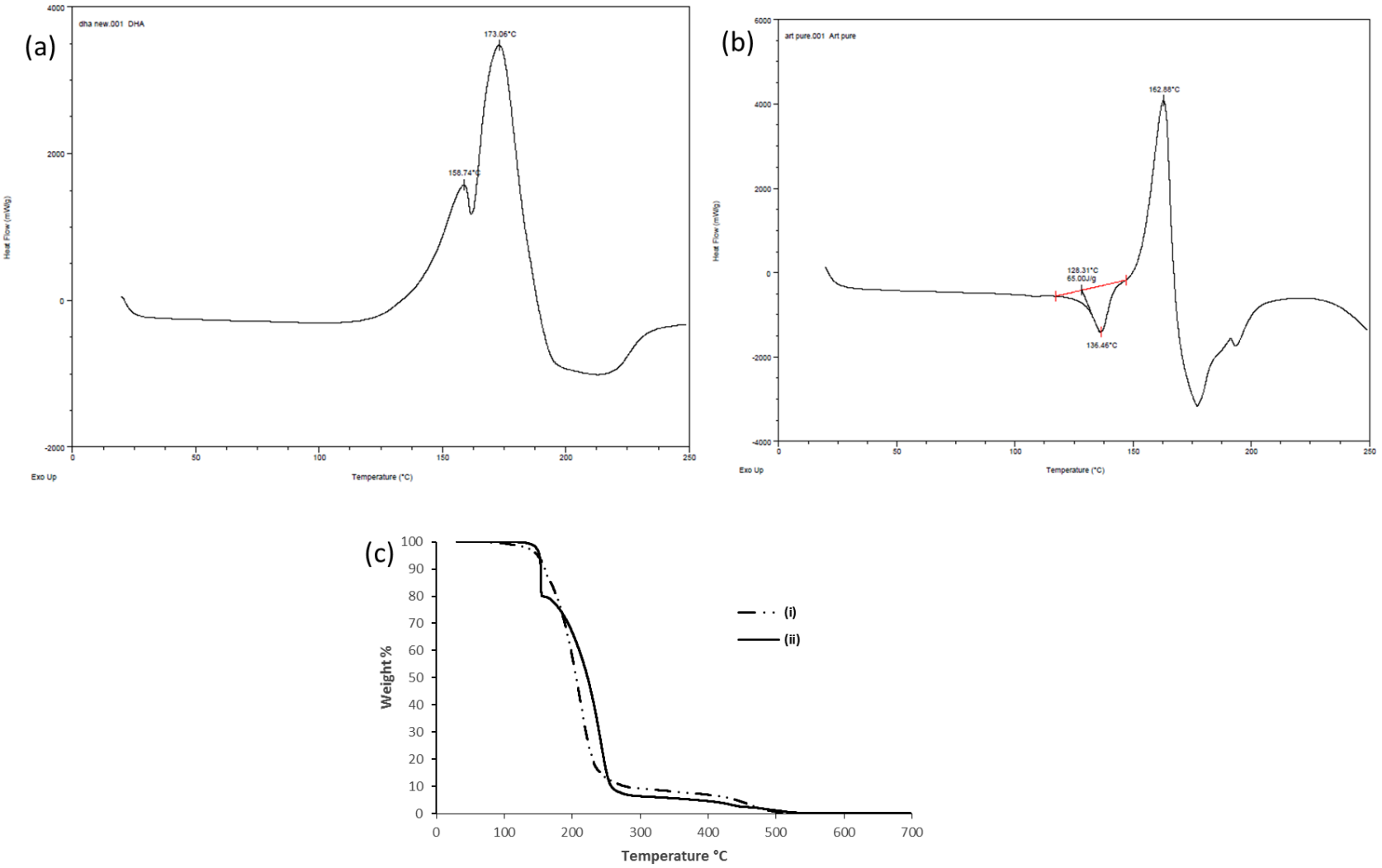

Figure 3.11: DSC thermogram of (a) DHA (b) DHA-Suc and (c) TGA thermogram of (i) DHA-Suc and (ii) DHA.

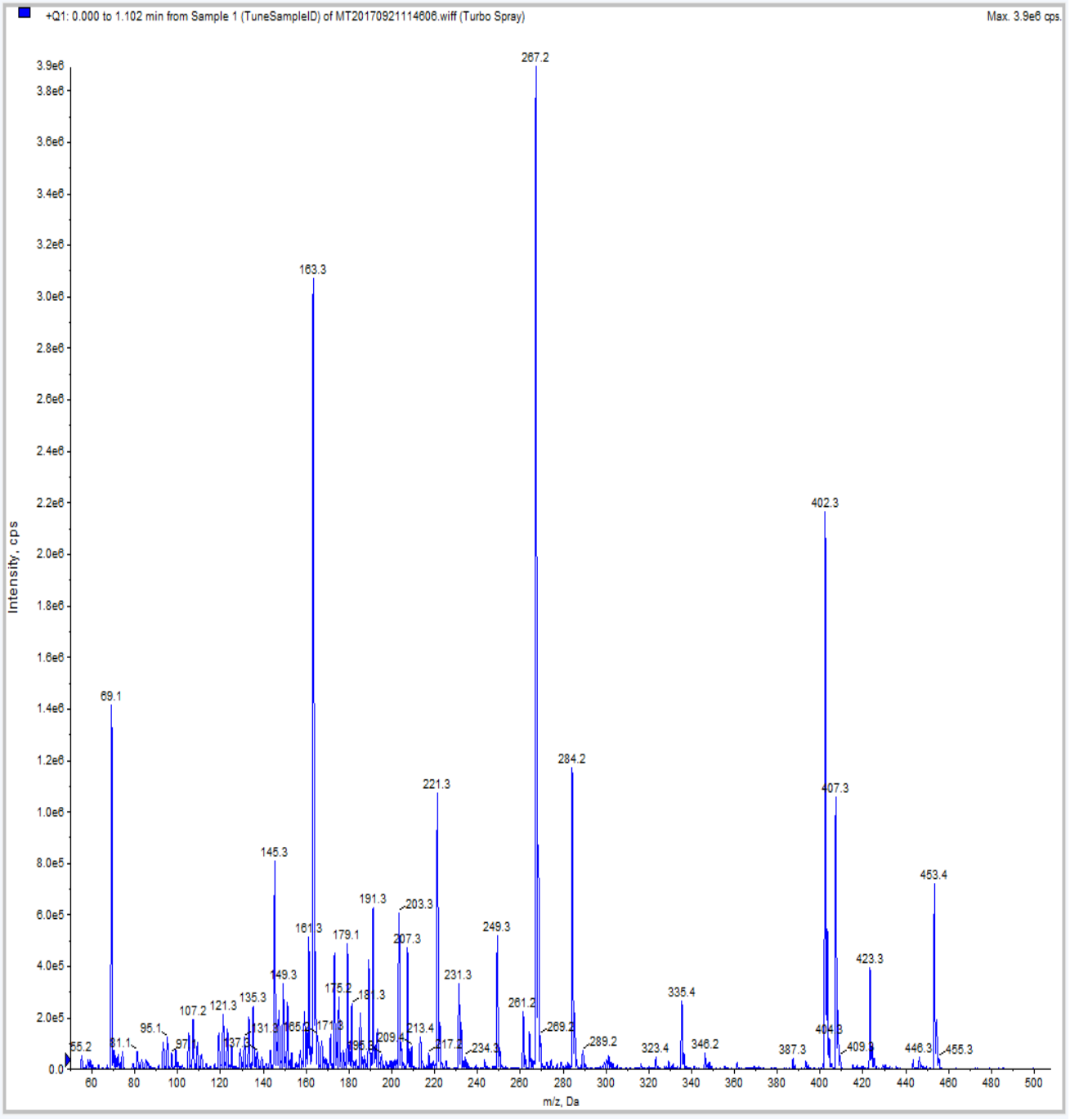

Figure 3.12: Mass spectra of DHA in mobile phase ammonium formate 20 mmol l^{-1} (pH 4.0) as phase A (35 %) and acetonitrile as phase B (65 %).

Stability of DHA was studied in HCl, acetate buffer and phosphate buffer (pH ranging range 2.00-7.40). The degradation of DHA was followed at concentration of 600 µg mL^{-1} at 37 ˚C for 24 h. Sampling was done at different time intervals and the samples were snap frozen in liquid nitrogen and later freeze-dried. The rate of decomposition of DHA shown in **Figure 3.15** in each buffer solution was found by plotting the peak area over time (min), were the peak at

6.86 in **Figure 3.16 (a)** was monitored overtime. **Figure 3.15** shows that DHA is unstable within pH range 1.0 to 3.50 which are conditions that apply to the stomach and small intestine where the drug is absorbed. These pH condition promotes degradation of DHA, while at pH 4.50 to 7.40 DHA was relatively stable. These results are similar to results reported by Parapini et al. (2015) and to those reported for DHA-Suc (Artesunate) by Haydar (2011). Hayder observed that is stable in pH 5.50 to 7.50 and these results are similar to the DHA obtained in this work.

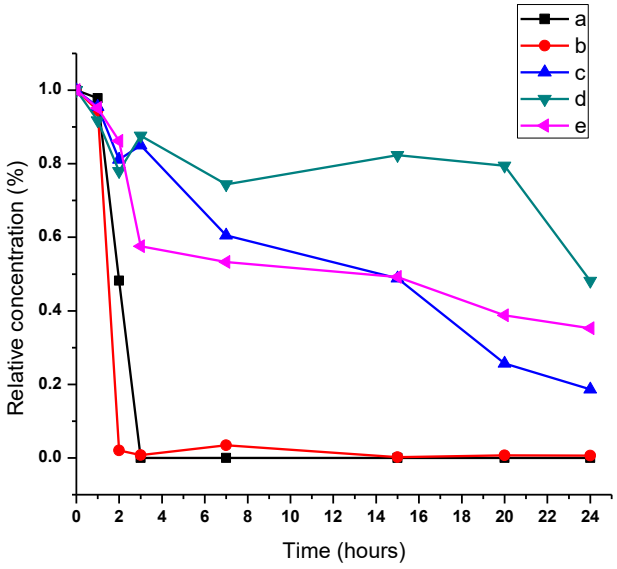

Figure 3.13: The degradation curve of DHA in pH (a) HCl 1.0 (b) Acetate buffer 3.50 (c) Acetate buffer 4.50 (d) PBS buffer 6.50 and (e) PBS buffer 7.40.

The major metabolite so far reported of cytochrome P450 enzyme metabolism of artemether, arteether and artesunate in the liver is dihydroartemisinin (MW=284.35) Dihydroartemisinin is further metabolized to α-dihydroartemisinin-β-glucoronide (MW=460.47). Artemisinin undergoes a different metabolic pathway to four metabolites namely, 9,10-dihydrodeoxyartemisinin (MW=217.3), deoxyartemisinin (MW=268.35), deoxydihydroartemisinin (MW=267) and crystal-7 (MW=247.15). Unlike dihydroartemisinin, none of these metabolites are active as they have lost the endoperoxide bridge (Kerb et al. 2009; Liu et al. 2011). To further investigate the degradation compounds, mass spectroscopy and a chromatogram of the decomposed products at 24 h are shown in **Figure 3.16 (i)-(ii)**. A new peak at *m/z* 284.2 was observed in the chromatogram in **Figure 3.16 (i)-(ii)** at retention time 6.1 min when DHA was put under acidic condition. The DHA parent ion are $[M+H]^+$), *m/z* 267.2, 231.3, 221.3, 163.3 as shown in **Figure 3.14**, DHA in acidic solution could have

degraded to form 9,10-dihydrodeoxyartemisinin , deoxyartemisinin, deoxydihydroartemisinin and crystal-7 as marked by red star. Therefore to improve the stability, DHA is conjugated to PEG and chitosan for intravenous and oral administration of the drug, respectively.

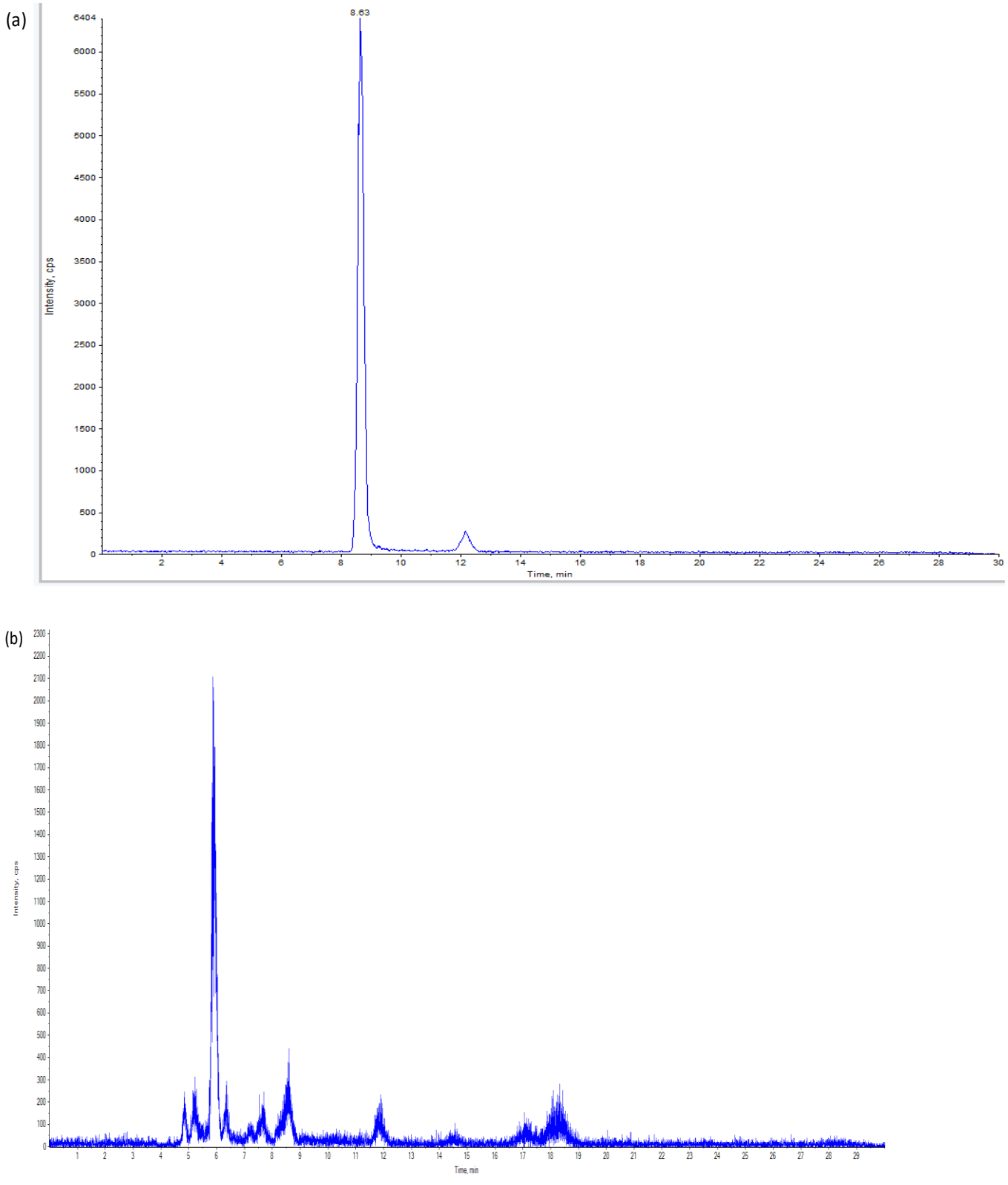

Figure 3.14 (i): Chromatogram of (a) DHA in PBS (pH 7.40), (b) HCl (pH 1.0).

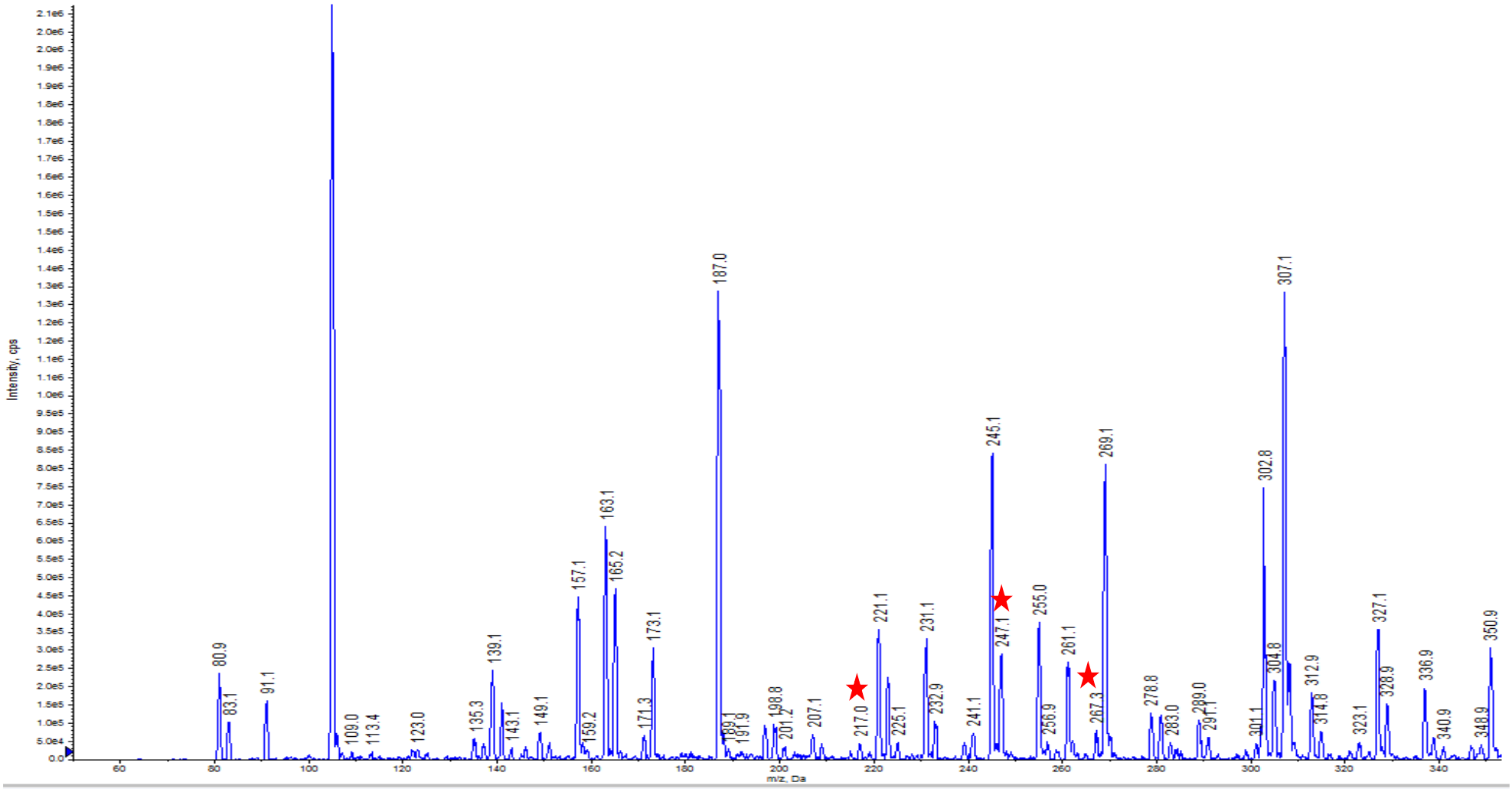

Figure 3.16 (ii): Mass spectrum of DHA in HCl pH 1.0 after 24 h.

3.2.4 Synthesis and physico-chemical characterization of PEG-Suc-DHA conjugate and chitosan-Suc-DHA conjugate

The formation of the amide bond linking DHA-Suc with PEG and chitosan shown in **Scheme 3.4** and **Scheme 3.5** respectively were accomplished using EDC/Sulfo-NHS as coupling reagents to enhance the yield of the amide bond. The synthesis of PEG-Suc-DHA was similar to the synthesis described above for PEG-BA. An activated complex of DHA-Suc was formed through nucleophilic attack of carbodiimide. This was reacted with sulfo-NHS to form a stable ester. After 2 h, the DHA-Suc-NHS ester was added dropwise to a solution of PEG-amine and left for 24 h. The product was then purified using a similar method to that used for the purification of PEG-BA.

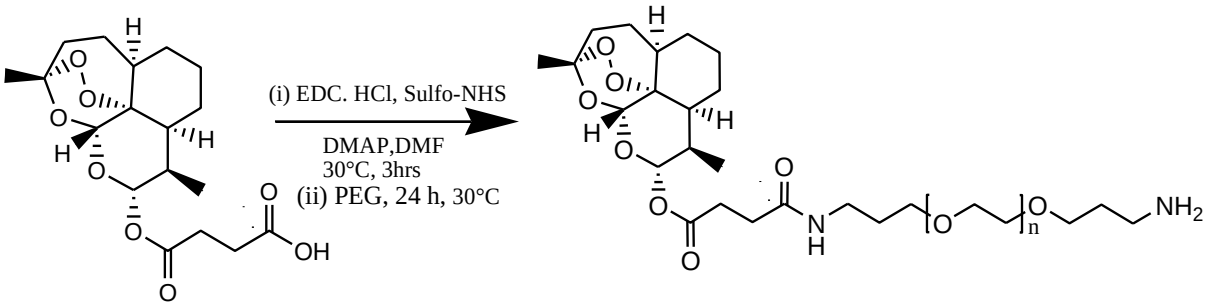

Scheme 3.4: Synthesis route for PEG-Suc-DHA.

3.2.4.1 NMR and FT-IR spectroscopy analysis

^{1}H NMR and FT-IR spectroscopy was used to verify the formation of the PEG-Suc-DHA conjugate. The conjugate showed characteristic protons of DHA-Suc at 0.8-2.9 ppm and the successful formation of amide bond was indicated by appearance of proton peak at 7.83 ppm (**Figure 3.17**). FT-IR spectra in **Figure 3.18 (c)** showed the formation of an amide bond by appearance of the absorption peaks at 1711.7 cm^{-1}, 1651.1 cm^{-1} and 1563.3 cm^{-1} due to the carbonyl (C=O) of amide stretching and also due to the amide N-H bending respectively.

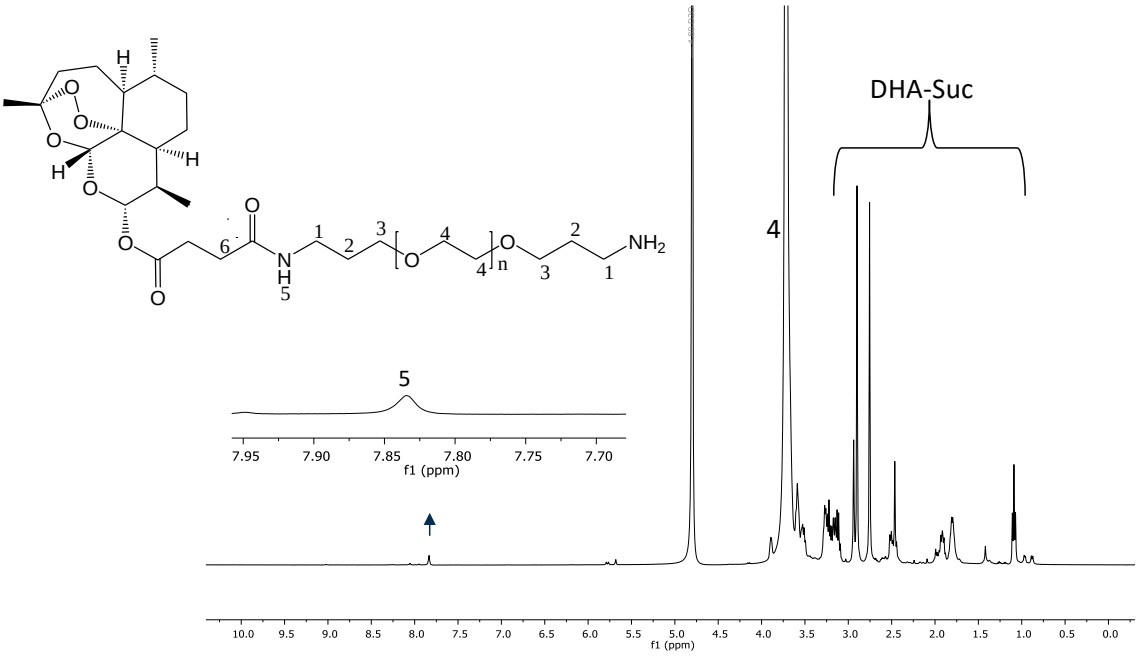

Figure 3.15: ^{1}H NMR (400 MHz, D_2O) spectrum of PEG-Suc-DHA.

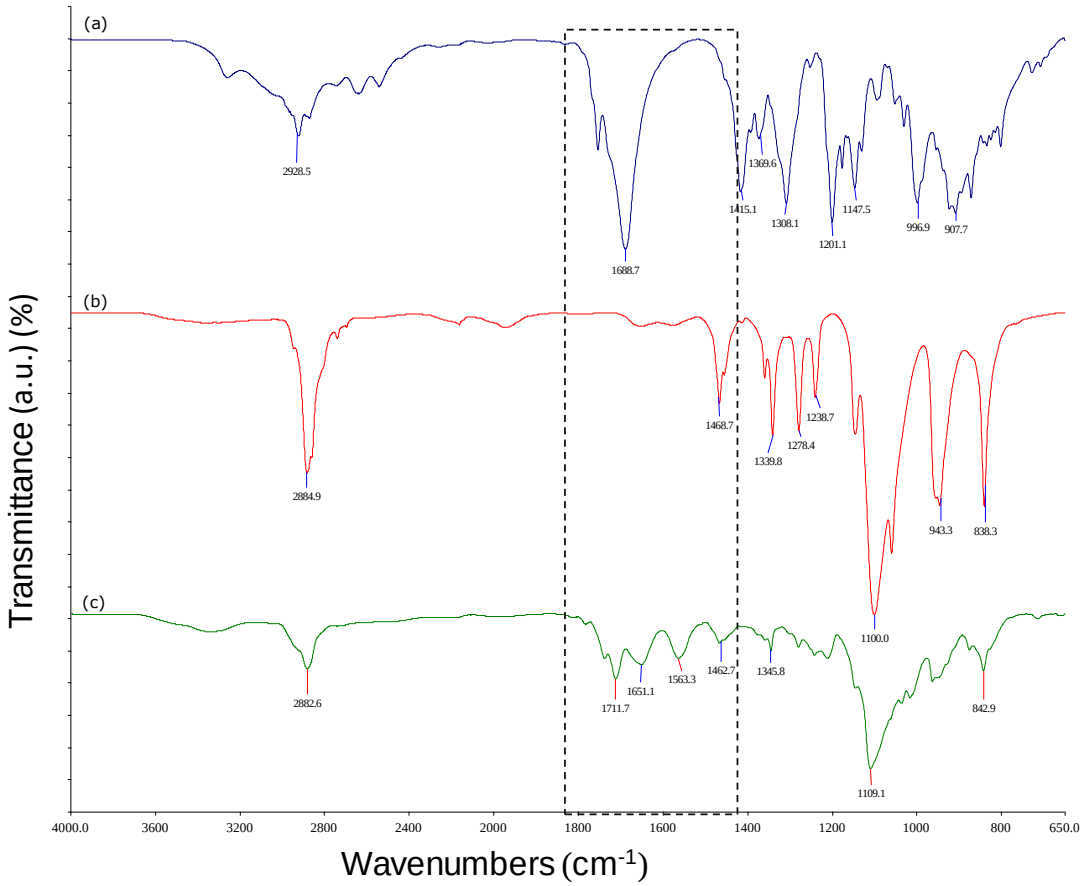

Figure 3.16: FT-IR spectra of (a) DHA-Suc (b) PEG and (c) PEG-Suc-DHA conjugate.

The conjugation of DHA-Suc to chitosan was carried in aqueous media because the low molecular weight chitosan is soluble in aqueous media. DHA-Suc was dissolved in a solution of sodium bicarbonate to make DHA-Suc-Na^+. This was then coupled with reagents EDC/Sulfo-NHS to form DHA-Suc ester, after 5 min of stirring this solution was added dropwise to a chitosan solution and the reaction was allowed to proceed for 3 h. Our standard purification protocol using precipitation-dissolution method, resulted in an impure conjugate showing traces of the coupling reagents. Therefore, couple alternative strategies were explored: (i) desalting column and (ii) dialysis to try obtain a pure product.

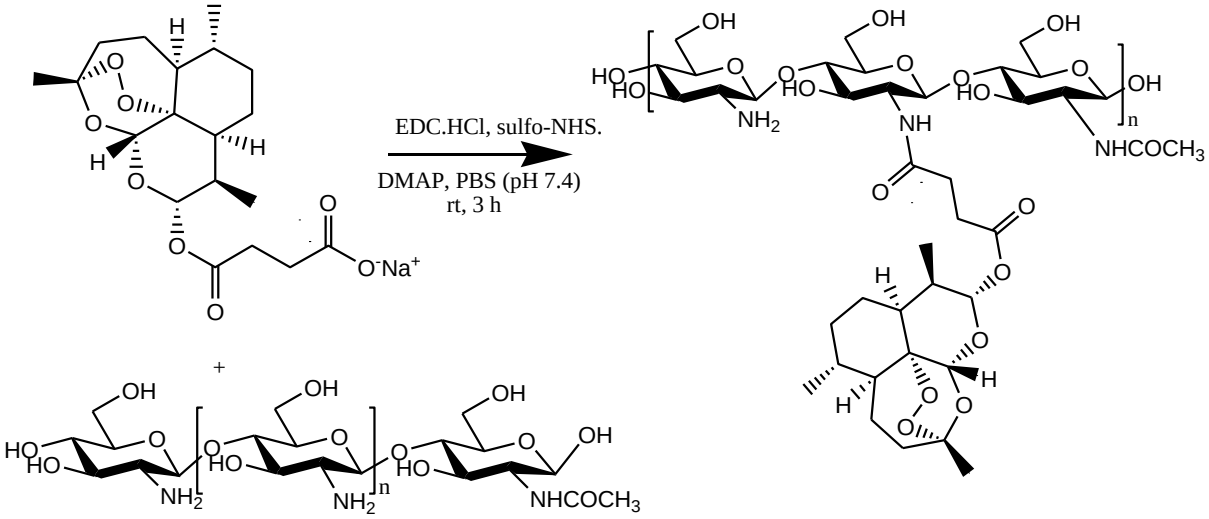

Scheme 3.5: Synthesis of chitosan-Suc-DHA conjugate.

A desalting column separates molecules based on molecular weight with bigger molecules eluting first. However, this method did not deliver a product of higher purity than the precipitation method. A pure compound was realised by gradient-based diffusion dialysis with PBS buffer pH 7.40. Following this step, the peaks of the coupling reagents and other impurities were no longer visible in the ^{1}H NMR spectrum (**Figure 3.19**). ^{1}H NMR and FT-IR spectroscopy were used for structural characterization of chitosan-Suc-DHA conjugate: ^{1}H NMR spectrum of chitosan (**Figure 3.19 (b)**) depicted characteristic proton peaks of aldohexose rings of the polysaccharide at 3.8-4.2 ppm, while proton peak at 1.90 ppm is due to acetyl methyl group of chitosan. The conjugate (**Figure 3.19 (c**)) showed the characteristic protons peaks of chitosan at 3.1-3.5 ppm and proton peaks of DHA-Suc at 0.77-2.9 ppm. The formation of an amide bond was seen by appearance of a new peak at 8.32 ppm suggesting a

secondary amide proton. FT-IR spectra in **Figure 3.20 (c)** also confirmed this by appearance of absorption peaks at 1706.6 cm^{-1}, 1643.1 cm^{-1}, 1555.9 cm^{-1} due to to carbonyl (C=O) stretching and N-H bending respectively.

The synthesized PEG-Suc-DHA had drug functionalization of 2mol% and chitosan-Suc-DHA had a drug loading of 12 mol% respectively determined using ^{1}H NMR spectra. This was done by comparing the ratio of integrated methylene proton for PEG (repeating units), chitosan characteristic peaks observed at 3.8- 4.2 ppm which are signals attributed to aldohexoses rings of the polysaccharide. These peaks are compared to the methyl proton peaks of DHA-Suc observed at 0.7-0.9 ppm. The percentage drug functionalization for PEG is lower compared to drug loading of chitosan. This is because the PEG used has two attachment points, while chitosan has repeating glucosamine units that allow higher drug loading capacity.

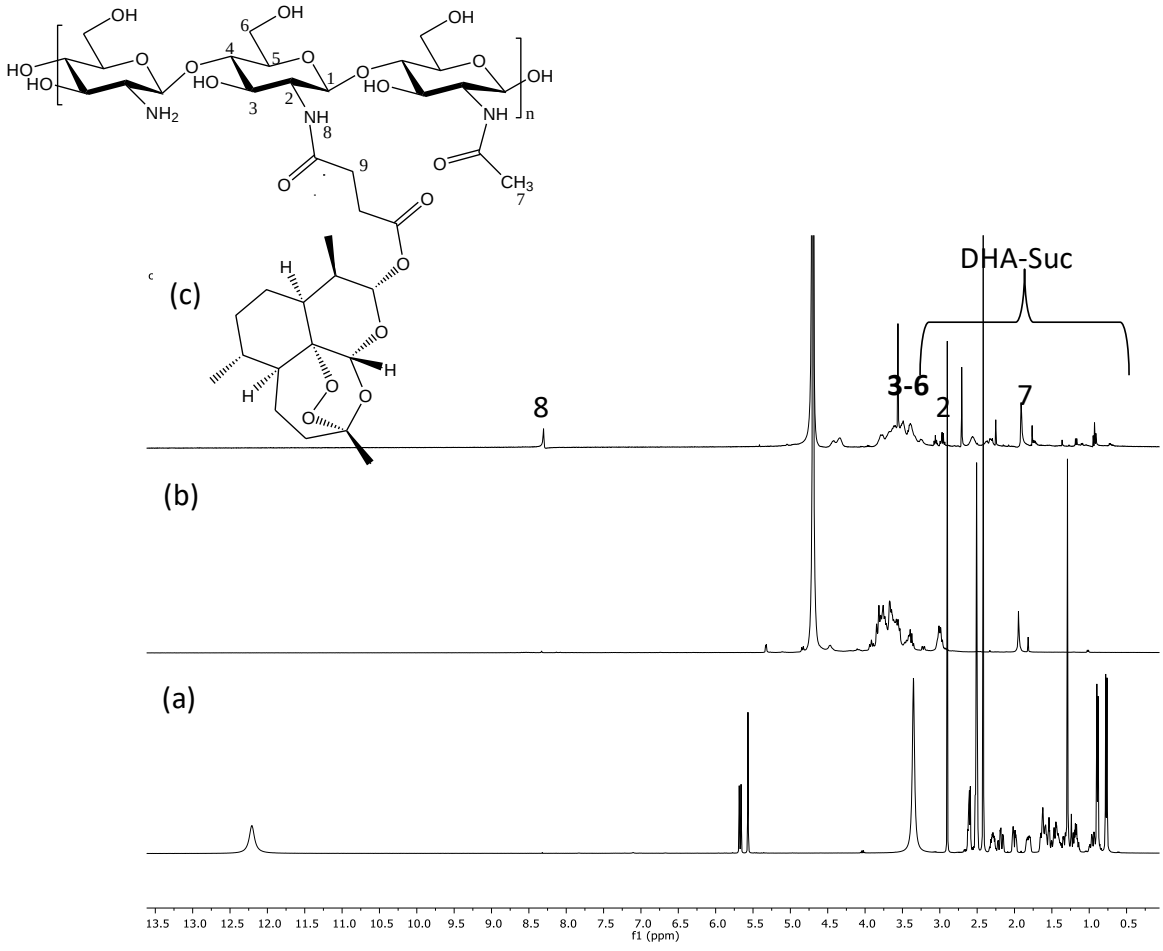

Figure 3.17: ^{1}H NMR Spectra of (a) DHA in DMSO-d_6, (b) chitosan (c) chitosan-Suc-DHA in D_2O.

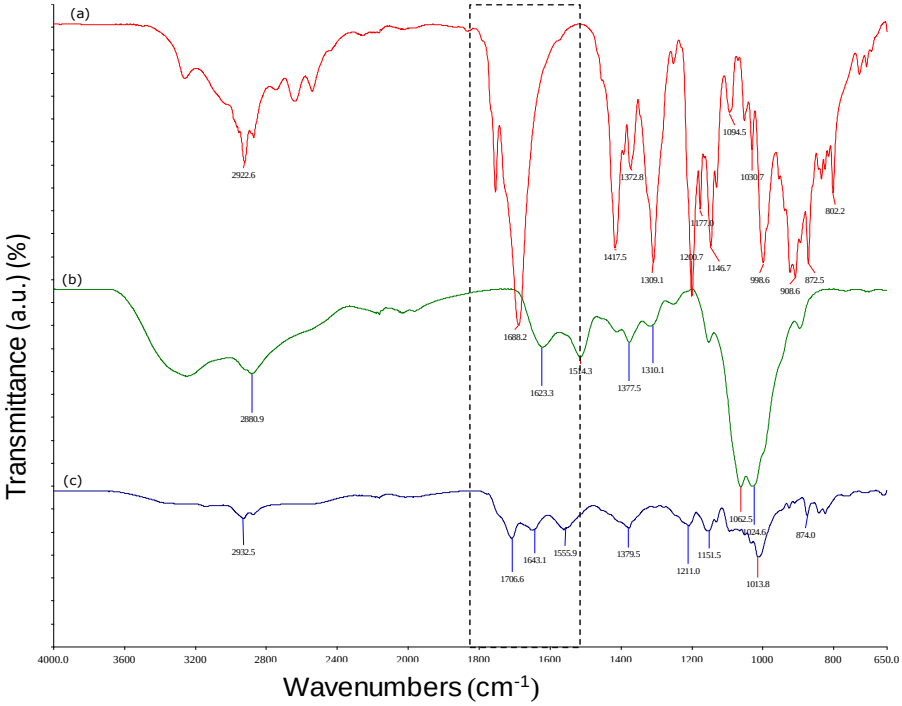

Figure 3.18: FT-IR spectra of (a) DHA-Su (b) chitosan and (c) chitosan-Suc-DHA conjugate.

3.2.4.2 Shape, Particle Size Distribution and solid material characterization of DHA-Suc polymer conjugates.

The TEM micrographs (**Figure 3.21 (a)**) revealed monodispersed spherical particles with an average size diameter of 26.92±2.36 nm (the white spot due to negatively charged phosphotungstic acid stain), while DLS showed a hydrodynamic size of 106.03±2.30 nm for PEG-Suc-DHA as shown in **Figure 3.21 (b)** and summarised in **Table 3.3:** Dynamic light scattering and Zeta potential of DHA-Suc polymer conjugates.**.** The chitosan-Suc-DHA conjugate showed irregular shaped particles with 29.89±5.23 nm with hydrodynamic size 125.7±8.95 nm as shown in **Figure 3.22**(**a-b**). The particle histogram (**b**) exhibited a skewed distribution towards formation of the particle size bigger than the average diameter. The because of agglomeration of the particles as seen in the chitosan conjugate TEM image. The DLS size are ideal for avoiding reticuloendothelial system clearance. The particles had a PDI less 0.4, this means in suspension the particles have a monodisperse size distribution. The zeta potential indicated that both conjugates were unstable at PBS 7.40 at 25 °C (**Table 3.3**) this could be due to aggregation, coagulation and flocculation of the material (Manaia et al. 2017).

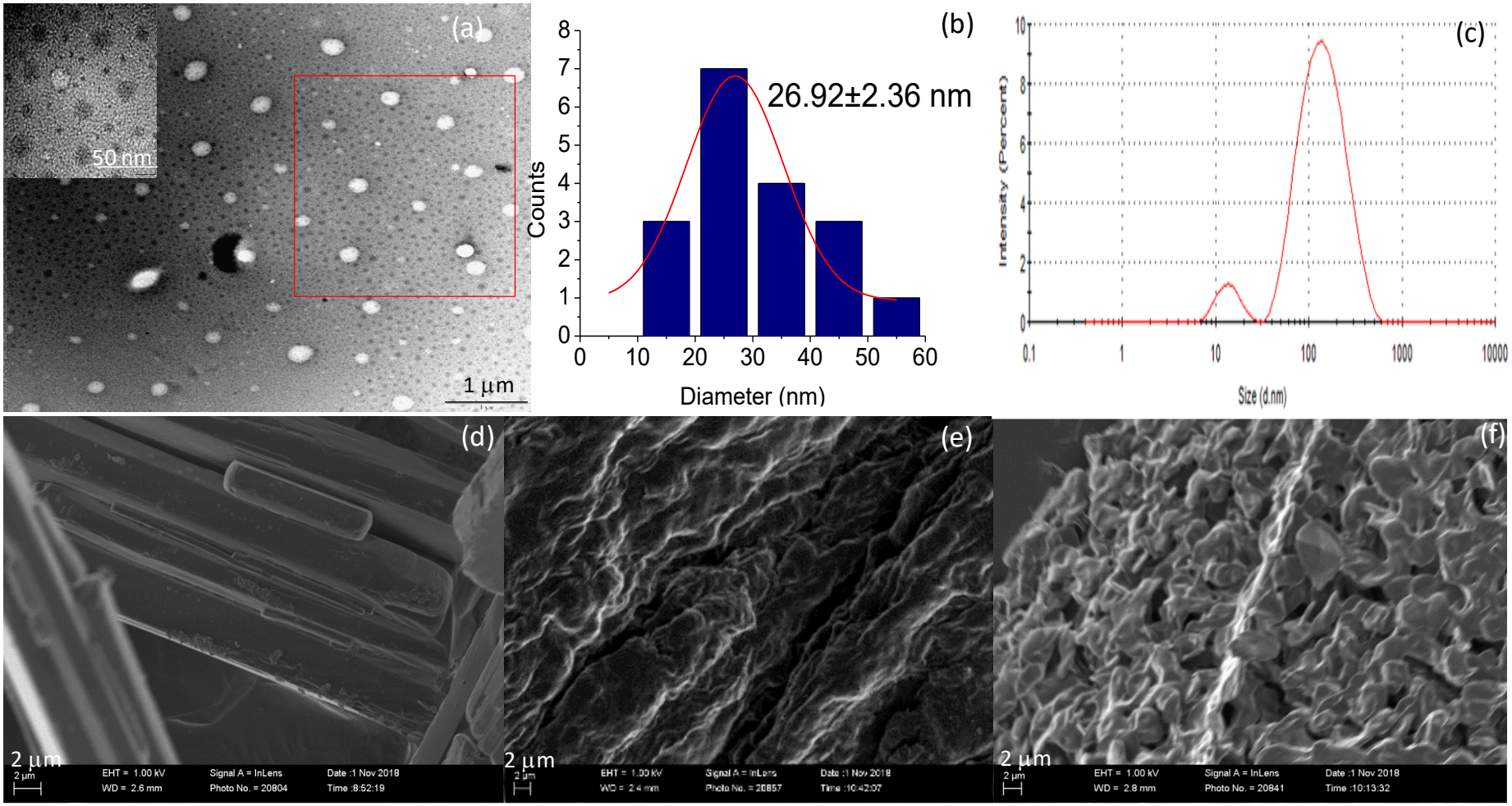

Figure 3.19: (a) TEM image, (b) Particle size distribution histogram, (c) DLS size, and SEM images of (d) DHA-Suc, (e) PEG, and (f) PEG-Suc-DHA conjugate.

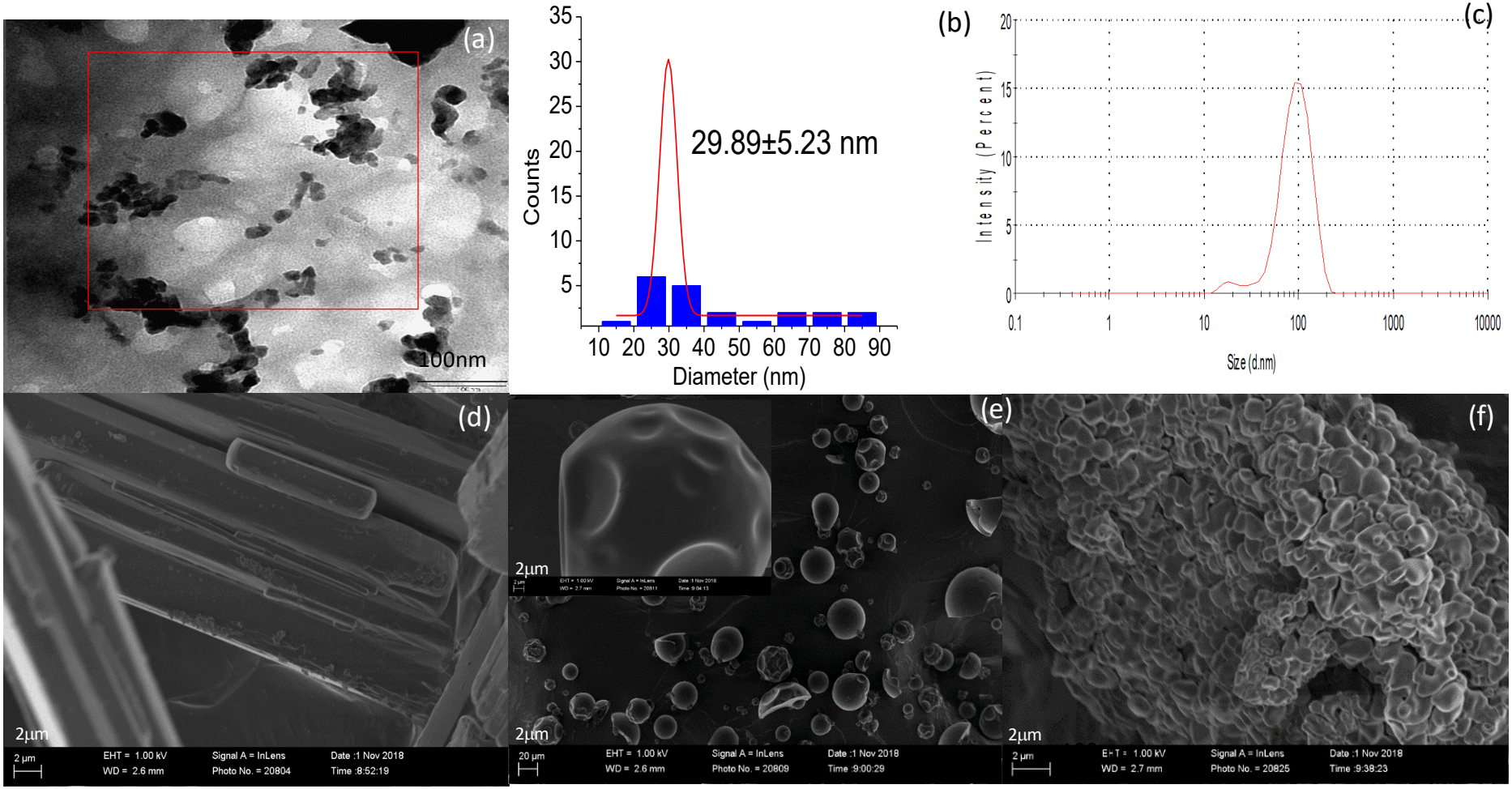

Figure 3.20: (a) TEM image, (b) Particle size distribution histogram, (c) DLS size, and SEM images of (d) DHA-Suc, (e) chitosan and (f) chitosan-Suc-DHA conjugate.

Table 3.3: Dynamic light scattering and Zeta potential of DHA-Suc polymer conjugates.

Parameters tested	PEG-Suc-DHA	Chitosan-Suc-DHA
Particle size distribution	106.03±2.30 (d.nm)	105.6±8.95 (d.nm)
PDI	0.387±0.007	0.276±0.020
Zeta potential	-1.55±1.60 (mV)	10.40±0.002 mV)
TEM size	26.92±2.36 (nm)	29.89±5.23 (nm)

Changes in physical structure of the polymer and drug upon conjugation were studied using SEM shown in **Figure 3.21(d-f)** and **Figure 3.22(d-f)** for PEG-Suc-DHA and chitosan-Suc-DHA respectively. The PEG conjugate showed irregular, amorphous particles and chitosan conjugate showed agglomerated irregular shaped particles. The SEM micrograph of the conjugates did not display crystalline morphology of the free drugs, indicating the absence of free drugs and further revealing that upon conjugation there was a change in the physical characteristic of the drug and polymer. These SEM results were complemented by the physical change observed in the PXRD.

The PXRD spectral analysis of the drugs and conjugate was studied to determine their physical changes. **Figure 3.23** shows PXRD of the PEG-Suc-DHA (i) and chitosan-Suc-DHA (ii)**,** as expected DHA showed sharp peaks indication crystalline nature as also seen with the SEM images. The PEG is also crystalline in nature, while chitosan is amorphous with broad peaks at 2θ =10.0° and 20.0° which are typical peaks for Chitosan (Smith, 1986). Upon conjugating DHA to either PEG or chitosan conjugate **(c)** reduced characteristic peaks of the DHA, PEG-suc-DHA and chitosan-Suc-DHA were observed. Indicating disruption of the physical nature of DHA-suc upon conjugation with PEG or Chitosan, this is also supported by the change in morphology observed in SEM images.

Thermal stability of the conjugates were analysed using TGA and DSC, the thermograms are shown in **Figure 3.24**. The changes in the temperature and also in endotherm peaks upon conjugation will give information about the stability and interaction of the drug with polymer (Monajjemzadeh et al. 2015). TGA thermogram in **Figure 3.24(a)** showed thermal stability until 259 °C to 381°C having weight loss of 88.0 % due to decomposition of amine. DHA-Suc

TGA thermogram showed to have decomposition between 113 °C and 240 °C due to decomposition of the compound with a weight loss of 84 %. The PEG-Suc-DHA conjugate weight loss occurred in 3 steps at 63 °C, 168 °C and 310 °C with weight loss of 2.62 %, 27.30 % and 54.15 % respectively. These are attributed to loss of moisture or water molecules, also due to the decomposition of the drug, thus decomposition of the amide bond (Nagarajan et al. 2009) and thermal decomposition of the polymer backbone. The results show that the conjugate had lower thermal stability than the pure drug and polymer. This may be due to the particles having greater surface area since they are more reactive than the polymer as the conjugate is now in a nano-range, therefore decomposition occurs quicker (Mainardes, Gremião and Evangelista, 2006). These results were also observed in DSC thermogram (**Figure 3.24 c**), as the conjugate showed a shift of the PEG endothermic peaks from 52.24 °C to 45.21 °C and also a shift in the DHA-Suc from 136.46 °C to 108.93 °C indicating low thermal stability.

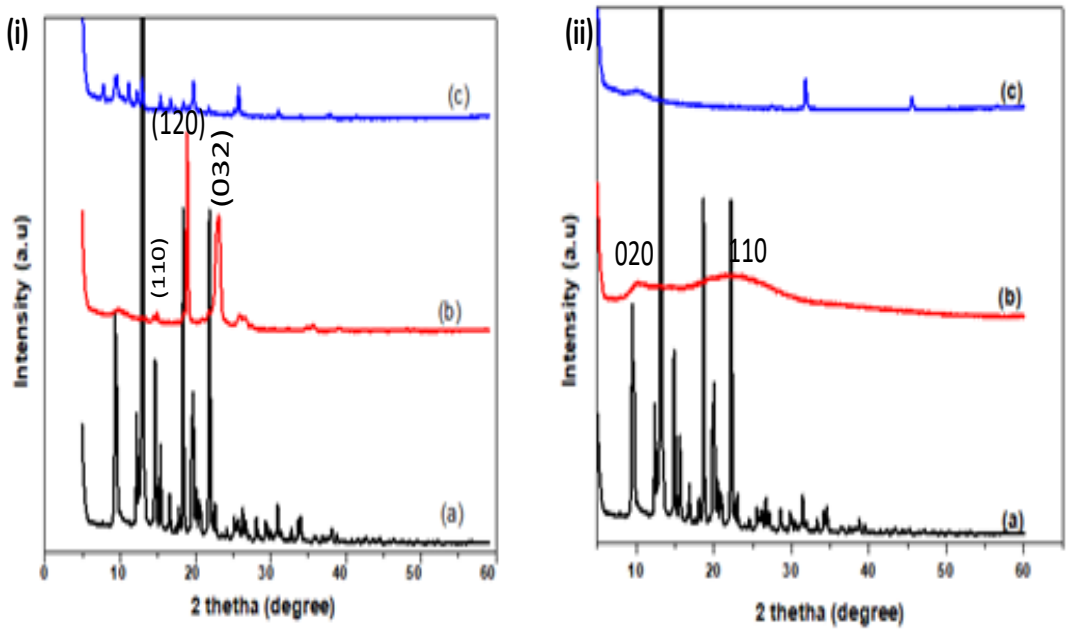

Figure 3.23 (i): X-ray diffraction of (a) DHA-Suc, (b) PEG and (c) PEG-Suc-DHA, **(ii)** (a) DHA-Suc, (b) Chitosan and (c) Chitosan-Suc-DHA.

The TGA thermogram of pure chitosan (**Figure 3.24 (b)**) show that this polymer goes through two stages of weight loss in the range of 46 °C to 398.47 °C (Mainardes, Gremião and Evangelista, 2006). The first weight loss (0.004 %) is due to loss of absorbed water molecules from 46 °C to 100 °C. There was thermal degradation of chitosan 184.24 °C to 398.47 °C with weight loss of about 70 %. The conjugate showed more thermal stability by having a weight

loss of 12 % at 280.13 °C to 454.7 °C. This was also supported by the shift in the endotherm peak of DHA-Suc to 153.25 °C from 136.46 °C in the DSC thermogram. The TGA and DSC results support that upon conjugation there is a change in the physical nature of the conjugate as also seen in the SEM micrograph and PXRD.

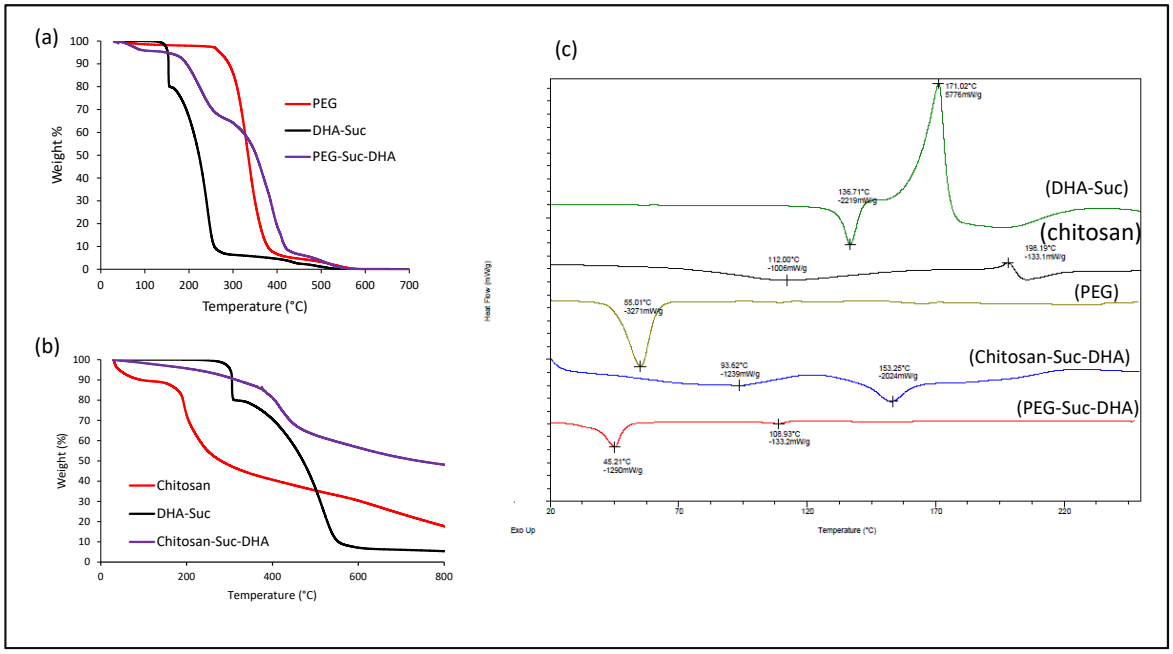

Figure 3.21: TGA thermograms of (a) PEG-Suc-DHA, (b) Chitosan-Suc-DHA and (c) DSC thermograms of conjugates.

3.3 Cytotoxicity studies

The conjugates were submitted for *in vitro* cytotoxicity, these studies were done to compare the potency of the free drug and polymer-drug conjugates. The cytotoxicity of the free BA and PEG-BA were evaluated using a pancreatic cancer cell line (MIA PaCa-2) and for healthy cells, Vero cells were used (**Figure 3.25**). PEG-BA showed lower IC_{50} values than the free BA for both cell types, indicating an enhanced potency from conjugation. For the MIA PaCa-2, the Peg-BA had IC_{50} =1.36±0.11 µM and it was IC_{50} = 9.84 ±0.10 for the Vero cells (**Figure 3.25** and **Table 3.4**) indicating that upon conjugation with PEG, BA became more potent. Furthermore, both BA and PEG-BA were less toxic to normal cells, showing great specificity to cancer cells.

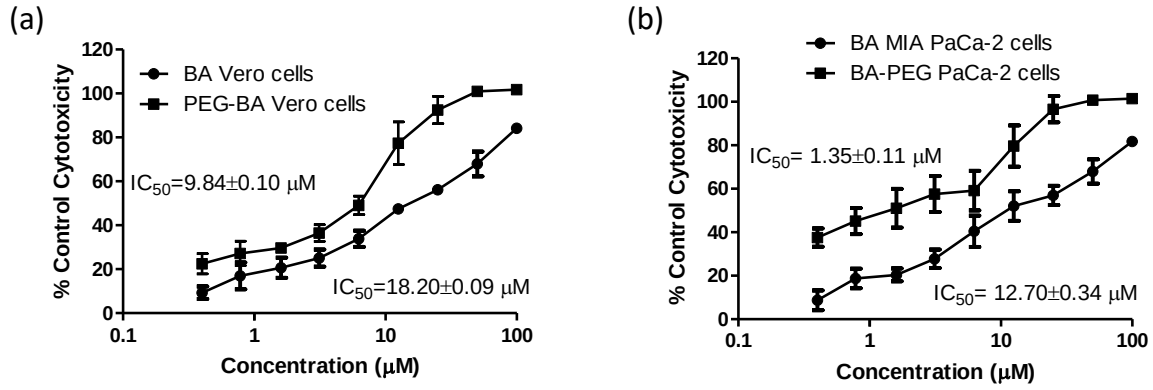

Figure 3.22: The effect of different concentration (µM) of BA and PEG-BA conjugate on the viability of (a) Vero cells and (b) MIA PaCa-2.

Analysis of *in vitro* cytotoxicity for the DHA conjugates illustrated in **Figure 3.26** and **Table 3.4** showed that the conjugates PGE-Suc-DHA (7.88±0.20) and chitosan-Suc-DHA had lower IC_{50} compared to free DHA (12.76±0.30) for MIA PaCa-2 cells indicating that a higher concentration of DHA was needed to kill 50 % of the MIA PaCa-2 cells than the conjugate i.e. the potency of the free drug was improved by conjugation. Interestingly, DHA and PEG-Suc-DHA were more toxic for the normal cells, indicating less specificity to MIA PaCa-2 cells compared to the chitosan-Suc-DHA which was more toxic to cancer cells. Conjugation of DHA to chitosan reduced it's toxicity to normal cells which holds promise for anti-malarial applications in addition to anti-cancer applications.

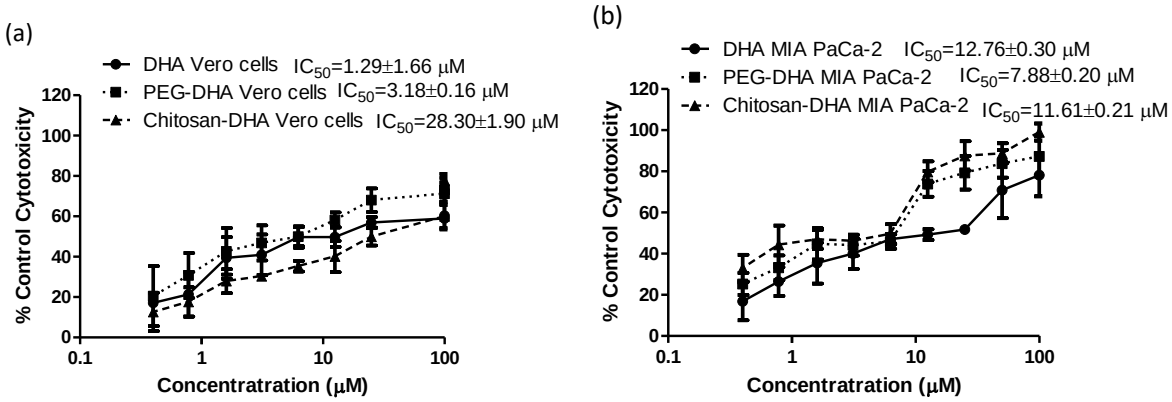

Figure 3.23: The effect of different concentration (µM) of DHA, PEG-Suc-DHA, and Chitosan-Suc-DHA on viability of (a) Vero cells and (b) MIA PaCa-2 cells.

Table 3.4: Summary of the cytotoxic studies showing the IC_{50} of the polymer-drug conjugates.

	IC_{50} values (µM)	
Compound name	***MIA PaCa-2***	***Vero cells***
BA	12.70 ±0.34	18.20±0.09
PEG-BA	1.36±0.11	9.84 ±0.10
DHA	12.76±0.30	1.29±1.66
PEG-Suc-DHA	7.88±0.20	3.18±0.16
Chitosan-Suc-DHA	11.61±0.21	28.30±1.90

3.4 Conclusion

The physico-chemical properties of the synthesized PEG and chitosan conjugate were evaluated in this work. Proton NMR and FT-IR spectroscopy showed successful conjugation by shifting in proton or appearance of a new absorption peak respectively. Due to the hydrophobicity of the drug, NMR spectra of PEG-BA conjugate in aqueous solvent suggested that the conjugate could be a micellar or globular structure as the proton peaks of the drugs were not visible. All the synthesized hydrodynamic size less than 130 nm, these size are ideal to avoid reticuloendothelial system clearance. PXRD, DSC and TGA further showed that upon conjugation, the structure and thermal properties of the polymer were changed forming amorphous particles. The chemical changes resulted in a decrease in the concentration needed to kill 50% of the MIA PaCa-2 cells for all the polymer-drug conjugate compared to the free drug. These results suggest that upon conjugation, the pharmacological activity of the natural-derived compounds could be improved.

Chapter Four:
Synthesis of polymer conjugates for antimalarial combination therapy drugs

4.1 Introduction

The World Health Organization (WHO) recommends artemisinin-based combination therapy (ACT) for the treatment of uncomplicated malaria caused by *P. falciparum* (World Health Organization, 2015). Combination is a general term normally used in therapeutics as the simultaneous administration of two or more pharmacologically active agents (Yap, Omlin and De Bono, 2013; Mokhtari et al. 2017). In malaria chemotherapy, two or more blood schizontocidal drugs with independent modes of action are used. This is to prevent or delay drug resistance and the commonly used ACT is Coartem®, which is a combination of a fast-acting drug artemether with lumefantrine (Lum). Artemisinin and its derivatives provide rapid relief of the clinical symptoms but must be co-administered with a slow acting agent when treating uncomplicated malaria. Coartem (artemether [20 mg] + lum [120 mg]) is administered orally twice a day for a period of three days (Agtmael, 2017; Djimdé and Lefèvre, 2009). Complicated or severe malaria, where the patient cannot ingest ACT orally, is first given injectable intravenous (I.V.) artesunate (DHA-Suc discussed in **Chapter 3**) for at least 24 h. Lum is not water soluble and cannot be administered at this stage using I.V. Therefore, artesunate I.V. is followed by a 3 day course of coartem (World Health Organization, 2016). Polymer drug conjugation as a delivery technology offers an alternative route to increase the solubility of the drugs to be administered using I.V. for severe malaria.

The WHO, recommends addition of PQ (0.25 mg per kg) to current regimens to prevent transmission by acting against the gametocytes. It is also used to prevent relapse of malaria for *P. ovale* and *P. vivax*. It is the toxicity of the PQ that limits its clinical use, the most serious side effect is hemolysis in individuals with Glucose-6-phosphate dehydrogenase (G6PD) deficiency (World Health Organization, 2012). In addition to its toxicity, it is readily absorbed, metabolized (converted to carboxyprimaquine) and eliminated. Carboxyprimaquine has a 10 times higher plasma level than the parent drug but is less potent (Azad et al. 2017; Chairat et al. 2018). It has been shown that only 30% of PQ reaches the liver after I.V. injection into the

mice ((Pirson, Steiger and Trouet, 1982). Due to these limitations prolonged doses are required which amplifies toxicity.

Chapter 3 described the use of PEG to synthesize water-soluble conjugates for intravenous delivery of nature derived medicinal products. However, PEG has only two terminal functional groups for attachment of drugs, which limits the drug loading potential. Radial or branched PEG architectures have been developed to address this but often the branched polymers have less than ten points of attachment. Dai and colleagues used a 4-arm PEG and an 8-arm PEG as the polymeric carrier for DHA and BA, respectively (Dai et al. 2014). Increasing the valency of the polymeric carrier allows for higher drug loading, which is important for drugs that may require higher dosing.

In this chapter, two multivalent water-soluble polymers, poly(*N*-acryloylmorpholine) macromonomers-co-acrylic acid (p(NAM-stat-AA)) and polyglutamic acid (PGA), were investigated as carriers for the antimalarial drugs DHA, Lum and PQ which make up the WHO's triple combination therapy for the treatment of uncomplicated malaria. Multivalency also allows for drugs to be combined on a single polymer chain but this combination strategy is not ideal for the three-drug combination investigated here as they have different sites of pharmacokinetic activity. As the active metabolite of other artemisinin derivatives like artemether and artesunate, the strategic and rational delivery of DHA (active metabolite of artemisinin) will be directed to the asexual stage of the *Plasmodium* parasite to elicit rapid relief of clinical symptoms and patient stabilization. This will be used in combination with Lum, which is a longer acting agent in the ACT for the removal of residual parasite remaining after treatment with DHA. The third drug, primaquine, is administered as a transmission blocker and it acts against the sexual, gametocyte stage. It will therefore not be a prudent design to combine any two of the drugs on a single polymer but multivalency is important for increasing the amount and concentration of the drugs at the target sites.

PGA is non-toxic, edible, non-immunogenic, non-mutagenic and unlike PEG and p(NAM-stat-AA) it is also biodegradable (Bajaj and Singhal, 2011; Luo et al. 2016; Ogunleye et al. 2015). PGA was conjugated to various anticancer drugs like paclitaxel and camptothecin that went into clinical trials (Pang et al. 2013). Compared to the PEG conjugate, the camptothecin conjugated to PGA had enhanced aqueous solubility due to the charged nature of the polymer

compared to PEG which is a neutral polymer. This means less PGA is needed to deliver a fixed dose of the drug.

The p(NAM-stat-AA) is an amphipathic copolymer made of neutral hydrophilic acrylamide monomer and this polymer can be used as an alternative for PEG. Similar to PEG this polymer is biocompatible, non-biodegradable and is soluble in a wide range of aqueous or organic solvents (Sartore, Vic and Ranucci, 1997; Anastasaki et al. 2014; Chamignon et al. 2016). It has also shown low toxicity and low incidence of provoking immunological reaction *in vivo* (Jo et al. 2008). Compared to linear or branched PEG, p(NAM-stat-AA) has higher structural stability and longer blood circulation (Schiavon et al. 2000). Similar to PGA, p(NAM-stat-AA) also has more points of attachment depending on the molecular weight of the polymer. Even though this polymer has been suggested as an alternative for PEG, few studies have been reported for its use more especially as a delivery system for malaria. Therefore, in this chapter p(NAM-stat-AA) and PGA will be conjugated to DHA, Lum and PQ as intravenous combination therapy for malaria.

The aims of this chapter are to synthesize conjugates for malaria triple combination therapy using multivalent polymers (p(NAM-stat-AA) and PGA) and also to characterize their physio-chemical properties.

4.2 Results and discussion

4.2.1 Synthesis of p(NAM-stat-AA) conjugates.

4.2.1.1 p(NAM-stat-AA)-DHA conjugate.

The p(NAM-stat-AA) used to conjugate DHA has 21 carboxylic acid functional groups (20 intra-chain and one terminal), which could be activated for conjugation to DHA via an ester link (**Scheme 4.1)**. 20-molar equivalents of DIC to p(NAM-stat-AA) were used to activate the carboxylic acids. Only 4 molar equivalents of sulfo-NHS were used because this stabilization reagent is recovered after substitution by DHA. DIEA was used to adjust the pH of the reaction to basic as the carbodiimide reaction proceeds more favourably under basic conditions (Hermanson, 2008). After 24 h, the crude conjugate was purified by gradient-based diffusion dialysis using a cellulose membrane (MWCO = 12 kDa) in PBS buffer (pH = 7.40) for 3 days. The pure conjugate was dried by lyophilisation to obtain a white powder.

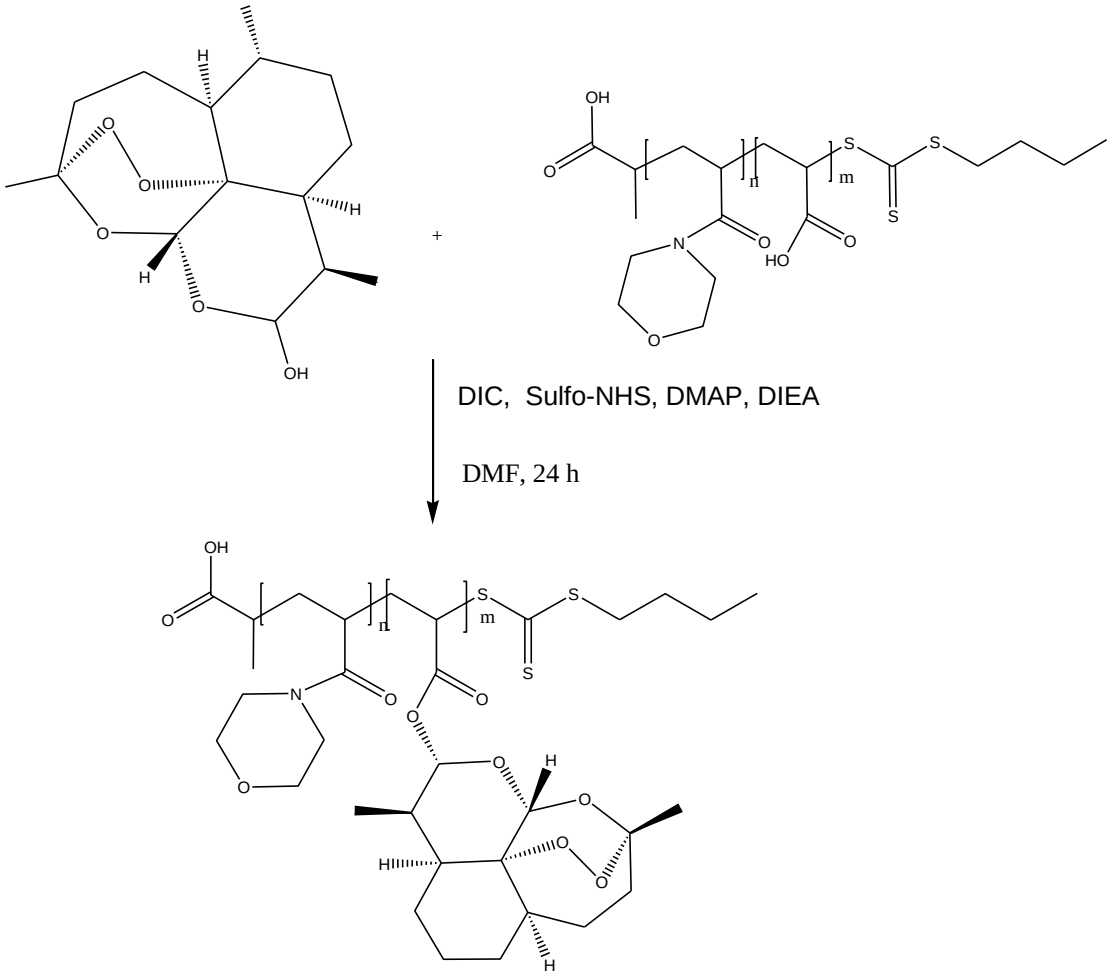

Scheme 4.1: Synthesis of p(NAM-stat-AA)-DHA conjugate.

Analysis of the ^{1}H NMR spectrum (**Figure 4.1**) suggested there could be conjugation by absence of the interchangeable anomer proton peaks of the DHA at 4.75 ppm and 5.60 ppm as one epimer is favoured as discussed in **Chapter 3** and the corresponding appearance of the doublet at 6.59 ppm. These results are similar to when DHA was converted to DHA-Suc, suggesting successful conjugation of the polymer to the drug. Also due to conjugation, there is broadening of the drug peaks downfield as the drug peaks are mixed with the broad peaks of the polymer. The FT-IR spectrum cannot confirm conjugation as it is not easy to distinguish between the carbonyl (C=O) stretching frequency absorbance at 1614 cm^{-1} for the carboxylic acid in the polymer and ester in the conjugate as seen in **Figure 4.2 (b)-(c).**

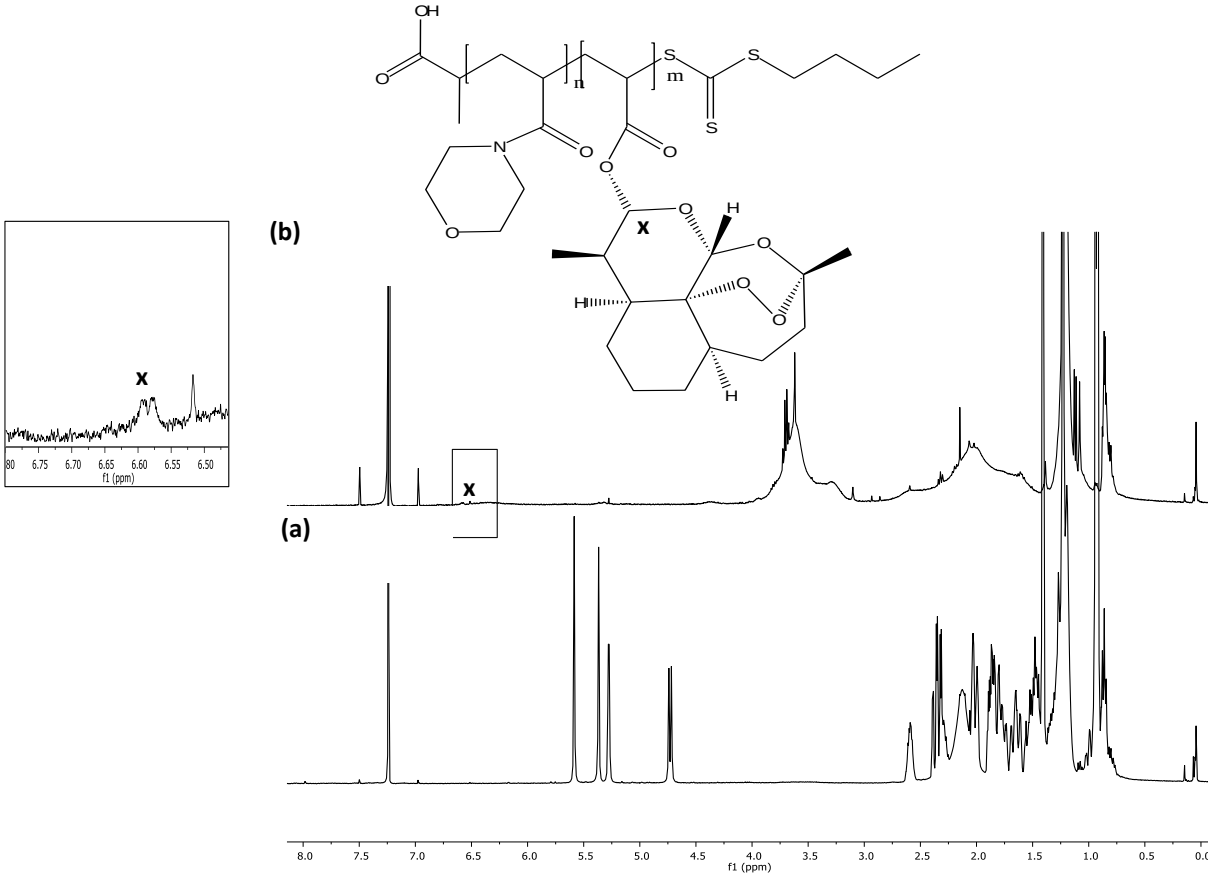

Figure 4.1: ^{1}H NMR (400 MHz, in $CDCl_3$) spectrum of (a) DHA and (b) p(NAM-stat-AA)-DHA. conjugate.

.

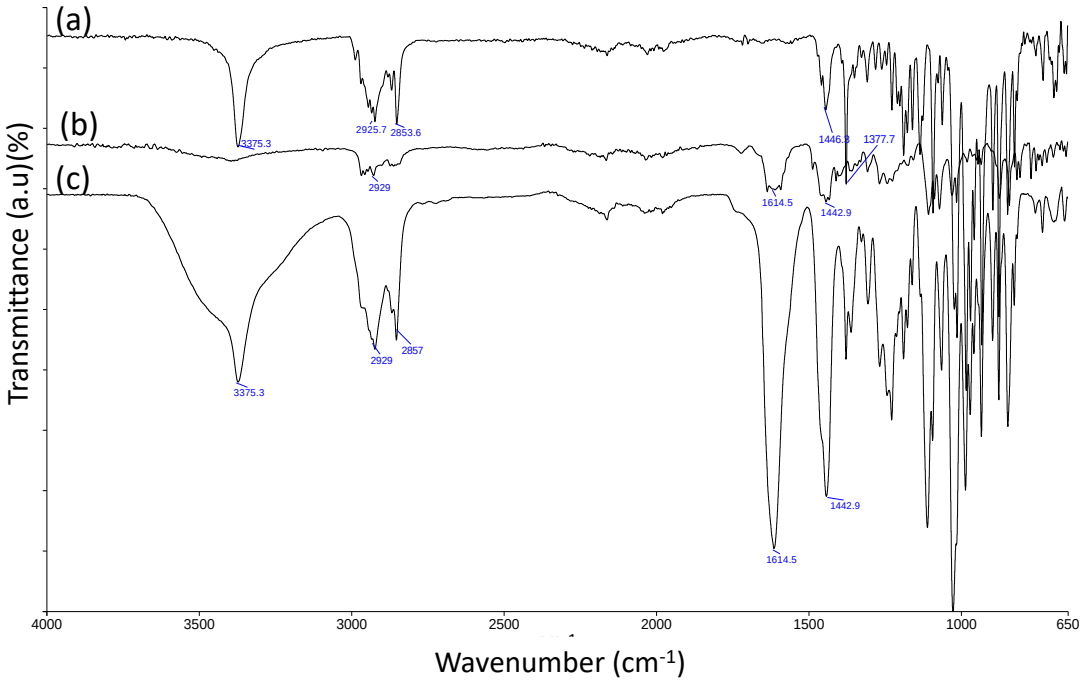

Figure 4.2: FT-IR spectra of (a) DHA, (b) p(NAM-stat-AA) and (c) p(NAM-stat-AA)-DHA conjugate.

.

The percentage drug loading was determined to be 4.0mol% from the ratio of the integrated peaks of DHA (methyl terminal protons) and p(NAM-stat-AA) proton peaks at 3.5 to 3.9 ppm in the ^{1}H NMR ($CDCl_3$) spectrum (**Figure 4.1**) This is a very low drug loading given that DHA was reacted at 15 molar equivalents. This poor loading may be attributed to the steric hindrance that would be encountered by the DHA molecules conjugating to carboxylic acids on adjacent methine carbons. With no spacer carbons on the chain, several carboxylic acids proximal to a conjugated DHA would be prohibited from reacting with another DHA molecule.

The poor loading could be suggesting a need to optimize the synthesis method using a different coupling agent under different conditions. It could also imply that p(NAM-stat-AA) will not be suitable for a drug such as DHA that is relatively easy to solubilize. With about 90% of the repeating units of p(NAM-stat-AA) not conjugatable but serving as the water-soluble moiety, the polymer will not offer significant advantage over other more established drug carrier polymers like PEG or even small alkyl chains such as succinic acid.

4.1.1.1 p(NAM-stat-AA)-Lum conjugate.

Lum has an aqueous solubility of about 2.6 x 10^{-9} g/mL, which is six orders of magnitude lower than the 0.15 x 10^{-3} g/mL solubility of DHA. Solubilizing Lum to a therapeutically significant concentration by conjugation to a small molecule like succinic acid had not been successful. The first water soluble Lum conjugate has been reported by Fortuin et al. (2020), as they conjugated it using copolymer of poly(*N*-vinylpyrrolidone) and poly(α-allylvalerolactone). In this work p(NAM-stat-AA), with its long water-soluble block, was deemed suitable for solubilizing multiple molecules of Lum to obtain a therapeutically significant aqueous concentration of the drug.

p(NAM-stat-AA) was conjugated to the secondary hydroxyl group of Lum in a chemical reaction similar to the p(NAM-stat-AA)-DHA experiment and with the same stoichiometry of reagents (**Scheme 4.2**). The crude product was purified by concentration gradient dialysis with cellulose membrane (MWCO = 12 kDa) in PBS buffer (pH = 7.40) for 72 h. The pure conjugate was dried by lyophilisation to obtain a yellow powder.

Conjugation was suggested by the downfield shift of the oxymethine proton (5.19 ppm) which is a doublet of doublets, to a broad single peak at 5.55 ppm (**Figure 4.4**). Peak broadening, which is often attributable to interaction of the drug with the polymer, was observed. FT-IR showed a carbonyl peak at 1614.5 cm^{-1} due to carbonyl stretching which is a sharp peak compared to the carbonyl peak of the free polymer **(Figure 4.3**).

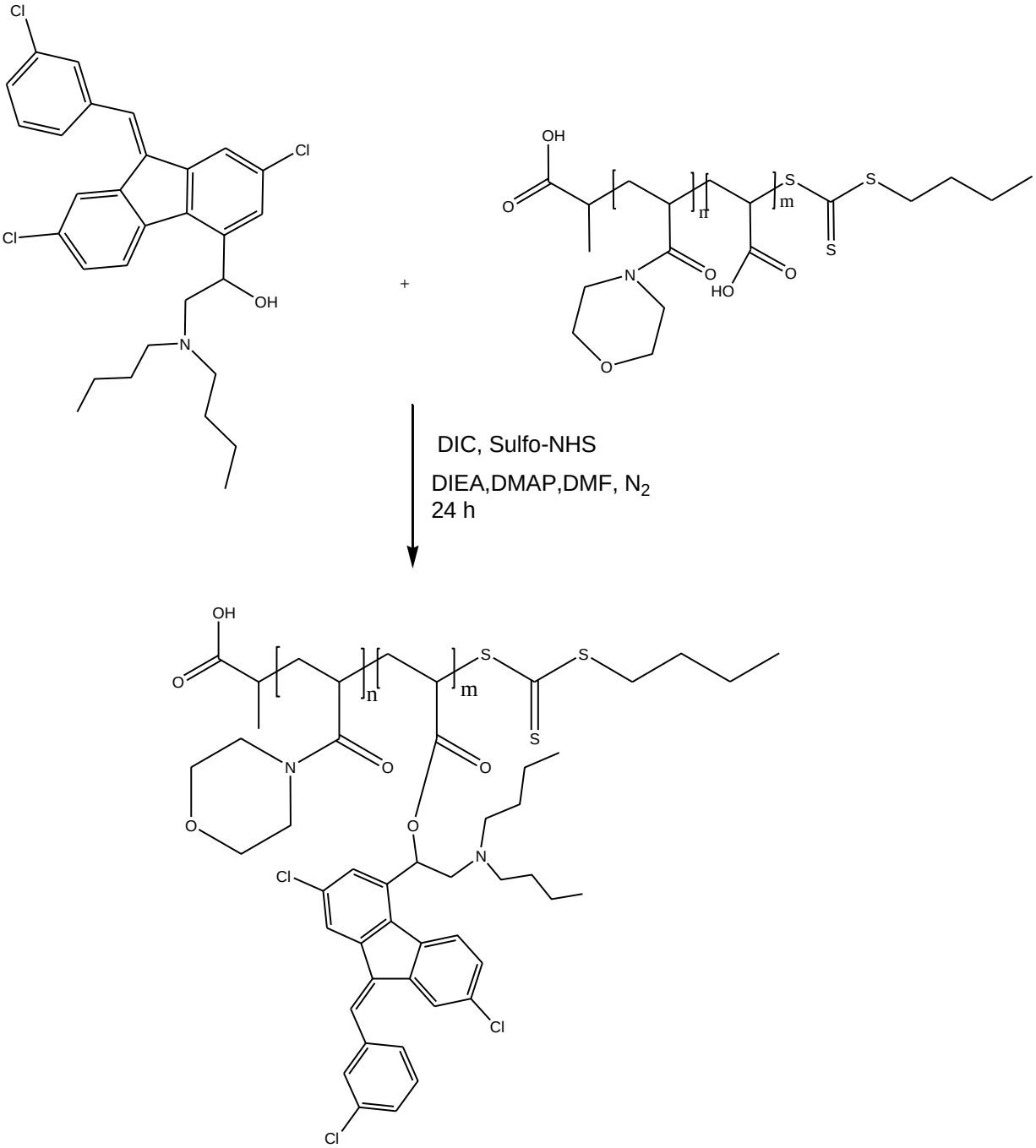

Scheme 4.2: The synthesis of p(NAM-stat-AA)-Lum conjugate.

Another notable observation is that when the p(NAM-stat-AA)-Lum conjugate ^{1}H NMR experiment was conducted in D_2O, the aromatic region protons of the drug were not visible. As explained in **Chapter 3** for the PEG-BA conjugate, this could have been due to either aggregation of the conjugate into micellar assembly (**EXP-I**) or each P(NAM-stat-AA)-Lum

conjugate adopting a globular conformation where the polymer block wraps around the drug-containing block (**EXP-II**).

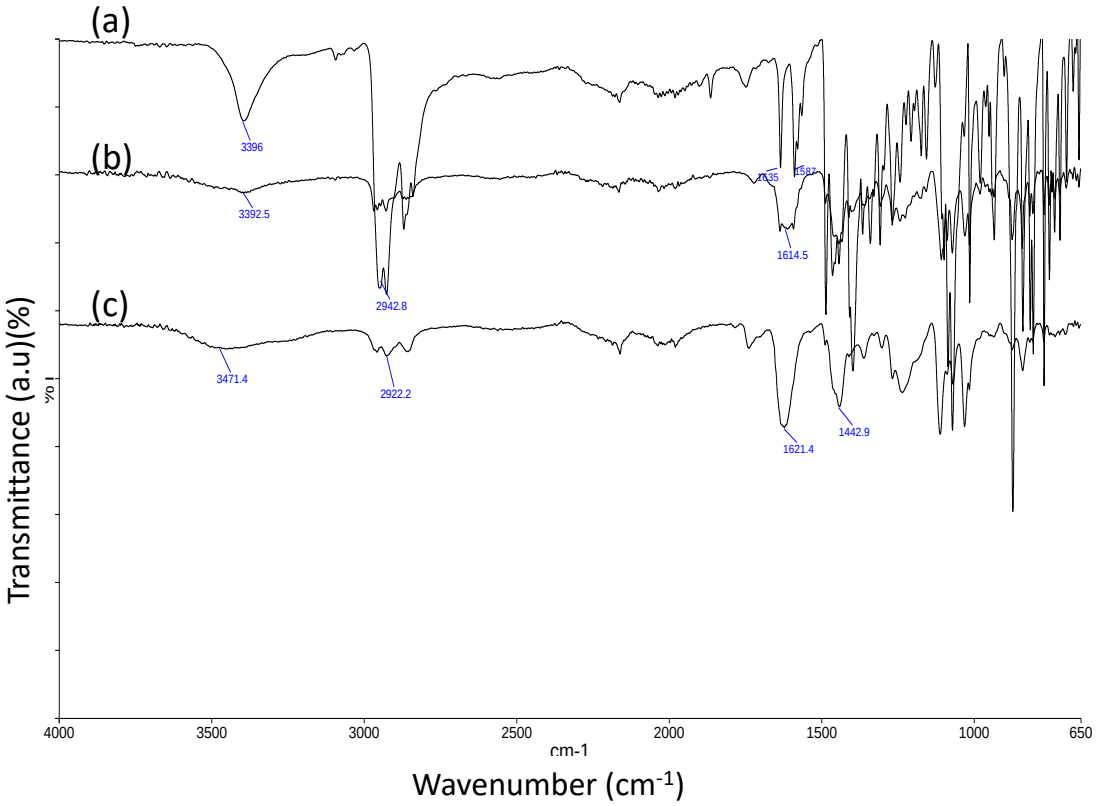

Figure 4.3: FT-IR spectra of (a) Lum, (b) p(NAM-stat-AA) and (c) p(NAM-stat-AA)-Lum conjugate.

The percentage drug loading was determined to be 12.2 mol% using protons marked 13-16 for the polymer and the aromatic (7.0 ppm) and methyl (0.7 ppm) proton peaks of the drug. Although this is about three times higher than the loading obtained for DHA on p(NAM-stat-AA), it is still significantly lower given that 15 molar equivalents of the drug used in the reaction. The same explanation given for the low loading of DHA could also be provided here, i.e. steric hindrance prevents the Lum molecules from occupying all available activated carboxylic acid sites.

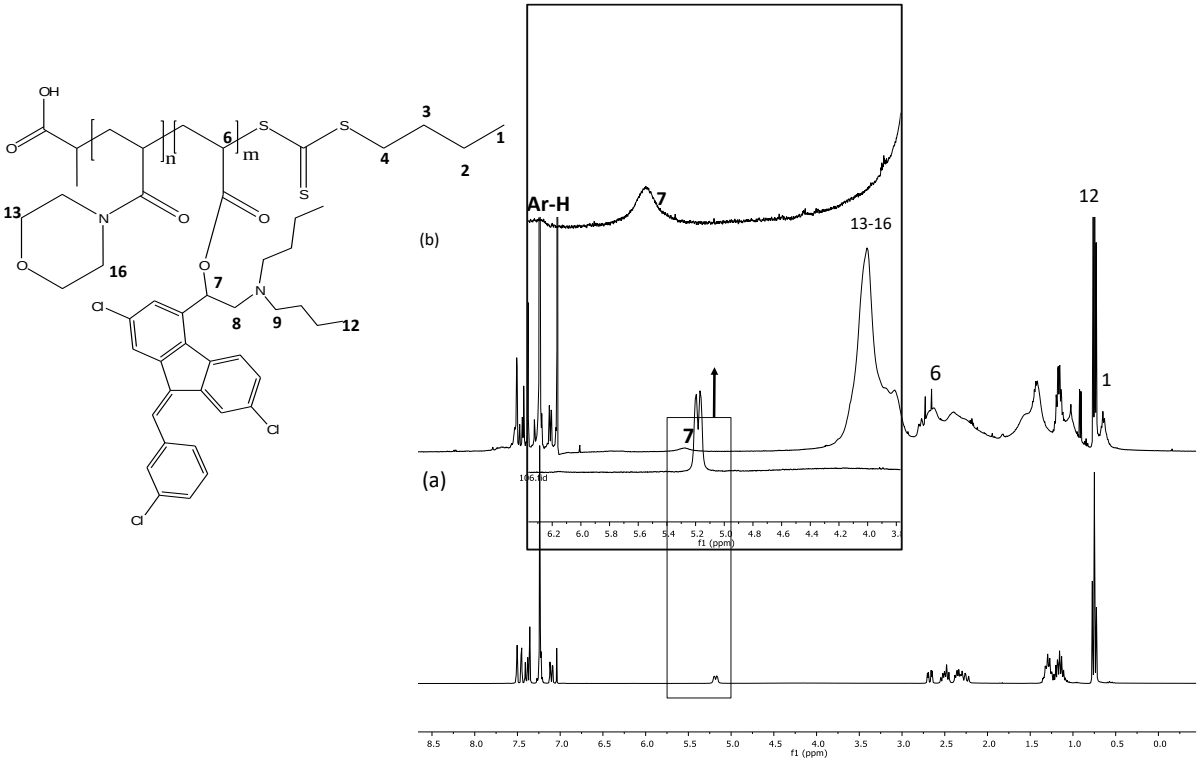

Figure 4.4: ^{1}H NMR (400 MHz in $CDCl_3$) spectrum of (a) Lum and (b) p(NAM-stat-AA)-Lum conjugate.

Lum is administered, orally, in a 6:1 ratio with artemether. It is interesting to note, in this context, the 3:1 drug loading ratios of Lum (12.2 mol%) and DHA (4.0 mol%) on p(NAM-stat-AA). This could make the development of intravenous formulations of these conjugates simpler, especially since this route of administration bypasses the biological barriers of the oral route, i.e. poor gastrointestinal absorption, epithelial membranes and first-pass liver metabolism, that would have informed the high excess of lumefantrine administered. The drug loading of these conjugate might also be improved by changing the synthesis methods.

Another useful NMR experiment to determine conjugation is diffusion ordered spectroscopy (DOSY). DOSY is primarily used to analyse mixtures of small molecules and the oligomeric state of biomolecules. DOSY is a two-dimensional NMR technique that measures the transitional diffusion coefficient of polymers. The diffusion coefficient provides a measure of the polymer hydrodynamic radius through the Stokes-Einstein **Equation 4.1** below. Where k is the Boltzmann constant, T is the absolute temperature, and η is the viscosity of the solvent (Gu et al. 2018).

$$D = \frac{KT}{6\pi\eta RH} \qquad \textbf{Equation 4.1}$$

During a DOSY experiment, a series of NMR spectra are collected at different gradient pulse amplitudes. The rate of signal decay is determined by the diffusion coefficient of the molecule. The diffusion coefficient reveals information about the size, molecular weight and hydrodynamic radius of each molecule in a mixture. For example, small molecules diffuse faster than macromolecules like polymers and their NMR signals decay more rapidly than those of polymers (Li, 2012).

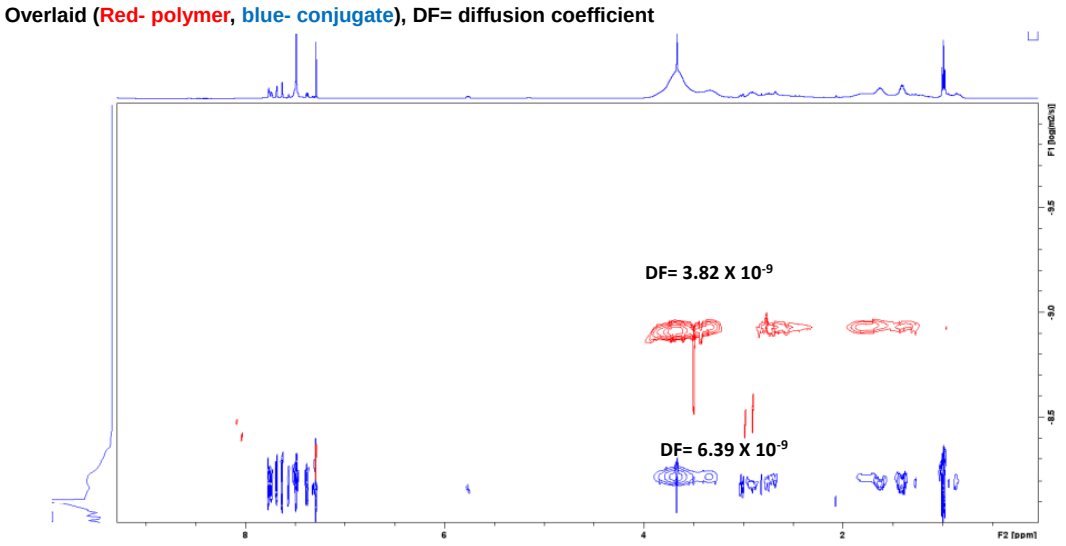

Figure 4.5: Overlaid DOSY-NMR (500 MHz in $CDCl_3$) spectra of p(NAM-stat-AA) (red) and the p(NAM-stat-AA)-Lum conjugate (blue).

DOSY NMR was used to further confirm conjugation of Lum to p(NAM-stat-AA), this analysis provides two-dimensional correlation maps with chemical shifts on the horizontal axis and diffusion coefficients on the vertical axis. NMR signals of nuclei on the same molecule are correlated with the same diffusion coefficient, in the absence of intermolecular interactions or chemical exchange, allowing for differentiation of the NMR signal produced by molecules of different sizes. The DOSY spectrum of the p(NAM-stat-AA)-Lum conjugate in **Figure 4.5** in blue shows that the polymer and Lum drug have the same translational mobility indicating that these molecules are linked together and conjugation was successful, these results are similar to published results by Fortuin et al. (2020). The results further show that the diffusion coefficient for the conjugate is 6.39×10^{-9} which is twice the magnitude of the diffusion coefficient of the

free polymer (DOSY spectrum shown in red), consistent with the expected faster diffusion of smaller molecules.

Solubility of P(NAM-stat-AA)-Lum conjugate

The mass ratio of Lum in the conjugate was detected using UV-VIS spectroscopy. p(NAM-stat-AA)-Lum conjugate was dissolved in deionized water. Lum has three absorbance peaks at 266, 306 and 314 nm, as seen in **Figure 4.6**, while p(NAM-stat-AA) absorbs at 310 nm then the absorbance at 310 nm for p(NAM-stat-AA)-Lum conjugate was determined and used to calculate the solubility of the conjugate. A standard calibration curve with correlation coefficient of 0.99 was obtained from the Lum, the absorbance of Lum corresponds to the concentration (μg/mL, the dilution factor was taken into account) and thus the amount of drug soluble in the sample. The equation of the straight line was used to calculate the solubility of the polymer-drug conjugate. The percentage mass ratio was determined by dividing the known concentration with the measured concentration. At 2 mg/mL, the conjugate solubility is 8 μg/mL, while for 6 mg/mL solubility is 11.82 μg/mL. This means that for 2 mg/mL, about 6 mg/mL of the drug is soluble in water (**Table 4.1)**. This indicates an improvement on solubility of Lum since the unconjugated drug is insoluble in water and the solubility could be higher as you increase concentration as 6 mg/mL is not the point of saturation for the conjugate. These results give the possibility of Lum being injected together with artesunate for the treatment of complicated malaria.

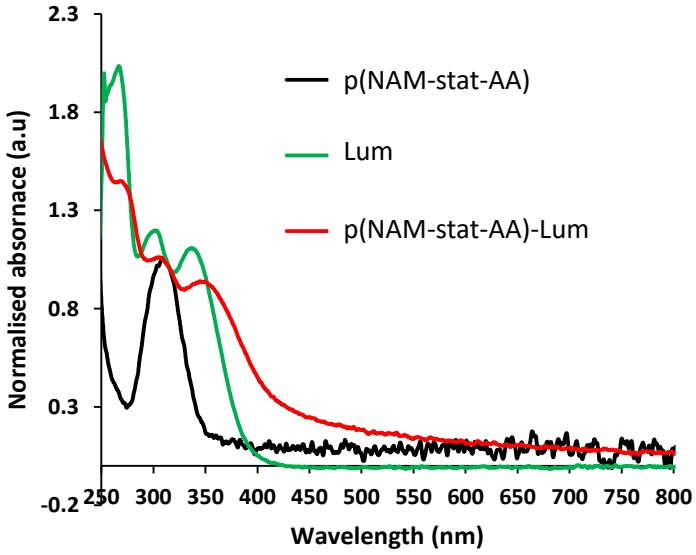

Figure 4.6: UV-VIS spectra of p(NAM-stat-AA) in water, Lum (DCM) in a and p(NAM-stat-AA)- Lum conjugate (water).

Table 4.1: Solubility studies of p(NAM-stat-AA)-Lum conjugate at different concentrations.

p(NAM-stat-AA)-Lum concentration (mg/mL)	Solubility (µg/mL)
2	8.00
4	10.21
6	11.82

4.1.1.2 Synthesis of p(NAM-stat-AA)-PQ conjugate.

Primaquine, commercially available and clinically administered as the bisphosphate salt, has an aqueous solubility of 10 mg/ml. This is forty times the recommended per kilogram body weight single dose. Solubility is therefore not a major problem with primaquine. The two main challenges, which require a delivery system, are the risk of life-threatening hemolysis in G6PD-deficient patients and the rapid metabolic deactivation to carboxyprimaquine. Conjugating primaquine to a carrier polymer via the primary amine is expected to prevent oxidation to the

carboxy metabolite. Also, conjugation results in a prodrug that should be less toxic to red blood cells.

The conjugation of p(NAM-stat-AA) to the primary amine group of PQ to form an amide bond was carried out using one step as illustrated in **Scheme 4.3**. As both the polymer and drug are water-soluble, conjugation was done in an aqueous solution of EDC (20 molar equivalents) and sulfo-NHS (4 molar equivalents). Except for the slightly higher EDC equivalents used, the stoichiometry of this reaction was similar to the DIC experiments for DHA and lumefantrine. The carboxylic acid groups of p(NAM-stat-AA) were activated using EDC/sulfo-NHS coupling reagents in deionized water. This was quickly followed by addition of the primaquine at 15 molar equivalents with an aim to load 15 units of the carboxylic units of polymer with a drug and reaction was allowed to continue for almost 3 h in the dark. Purification of the product by semipermeable membrane methods was however complicated by colour changes that occurred with the crude reaction solution. Different methods were used to test the stability of the conjugate (**Figure 4.7).**

a) Semi-permeable membrane bags (cellulose membrane, MWCO 12 kDa) that uses gradient diffusion method.
b) Semi-permeable membrane tubes (cellulose membrane, MWCO 3 kDa) that uses ultra-filtration by centrifuge.
c) Gradient-based diffusion dialysis by centrifugation in a Vivaspin^{TM} ultrafiltration tube (PES membrane, MWCO 3 kDa).

All these purification methods were conducted in the dark to avoid photo-degradation (Al-Badr, 2005) but a green coloured solution was observed within the first 30 min.

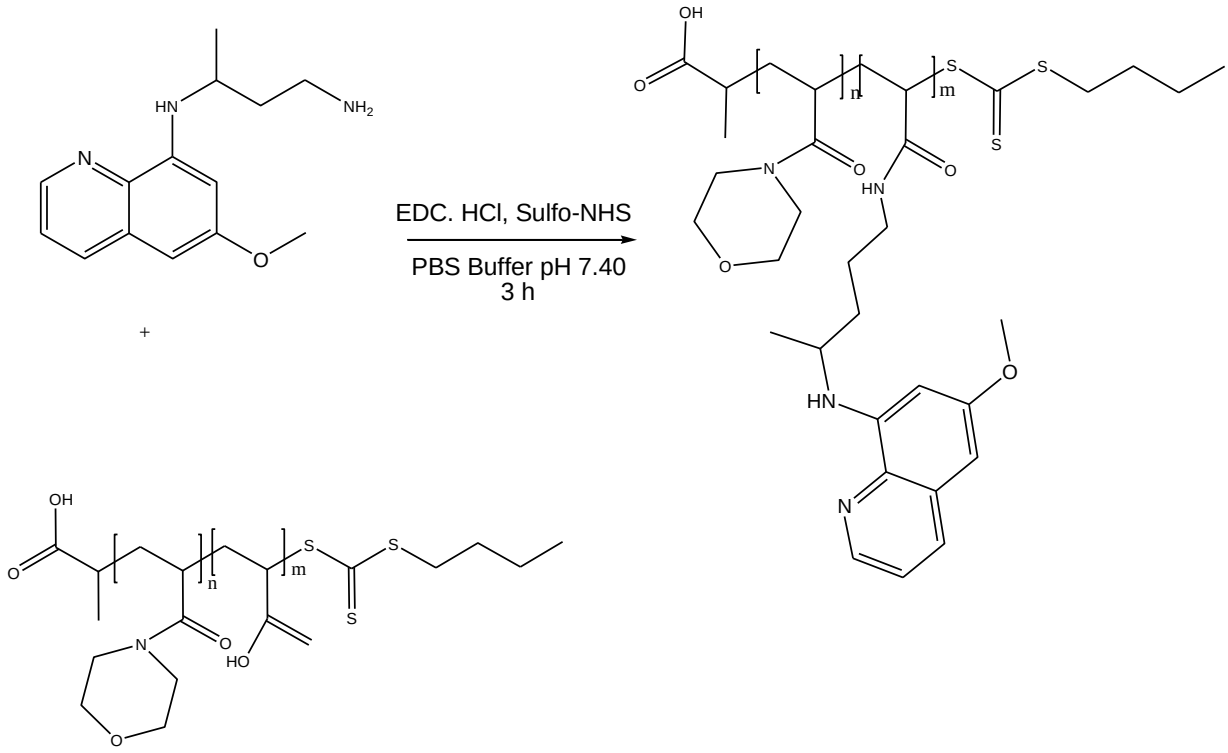

Scheme 4.3: Synthesis of p(NAM-stat-AA)-PQ conjugate.

In order to try to overcome this problem, it was decided to carry out a meticulous control of the experimental conditions. To do this several aspects of the experimental process were carefully investigated. These included:

1. Change of coupling reagent
2. Investigating stability of the reactants over longer reaction time
3. Stability at lower temperature using different purification methods

1. Change of coupling reagents.

The reaction was carried out as described above with a change in coupling reagents, EDC/ Sulfo-NHS to DIC/Sulfo-NHS in DMF under nitrogen gas for 24 h at ambient temperature. After 24 h; DMF was removed under vacuum and PBS pH 7.40 was added to the solution and transferred to dialysis bag MWCO 12 kDa. It was observed that after 5 h the solution had turned green.

2. Stability of the reactants over 24 h

The stability of the reactants was investigated over 24 h in PBS buffer pH 7.40, the tests were conducted as shown **Figure 4.6**. This was to investigate whether excess unreacted reagent was responsible for the colour change. After 24 h the PQ alone and P(NAM)-stat-AA with EDC/sulfo-NHS has no colour change and the PQ with EDC/sulfo-NHS showed a fainted yellow colour after 24 h observations are summarized in **Table 4.2**. These results indicated that the coupling reagents might not have an impact on the colour change.

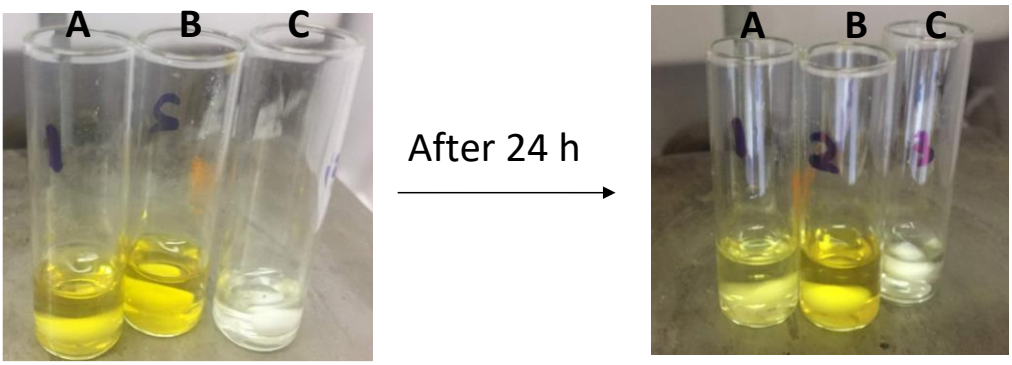

Figure 4.7: Test of stability of the (A) PQ with EDC.HCl and NHS (B) PQ and (C) P(NAM-stat-AA) with EDC.HCl and NHS in PBS buffer pH 7.40.

Table 4.2: Summary of the stability of the reactants after 24 h.

Label	**Observation**
A	Yellow to faint yellow after 3 h to 24 h
B	No colour change
C	No colour change

3. Change in temperature during purification

The effect of temperature was also investigated, EDC/Sulfo-NHS were used as coupling reagents. The solution after 2.5 h was transferred to either a gradient-based diffusion dialysis bag (MWCO 12 kDa or 1 kDa) or a semi-permeable ultrafiltration membrane with centrifugation (3 kDa, 10 000 rpm) as shown in **Table 4.3**. The purification was carried out at room temperature and at 22 °C for centrifugation, but the solutions still turned green. The temperature was lowered for both purification methods, to 4 °C for dialysis bags (done in the

refrigerator) and the centrifuge was lowered to 6 °C for ultra-filtration. It is the latter method that yielded a pure stable product that was lyophilized and stored under N_2 at -80 °C.

The stable p(NAM-stat-AA)-PQ conjugate was analysed using ^{1}H NMR spectroscopy shown in **Figure 4.8**. The NMR spectrum showed characteristic peaks of PQ due to (Ar-H) aromatic peaks at 8.5-6.2 ppm. The specific site of amide formation is unclear because of the interference of the broad p(NAM-stat-AA) peaks down field. A new peak is observed at 7.9 ppm and this could be assigned to the proton peak of secondary amine (N-H). The other new proton peak is observed at 9.5 ppm, which could be due to protons of the newly formed secondary amide or the unreacted carboxylic acid O-H groups. The drug loading was determined to be 2 mol%, using the aromatic peaks at 7.4 ppm for the drug and polymer peaks repeating peaks around 3.0-3.7 ppm. FT-IR spectra in **Figure 4.9**, clearly shows the formation of amide bond through the shift of the acid carbonyl (1614.5 cm^{-1}) in the p(NAM-stat-AA) to amide carbonyl (1632.8 cm^{-1}) in the conjugate.

Table 4.3: Different methods tested to purify P(NAM-stat-AA)-PQ conjugate to get stable conjugate.

<table>
<tr><td>Method of purification</td><td colspan="2">Ambient temperature after 12 h</td></tr>
<tr><td rowspan="2">Dialysis (12 kDa, cellulose membrane)</td><td colspan="2">(a)  (b)  </td></tr>
<tr><td>Ambient temperature after 12 h</td><td>Left at 4 °C for 12 h</td></tr>
<tr><td>Dialysis (1 kDa, cellulose membrane)</td><td>  </td><td>  </td></tr>
</table>

Viva spin™ (3 kDa,PES membranes)		

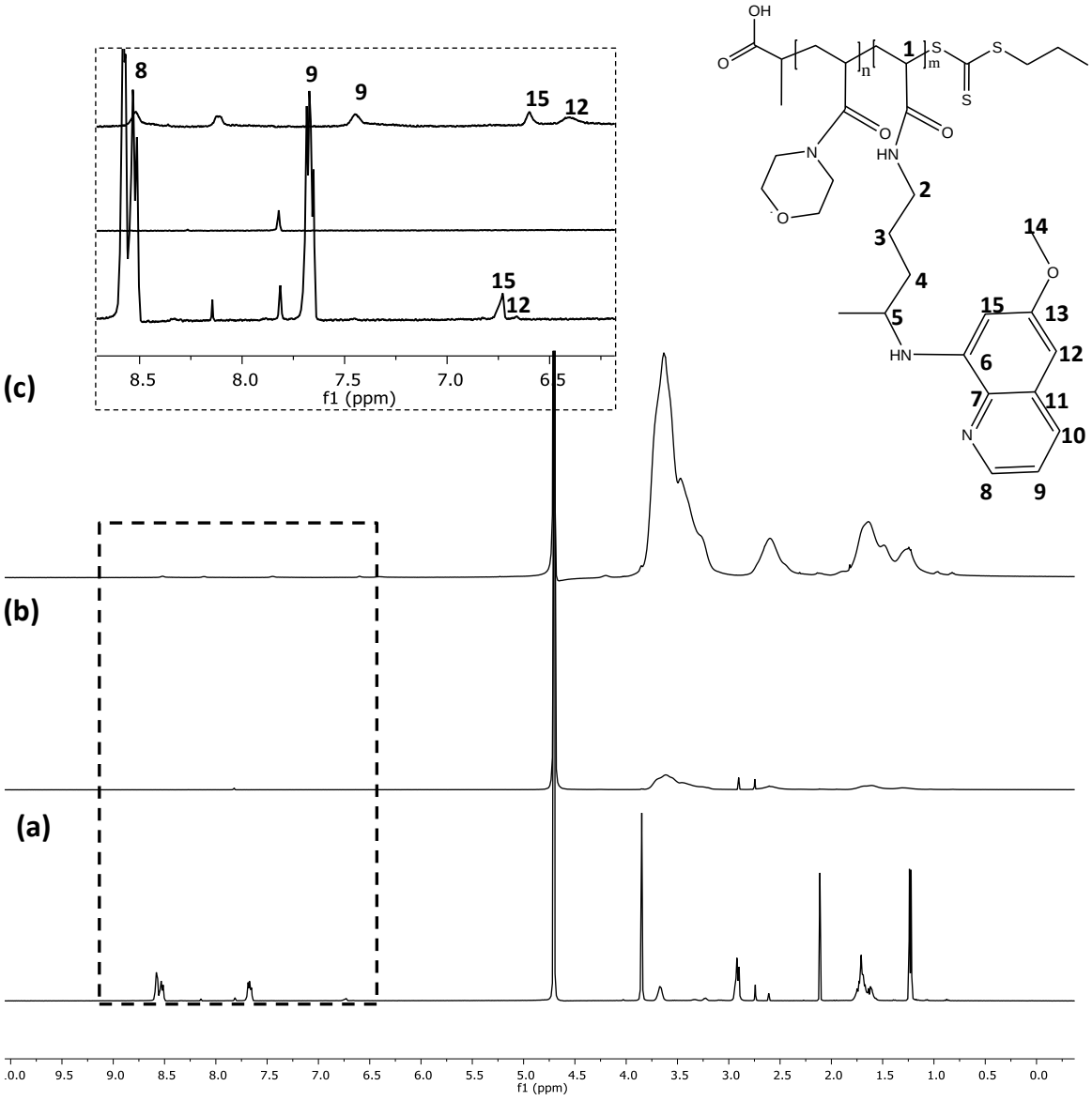

Figure 4.8: ^{1}H NMR (400 MHz in D_2O) spectra of (a) PQ, (b) p(NAM-stat-AA) and (c) p(NAM-stat-AA)-PQ.

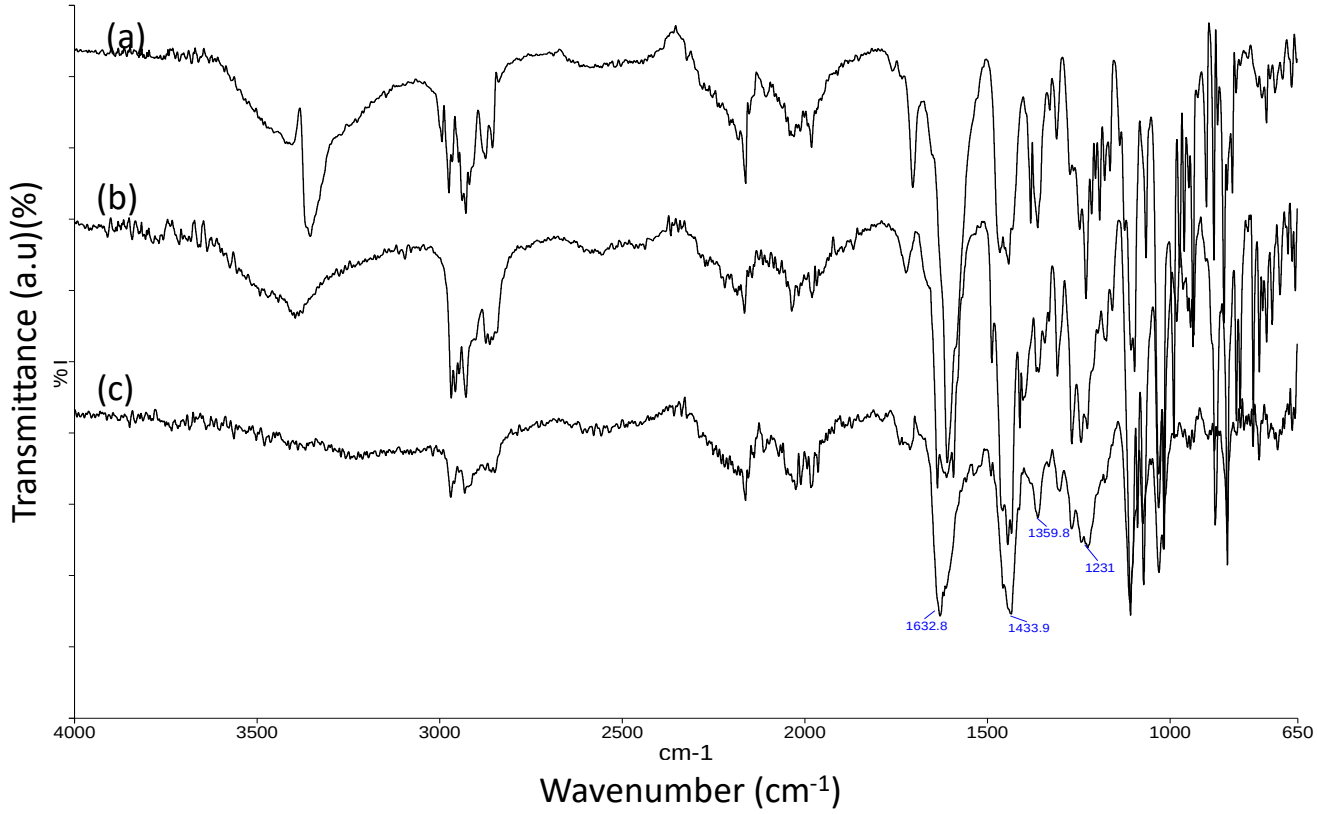

Figure 4.9: FT-IR spectra of (a) PQ, (b) p(NAM-stat-AA) and (c) p(NAM-stat-AA)-PQ conjugate.

4.1.1.3 TEM, Hydrodynamic size and charge of p(NAM-stat-AA)-drug conjugates.

The hydrodynamic size and zeta potential, measured by DLS, of the p(NAM-stat-AA)-drug conjugates are shown in **Figure 4.10** and **Table 4.4**. p(NAM-stat-AA)-DHA showed a bimodal hydrodynamic size profile around 12.71 nm and 490.40 nm and TEM average size was calculated to be 6.58±0.2 d.nm. The bimodal size distribution in DLS could be due to the size related to the small monodispersed particles and big globular structure on the surface of the smaller particles as seen in the TEM image. The small particles were spherical in shape. p(NAM-stat-AA)-Lum and p(NAM-stat-AA)-PQ conjugates had unimodal hydrodynamic sizes 217.2±2.2 and 161.3±6.2 respectively. The TEM size was 116.61±0.7 nm for p(NAM-stat-AA)-Lum with a mixture of spherical and elongated structured particles, while for p(NAM-stat-AA)-PQ conjugate the particles were monodispersed with an average particle size of 7.63±0.16 nm. As mentioned in **Chapter 3**, TEM measured dimensions are smaller than those measured by DLS because the latter is affected by both the solvent and the shape of the particles. The Lum conjugate had a bigger TEM and DLS size compared to the other conjugates. This could be due to amphiphilic character of the conjugate with the polymer being

hydroscopic and the Lum being hydrophobic nature: Lum (logp 8.34) compared to DHA (logp 2.5). The particles had PDI values below 0.2 for the Lum and PQ conjugate, which is an indication of the relatively homogeneous size distribution achieved using carbodiimide chemistry. A PDI greater than 0.4 as calculated for the DHA conjugate indicates that the sample is polydisperse with multiple size distributions as seen by the bimodal size distribution curve. The particles had a negative charge at pH 7.40 indicating not all the carboxylic acid groups of p(NAM-stat-AA).

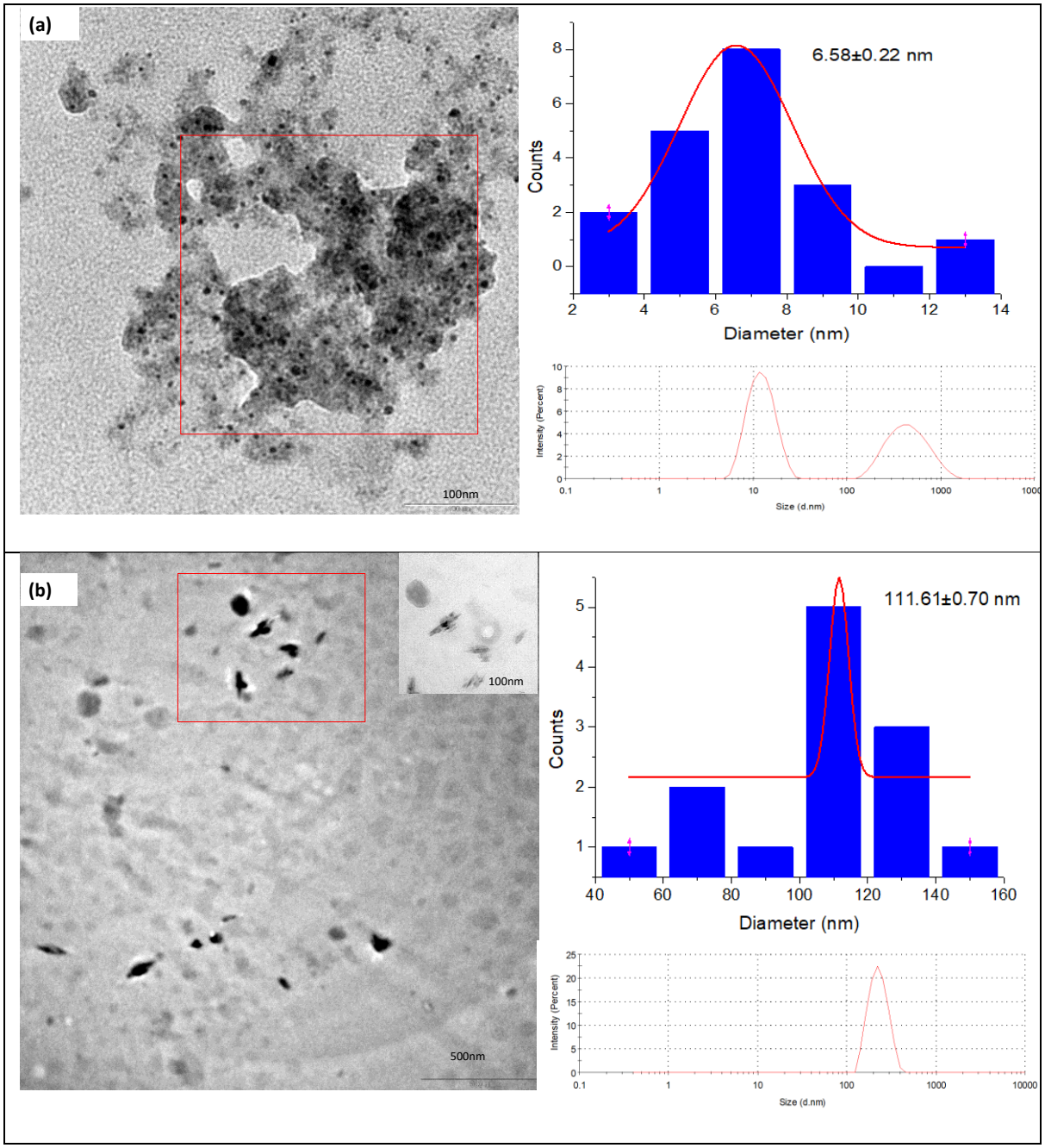

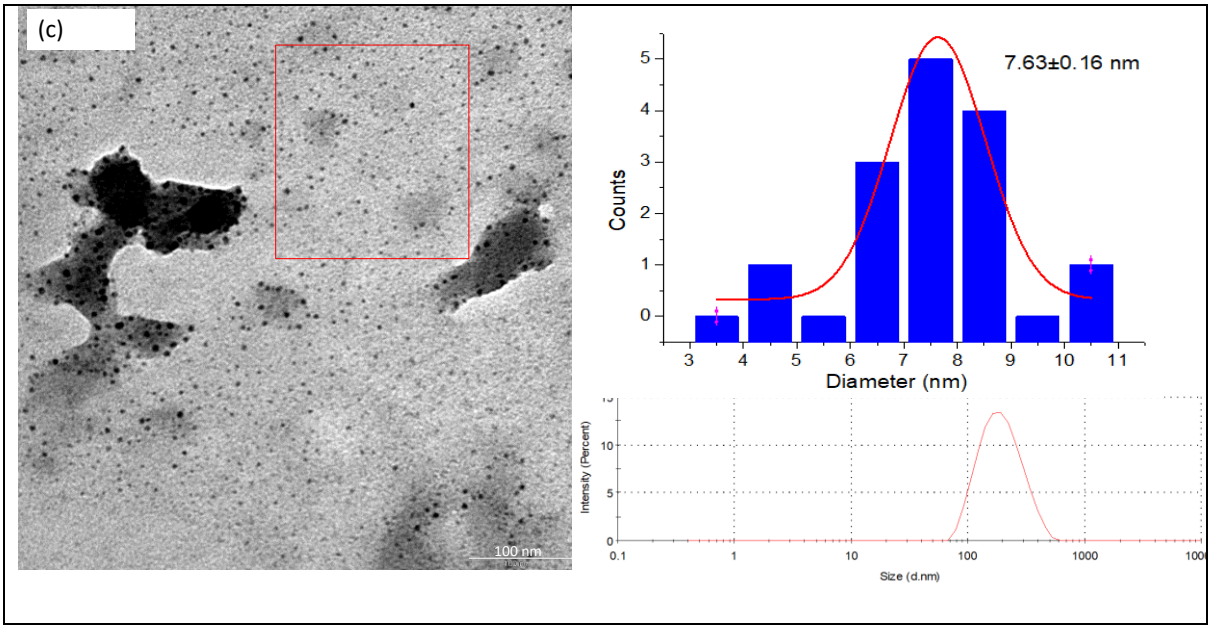

Figure 4.10: TEM image, Particle size distribution histogram and hydrodynamic size of p(NAM-stat-AA) (a) DHA, (b) Lum and (c) PQ conjugates.

Table 4.4: TEM, Hydrodynamic size of PGA conjugate with PDI and zeta potential values.

Parameters tested	p(NAM-stat-AA)-DHA	p(NAM-stat-AA)-Lum	p(NAM-stat-AA)-PQ
Hydrodynamic size	21.51±4.1 d.nm	217.1±2.2 d.nm	161.3±6.2 d.nm
PDI	0.619±0.3	0.068±0.03	0.320±0.03
Zeta Potential	-3.25±0.12 mV	-21.8±0.1 mV	-12.9±3.3mV
Tem size	6.58±0.2 nm	111.61±0.7 nm	7.63±0.2 nm

4.2.1 Synthesis of PGA-drug conjugates.

4.2.1.1 Conversion of sodium polyglutamate to polyglutamic acid

PGA was received as the sodium salt, sodium polyglutamate, from Professor Maria Vicent of the Polymer Therapeutics Laboratory, CIPF, Spain. Sodium polyglutamate (PG-COO^- Na^+) is the water-soluble salt of PGA and to carry out reactions in organic solvents, as is required for lumefantrine, it has to be converted back to the organic acid (-COOH) form. PGA was formed by addition of 2 M HCl dropwise to an aqueous solution of PG-COO^- Na^+ (1.0 g) until pH 4.0

was reached, this solution was allowed to stir for 24 h at 4 °C (**Scheme 4.4**). The product formed as a white precipitate after 24 h and the yield was 58 %.

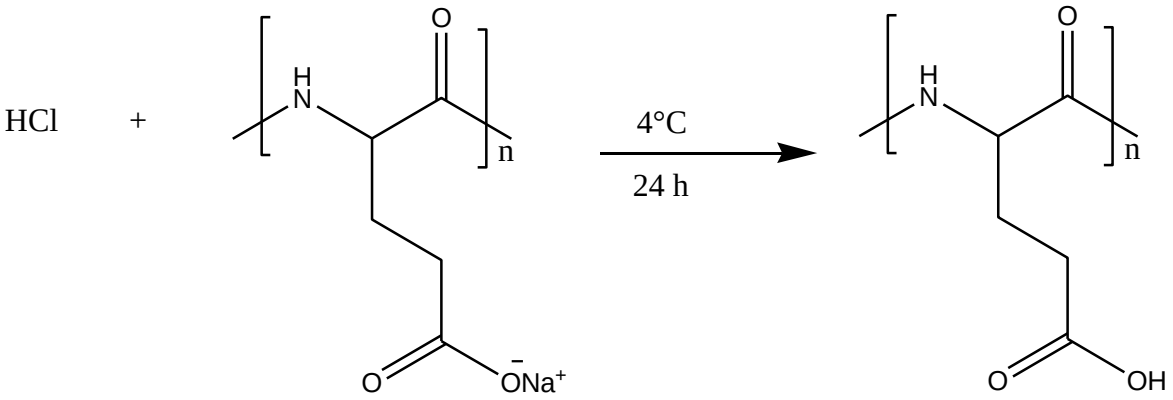

Scheme 4.4: Synthesis of polyglutamic acid from sodium polyglutamate.

The ^{1}H NMR spectrum (**Figure 4.11**) showed a chemical shift at 3.47 ppm that is attributed to the α-H. The peak at 1.54 ppm is due to γ–H , the peaks at 0.8 and 1.23 ppm are due to β-H. These results are consistent with the characteristic peaks of PGA reported by Lai and Huang (2015). The ^{1}H NMR does not provide definitive characterization information to distinguish the salt from the acid. DSC thermogram (**Figure 4.12**) was further used to confirm conversion of polyglutamate (**a**) to polyglutamic acid (**b**). The crystallinity of PGA was further confirmed using DSC, which exhibited two endothermic peaks at 71.46 °C and at 268.05 °C. These peaks correspond a glass transition and a melting temperature respectively (Margaritis and Manocha, 2010). Introduction of the hydrogen, forming –OH resulted in a decrease in these values to 60.40 °C and 245.97 °C, this could be due to the changes in the polymer as the Na^{+} is replaced by hydrogen.

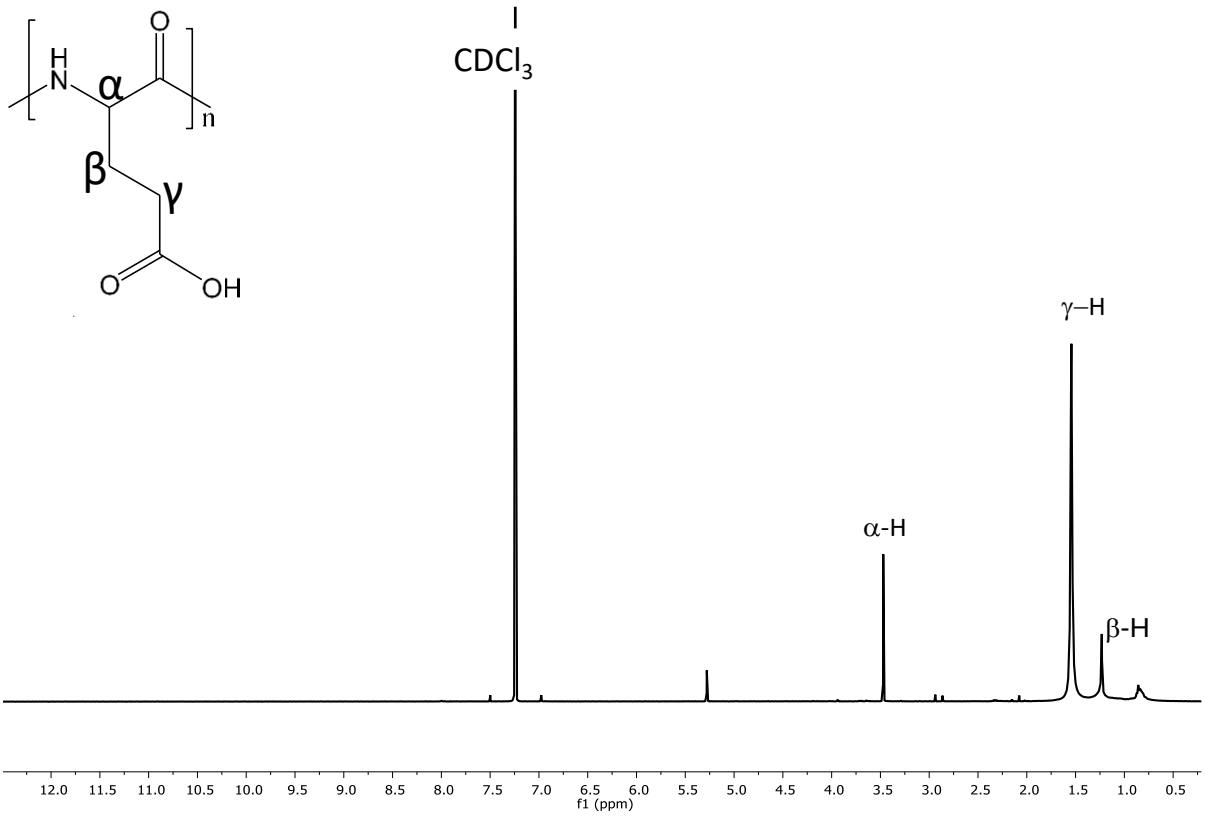

Figure 4.11: ^{1}H NMR (400 MHz) spectrum of PGA in $CDCl_3$.

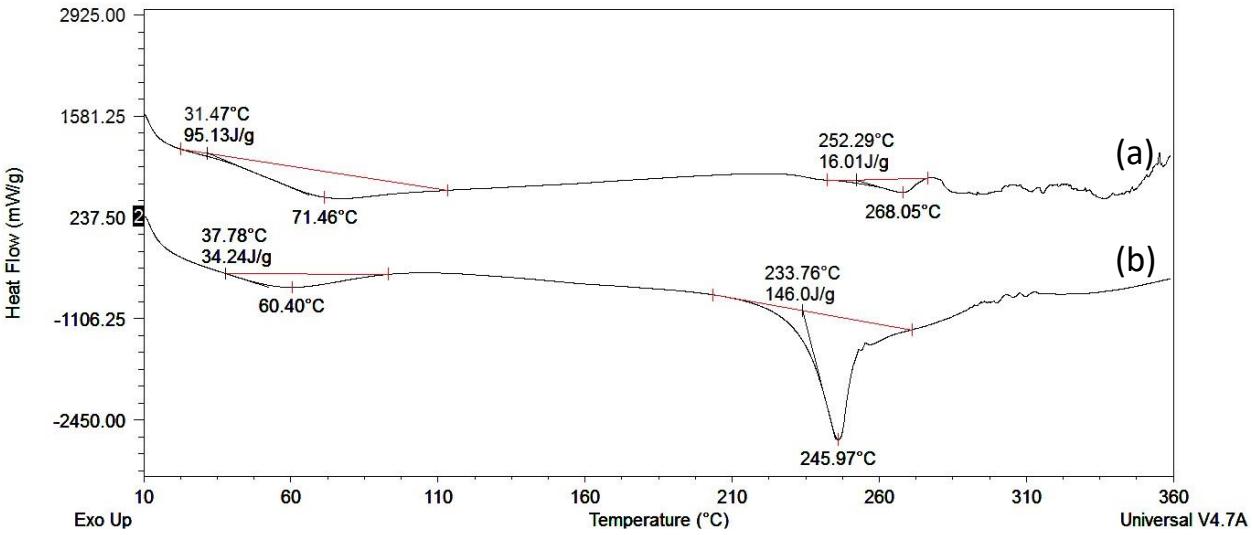

Figure 4.12: DSC thermogram of (a) polyglutamate and (b) polyglutamic acid.

4.2.1.2 Synthesis of PGA-DHA conjugate.

PGA was successfully esterified by a two-step reaction using DIC/HOBt as coupling reagents (**Scheme 4.5**). HOBt is recommended for the formation of esters and amide with carboxylic acid, in order to enhance reactivity and also reduce formation of epimers. It also minimizes the formation of N-acylurea (Windridge and Jorgensen, 1973; Gopi, 2014) which reduces the reaction yield and also complicates work-up and isolation of the desired ester (Siengalewicz, Mulzer and Rinner, 2014; Yang, 2016). The conjugate was purified using gradient-based diffusion dialysis with MWCO 12 kDa in PBS (pH 7.40) for 72 h.

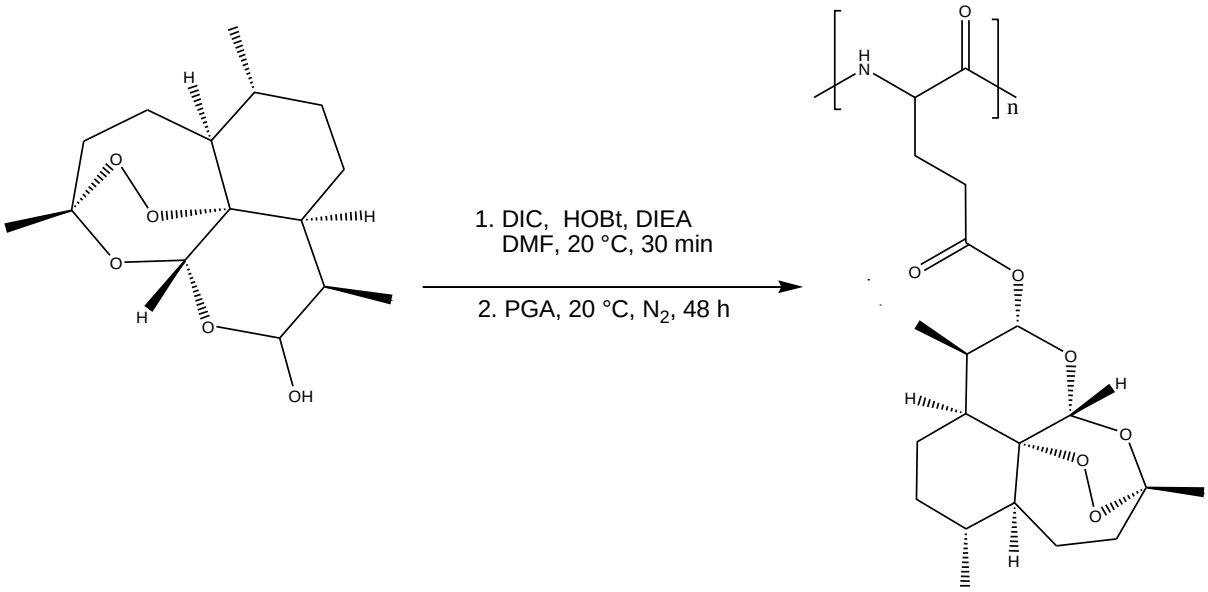

Scheme 4.5: Synthesis of PGA-DHA conjugate.

^{1}H NMR spectra in **Figure 4.13** shows (a) DHA, (b) PGA and (c) PGA-DHA conjugate, where the peaks at 0.80-2.90 are characteristic proton peaks of DHA. While the proton peaks at 3.51 ppm and around 1.51 ppm are due α-H and β-H of PGA. Successful esterification was confirmed by a shift in the γ-H proton of PGA from 1.54 ppm to 1.71 ppm. The doublet at 4.78 ppm due to the acetal methine (-CH) proton in DHA also shifted to 5.3 ppm indicating successful formation of the ester bond, a similar observation was reported by Liu et al. (2016) when DHA was conjugated to multi-arm PEG-OH. The percentage drug loading was determined to be 6 mol% using the methine proton of DHA and methylene protons of polymer (labelled 2 and 3). FT-IR spectra in **Figure 4.14** further confirmed this by appearance of the absorption band at 1600 cm^{-1} as pure DHA does not have this peak.

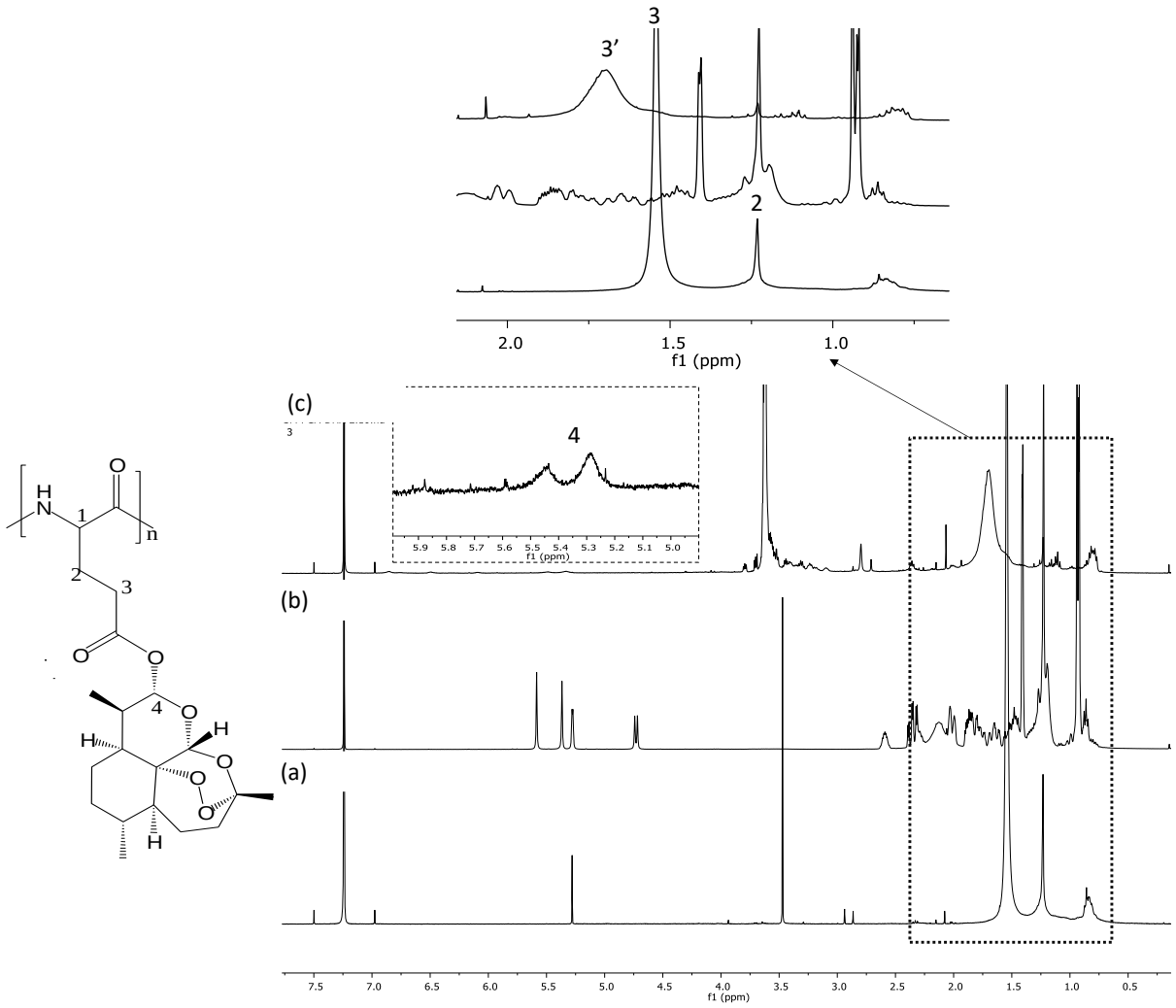

Figure 4.13: ^{1}H NMR spectra (400 MHz in $CDCl_3$) of (a) PGA, (b) DHA and (c) PGA-DHA conjugate.

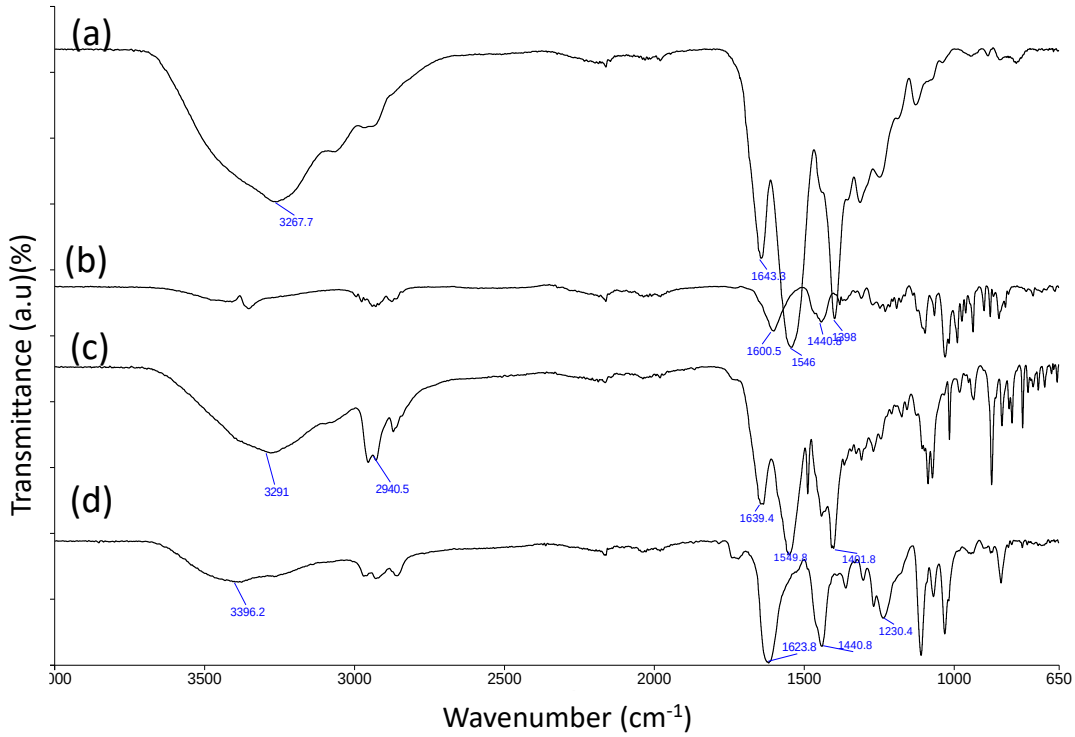

Figure 4.14: FT-IR spectra of (a) PGA, (b) PGA-DHA, (c) PGA-Lum and (d) PGA-PQ

4.2.1.3 Synthesis of PGA-Lum conjugate.

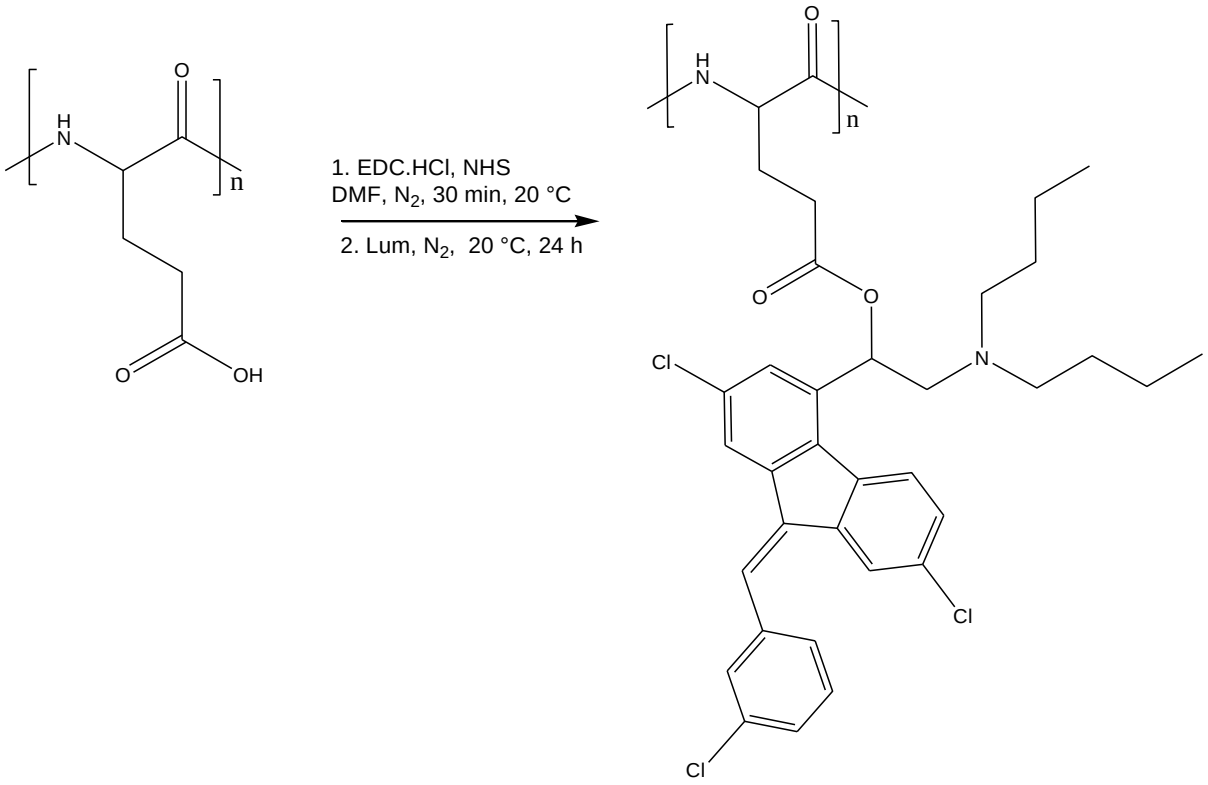

Scheme 4.6: Synthesis of PGA-Lum conjugate.

The conjugation of the PGA to Lum to form an ester bond was carried out in a two-part reaction as illustrated in **Scheme 4.6**, using EDC/NHS as coupling reagents. After 24 h the solvent was removed *in vacuo*. The conjugate was purified using gradient-based diffusion dialysis (MWCO 12 kDa) in PBS (pH 7.40). The PBS buffer was used to avoid the hydrolysis of the formed ester bond. The conjugate was purified for 72 h with frequent changing of PBS buffer and the pure conjugate was lyophilized for 3 days to form a yellow powder. The successful conjugation and percentage drug loading was determined using ^{1}H NMR spectroscopy (400 MHz in $CDCl_3$) in **Figure 4.15.**

The ^{1}H NMR spectrum of Lum in $CDCl_3$ showed proton peaks of CH of the aromatic groups between 7.51-7.04 ppm. At 5.20-5.16 ppm a doublet of doublets due to the proton of the hydroxyl group (labelled-4) is seen. The multiplet at 2.68- 2.65 ppm was attributed to the diasterotopic protons (labelled 5) and due to methylene proton of the alkyl chain resulted in the multiplets from 2.55 to 1.08 ppm. At 0.97-0.93 ppm a triplet was observed due to the protons of the terminal methyl groups of the butyl chains. Upon formation of the polymer drug conjugate with PGA, there is a shift in chiral proton (4) of Lum from 5.20 ppm (doublet of

doublet) to 6.23 ppm (single broad peak). There was also broadening of the drug proton peaks due to the interaction of the drug and polymer. This could indicate successful conjugation and successful esterification was shown by the shift in the proton peaks of the polymer (γ–H) from 1.54 ppm to 1.59 ppm shown in the insert in **Figure 4.15** (labelled 3). The percentage drug loading was calculated to be 17.5 mol% by using the γ proton of the polymer and methine peak at 6.23 ppm of the drug. The FT-IR spectrum (**Figure 4.14 c**) confirmed conjugation by a shift of the carbonyl peak to 1639.4 cm^{-1}. The solubility studies (**Table 4.5**) were conducted using similar method to the one explained for p(NAM-stat-AA)-Lum conjugate, the aqueous solubility of Lum was significantly improved from being insoluble to being soluble at the highest concentration measured.

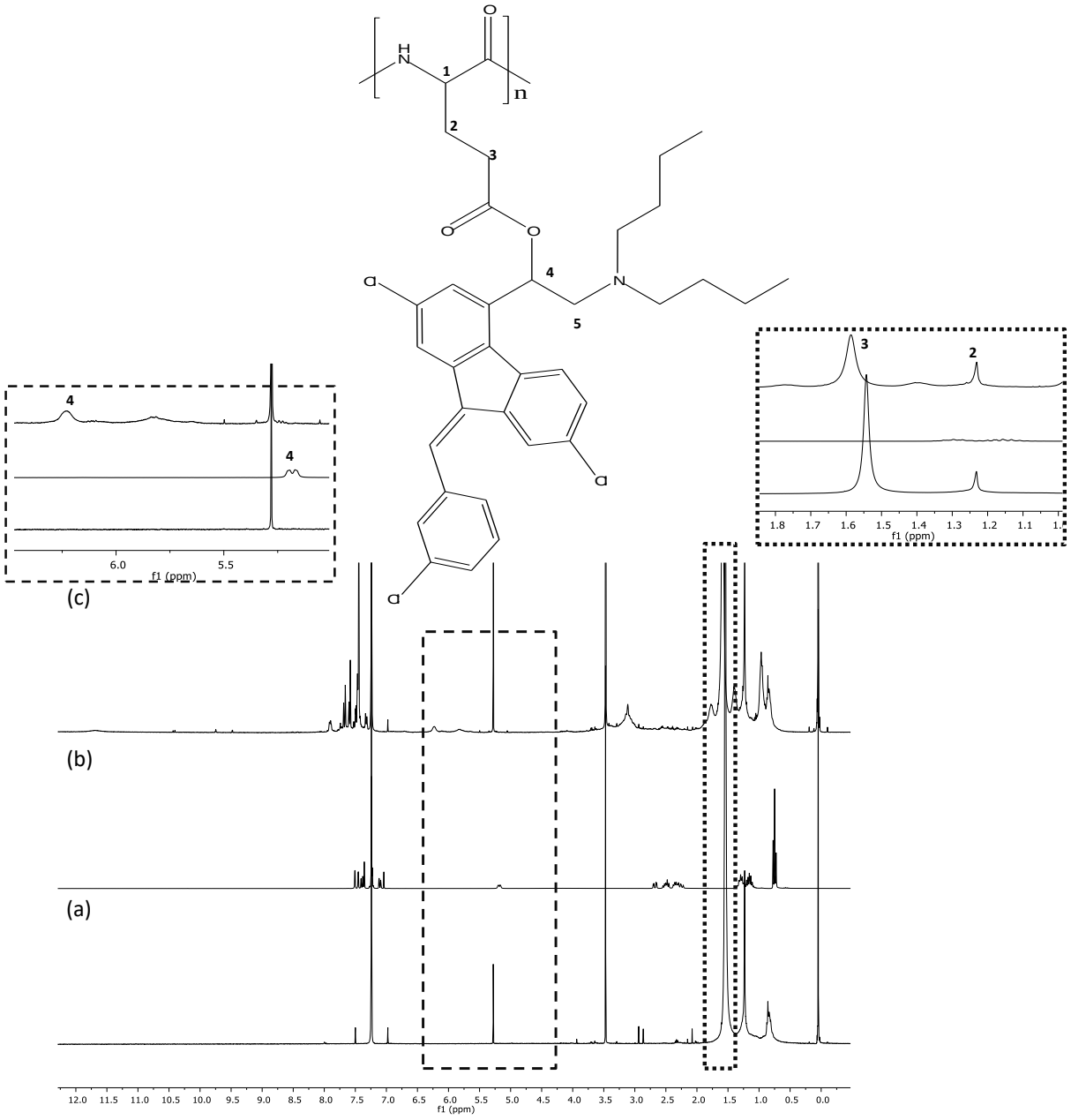

Figure 4.15: ^{1}H NMR (400 MHz in $CDCl_3$) spectra of (a) PGA, (b) Lum and (c) PGA-Lum conjugate.

Table 4.5: Solubility studies of PGA-Lum conjugate

PGA-Lum concentration (mg/mL)	Solubility (µg/mL)
2	8.61
4	11.82
6	11.40

2.9.1.1 Synthesis of Sodium polyglutamate-PQ conjugate.

The conjugation of PQ to sodium polyglutamate through amide bond formation required a one-step reaction carried out in PBS pH 7.40. The formation of amide bond was realized by the use of water-soluble coupling reagents, EDC/Sulfo-NHS in the dark to avoid degradation of PQ (**Scheme 4.7**). The reaction was left for 2 h and the product was purified by ultra-filtration using semi-permeable tubes (MWCO 3 kDa) and centrifugation. To avoid the product degradation, previously experienced with conjugation of PQ to p(NAM)-stat-AA, this purification method was chosen as it is quick. The purification was completed within 30 min, the centrifuge speed was 12000 rpms and temperature kept at 6 °C to avoid drug degradation. The final concentrate was lyophilized to yield pure conjugate that was analyzed using ^{1}H NMR spectroscopy and a drug loading was determined to be 0.2 mol%.

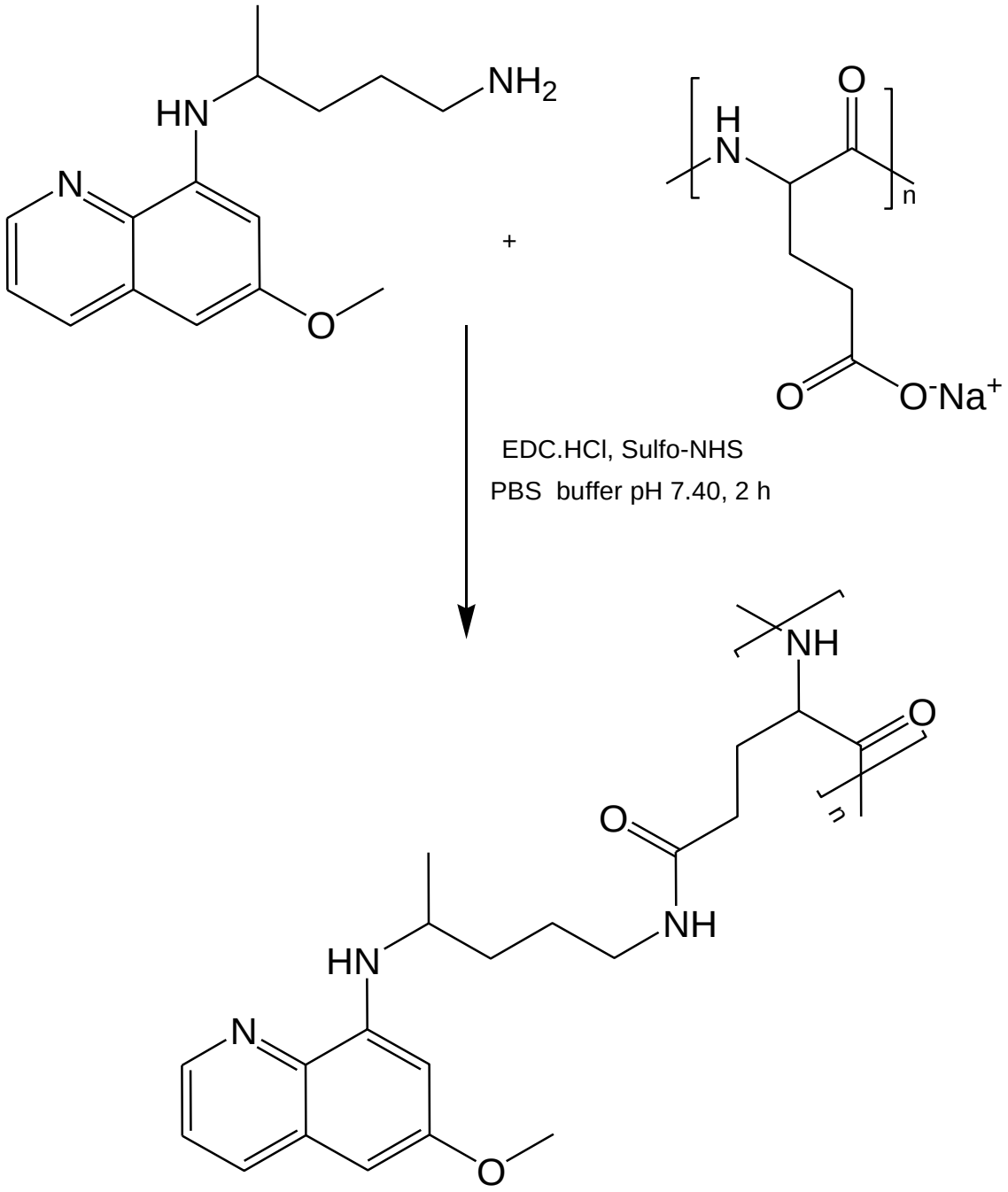

Scheme 4.7: The synthesis of PGA-PQ conjugate.

A comparison of the ^{1}H NMR spectra presented in **Figure 4.16**, indicated that the conjugate contained both PGA and PQ proton peaks. The formation of an amide bond was confirmed by the disappearance of the peak at 9.75 ppm due to protons of the amine (-NH_2) of PQ (Al-Badr, 2005), the shift in CH_2N proton of the polymer (marked 3) and a new peak appearing at 7.93 ppm due to new secondary amide (N-H) proton. The appearance of the amide (C=O) absorption peak at 1623.8 cm^{-1} in the FT-IR spectrum (**Figure 4.14 (d)**) confirmed that conjugation had taken place. The percentage drug loading determined by ^{1}H NMR

spectroscopy was 9.0 mol% by integrating the aromatic peaks of the drug around (6.5-8.5 ppm) and compared to the γ-proton of the polymer (marked-2).

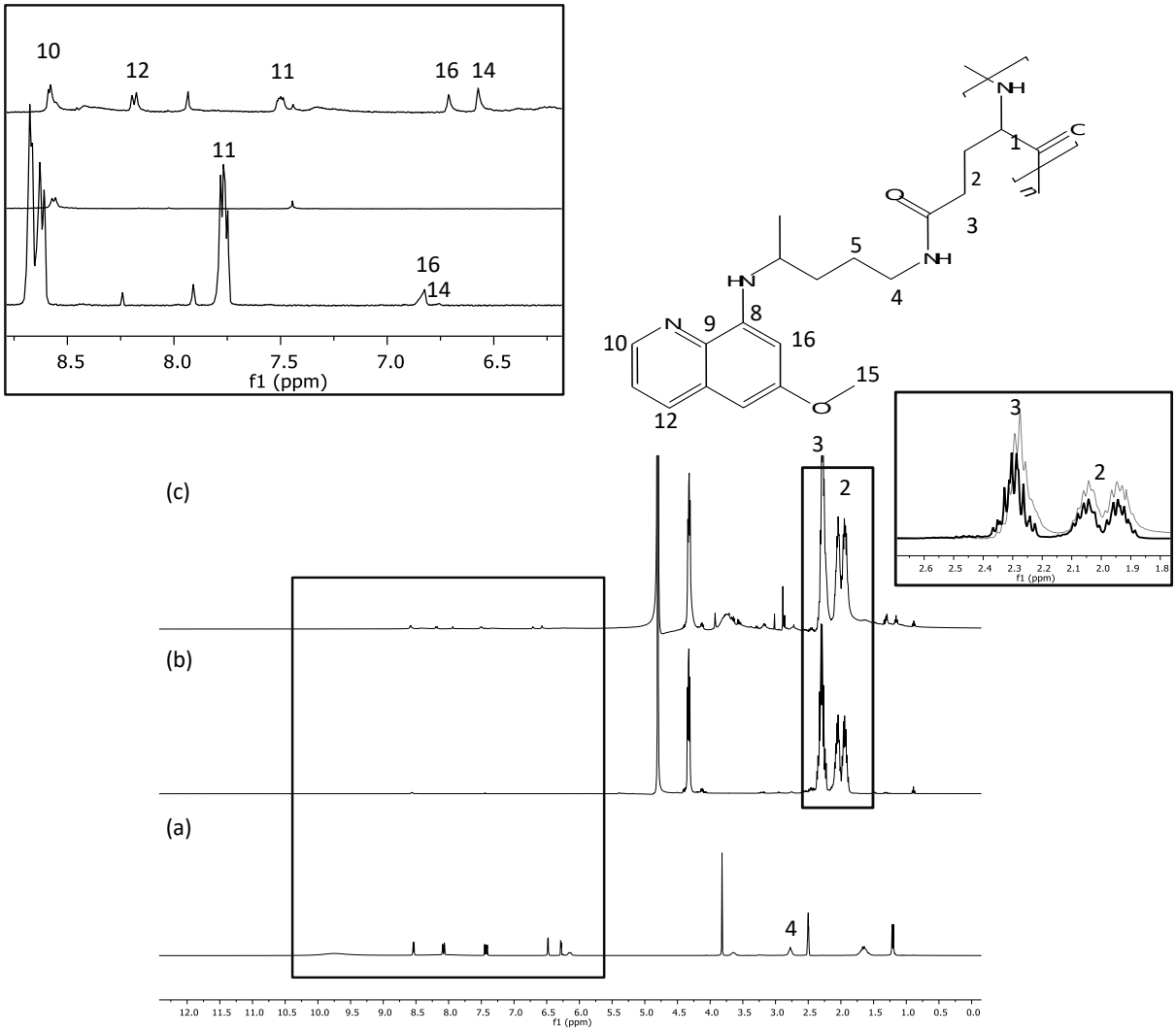

Figure 4.16: ^{1}H NMR spectra (400 MHz in D_2O) of (a) PQ (b) PG sodium salt and (c) PGA-PQ conjugate.

2.9.1.2 TEM, Hydrodynamic size and charge of PGA-drug conjugates.

The PGA conjugates had hydrodynamic size ranges from 169.8±6.7 d.nm to 185.7±18 d.nm as shown in **Table 4.6 and Figure 4.17**. The TEM microgram showed that the particles are heterogeneous with the PGA-DHA conjugate having spherical and irregular shaped particles with a size of 56.0±4.4 nm. The PGA-Lum had aggregated spherical particles lying on the surface of squared shaped sheets with averaged particles size of 238.47±15 nm. The PGA-PQ conjugate also had a mixture of spherical and irregular shaped particles with average particle

size of 210.12±0.1 nm. The Lum and PQ conjugate had differed from the observed norm that TEM size is smaller than DLS size. This could be due to that DLS is mostly used to measure spherical particles, the conjugates are heterogeneous with a mixture of spherical and non-spherical particles. For the non-spherical particles, rotational diffusion is not considered and these could have an impact on the micron size seen in PQ or reduced size compared to the TEM measurement (Arenas-Guerrero et al. 2018). The TEM size is calculated by measuring the cross-sectional area of the particles and this is converted to equivalent spherical diameter. The PDI values were more than 0.5 indicating a broad size distribution that could be caused by the difference in shape of the particles.

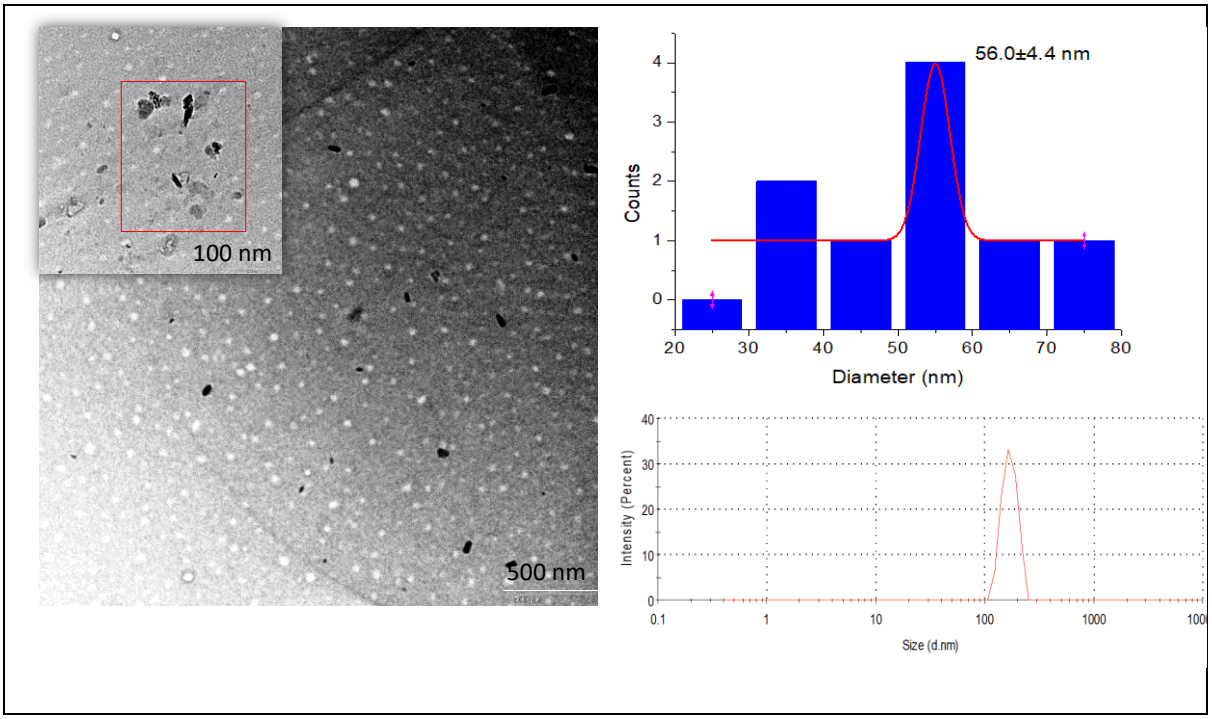

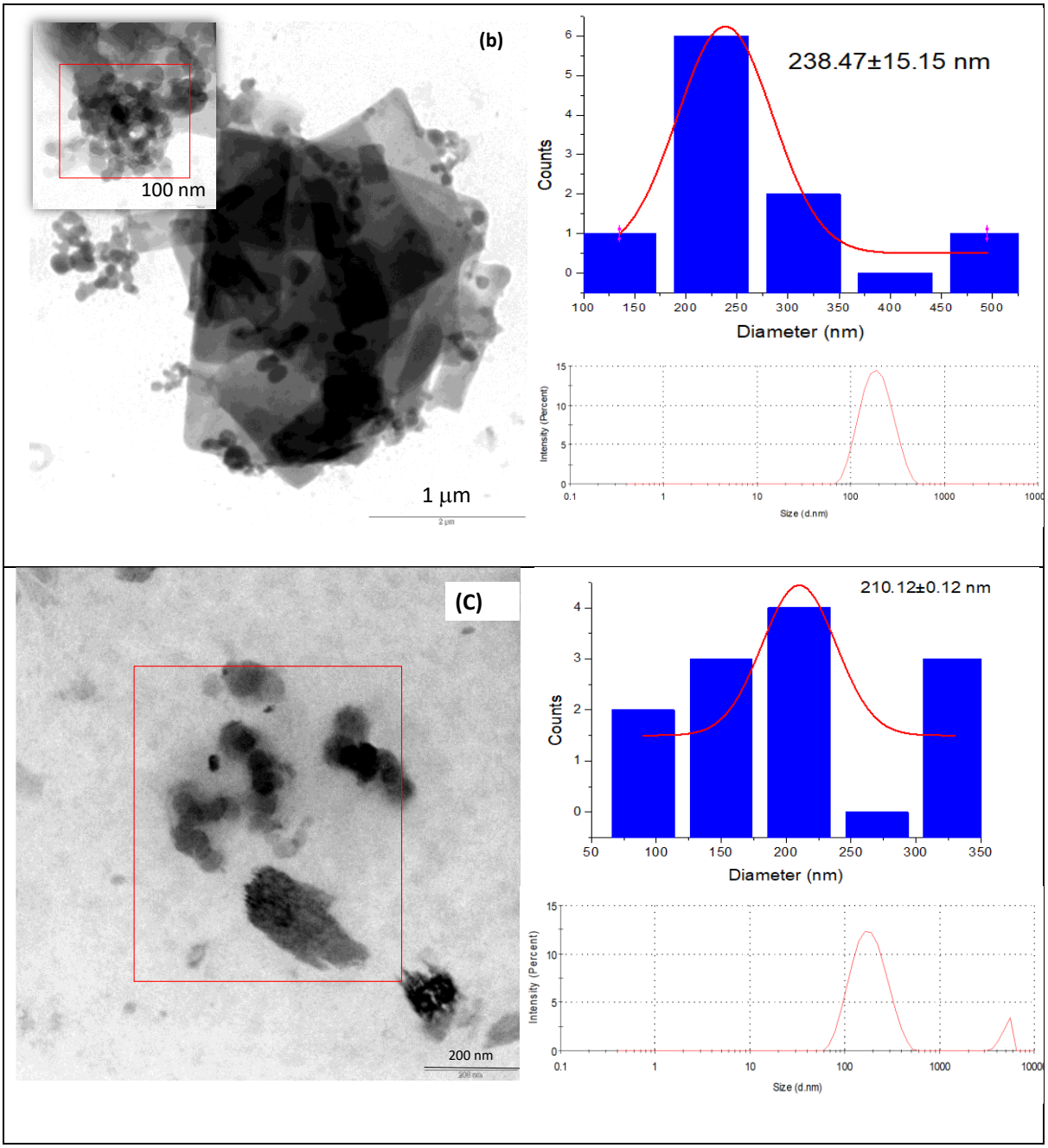

Figure 4.17: TEM image, Particle size distribution histogram and hydrodynamic size of PGA (a), DHA (b) Lum and (c) PQ conjugates.

The zeta potential was also evaluated to check the charge and overall stability of the particles in PBS buffer pH 7.40. The results, summarized in **Table 4.6**, indicated that the conjugates had a negative net surface charge. These results suggest that not all the carboxylic acid of the PGA are chemically bound to a drug as at neutral pH, the free carboxylic acid losses a proton and becomes negatively charged (Cao et al. 2013).

Table 4.6: TEM, Hydrodynamic size of PGA conjugate with PDI and zeta potential values.

Parameters tested	PGA-DHA	PGA-Lum	PGA-PQ
Hydrodynamic size	169.8±6.7 d.nm	175.4±0.7 d.nm	185.7±18 d.nm
PDI	0.80±1.3	0.55±0.01	0.65±0.1
Zeta Potential	-6.60±6.8 mV	-26.5±0.3 mV	-18.2±0.61 mV
TEM size	56.0±4.4 nm	238.47±15 nm	210.12±0.1 nm

4.2.2 Solid-state characterization using SEM, XRD, DSC and TGA.

The SEM micrograms revealed that upon conjugating the drugs to the polymer, there is a change in the shape and morphology of starting material. Tthis is similar to results published by Monacha and Margaritis (2010) and Dai et al. (2015). In **Figure 4.18 (a)-(b)** reveals that PGA and p(NAM-stat-AA) respectively are irregular in shape, while DHA **(c),** showed rod like material, **(d)** Lum and **(e**) PQ showed irregular sheet like material. Upon conjugation, there was a complete change in morphology. p(NAM-stat-AA)-DHA (**f**) showed agglomerated irregular shaped particles, while p(NAM-stat-AA)-Lum (**Figure 4.18** (**g**)), showed irregular shaped particles and agglomerated spherical shaped particles were observed for p(NAM-stat-AA)-PQ (**h**) conjugate. The PGA-DHA (**i**) conjugate showed agglomerated mixtures of morphologies from rod like to irregular shaped. The PGA-Lum conjugate (**j**) showed big spheres that have small spherical material on the surface (insert picture with 200nm). The PGA-PQ **(k)** conjugate had agglomerated irregular shaped particles. These results indicate that upon conjugation, there was a significant change in the shape and morphology of the pure drug and polymer. The SEM results were further complemented by the physical changes observed in PXRD.

In order to further study the physical state of the particles, PXRD studies (**Figure 4.19**) were carried out on the lyophilized conjugates. As seen in the SEM images, DHA, Lum and PQ are crystalline in nature with well-defined patterns (black solid lines). Upon conjugation with amorphous polymers (p(NAM-stat-AA) and PGA, Lum and PQ conjugates had no crystalline

peaks indicating that the conjugate were amorphous in nature. These results support the physical changes seen from the SEM images. The DHA conjugates showed some crystallinity with peak intensities that are different from the pure drug peaks. This may be attributed to the crystal orientation of the conjugate changing as there is also a change in morphology as seen in the

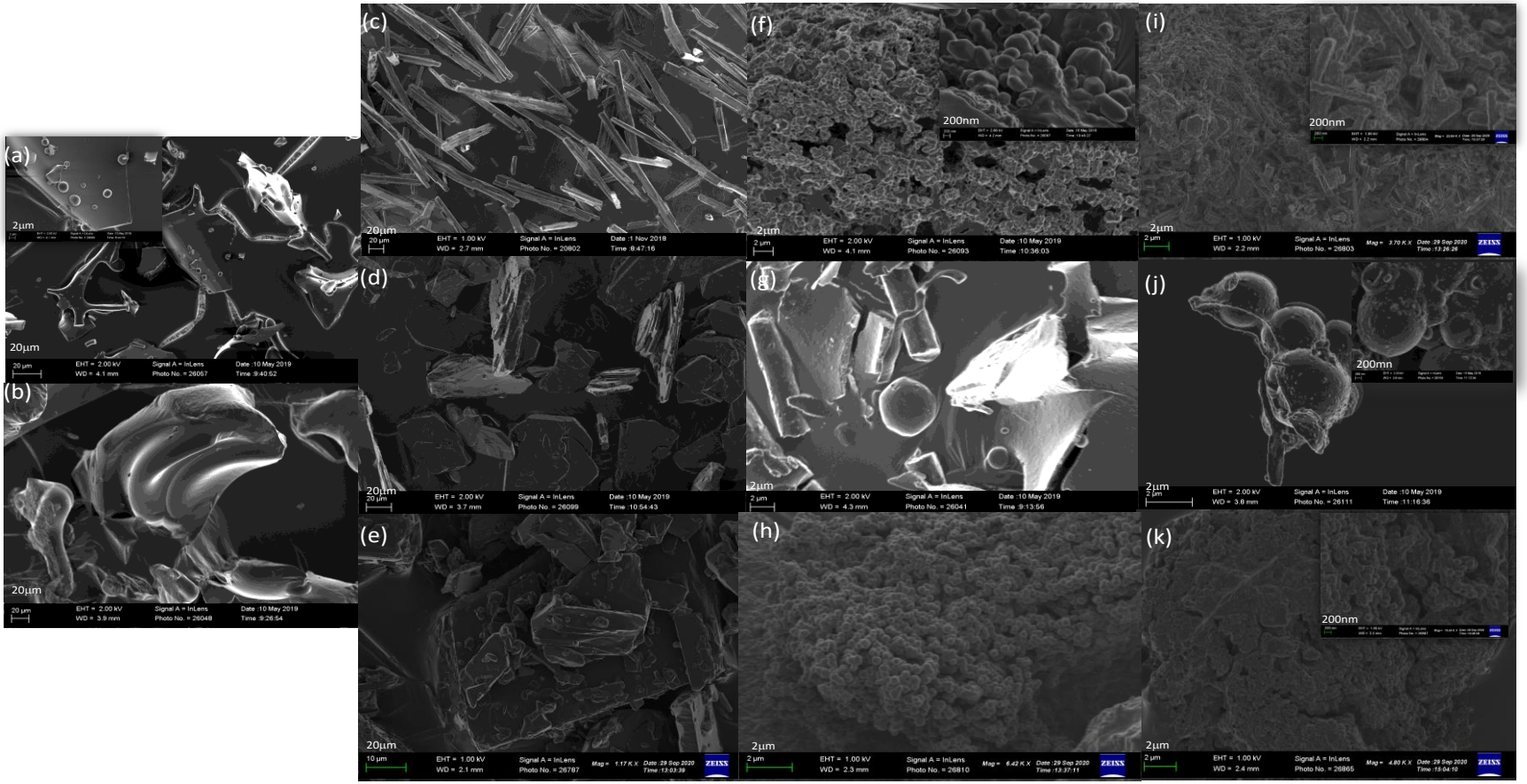

Figure 4.18: SEM images of (a) PGA, (b) p(NAM-stat-AA), (c) Lum, (d) DHA, (e) PQ, (f)-(h) p(NAM-stat-AA)-drug conjugates and (i)-(k) PGA-drug conjugates.

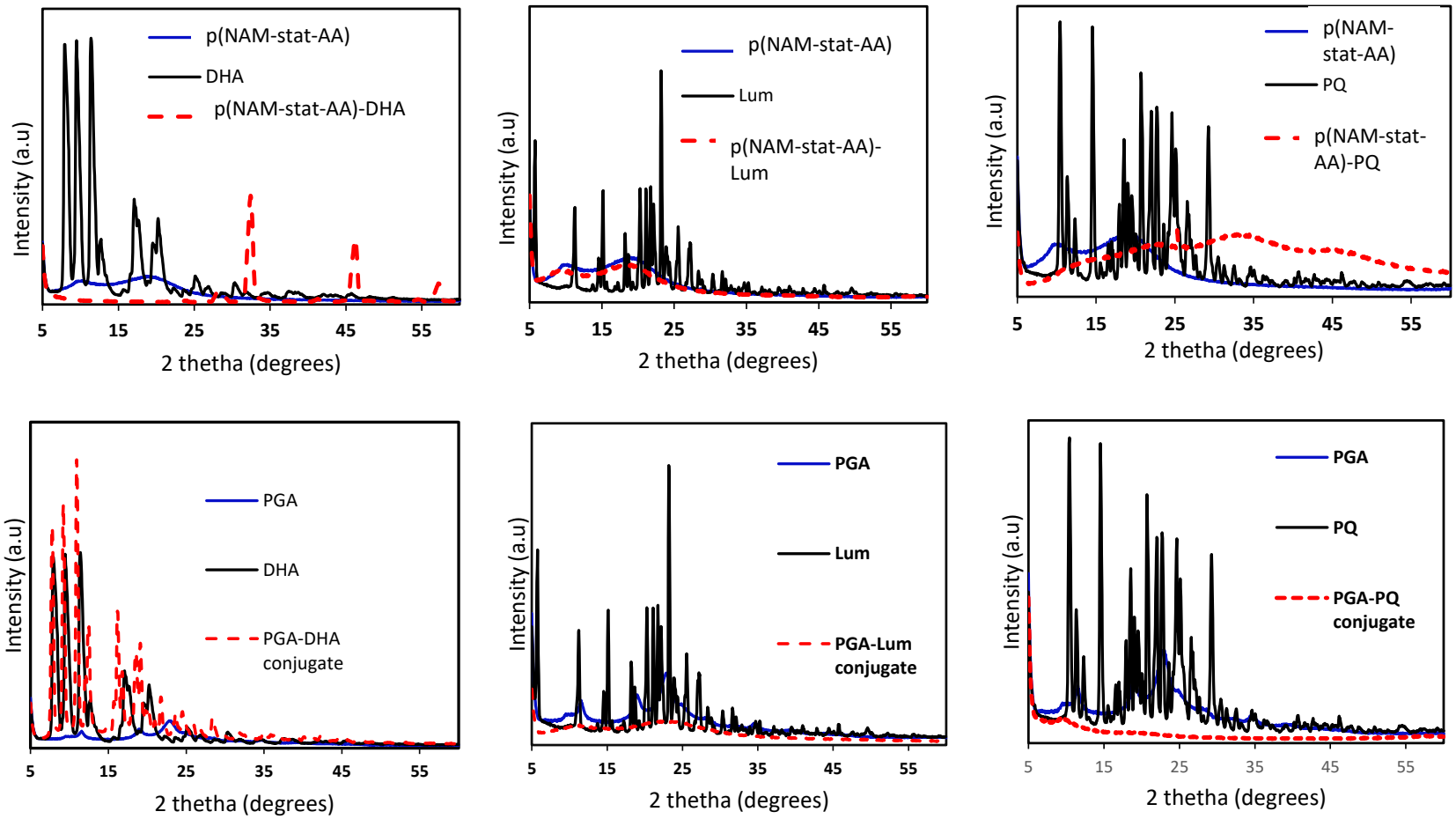

Figure 4.19: PXRD of p(NAM-stat-AA)-drug conjugates and PGA-drug conjugates.

SEM images. These results indicate that upon conjugation, the drugs changed their physical state. The change to an amorphous material is important in pharmaceuticals to improve properties such as dissolution rate and bioavailability (Vranic, 2004).

The p(NAM-stat-AA) and PGA drug conjugates were evaluated for their thermal stability using TGA and DSC thermograms shown in **Figure 4.20** and **Figure 4.21**. All the samples showed an initial weight loss of 2 % to 5 % attributed to loss of water. Low quantities of water are desirable whereas high moisture content can result in degradation and microbial contamination during storage (Vauthier and Bouchemal, 2009). The TGA of p(NAM-stat-AA), DHA and the p(NAM-stat-AA-DHA) conjugate in **Figure 4.20 (a)**, shows that p(NAM-stat-AA) underwent decomposition from 159.79 °C to 393 °C with a weight loss of about 60 %. This could have been due to the breaking of the ether bonds (Movagharnezhad and Moghadam, 2016) and decomposition of the polymer (Al-Sagheer, Ibrahim and Khalil, 2014). The conjugate, p(NAM-stat-AA)-DHA underwent continuous decomposition starting at 158.81 °C and 205.15 °C with weight loss of 17 % and 39.21 % respectively, which could have been due to breaking of the ester linkage and ether bond from the p(NAM-stat-AA). These changes were also observed in the DSC thermogram, with the appearance of new peaks at temperatures of 113.67 °C, 180.16 °C and 207.87 °C. These results show that the structure of the pure DHA and p(NAM-stat-AA) were changed upon conjugation. A similar result was seen in the p(NAM-stat-AA)-Lum conjugate were ester and ether bond breakage were seen starting at temperatures of 143.47 °C and 320.64 °C in **Figure 4.20 (b**) with at with 1.08 % and 38.65 % weight loss. The DSC thermogram shows the change in the physical structure of the starting material by a lack of appearance of the Lum endotherm indicating that the there is a change in crystallinity and nature upon conjugation (Thompson et al. 2008). A similar observation was seen in the DSC thermogram (**Figure 4.20 (c'**)) of p(NAM-stat-AA)-PQ conjugate, where the PQ exothermic peak was not visible in the conjugate. TGA thermogram of p(NAM-stat-AA)-PQ in **Figure 4.20 (c)** showed several decomposition temperatures from 70 °C to 176.13°C with a weight loss of 18.12 % this could have been due to loss of water molecules absorbed by the molecule. There is further decomposition from 202.07 °C to 393.78 °C with weight loss of 43.18 % and this could be due to breaking amide bond linkage (Movagharnezhad and Moghadam, 2016). Also beyond the 250 °C there is a possibility of decarboxylation of the free carboxyl groups from the polymer (Wang et al. 2007). These results show that upon conjugation there were changes in the physical structure of the conjugate that resulted in changes in the TGA and DSC thermogram compared to the free drugs and p(NAM-stat-AA).

PGA conjugates are represented in **Figure 4.21**, TGA shows that PGA has two decomposition temperatures. The initial one observed below 200 °C was due to the release of water as the polymer is highly hydrophilic due to the carboxylic acid functionalities (Portilla-Arias et al. 2007). The second decomposition step occurs from 202 °C to 395 °C with a weight loss of about 56.68 %. The DSC thermogram also showed these decompositions at 65.99 °C and 249.03 °C due to the loss of water molecules and breaking down of the polymer (Yang, 2011). TGA of the PGA-DHA conjugate shown in **Figure 4.21 (a)** showed evaporation of moisture at 122.88 °C with a weight loss of 3.80 %. This was followed by decomposition of at 200 °C and 583.23 °C with weight losses of 35.25 % and 6.2 % respectively. These could be due to the breaking of the ester bond and also decomposition of the polymer backbone. The PGA-DHA curve reflects the heterogeneous nature of the interaction between the drug and polymer (Margaritis and Manocha, 2010). The DSC thermogram in **Figure 4.21 (a')** showed that the conjugate is still crystalline in nature by appearance of the DHA exothermic peak at 164.17 °C. This was also observed in the DSC thermogram of PGA-Lum with appearance of both polymer and drug endothermic peaks (**Figure 4.21 (b'**)). The TGA for PGA-Lum in **Figure 4.21 (b)** showed decomposition temperatures at 258.15 °C and 592 °C corresponding to weight loss of 41.18 % and 4.19 % respectively. Since the PGA-PQ conjugate was prepared from the sodium form of the PGA polymer, the TGA analysis of the conjugate is compared to that of the sodium form of the PGA polymer (**Figure 4.21 (c)**). This explains the difference in the TGA thermogram of PGA compared to the previous analyses as the acid (PGA) form was used in **Figures 4.21** (**a)** and (**b)**. The DSC thermogram in **Figure 4.20 (c')** of the conjugate showed the endothermic peak of the polymer with no drug peaks. While TGA of the conjugate shown in **Figure 4.21 (c)** showed decomposition temperature at 206.22 to 411 °C having a 55.8 % weight loss.

The TGA results showed many decomposition temperatures compared to the pure drug and polymer. This could be due to formation of the nanoparticles that have a greater superficial area resulting in thermal decomposition occurring much faster (Mainardes, Gremião and Evangelista, 2006). This could also indicate the heterogeneous nature of the conjugate due to covalent bonding of the carboxylic groups from the polymers with the hydroxyl and amine groups of the drugs (Margaritis and Manocha, 2010). The DSC results support the results observed in PXRD, where DHA conjugate still showed some form of crystallinity, while the Lum and PQ conjugate showed an amorphous nature.

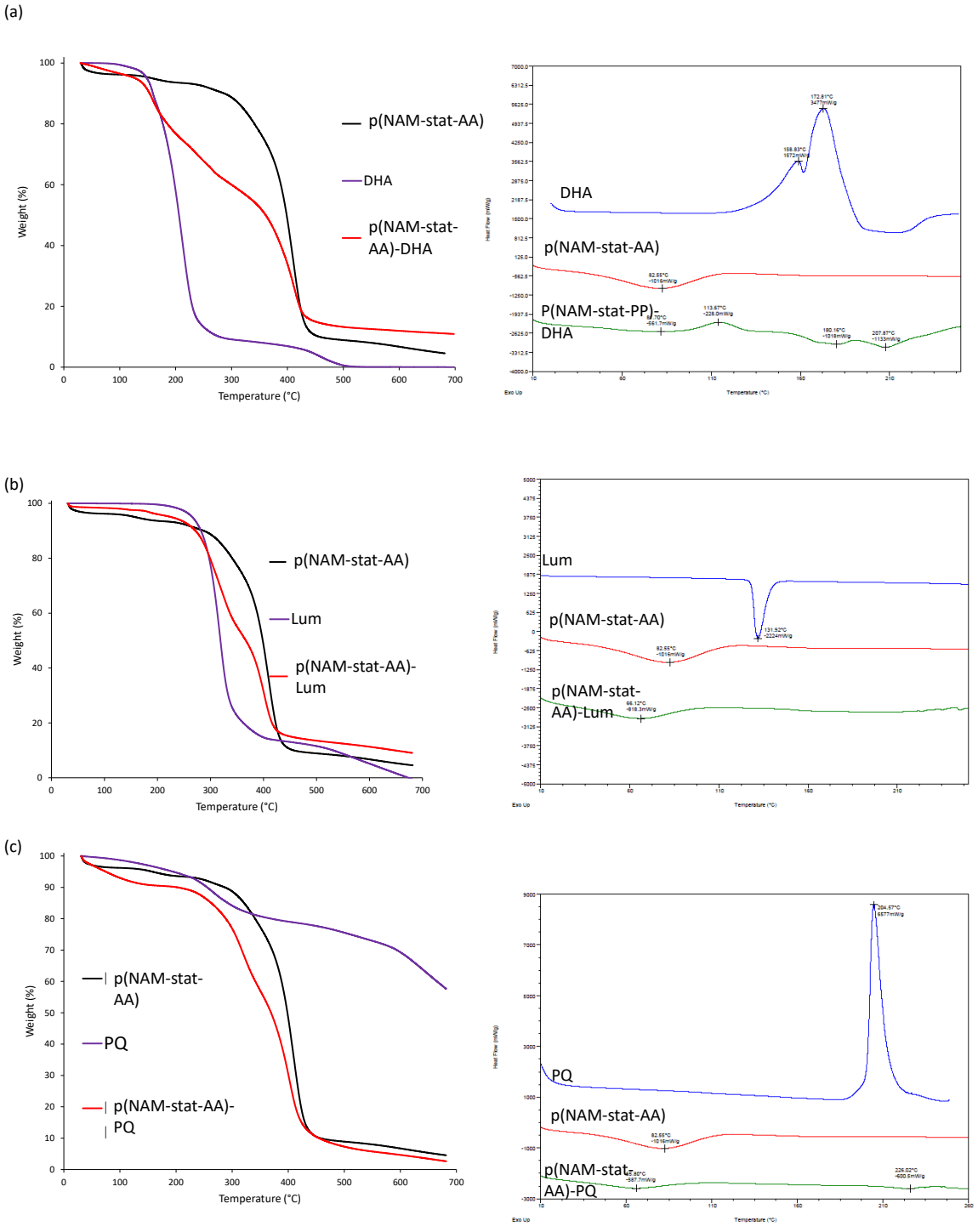

Table 4.20: TGA thermogram of (a) p(NAM)-stat-AA-DHA, (b) p(NAM)-stat-AA-Lum and (c) p(NAM)-stat-AA-PQ conjugates with their corresponding DSC thermograms.

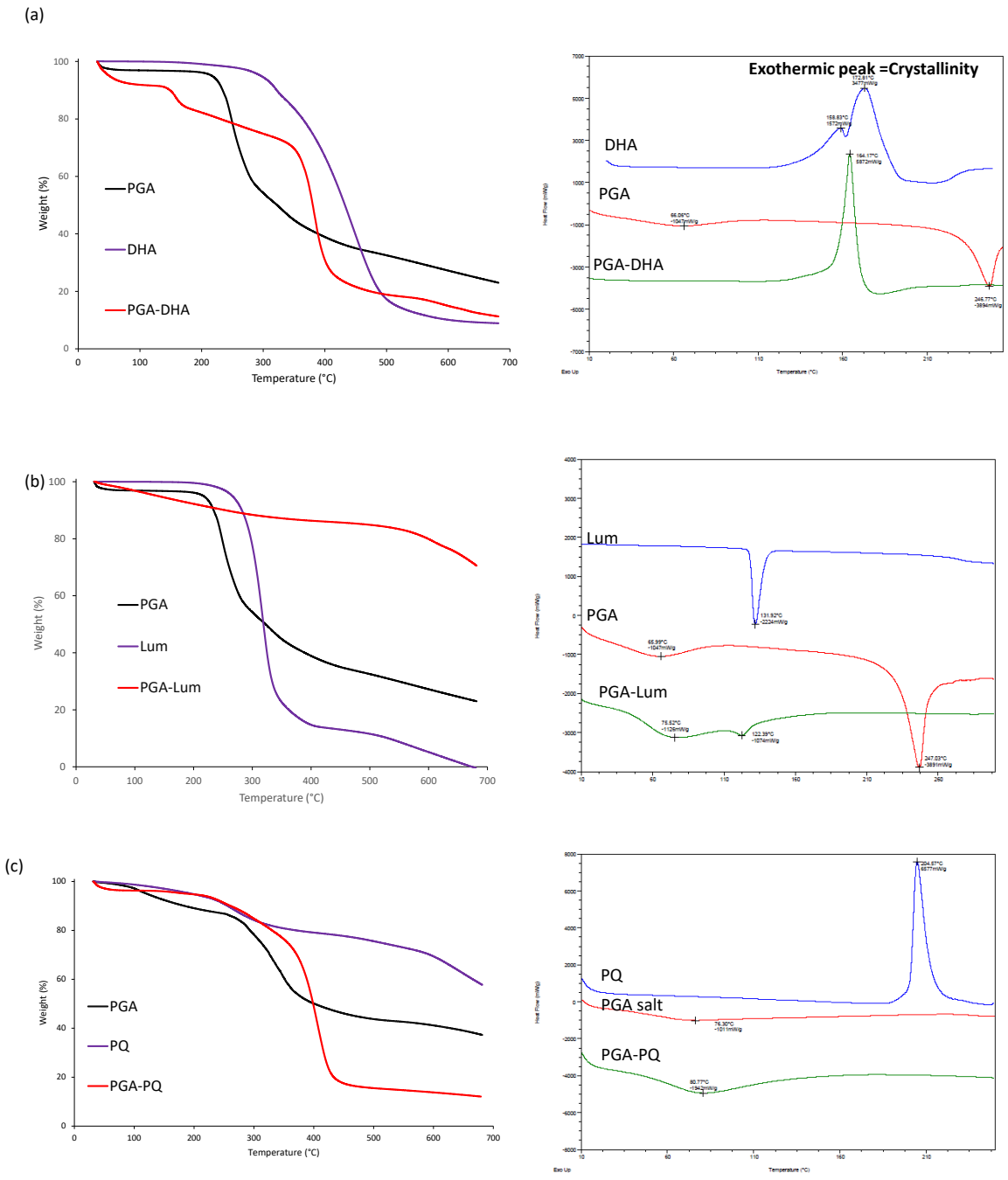

Figure 4.21: TGA thermograms of (a) PGA-DHA, (b) PGA-Lum and (c) PGA-PQ conjugates with their corresponding DSC thermograms.

4.2.3 Cytotoxicity studies

The conjugates were submitted for toxicity studies. These studies were conducted to compare the concentration of the free drug, polymer and conjugates that can cause 50 % mortality. Lethal concentration (LC_{50}) were tested using Vero cells (African green Monkey kidney cells) and Caco-2 cells using 3-(4,5-dimethylthiazol)-2,5-diphenyl tetrazolium bromide (MTT) assay (Mosmann, 1983; McGaw et al., 2007). The MTT assay is a colorimetric assay that measures cell proliferation as well as reduction in cell viability when metabolic events lead to cell death. It can also be used to assess the rate of survival of a given cell line and provide information about toxicity profiles of the new chemical entities to avoid unwanted exposure of animals to toxic material. **Table 4.7** is a summary of the results for the LC_{50} results of free drug, polymers and conjugates.

Table 4.7: LC_{50} of free drugs, polymers and polymer-drug conjugates in both Vero cells and Caco-2 cells in mg/mL.

Compound	***Vero cells (mg/mL)***	***Caco2- cells (mg/mL)***
DHA (control)	0.005 ± 0.0002	0.04 ± 0.003
p(NAM-stat-AA)-DHA	0.04 ± 0.002	0.09 ± 0.0009
PGA-DHA	0.03 ± 0.0005	>0.4
Lum (control)	>0.4	>0.4
p(NAM-stat-AA)-Lum	>0.4	>0.4
PGA-Lum	>0.4	>0.4
PQ (control)	0.13 ± 0.0115	0.012 ± 0.0004
p(NAM-stat-AA)-PQ	>0.4	0.13 ± 0.011
PGA-PQ	>0.4	>0.4
p(NAM-stat-AA) (control)	>0.4	>0.4
PGA (control)	>0.4	>0.4

A comparison of the LC_{50} values for Vero and Caco2 cells show that for the controls, LC_{50} for Lum, p(NAM-stat-AA) and PGA was greater than 0.4 mg/mL for both Vero cells and Caco-2 cells. While for DHA there was an increase in the concentration of the drug needed to cause 50% mortality from 0.005 ± 0.0002 to 0.04 ± 0.003, there was a decrease for PQ from 0.13 ± 0.0115 to 0.012 ± 0.0004. An increase in concentration needed to cause mortality, means the substance is less toxic. Therefore, these results indicate that DHA is more toxic towards Vero cells than Caco2 cells, while PQ is toxic in Caco-2 cells and other controls non-toxic for both cells.

There is a general decrease in toxicity for the conjugates corresponding to an increase in the lethal concentration. These results support the idea that polymeric carriers attenuate the activity of drugs by creating pro-drugs with reduced toxicity. This concurs with a previous report that conjugation reduced the toxicity of DHA, which is generally a toxic compound (Chaturvedi et al. 2010). These results also support the idea that polymers like PGA are non-toxic.

4.3 Conclusion

DHA, Lum and PQ, the three drugs recommended for triple combination therapy for malaria, were individually covalently conjugated to non-toxic multivalent polymers (p(NAM-stat-AA) and PGA). Proton NMR spectroscopy confirmed conjugation by shift in some NMR proton peaks or broadening of peaks indicating interaction between the drug and polymer. The appearance of some new carbonyl absorption bands in FT-IR spectroscopy further confirmed conjugation.

Multivalent polymers were used in an attempt to improve the percentage drug loading. Proton NMR spectroscopy was also used to calculate the percentage drug loading, for both PGA and p(NAM-stat-AA) conjugates loading was lower than the molar equivalents used in the reactions when coupling to the polymer (4 mol % p(NAM-stat-AA)-DHA, 12 mol % p(NAM-stat-AA)-Lum and 2 mol % p(NAM-stat-AA)-PQ. This could have been due to steric hindrance, more especially for Lum and DHA, preventing the drugs from occupying activated carboxylic acid sites. Zeta potentials further confirmed this as at pH 7.40 the zeta potential was negative, indicating not all carboxylic acid groups were conjugated. Therefore, these multivalent polymers do not offer an advantage over popular polymers like PEG.

Upon conjugation, the physico-chemical properties of the conjugates were evaluated. The thermal studies showed that upon conjugation there is a change in the physical nature compared to the free drug and polymer, resulting in a different thermogram. This supported the SEM images and PXRD diffraction results that upon conjugation the crystalline drugs changed their physical state to amorphous material. Amorphous material is desired for drugs as this improves the bioavailability of the compound though improving the solubility of the compound. The Lum conjugate showed improved solubility at the maximum concentration tested in this study (6 mg/mL) by having over 50 % of the drug soluble in water for both p(NAM-stat-AA) and PGA. Conjugation also reduced toxicity of drugs like DHA.

The physico-chemical properties reported in this work are similar to the recently reported self-assembly aggregate of artemether and Lum synthesized by Fortuin et al. (2020) using a copolymer of poly(*N*-vinylpyrrolidone) and poly(α-allylvalerolactone). Where Lum was conjugated using an acid-labile acetal linkage and artemether was entrapped within the hydrophobic core of the self-assembled aggregates forming a micelle. Compared to our work, these authors reported high drug loading of 14 wt% and 27 wt% for Artemether and Lum respectively. Similar to this study, the polymer size measured by TEM was lower than that measured by DLS. Both studies showed that conjugation decreases the toxicity of the drugs.

The conjugation of DHA, Lum and PQ to multivalent polymers (p (NAM-stat-AA) and PGA) have illustrated improved physico-chemical properties and reduced toxicity of the drugs. Unfortunately, drug loading remained poor in spite of using multivalent polymers. We hypothesized that this could be due to steric hindrance limiting access to all reactive sites. Use of linkers between the polymer and the drug, may be a possible solution to the problem and the linker chemistry will be discussed in the next chapter.

Chapter Five:
Synthesis of polymer-drug conjugates using physiologically cleavable linkers

5.1 Introduction

According to Ringsdorf's definition, polymer-drug conjugates do not only contain a water soluble polymer and a bioactive agent but they also contain a physiologically labile linker that is chemically stable. A linker is a molecule that joins a drug to a polymer (Chang et al. 2015) and it can be cleaved by a stimulus such as a change in pH (Pang et al. 2016; Le and Neralla, 2020; Zhou et al. 2020) or the presence of a specific enzyme (Chen et al. 2018; Erez et al. 2009; Slor and Amir, 2021). The role of a linker goes further than binding a drug to a polymer, as it ensures stability during transportation of the conjugate but is able to release the drug at the targeted site (Duncan, 2006; Lavignac et al. 2009; Larson and Ghandehari, 2012). In addition, a linker is able to increase the percentage drug loading as was shown by Singer et al. (2001) when they interrogated the effect of a small linker glycine coupled between PGA and camptothecin (CPT). PGA with CPT without glycine had 15% w/w drug loading and the conjugate with a glycine linker had increased percentage drug loading to 50% w/w (Singer et al. 2006). The chemistry of a linker is also important as it provides control of drug release and thus enhances therapeutic efficacy. This was shown by Quan et al. (2013) when they compared HPMA– dexamethasone polymeric system designed by incorporating hydrazone and hydrazone benzyl ester linkers. These are slow and fast releasing polymeric prodrugs respectively, and they were evaluated in an adjuvant-induced arthritis rat model. After a single I.V. injection, the slow releasing hydrozone linked conjugate maintained a longer duration of therapeutic activity than the hydrozone benzyl ester linked conjugate that has faster release kinetics, resulting in better joint protection. Thus, the rational design of the polymer-drug conjugate is very important to ensure that the conjugate is stable, the amount of drug loaded is optimum and the drug is released to elicit the desired therapeutic effect. In addition, the type of drug used and the site and action of mechanism have to be considered in the rational design of polymer-drug conjugates.

Malaria infected red blood cells (RBCs) are reported to have new permeability pathways (NPPs) shown in **Figure 5.1**, that develop in the plasma membrane of the infected RBCs within

12-16 h after infection (Biagini, Ward and Bray, 2005; Santos-Magalhães and V. C F Mosqueira, 2010; Santos-magalhães, Carla and Mosqueira, 2010; Urbán et al. 2014). These NPPs are important for the parasite to exchange material with the environment as the RBCs lack an endocytotic system. These channels have a size range of 50-80 nm diameter and are permeable to biomacromolecules. They present an attractive route for passive concentration of the conjugate into the cells that provides discrimination between infected and non-infected RBCs. These channels could direct the conjugate into the gut of the parasite via the permeable parasitophorus vacuole membrane (PVM), which is acidic and suitable for cleaving acid-labile bonds like esters and imines. This compartment has a pH range of 5.2-5.8, it is in this vacuole that most antimalarial are believed to work by inhibiting hemozoin synthesis.

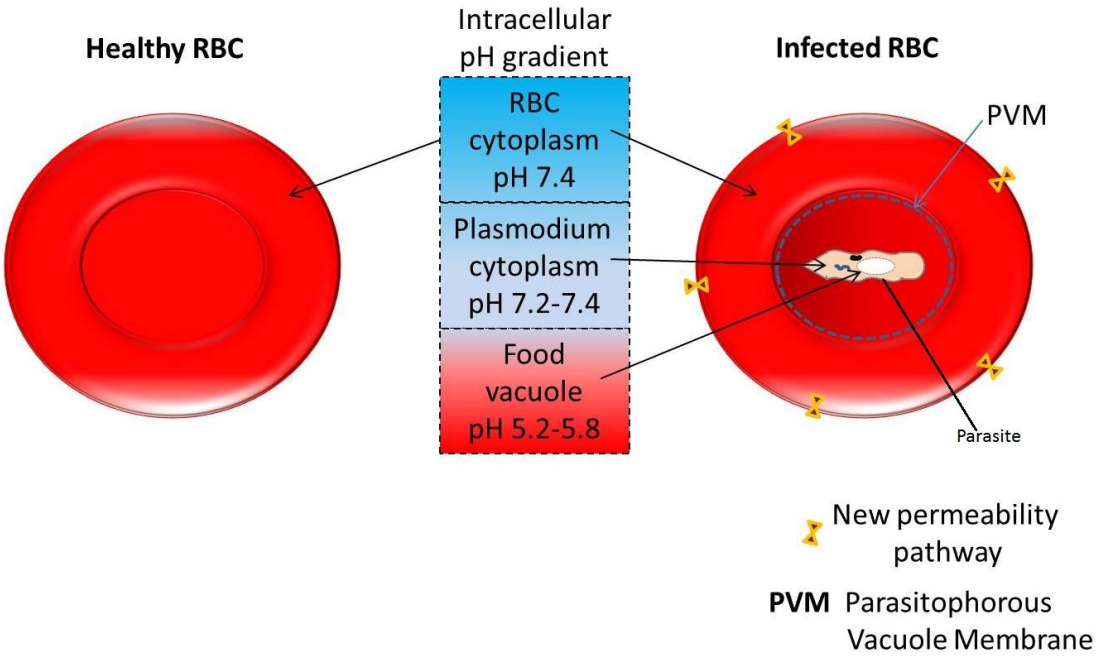

Figure 5.1: Schematic representation the new permeability pathways (NPPs) and pH gradation of infected RBCs.

Designing an appropriate linker is indispensable in obtaining an effective polymer therapeutic. Previously, in **Chapter 4**, Lum was linked directly to p(NAM)-stat-AA and PGA via an ester bond with no intervening alkyl chain. Also, earlier in **Chapter 3**, DHA was linked to PEG amine and chitosan through the dicarboxylic acid linker succinic acid. In this chapter the amino acid glycine is investigated as a potential linker for Lum as shown in **Scheme 5.1**. As a heterobifunctional molecule, glycine offers the potential of an asymmetrical bonding chemistry

between the drug Lum and a polymer bearing a carboxylic group. This is important as the homobifunctional succinic acid does not allow for linkage of Lum to a carboxylated carrier polymer like p(NAM)-stat-AA and PGA.

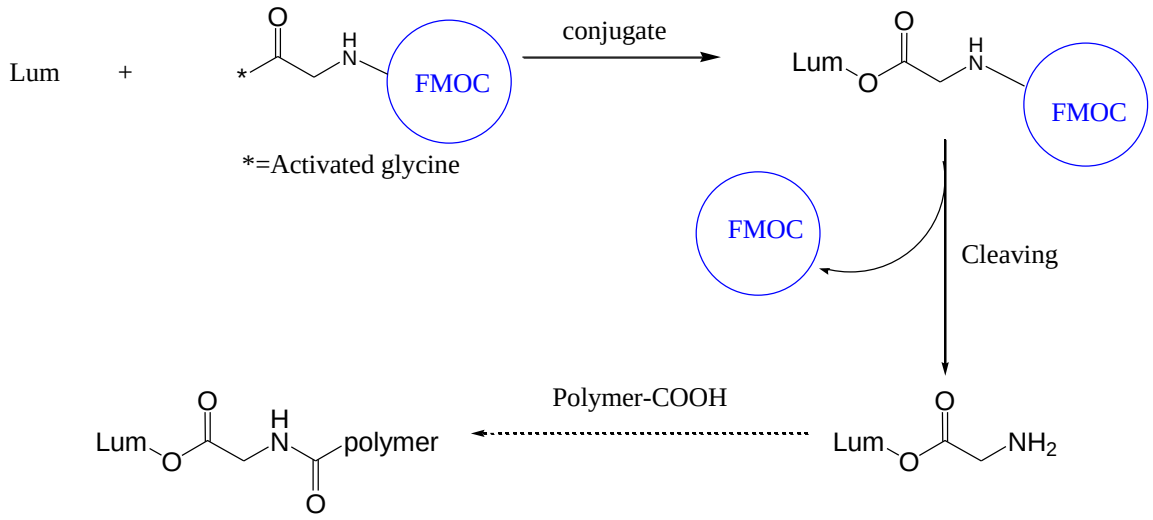

Scheme 5.1: Schematic representation of the work planned.

5.2 Results and Discussion

5.2.1 Synthesis and characterization

5.2.1.1 Synthesis of Fmoc-gly-Cl

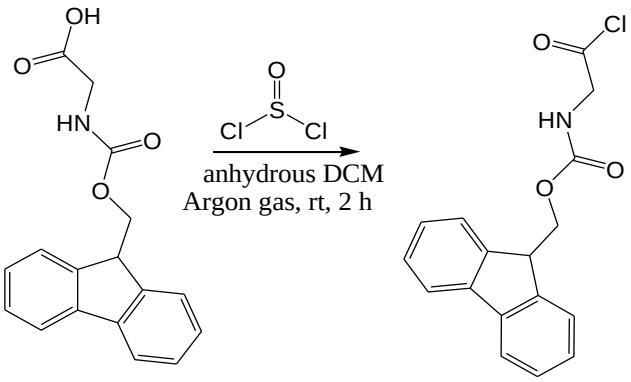

Scheme 5.2: Synthesis of Fmoc-gly-chloride.

The conversion of carboxylic acid (Fmoc-gly-OH) to an acid chloride was carried out using a method published by Gawande and Branco (2011) with slight modifications. The synthesis was done using thionyl chloride at room temperature in an aprotic solvent (DCM) as shown in **Scheme 5.2**. The crude product was isolated as a white solid powder after concentration under reduced pressure followed by precipitation using cold hexane. TLC analysis (hexane : EtOAc

(1:3)) revealed that the purified Fmoc-gly-Cl product has an increased R_f (0.72) value compared to the Fmoc-gly-OH (0.16). The ^{1}H NMR spectrum in **Figure 5.2** clearly shows the disappearance of the acidic proton at 12.59 ppm (indicated by dashed box). Also upon substitution with the chlorine atom there is deshielding of the methylene protons (labelled 8) caused by electronegativity and electron crowding of the chlorine group. Also the ^{1}H NMR intergrals of the diagnostic peaks gave the expected number of protons for the acid chloride (**Figure 1C, Appendix**) and these results are similar to those published by Gawande and Branco (2011), the Fmoc-gly-OH NMR spectrum has an impurity peak marked by an asterisk. The product was stored under nitrogen at room temperature to avoid product degradation as chloride is a good leaving group. The successfully synthesized Fmoc-gly-Cl product was immediately used in the next step in an attempt to synthesize Fmoc-gly-Lum.

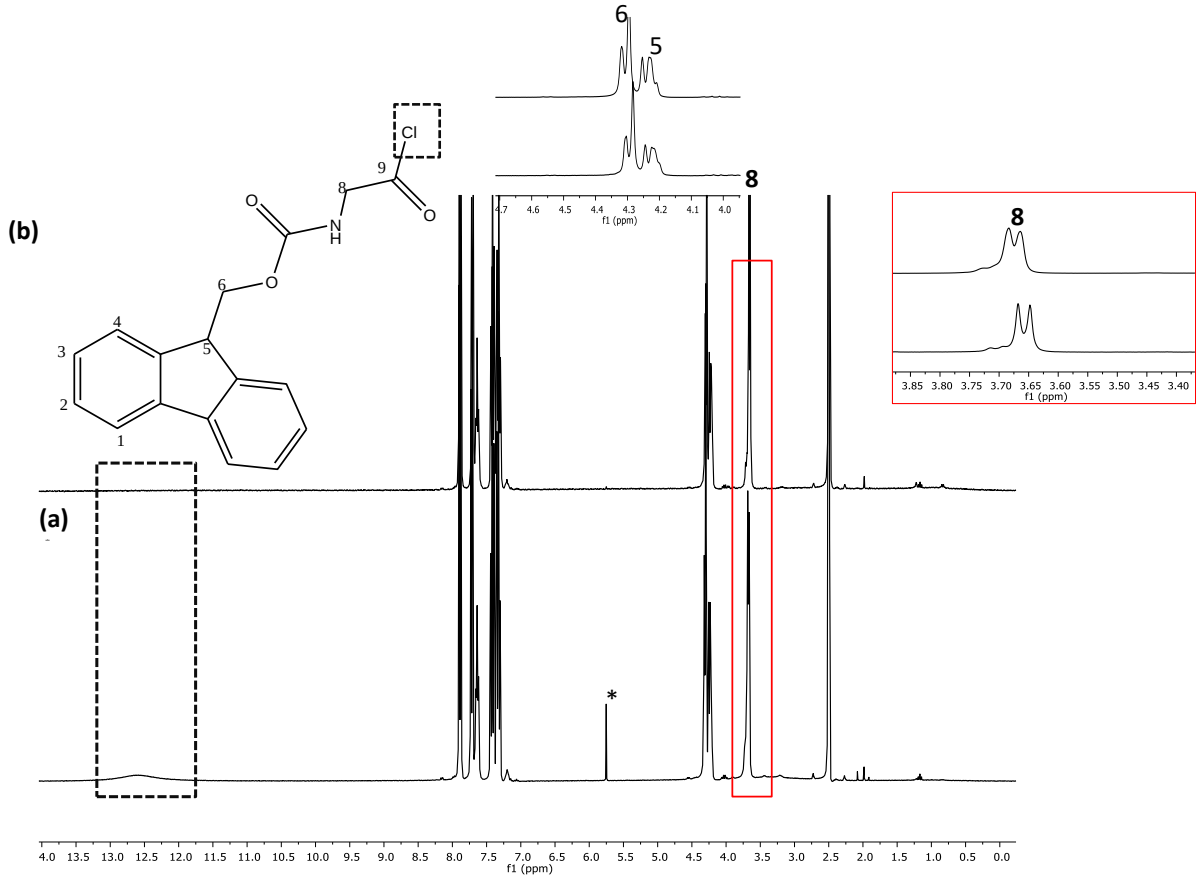

Figure 5.2: ^{1}H NMR (300 MHz, DMSO-d_6) spectrum of (a) Fmoc-gly-OH and (b) Fmoc-gly-Cl.

5.2.1.2 Synthesis of Fmoc-gly-Lum.

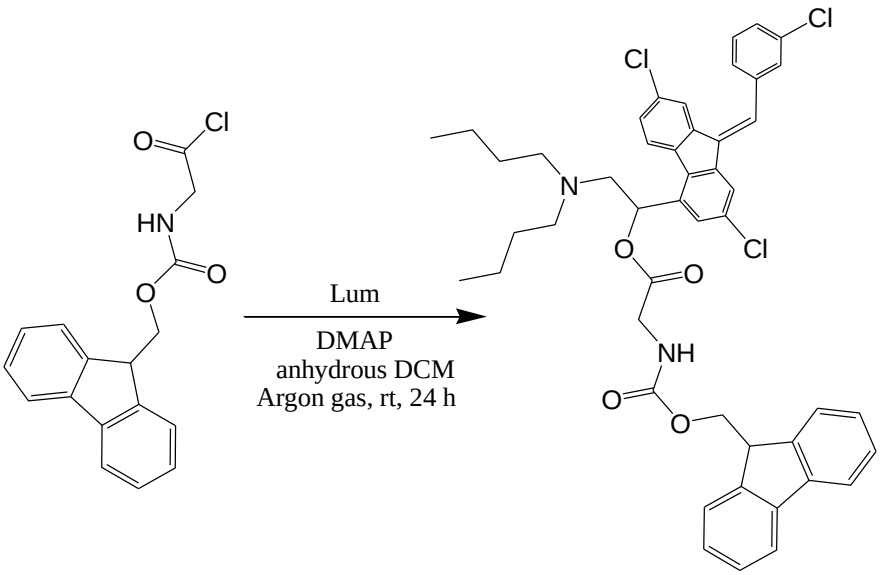

Scheme 5.3: Synthesis of Fmoc-gly-Lum.

Coupling of Fmoc-gly-Cl to Lum was initially carried out as shown in **Scheme 5.3** using DMAP to neutralize the HCl liberated from the reaction. The formation of Fmoc-gly-Lum was monitored after 24 h by TLC (hexane: EtOAc (3:1) R_f = 0.33) and the reaction mixture showed the presence of a new spot with a lower retention factor compared to Lum (R_f = 0.53) indicating increased polarity from an increased number of polar groups. The product was purified by flash silica column chromatography using hexane: EtOAc (3:1) as eluent. The ^{1}H NMR intergrated spectrum in **Figure 5.3** shows that upon purification of the crude product the ester bond was hydrolyzed as there is no shift in Lum oxymethine proton marked x at 5.44 ppm and the methylene proton peaks of the glycine are also not visible (red box) as impurities are observed, also the intergrated peaks gave the proton number of free Lum. Similar to the DHA-Suc in **Chapter 3,** the column was basified using trimethylamine to neutralize the silanol groups on the silica but this still yielded undesired product.

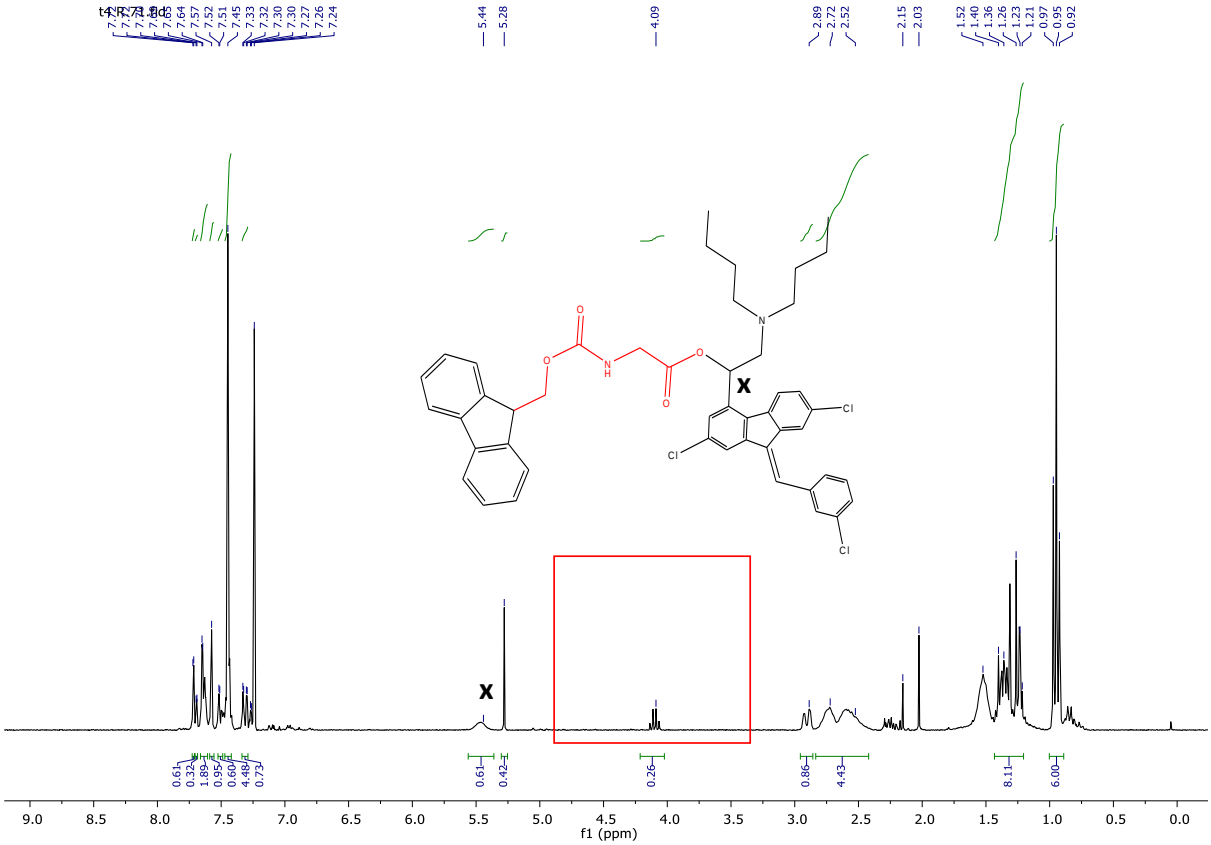

Figure 5.3: ^{1}H NMR (300 MHz, $CDCl_3$) spectrum of the isolated undesired product.

Braslau, Axon and Lee (2000) reported that the nature of the base is important as pyridine leads to formation of *O*-protected hydroxylamines as a major product. Since DMAP is a derivative of pyridine and more basic than pyridine (Scriven and Murugan, 2005), trimethylamine was used as a base but the same undesired product formed under both basified and unbasified column chromatography. Acid halides are good leaving groups (Ayers et al. 2005), this makes them unstable and thus other methods were explored in an attempt to synthesize the desired Fmoc-gly-Lum product in higher yields.

5.2.1.3 Synthesis of Fmoc-gly-Lum using carbodiimide chemistry.

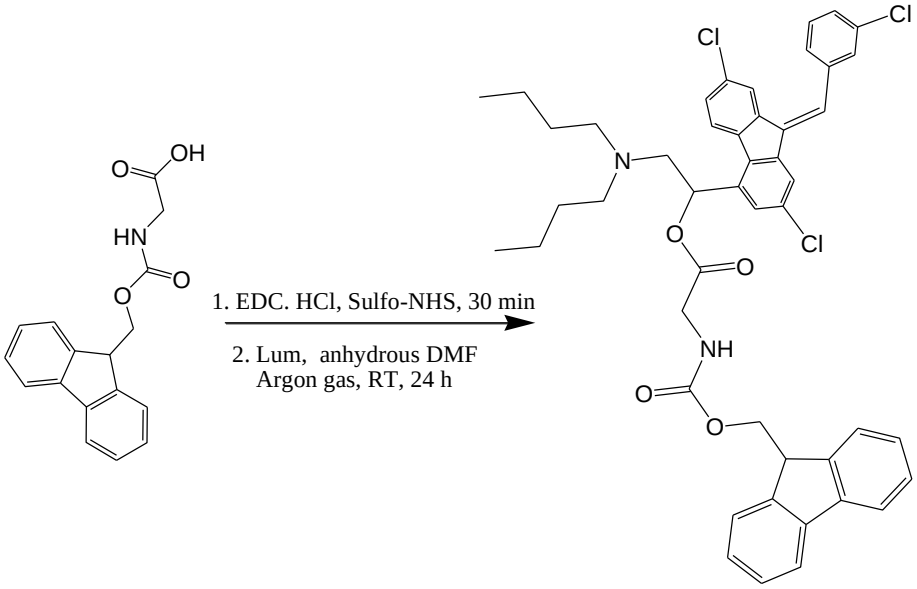

Scheme 5.4: Synthesis of Fmoc-gly-Lum conjugate using EDC/Sulfo-NHS.

Esterification of Lum to Fmoc-glycine via carbodiimide coupling methodology using EDC and sulfo-NHS under inert conditions to avoid hydrolysis of the ester bond was explored (**Scheme 5.4)**. EDC was chosen since it is a water-soluble carbodiimide reagent and its isourea by-product is also water soluble (Hermanson, 2008). Therefore, instead of using column chromatography that yielded undesired product, the crude Fmoc-gly-Lum was purified by precipitation in deionized water and washed 5 times using PBS buffer pH 7.4 to remove water soluble reagents and byproducts and this yielded the desired Fmoc-gly-Lum.

FT-IR analysis, presented in **Figure 5.4**, confirmed conjugation by the appearance of the absorption at 1706.3 cm^{-1} for the conjugate due to carbonyl (C=O) stretch of an ester bond, this is a new peak from the urethane linkage joining the glycine to the Fmoc which appears at 1636.9 cm^{-1}. This was supported by the ^{1}H NMR spectrum in **Figure 5.5** which showed a shift of the methine proton from 5.20 ppm (labelled 10*) to 5.92 ppm (labelled 10). There is also the appearance of the glycine methyl protons around 3.73-4.1 ppm (labelled 6 to 8). The appearance of the ester carbon at 170.06 ppm in the carbon spectra conducted in DMSO-d_6 further confirms the results, unfortunately when NMR spectra were run in $CDCl_3$ it was not easy to see this peak (see **Figure 1E, Appendix)**.

The glycine used in this work is Fmoc protected, which was chosen to allow formation of an ester bond with the drug instead of an amide bond between two glycine molecules. This is

because the primary amine of glycine will outcompete the less nucleophilic hydroxyl group of Lum. Amide bonds have been reported to show high stability towards various reaction mechanism conditions (acidic and basic conditions), high temperature and in the presence of other chemicals (Bond et al. 2018). This is because amide bonds resonate to provide a stabilizing a double bond character to the amide C-N bond.

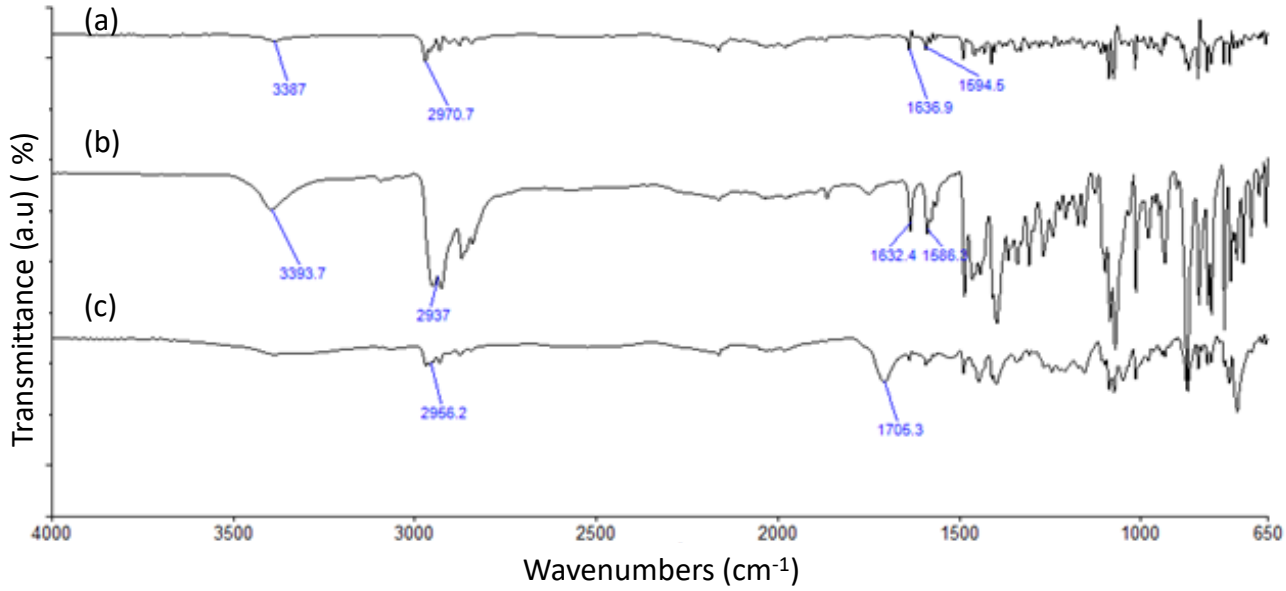

Figure 5.4: FT-IR spectra of (a) Fmoc-glycine-OH, (b) Lum and (c) Fmoc-gly-Lum.

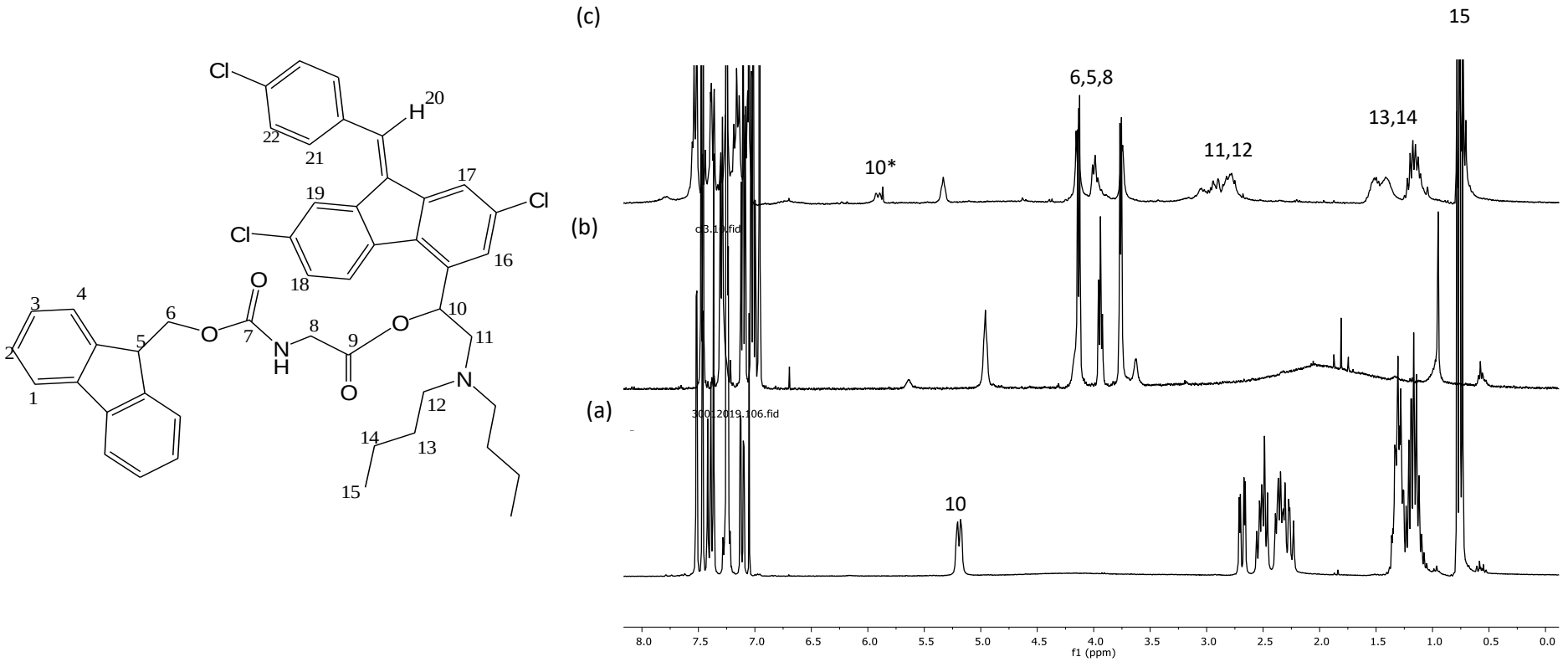

Figure 5.5: ^{1}H NMR spectra (300 MHz, $CDCl_3$) of (a) Lum, (b) Fmoc-gly-OH and (c) Fmoc-gly-Lum.

5.2.1.4 Cleaving of the Fmoc group.

After the coupling reaction, 80 mg of Lum-gly-Fmoc was treated with 20% v/v piperidine in DMF at room temperature to deprotect the amino group of Fmoc. The Fmoc removal mechanism has two steps, the initial deprotection of the fluorenyl system by elimination that yields dibenzofulvene (DBF) and carbamic acid by-products (**Scheme 5.5**). The carbamic acid then decomposes spontaneously to release carbon dioxide along with a free amine. DBF is scavenged by a nucleophile (piperidine) reacting with the free amine to form a piperidine-DBF adduct. It is important to note the reaction was done in DMF to avoid formation of an amine salt precipitate (Fields, 2014). The crude product was purified by column chromatography but this resulted in an undesired mixture of Lum – implying premature ester hyrolysis, DBF (marked 1) and piperidine-DBF (marked 2) as seen in ^{1}H NMR spectrum (**Figure 5.6)** and this also resulted in the loss in quality of the aromatic proton peaks. Therefore, other deprotection methods were explored in an attempt to get the desired product.

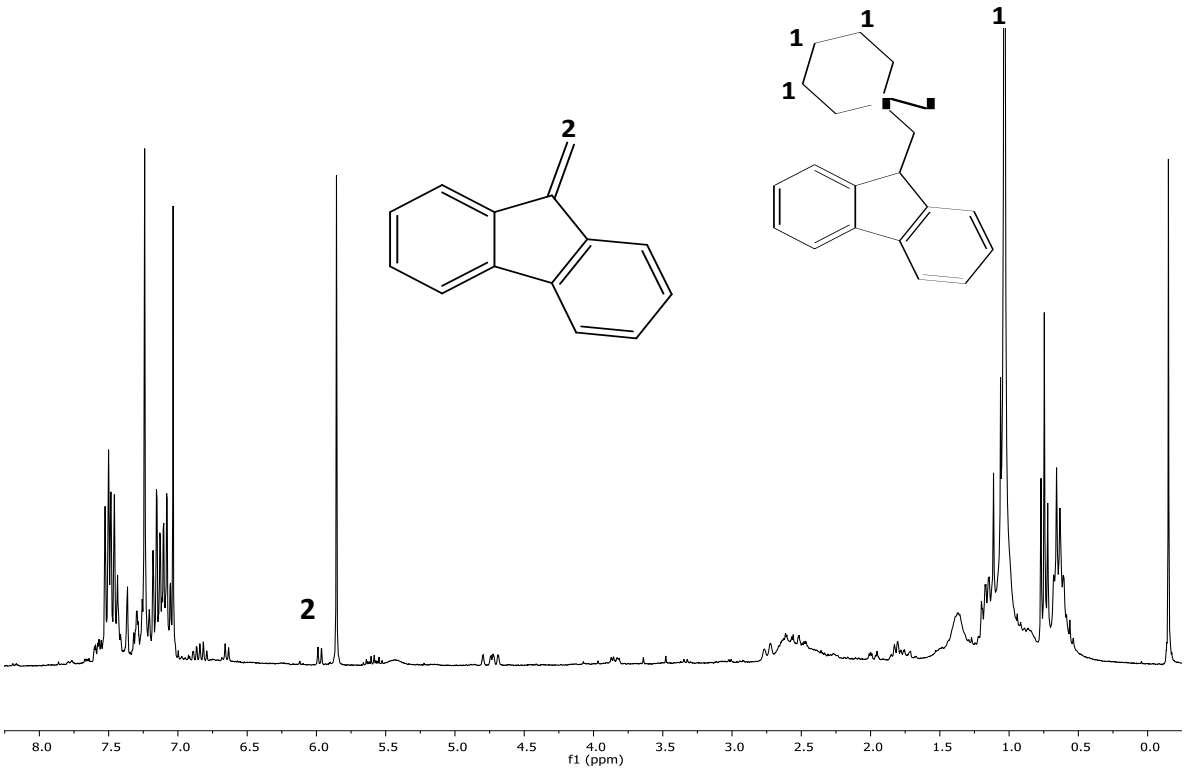

Figure 5.6: ^{1}H NMR (300 MHz, $CDCl_3$) spectrum of isolated undesired product with DBF and piperidine-DBF.

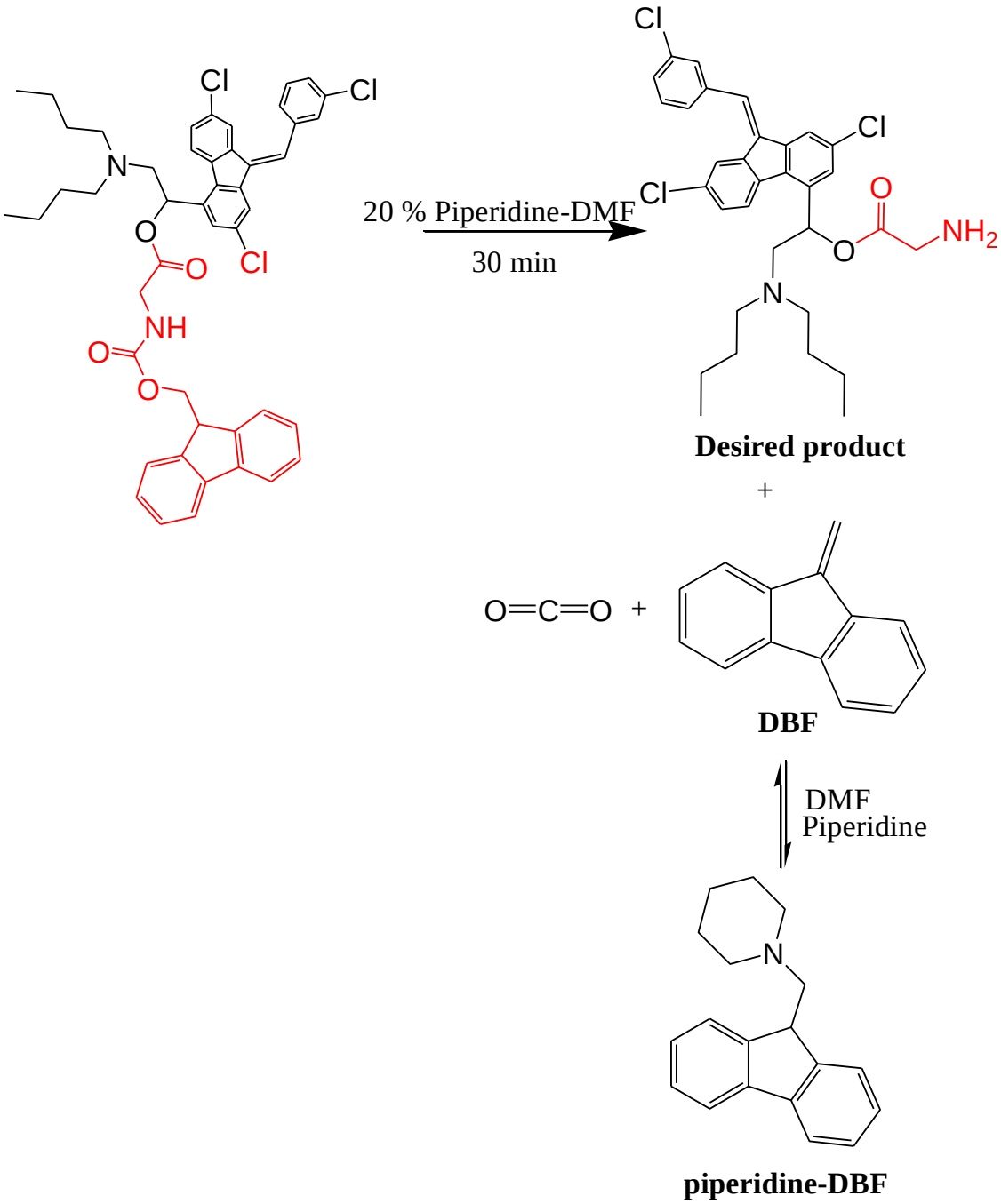

Scheme 5.5: Cleaving of the Fmoc from the amine.

5.2.1.4.1 Change in base.

Deprotection of the Fmoc group using morpholine was also explored, this base is preferred to piperidine for its low pKa values (8.3) compared to the piperidine (pKa = 11.1) (Fields, 2014). The lower the pKa value the less the chances of side reactions. The Fmoc was cleaved by using morpholine 50% v/v in DCM or DMF (removal time 15 min to 45 min). This was purified in the column flash chromatography but did not yield the desired product.

5.2.1.4.2 One-pot reaction

Cleavage of Fmoc was attempted in a one-pot reaction. Coupling with EDC/Sulfo-NHS as explained in Section 5.2.1.3, without product purification was followed directly by treatment with 20% v/v piperidine and reaction was monitored by TLC (ethyl acetate: hexane, 3:1) for 45 min. The crude product was concentrated *in vacuo* and purification by column chromatography was attempted. It was observed after NMR analysis, with the appearance of the methylene proton marked 1 and also the oxymethine or chiral peak labelled 2 shifted upfield indicating formation of ester bond in **Figure 5.7**, the desired deprotected Lum-gly was obtained but with the presence of by-products labelled 3 (DBF and piperidine-DBF). It is important to remove the by-products, which are formed from dibenzofulvene (DBF), before proceeding to conjugate the Lum-Gly to a polymer. These by-products are a potential cause of side reactions (Fields, 2014; Takahashi, Inomata and Fukui, 2017). Due to this alternative purification methods were then explored.

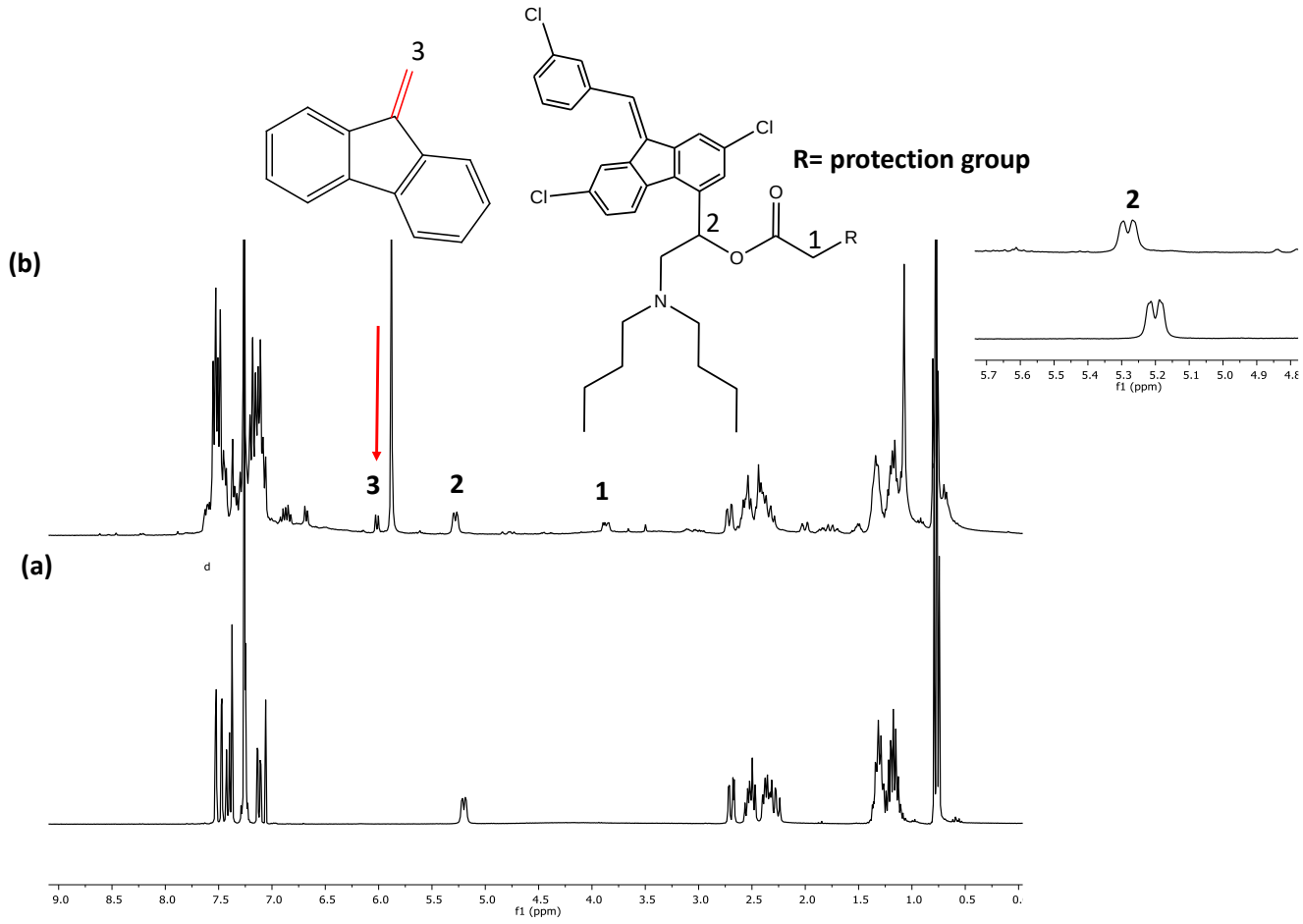

Figure 5.7: ^{1}H NMR (300 MHz in $CDCl_3$) spectrum of (a) Lum and (b) deprotected Lum-gly with by-product (DBF and piperidine-DBF).

5.2.1.4.3 Different purification methods.

Liquid-liquid extraction with a hexane-DMF (10 mL each) binary solvent system was attempted to purify the Lum-Gly. This was however not successful as the NMR analysis of the extract still showed the presence of undesired by-product (DBF) contaminating the Lum-Gly product.

The use of acidic solvent to remove the by-products has been suggested in the literature (Takahashi, Inomata and Fukui, 2017). Due to the instability of ester bonds in acidic conditions this option was not considered suitable for the current design of Lum-Gly. Therefore, automated flash chromatography was explored to purify the product as literature suggests automated chromatographic methods (e.g. HPLC) to be better at purifying Fmoc-protected groups (Welling and Atherton, 1997).

5.2.1.4.4 Purification method using automated flash chromatography

The crude product was purified using automated flash silica chromatography with a UV-VIS detector shown in **Figure 5.8.** This chromatographic technique has an advantage of being fast, separation can be optimized easily, and it is said to work well for both crystalline and non-crystalline compounds (Kramer and Deming, 2010). Compared to other chromatographic techniques such as High Pressure Liquid Chromatography (HPLC), it has the advantage of using smaller quantities of hazardous solvents (Kramer and Deming, 2010; Patsavas, Byrne and Liu, 2013). It has also been shown to have a 10-fold improvement in terms of production of purified compounds compared to preparative / semi-preparative HPLC (Liu, Patsavas and Byrne, 2011; Patsavas, Byrne and Liu, 2013). In this work it is explored for the purification of glycine coupled to Lum.

Figure 5.8: Automated flash chromatography system with UV-VIS detector.

Purification of Lum-gly was attempted using an isocratic solvent system of hexane and ethyl acetate (1:3) at a flow rate of 5 mL/min. The eluates were collected and solvent was removed using vacuum and air-drying overnight. The proton NMR spectrum showed a mixture of

free Lum with some impurities believed to result from hydrolysis as the product passed through the column. The purification of the final product is a huge problem as hydrolysis is observed and maybe one can consider using a different protecting group for the glycine linker or the use of other primary and secondary amines to remove the FMOC group.

5.3 Conclusion

The aim of this chapter was to synthesize a Lum-gly polymer conjugate. This was not achieved as purification of the deprotected Lum-gly was the challenge, due to the difficulties of removal of by-products formed during the cleaving of the Fmoc. Different purification methods such as column flash chromatography, liquid-liquid extraction, precipitation and automated flash chromatography with a UV-VIS detector were used to purify the crude Lum-gly from the cleaved Fmoc byproducts. The removal of by-products is crucial to avoid side reactions, but this was not achieved in this work due to the instability of the product. Even though, researchers in the field have successfully coupled glycine to other drugs for cancer therapeutics, it is yet to be achieved for malaria. This work has revealed that the Lum-glycine ester bond is readily hydrolyzed. The reason for the susceptibility of this ester bond to hydrolysis should be explored and will inform the rational design of linkers for Lum conjugates in future.

Chapter Six:
Conclusions and Future work

Malaria continues to be one the most fatal infectious diseases, even though it has been around for millennia. There was a decline in the development of new antimalarial drugs between 1980 and early 2000s. The majority of the drugs currently used are several decades old, making them vulnerable to the development of drug resistance. The newly developed drugs in the pipeline also have intrinsic therapeutic challenges due to poor pharmacokinetics that is caused by poor aqueous solubility, poor bioavailability, toxicity, stability and high lipophilicity. Nanomedicine using polymer therapeutics offers a powerful technology that managed to reduce the toxicity and improve the solubility of anticancer drugs. However, infectious diseases like malaria have not benefited from this state of the art technology. Therefore, this research aim was to explore the chemistry of developing polymer-therapeutics for antimalarials and investigate the physico-chemical changes using analytical techniques. The characterization of these is important as the formed covalent bond results in a new chemical entity.

In designing a synthesis of these new chemical entities one needs to consider the pharmacodynamics and pharmacokinetics of the drug desired in the polymer therapeutics. In this work, polymer-drug conjugate using nature derived compounds such as BA and DHA were synthesized first. Nature-derived compounds are normally administered orally, chitosan which has muco-adhensive properties was used as a polymer for the synthesis of a DHA conjugate for potential oral delivery. Malaria infects the RBCs, therefore it would be ideal to have a long circulating antimalarial conjugate that would persist in the blood for long period of time. PEG which is a non-immunogenic, non-toxic, water soluble polymer with long blood circulating properties have been used in this work. PEG was conjugated to the nature-derived compounds and long circulation of these compounds will also benefit patients with cerebral malaria, as the long circulation gives the possibility to also deliver to the brain.

This work also considered the commendations made by the WHO for using combination therapy for malaria to delay drug resistance. Triple combination therapy was considered in this work with respect to conjugating DHA, Lum and PQ to multivalent polymers, p(NAM-

stat-AA) and PGA which have more points of attachment compare to divalent PEG. Even though these polymers can allow conjugation of more than one drug this was not seen to present an optimal design for malaria combination therapy as these drugs have different sites of pharmacokinetic activity. Thus, in this work each drug was conjugated on its own polymer. The multivalent polymer p(NAM-stat-AA) has similar properties to PEG but with high structural stability and longer blood circulation. While, PGA has more repeating units of carboxylic acid it was reported to yield high percentage drug loading for anticancer drugs.

The covalent bond formed through conjugating the drugs to the polymers was confirmed using spectroscopic techniques (^{1}H NMR and FT-IR). The percentage drug loading, determined by ^{1}H NMR analysis, showed an increase in loading from PEG to multivalent p(NAM-stat-AA) for DHA but the drug did not occupy all the available activated carboxylic acid sites for the multivalent polymers. The percentage drug loading was expected to be higher as high molar equivalents of the drug were used. The poor drug loading was suggested to be due to steric hindrance, indicating the important role that chemistry plays in conjugation. ^{1}H NMR spectroscopy, also showed that the type of solvent used during analysis plays a role in the NMR spectrum. The PEG-BA or p(NAM-stat-AA)-Lum conjugates in aqueous solvent was hypothesized to form micelle structures or globular structures due to the polymer wrapping around the drug resulting in invisible NMR proton drug peaks. In the future, researchers in the field can explore if the conjugation of a drug with low aqueous solubility or high lipophilicity yields an amphiphilic therapeutic agent with a tendency to form structures with hydrophilic corona. The TEM and DLS analysis showed bigger sizes for Lum conjugated to p(NAM-stat-AA) and PGA compared to DHA conjugated to these polymers: Lum, which is a lipophilic drug with low aqueous solubility compared to DHA, had hydrodynamic size of 217.1 d.nm and 175.4 d.nm when conjugated to p(NAM-stat-AA) and PGA respectively while the size of p(NAM-stat-AA)-DHA was 21.51 d.nm and was 169.8 d.nm for PGA-DHA. Researchers can also investigate the effect of high percentage drug loading of hydrophobic drugs in polymer conjugates on the formation of structures with hydrophilic corona since a high percentage of hydrophobic drug on a polymer could affect the size and amphiphilic nature of the conjugate.

One must note that, even though TEM enables visualization of the nanoparticle morphology and DLS gives you insight on size in solution, these instruments give different sizes.

Researchers need to keep in mind the advantages and disadvantages associated with each technique. The use of these techniques will lead to one getting an estimation on the behavior of the conjugates in a biological system. The conjugates synthesized in this work had sizes less than 70 nm according to the TEM results, while the DLS showed larger sizes, this is expected due to solvating layer from conducting hydrodynamic size analysis in a liquid. Sizes less than 70 nm are important for the passive accumulation of the conjugate in the infected RBCs through the NPPs and these are estimated to have diameter between 50-70 nm. In the future it would be ideal to do a statistical study on TEM samples to be sure about the true size of the conjugate.

The analytical techniques SEM and PXRD showed that conjugation of the drug to the polymer resulted in an amorphous material that had improved solubility as seen in the p(NAM-stat-AA)-Lum or PGA-Lum conjugates. The conjugates also displayed reduced cytotoxicity compared to the free-drugs tested in Vero cells and Caco-2 cells of the African green Monkey kidney cells. In the future, it would be valuable to test the mean parasite clearance of these conjugate by testing for antiplasmodial activity and their plasma stability.

During the design of a delivery system in polymer therapeutics, the drug, polymer and type of linker need to be carefully selected. In Chapter 5, Lum was coupled to aminopropanoic acid (glycine) linker with the hope to conjugate to multivalent polymers such as p(NAM-stat-AA). Lum was chosen over DHA, as the latter is unstable due to the endoperoxide bridge and sensitive stereocentres. In addition, a water soluble form of DHA, artesunate - DHA coupled to succinic acid, does exist. It would be more valuable to have a water soluble Lum in combination with artesunate for people with severe malaria. Conjugation of Lum to a multivalent polymer has the possibility of yielding higher percentage drug loading, but steric hindrance is likely to block some sites for direct conjugation of the polymer to the drug as outlined in Chapter 4. In the future, optimization of the synthesis procedure can be explored to improve the percentage drug loading. For the anticancer drug, camptothecin, the percentage drug loading was improved when the PGA conjugate had a glycine linker. Thus in this work, a heterobifunctional linker such as glycine was used. As a heterobifunctional molecule, glycine offers the potential of asymmetrical bond chemistry between Lum and a carboxylic bearing polymer. Fmoc protected glycine was used to reduce the competition of the carboxylic acid and amino group, selectivity in reaction was required as amine has more

potential to be conjugated to carboxylic acid of another molecule than the hydroxyl of Lum. The synthesis using carbodiimide chemistry was successful but the removal of the Fmoc caused hydrolysis of the ester bond that hindered progress to further conjugate to a polymer. Therefore, researchers continuing with this work can consider using tert-butyloxycarbonyl (BOC) protected glycine linker as it was used in the camptothecin conjugation as the researchers did not report any difficulties. Also the use of other drugs similar to Lum such as Halofantrine, which is also an aryl alcohol with the same lipophilicity as Lum but with a less hindered stereogenic hydroxyl group could be considered. Researchers can also explore the use of less hydrophobic or less hindered antimalarial drugs.

The research through the three different chapters has revealed that even though polymer-therapeutics has been reported to have shown great success for cancer treatment the approach is not directly transferable to other diseases. One needs to carefully consider the pharmacodynamic and pharmacokinetic activities of the drugs thus informing the type of polymer used or type of combination therapy. After careful consideration of these, this work has demonstrated that malaria chemotherapy can also benefit from this technology. This work revealed that upon conjugation, the physico-chemical properties of the drug or polymer are changed resulting in improved intrinsic properties (improved solubility, reduced toxicity) of the polymer-drug conjugate. Analysis of the conjugates revealed that conjugation to the same polymer does not yield the same physico-chemical properties, each drug is different and thus each conjugate must be analyzed properly to understand their behavior in the biological system. Finally, the cost of producing polymer-therapeutics for malaria should be a primary consideration, as it is very important to use cheap polymers and linkers so that everyone can benefit from the improved properties created by this technology more especially for malaria as it is to be a disease of less wealthy tropical countries and it mostly affects people in sub-Saharan Africa.

Chapter Seven:
Experimental

7.1 General

7.1.1 Materials and Reagents

Dihydroartemisinin (DHA), lumefantrine (Lum) and chitosan (MW = 3000 Da) were purchased from DB Fine Chemicals, South Africa. Succinic anhydride, imidazole, dichloromethane (DCM), 1-ethyl-3-(3-dimethylaminopropyl) carbodiimide (EDC), *N*,*N*-diisopropylethylamine (DIEA), poly(ethyleneglycol) bis(3-aminopropyl) terminated (MW = 1500 Da), dimethylformamide (DMF), all deuterated solvents, primaquine bisphosphate (PQ), betulinic acid (BA), hydroxybenzotriazole (HOBt), ethyl acetate (EtOAc), hexane, sodium bicarbonate ($NaHCO_3$), N-hydroxysuccinimide (NHS), *N*-hydroxysulfosuccinimide sodium salt (sulfo-NHS), hydrochloric acid (HCl), *N*,*N'*-diisopropylcarbodiimide (DIC), N-[(9H-fluoren-9-ylmethoxy)carbonyl]glycine (Fmoc-gly-OH), thionyl chloride ($SOCl_2$), piperidine, morpholine, tetrahydrofuran (THF), phosphotungstic acid hydrate and Pur-A-lyzer Mega 1000 dialysis kit were purchased from Sigma-Aldrich, South Africa, and were used as received. Column chromatography was performed with silica gel 60 (0.040-0.063 mm) supplied by Merck. Synthetic Polyglutamic acid sodium salt (nBu-PGA (210)[Na], Weight size distribution (Mn) = 4329 Da, DP = 198, Đ = 1.14) and poly(N-acryloylmorpholine)-stat-p-acrylic acid (p(NAM-stat-AA) Mn = 25725 Da, DP = 200, Đ = 1.25), were received as a gifts from Professor María Jesus Vicent of the Polymer Therapeutics Laboratory, CIPF, Valencia, Spain, and Ms Cheng Sun of Monash University, Melbourne, Australia, respectively. Vivaspin® 20 ultrafiltration polyethersulfone membranes (MWCO = 3000 Da), Sephadex G-25M PD10 pre-packed columns and Vivaspin® 20 (MWCO = 1000 Da) were purchased from GE Healthcare, Buckinghamshire, United Kingdom.

All moisture sensitive reactions were carried out under inert gas atmosphere using anhydrous solvents. Glassware was washed and dried in an oven at 90 °C before use. For experiments requiring strictly dry conditions, all non-melting equipment were further dried at 120 °C for a minimum of 12 h before use.

7.1.2 Equipment

The nuclear magnetic resonance (NMR) experiments were carried out on a Bruker Avance III 300 and 400 MHz instrument at 295.4 K (Germany). Fourier transform infrared spectroscopy (FT-IR) analyses were conducted on Perkin Elmer Spectrum 100 (United States of America) over the range 650-4000 cm^{-1} with 16 scans performed for every sample and the resolution was set at 4 cm^{-1}. Ultraviolet-visible spectroscopy (UV-VIS) analyses were performed on a Mettler Toledo UV5Bio (Switzerland) with samples in a quartz cuvette. Dynamic light scattering (DLS) and zeta potential experiments to determine particle size and charge, respectively, were conducted on a Malvern Zetasizer Nano series, Nano-ZS90 (Malvern Instruments, United Kingdom). The morphologies of the conjugates were visualized with a scanning electron microscope (SEM) using a Zeiss crossbeam 540 FEG SEM and a transmission electron microscope (TEM) JEOL JEM 2100 (Japan) at 100 kV. X-ray powder diffraction (XRD) patterns were recorded on a Bruker D8, Discover X-ray diffractometer equipped with a proportional counter and a Lynx-Eye detector, using Cu K_α radiation (λ=1.5405 Å, nickel filter). Differential scanning microscopy (DSC) thermograms were obtained on DSC, Q2000, TA Instruments (United States of America). The liquid chromatography - tandem mass spectrometry (LC–MS/MS) system used consisted of a Shimadzu Prominence Ultra-Fast Liquid Chromatography (UFLC) series system (Shimadzu Corporation, Kyoto, Japan) coupled with an AB Sciex 3200 QTrap Triple Quadrupole Tandem Mass Spectrometer equipped with Analyst 1.6 software (AB Sciex, Massachusetts, United States of America). Flash chromatography was conducted using CombiFlash® NextGen 300, UV-VIS automated flash chromatography system (Teledyne ISCO, United States of America).

Phosphate buffer saline (PBS) [*], 7.40 was used in the synthesis and purification of the polymer-drug conjugates unless stated otherwise in the method.

7.1.2.1 Thin layer chromatography

Thin layer chromatography (TLC) was carried out on Merck TLC plates (silica gel 60 F254 0.2 mm, 200 9 200 mm). TLCs were either visualized by staining with an ethanolic solution

[*] 0.01 $mol.l^{-1}$ PBS prepared, 0.2 g KCl, 8.0 g NaCl, 0.24 g KH_2PO_4 and 1.44 g $NaHPO_4$

of phosphomolybdic acid hydrate followed by charring with a heat gun or using UV-VIS lamp (254 nm). Lyophilisation was carried out on a Telstar LyoAlfa10 freeze-dryer (Spain) in 0.3 mbar, condenser temperature -60 °C.

7.1.2.2 Drug loading determination

Drug loading was determined by ^{1}H-NMR spectroscopy only for non-chromophoric compounds. For determination by ^{1}H NMR spectroscopy, approximately 10 mg/mL sample of lyophilised polymer-drug conjugate was dissolved in 600 µL of a suitable deuterated solvent and added to an NMR tube. ^{1}H-signals were acquired at 256 scans, 400 MHz. The percentage drug loading was determined from the integration of appropriate drug and polymer signals in the ^{1}H NMR spectrum.

7.1.2.3 Diffusion-coefficient spectroscopy (NMR)

Standard NMR samples were prepared by dissolving the polymer and polymer-conjugate in $CDCl_3$ (10 mg mL^{-1}). DOSY experiments were performed at 25 °C on a Bruker AVANCE III with a probe of type PA BBO 500 S1 BBF-H-D-05. To minimize convection, we waited 20 min to allow for temperature equilibration.

7.1.2.4 Solubility studies

The drug conjugate was dissolved in a suitable organic solvent (DCM) Mand the concentration was increased gradually from 1 mg/mL to 10 mg/mL. After shaking the solution was analyzed using UV-VIS spectroscopy and the equation y = mx + c ($R^2 \approx 1$) was obtained. The solubility was obtained by dissolving the polymer-drug conjugate in deionized water and the concentration was increased from 2 mg/mL, 4 mg/mL to 6 mg/mL. After shaking the solution filtered using 0.22 µm filter and the filtrate was analysed using UV-VIS specstroscopy and the obtained absorbance was substituted in the equation obtained from measured drug concentration and the solubility was calculated.

7.1.2.5 Cytotoxicity studies

The cytotoxic effect was assessed using the 2,3-bis-(2-methoxy-4-nitro-5-sulfophenyl)-2H-tetrazolium-5-carboxanilide (XTT) assay, an improved tetrazolium dye based assay which obviates the solubilisation step. A concentration of $1x10^{5}$ cells/mL each of adherent MIA

PaCa-2 and Vero cells were seeded into 96-well plates (BD Biosciences, California, USA) overnight before treatment with the compounds at concentrations ranging from 0.4 to100 µM for 72 h. Doxorubicin (0.2 µg/mL) was used as a positive control for cell death assessment while DMSO was used as a vehicle control. After treatment, washed cells were exposed to 125 µL of complete Dulbecco's Modified Eagle's Medium (DMEM) containing 25 µL of XTT solution and incubated (37 ºC, 5 % CO_2, 95 % humidity) for 4 h. The optical density of the mixture was measured at 450 nm with background at 690 nm using a Multiskan Ascent 96/384 microplate reader (Labsystem, Finland). Cell viability was determined as a percentage relative to the vehicle control. The IC_{50} was then calculated using Graphpad Prism 8 (GraphPad Software, Inc, California). Statististical significance was calculated using a two way analysis of variant (ANOVA) and the Bonferroni post-test to compare replicate means in Graphpad Prism 6 (GraphPad Software, Inc, California). A $p<0.05$ was considered to be statistically significant.

Half maximal cytotoxicity (LC_{50}) in mg/mL of the compounds against Vero cells (African green Monkey kidney cells) and Caco-2 cells (Human colon cells) as done by the MTT assay. The African green monkey cells (Vero cells) were maintained in minimal essential medium (MEM, Highveld Biological, South Africa) supplemented with 5 % foetal calf serum (Adcock-Ingram) and 0.1 % gentamicin (Virbac) in a 5 % CO_2 incubator. The human Caucasian colon adenocarcinoma (Caco-2, ATCC HTB 37) cell lines were grown in DMEM, (Highveld Biological, South Africa) supplemented with 10 % foetal calf serum (Adcock-Ingram), 1 % non-essential amino acids (Hyclone) and 1 % penicillin streptomycin (10,000 U/mL and 10 mg/mL streptomycin, Sigma) in a 5 % CO_2 incubator.

Cell suspensions were prepared from 70-80 % confluent monolayer cultures and seeded at a density of 5×10^4 cells into each well of sterile 96-well plates. Plates were incubated for 24 h at 37 ºC in a 5 % CO_2 incubator before exposure to the extracts or compounds. The crude plant extracts were dissolved in DMSO, and appropriate dilutions were prepared in the media and added to the wells. Cells were exposed to the various compounds' concentrations (0.4, 0.2, 0.1, 0.05, 0.025, 0.0125, 0.01, and 0.005 mg/ml) in quadruplicates for 48 h. The assay was repeated twice (n = 8). Doxorubicin (Pfizer) and DMSO served as positive and negative controls, respectively. After incubation for 48 h, the wells were rinsed twice with 200 µL of phosphate buffered saline (PBS, Sigma) and 200 µL of fresh medium was dispensed into the

wells. Then 30 µL (5 mg/mL) of MTT (Sigma) dissolved in PBS was added to each well and the plates were further incubated for 4h at 37 ºC. After this, the medium from the wells was discarded and 50 µL of 100 % DMSO was added to the wells to dissolve the formed formazan crystals. Absorbance was measured on a microplate reader (BioTek Synergy) at a wavelength of 570 nm. Each extract concentration was tested in quadruplicate and the assay was repeated twice. The equation resulting from plot of the log of the concentration versus absorbance was used to calculate the concentration causing 50 % lethality on cells (LC_{50}).

7.1.2.6 Preparation of Dynamic light scattering samples

For each DLS experiment, 1-3 mg of a polymer-drug conjugate was vortexed and filtered through a 0.2 µm syringe filter. Each experiment was run in triplicate. To determine the particle charge, the zeta potential of the conjugates was measured in the same experiment with a folded capillary cell. The results are expressed as mean ± standard deviation (SD).

7.1.2.7 Sample preparation for microscopic analysis

The SEM samples were prepared by placing the dry powder sample of the polymer-drug conjugate onto a dark carbon tape and sputtered with conductive carbon in a high-vacuum evaporator. SEM analyses were performed at an accelerating voltage of 1.00 kV. For TEM analyses, the samples were dissolved in an aqueous solution of phosphotungstic acid that was used as a negative stain. The solution was drop dried onto 300 square mesh copper 3.05 mm (G2300C) grids from Agar Scientific.

7.1.2.8 X-Ray diffraction analysis

The samples for XRD were placed in a silica low background sample holder and scanned from 2θ=5-60°, using a beam of Cu Kα radiation of λ = 0.1542 nm, operated at 45 kV, 40 mA. The scan speed and exposure time were 2366 °/s and 40 min, respectively.

7.1.2.9 Differential scanning calorimetry analysis

DSC experiments were carried out with 0.8 – 6.0 mg samples which were taken into the aluminium pan of the instrument, covered with a lid and sealed. DSC curves were obtained

under a nitrogen purge 50 mL/min at a heating rate of 10 °C/min with temperature range from 10 -250 °C.

7.1.2.10 Thermogravimetric analysis (TGA)

Thermogravimetric analysis were carried on purge nitrogen gas of 60 mL/min. Samples were weighed between 5 to 12 mg and placed into open aluminum pan. A heating of 10 °C/min was applied with a heating ramp from room temperature to 700 °C.

7.1.2.11 Liquid chromatography elution conditions

LC was performed using a 7 minutes gradient elution method with 35 % formic acid as mobile phase A and acetonitrile 65 % as mobile phase B at a flow rate of 0.2 mL/min on a Phenomenex Kinetex 5 µ C18 analytical column (100 mm × 4.60 mm). The mass spectrometer was operated in positive ion mode with the transition of 283.8 m/z - 163.2 m/z.

7.1.2.12 Flash silica chromatography

The sample were purified using Teledyne ISCO CombiFlash, UV-VIS automated flash silica chromatographic system. The column was a silica 12 g Teledyne ISCO Redi*Sep*. The column was conditioned first with the solvent system EtOAc: hexane (3:1). Then sample was injected into the top of the column from a plastic syringe. After column return to the system, the purification proceeded accordingly using isocratic system, flow rate 5 mL/min, monitored at wavelength 200-800 nm. The fractions isolated were dried and analysed using NMR spectroscopy.

7.2 Preparation of chapter three conjugates

7.2.1.1 Synthesis of PEG-BA conjugate.

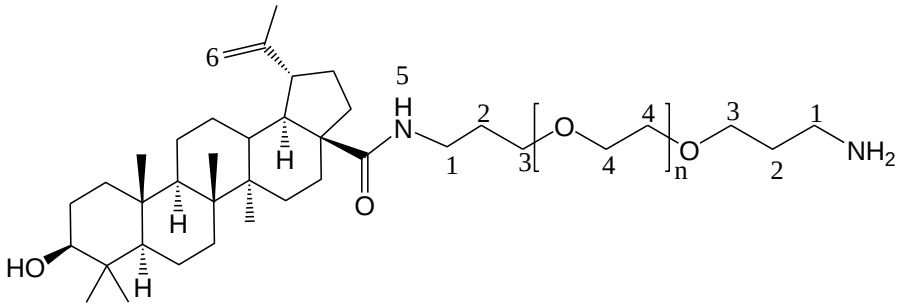

To a stirred solution of the acid, BA (6.09 mg, 0.01 mmol, 1.0 mol equiv) in DMF (2.0 mL) was added EDC (13.4 mg, 0.07 mmol, 5 mol equiv.) NHS (8.05 mg, 0.07 mmol, 5.0 mol equiv.), the reaction was allowed to processed for 2 h at 20 °C. Then, without product isolation the activated BA was added dropwise to a stirred solution of PEG amine (20 mg, 0.01 mmol, 1.0 mol equiv.) in DMF (2.0 mL) followed by DMAP (0.01 mol equiv.). The reaction was allowed to proceed at 20 °C for 24 h. At the end of this time, the solution was concentrated *in vacuo* on a rotary evaporator (4.0 mBar, 60 °C) and the crude product was re-dissolved in THF (1.0 mL). The conjugate was precipitated in cold diethyl ether (5.0 mL) to yield a yellowish waxy product, **^{1}H NMR (400 MHz, pyridine-d$_5$)**, δ 6.83 (s, 1H, H-5), 4.80 (d, *J* = 66.6 Hz, 2H, H-6), 3.67 – 3.23 (m, 4H, H-4), 2.67 (s, 1H), 2.02 (dddd, *J* = 12.7, 7.0, 5.4, 2.7 Hz), 1.40 – 1.18 (m), 1.08 (td, *J* = 7.2, 1.6 Hz), 0.98 (q, *J* = 2.1 Hz), 0.81 (d, *J* = 6.1 Hz). **FT-IR (υ in cm^{-1}):** 2880.1, 1734.8, 1655.8, 1554.9, 1465.9.

7.2.1.2 Synthesis of DHA-Suc

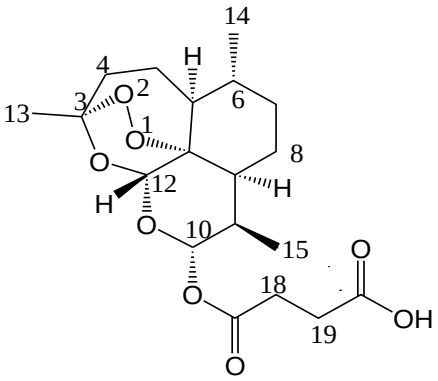

To a stirred solution of imidazole (0.47 mg) in anhydrous dichloromethane (5.0 mL) was added the alcohol, DHA (200 mg, 0.70 mmol, 1.0 mol equiv) with excess succinic anhydride (426.3 mg, 1.5 mmol, 3.0 mol equiv) and the reaction allowed to run at 35 °C for 24 h when a white precipitate was formed. The solvent was removed in vacuo on a rotary evaporator (395 mbar, 40°C) to yield a concentrate of the crude product, which was purified by flash silica column chromatography with a mobile phase of hexane: EtOAc (1:3). The pure product was obtained as a fine crystalline powder (1.33 g, 49.2 % yield) with *Rf* = 0.37, m.p. = 130-134 °C.

^{1}H NMR (400 MHz, DMSO-d$_6$) δ 5.67 (d, J = 9.7 Hz, 1H, H-10), 5.56 (s, 1H, H-12), 2.64 – 2.58 (m, 2H, H-18',H-19'), 2.60 (dd, J = 8.8, 5.7 Hz, 1H, H-19), 2.53-2.48 (m, 2H, H-18", H-19"), 2.18 (td, J = 13.9, 3.9 Hz, 1H, H-4'), 1.99 (ddd, J = 14.6 Hz, 2.8 Hz, 1H, H-4"), 1.81 (dq, J=10.4, 3.5 Hz, 1H, H-5'), 1.66 – 1.54 (m, 1H, H-7', H-8'), 1.58 – 1.49 (m, 1H, H-8a), 1.48 – 1.33 (m, 1H, H-8", H-6), 1.29 (s, 3H, H-13), 1.18 (dd, J = 11.3, 6.4 Hz, 1H, 5a), 1.01 – 0.83 (m, 1H, H-7"), 0.88 (d, J = 6.3 Hz, 3H, H-14), 0.76 (d, J = 7.1 Hz, 3H, H-15) ppm.**^{13}C NMR (101 MHz, DMSO- d$_6$)** δ 173.7 (C-20),171.50 (C-17), 104.0 (C-3), 92.2 (C-10), 91.1 (C-12), 80.3 (C-12a), 51.6 (C-5a), 45.0 (C-8a), 36.4 (C-4, C-6), 34.2 (C-7), 32.1 (C-9), 29.2 (C-18), 28.9 (C-19), 26.0 (C-13), 24.7 (C-5), 21.5 (C-8), 20.5 (C-14), 12.2 (C-15) ppm. FTIR (υ in cm-1): 3200, 2922, 1691, 838, 830, 737.

7.2.1.2.1 Method of DHA stability with LC-MS

DHA (6.0 mg) was dissolved in 2.0 mL absolute ethanol, then added to 98 mL of different buffer solutions (pH 2.0, 3.50, 6.50 and 7.40) to make a concentration of 60 µg/mL. All the samples were incubated in a dry-bath thermal shaker for 24 h at 37 °C and 2 mL aliquots were withdrawn at intervals, snap frozen and lyophilized. The samples were reconstituted in a mobile phase to 30 mg/mL and analysed with LC-MS. Then this was placed in a thermal shaker at 37°C for 24 h, with 2 mL aliquots taken at specific time.

The LC-MS system consisted of a binary pump using mobile phase ammonium formate 20 mmol/L (pH 4.0) as phase A (35%) and acetonitrile as phase B (65%). The acquisition data were atmospheric pressure chemical ionization (APCI), positive ionization, heat block 400°C, dry gas was 10 L/min, at a flow rate of 0.2 mL^{-1} and m/z 284.

Each batch of study samples was analyzed together with one blank sample, eight calibration standards and QCs in duplicates at low, medium and high concentrations worked up the same way as the study samples. The calibration curve was obtained by plotting the peak area ratio of the target molecule with the analyte concentration, from this the concentration of the sample at different buffer solutions was calculated in ng/mL.

7.2.1.3 Synthesis of PEG-Suc-DHA conjugate

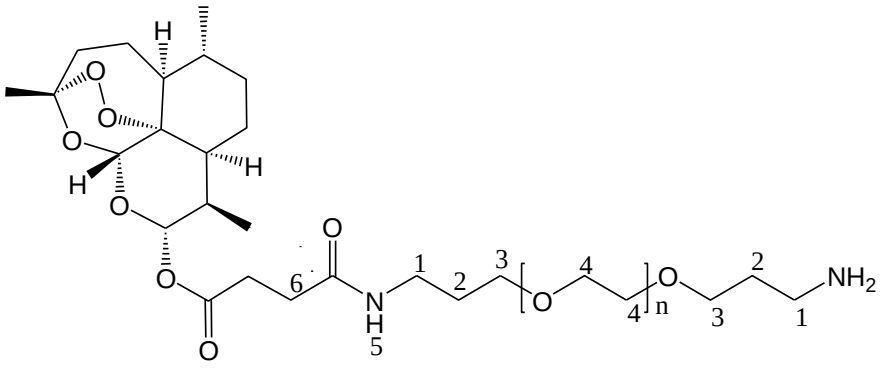

To a stirred solution of the acid, DHA-Suc (23.1 mg, 0.06 mmol, 1.20 equiv.) dissolved in DMF (2.0 mL) was added EDC (23.0 mg, 0.12 mmol, 3.0 mol equiv.), sulfo-NHS (13.80 mg 0.12 mmol, 3.0 mol equiv.) and DMAP (0.01 mol equiv.). The reaction was allowed to run for 2 h at room temperature (≈30 °C). Then without product isolation, the activated acid was added dropwise to a stirred solution of the PEG amine, (60.0 mg, 0.64 mmol, 1.0 mol equiv.) in DMF (1.0 mL). The reaction was allowed to proceed at 30 °C for 24 h. At the end of this time, the solution was concentrated *in vacuo* (4 mbar, 50 °C) and the crude product was dissolved in ethyl acetate (3.0 mL) followed by precipitated and dissolving of the crude product respectively in cold diethyl ether (3.0 mL) and deionized water (3.0 mL) three times. The purified conjugate was lyophilized to obtain a yellowish waxy solid. **^{1}H NMR (400 MHz, D_2O)**, δ 7.83 (s, 1H, H-5), 5.78 (d, J = 9.9 Hz, 1H), 5.68 (s, 1H), 3.72 (s, 1035H, H-4), 2.92 (d, J = 15.4 Hz, 50H), 2.75 (s, 38H), 2.55 – 2.42 (m, 24H), 1.93 (tt, J = 14.3, 6.7 Hz, 18H), 1.85 – 1.71 (m, 22H), 0.97 (d, J = 5.6 Hz, 2H), 0.88 (d, J = 7.1 Hz, 2H). **FT-IR (*υ* in cm^{-1}):** 2882.6, 1711.7, 1651.1, 1563.3, 1462.7, 1109.1.

7.2.1.4 Synthesis of Chitosan-Suc-DHA conjugate

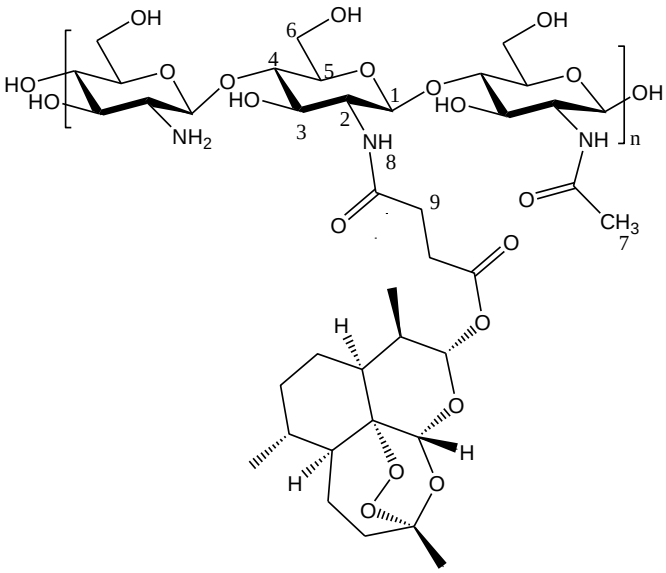

7.2.1.4.1 (i) Synthesis of Sodium Salt

To a stirred suspension of the DHA-Suc (DHA-Suc, 23.9 mg) in PBS (pH = 7.4, 2.0 mL) was added solid sodium bicarbonate until effervescence of CO_2 stopped, and to a final concentration of 2 M with no visible particulate suspension, to form the salt DHA-Suc-Na^+. The solution was diluted with PBS to a final volume of 3.5 mL and used in the next reaction (ii).

7.2.1.4.2 (ii) Synthesis of DHA Conjugate

To a stirred solution of the salt, DHA-Suc-Na^+ (23.9 mg, 0.06 mmol, 0.1 mol equiv.) dissolved in PBS (3.5 mL) was added EDC (36.43 mg, 0.19 mmol, 3.0 mol equiv.) and sulfo-NHS (21.85 mg, 0.19 mmol, 3.0 mol equiv.) and left to stir for 5 min. The solution was added dropwise to the polyamine, chitosan, (3 kDa, 100 mg, 0.6 mmol, 1.0 mol equiv.) in PBS (pH 7.40, 3.0 mL) and the reaction left to run for 3 h at 20 °C. The solvent was removed *in vacuo* on a rotary evaporator (21.0 mbar, 40 °C) and the crude product was purified by membrane dialysis (MWCO = 1 kDa) PBS (pH 7.40) for 72 h and lyophilized to yield a fine powder. **^{1}H NMR (400 MHz, D_2O)**, δ 8.30 (s, 1H, H-8), 4.38 (d, J = 33.7 Hz, 3H, H-1), 3.91 – 3.15 (m, 6H, H2-H6), 2.71 (s, 1H), 2.53 (d, J = 27.2 Hz, 2H), 2.45 – 2.17 (m, 2H), 1.75 (d, J = 9.0 Hz, 3H). **FT-IR (υ in cm^{-1}):** 2932.5, 1706.6, 1643, 1555.9, 1379.5, 1013.8.

7.3 Preparation of chapter three conjugates

7.3.1.1 Synthesis of p(NAM-stat-AA)-DHA conjugate

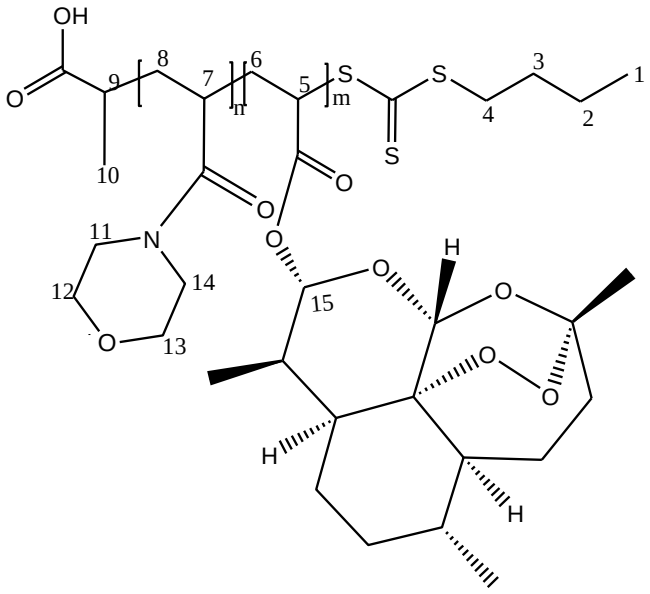

To a stirred solution of alcohol, DHA (9.30 mg, 0.03 mmol, 15 mol equiv.) in dry DMF (3.0 mL) was added, p(NAM-stat-AA) (30 mg, 0.002 mmol, 1 mol equiv.), DIC (0.50 mg, 0.044 mmol, 20 mol equiv.), sulfo-NHS (1.73 mg, 0.008 mmol, 4.0 mol equiv.), DMAP (0.01 mol equiv.) with a drop of DIEA. The reaction was allowed stirred for 24 h at room temperature (20 °C). At the end of this time, the solution was concentrated *in vacuo* on a rotary evaporator (4.0 mbar, 50 °C) and the crude mixture was re-dissolved in PBS buffer and purified by membrane dialysis (MWCO = 1 kDa) for 72 h with constant changing of PBS buffer every 12 h. The final product was lyophilized to yield a white powder of P(NAM)-stat-AA-DHA conjugate (0.25 mg,), **^{1}H NMR (400 MHz, $CDCl_3$)**, δ 7.51 (d, *J* = 2.0 Hz, 1H, Ar-H), 7.48 (d, *J* = 1.9 Hz, 1H, Ar-H), 7.44 (d, *J* = 1.9 Hz, 1H, Ar-H), 7.42 (d, *J* = 2.0 Hz, 1H, Ar-H), 7.38 (s, 1H), 7.12 (d, *J* = 2.0 Hz, 1H), 7.10 (d, *J* = 2.0 Hz, 1H), 7.03 (s, 1H), 5.54 (s, 1H, H-15), 3.25 (d, *J* = 133.1 Hz, 11H, H-11-14), 1.81 – 1.25 (m, 4H, H-15,H-16), 1.17 (d, *J* = 7.2, 2.3 Hz, 1H), 0.75 (t, *J* = 7.3 Hz, 6H, H-20, H-1). **FT-IR (υ in cm^{-1}):** 3365.0, 2924.6, 1629.2, 1440.9, 1371.5, 1228.8, 1090.0, 987

7.3.1.2 Synthesis of p(NAM-stat-AA)-Lum conjugate

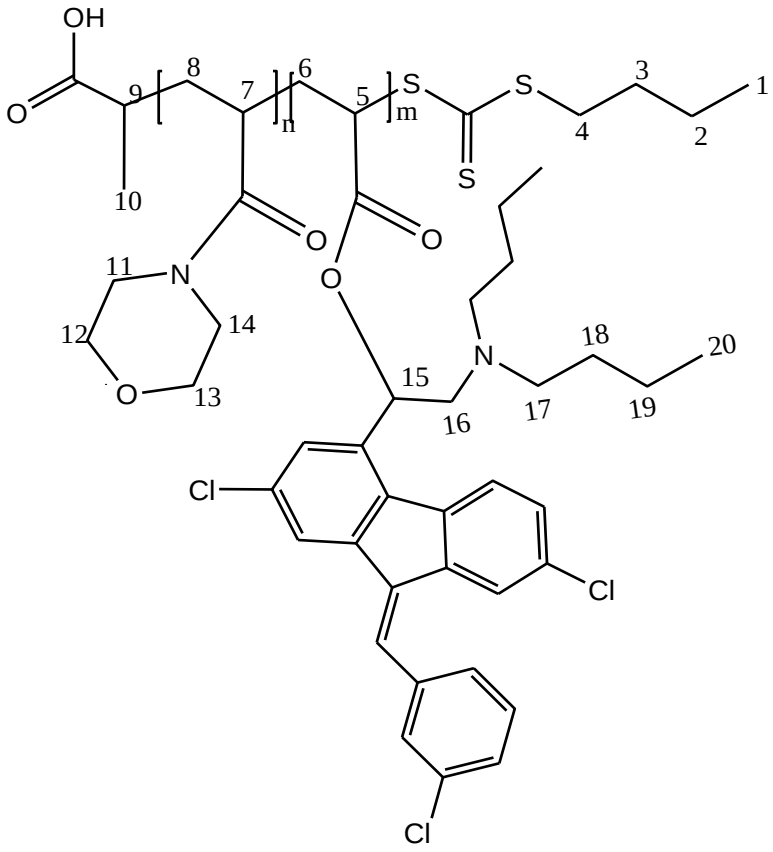

To a stirred solution of alcohol, Lum (17.47 mg, 0.033 mmol, 15 mol equiv.) in dry DMF (3.0 mL), was added p(NAM-stat-AA) (30 mg, 0.002 mmol, 1.0 mol equiv.), DIC (5.04 mg, 0.04 mmol, 20 mol equiv.), sulfo-NHS (1.95 mg, 0.009 mmol, 4.0 mol equiv.) and DMAP (0.01 mol equiv.) and a drop of DIEA. The reaction was allowed to proceed stirred at 20 °C for 24 h under nitrogen gas. At the end of this time, the solution was concentrated *in vacuo* on a rotary evaporator (4.0 mbar, 50 °C). The crude product was re-dissolved in PBS buffer (15 mL, pH 7.40) and purified using membrane dialysis (MWCO = 12 kDa) and stirred for 72 h with constant changing of the PBS buffer every 12 h. The final product was lyophilized to yield a yellow powder of p(NAM-stat-AA)-Lum. **^{1}H NMR (400 MHz, $CDCl_3$)**, δ 7.51 (d, *J* = 2.0 Hz, 1H, Ar-H), 7.48 (d, *J* = 1.9 Hz, 1H, Ar-H), 7.44 (d, *J* = 1.9 Hz, 1H, Ar-H), 7.42 (d, *J* = 2.0 Hz, 1H, Ar-H), 7.38 (s, 1H), 7.12 (d, *J* = 2.0 Hz, 1H), 7.10 (d, *J* = 2.0 Hz, 1H), 7.03 (s, 1H), 5.54 (s, 1H, H-15), 3.25 (d, *J* = 133.1 Hz, 11H, H-11-14), 1.81 – 1.25 (m, 4H,

H-15,H-16), 1.17 (d, *J* = 7.2, 2.3 Hz, 1H), 0.75 (t, *J* = 7.3 Hz, 6H, H-20, H-1). **FT-IR (υ in cm^{-1}):** 3253.9, 1617.4, 1522.2, 1403.3, 1226.8, 1026.6.

7.3.1.3 Synthesis of p(NAM-stat-AA)-PQ conjugate

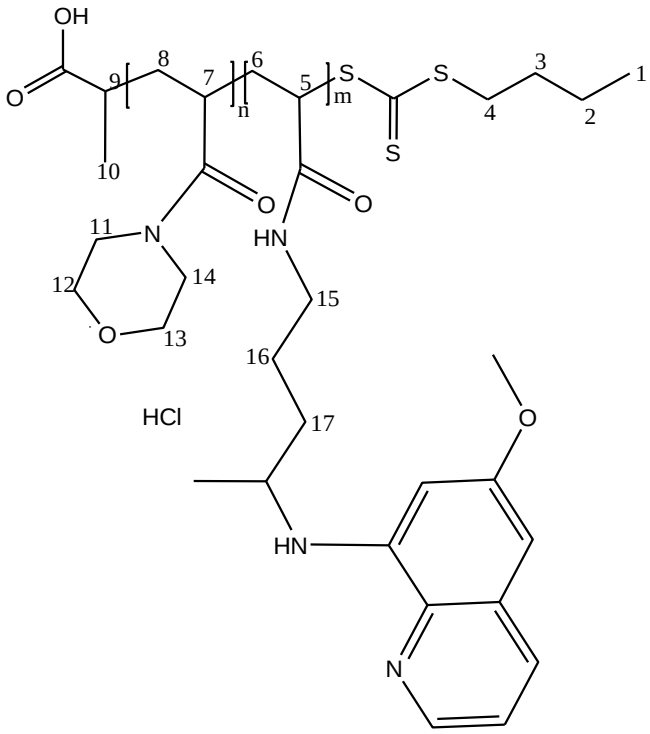

To a stirred solution of the carboxylic acid, p(NAM-stat-AA) (30 mg, 2.2 µmol, 1.0 mol equiv.) in deionized water (3.0 mL) was added EDC (8.43 mg, 44.0 µmol, 20 mol equiv.) and sulfo-NHS (1.95 mg, 9.0 µmol, 4.0 mol equiv.) followed immediately by addition of the PQ (8.55 mg, 33.0 µmol, 15 mol equiv.). The reaction was allowed to proceed at 20 °C in the dark for 2.5 h. At the end of this time, the solution was transferred to a Vivaspin™ (PES membrane, MWCO = 3 kDa) and centrifuged at 12000 rpm and 6 °C. The final product was lyophilized to yield a yellow solid. **^{1}H NMR (400 MHz, DMSO-d$_6$)**, δ 9.25 (s, 1H, H), 8.54 (dd, *J* = 4.2, 1.7 Hz, 1H, Ar-H), 8.09 (dd, *J* = 8.3, 1.7 Hz, 1H, Ar-H), 7.43 (dd, *J* = 8.2, 4.2 Hz, 1H, Ar-H), 6.49 (d, *J* = 2.5 Hz, 1H, Ar-H), 6.29 (d, *J* = 2.5 Hz, 1H), 6.01 (dd, *J* = 13.6, 7.4 Hz, 2H). **FT-IR (υ in cm^{-1}):** 3265.8, 1621.3, 1538.1, 1399.3, 1236.7.

7.3.1.4 Conversion of PGA-sodium to PGA

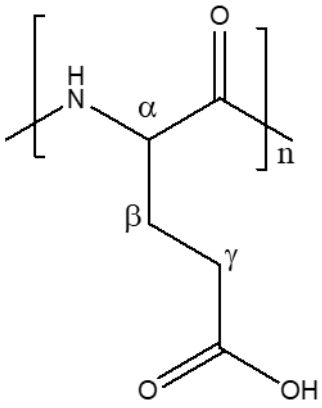

To a stirred solution of the sodium salt of PGA (1.0 g) dissolved in deionized water (25 mL), 2 M HCl was added dropwise until pH 4.0 was reached. The solution was allowed to stir for 12 h at 4 °C and a white precipitate was observed. The solution was centrifuged at 10 °C and the product was washed several times with deionized water until the pH reached 7.0 and then lyophilized to obtain a white powder of PGA. **^{1}H NMR (400 MHz, $CDCl_3$)**, δ 3.47 (s, 1H, α-H), 1.54 (s, 25H, γ-H), 1.28 – 0.74 (m, 6H, β-H). **FT-IR (*υ* in cm^{-1}):** 3339.6, 1730.7, 1603.5, 1539.8, 1406.6, 1167.7.

7.3.1.5 Synthesis of PGA-DHA conjugate

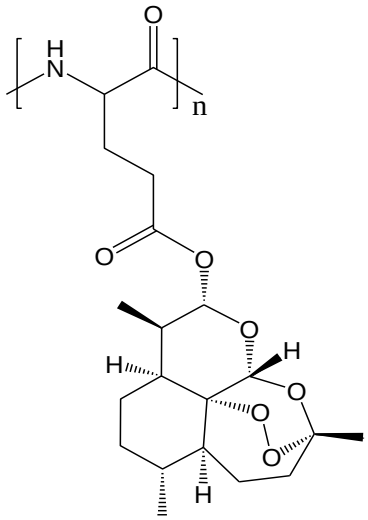

To a stirred solution of the acid, PGA-OOH (10 mg, 0.08 mmol, 1.0 mol equiv.) in anhydrous DMF (3.0 mL) was added DIC (25.24 mg, 0.2 mmol, 3.0 mol equiv.), HOBt (27.02 mg, 0.2 mmol, 3.0 mol equiv.) and DIEA (2 drops). The reaction was allowed to proceed under nitrogen gas at 20 °C for 30 min followed by addition of DHA (10 mg, 0.08 mmol, 1.0 mol equiv.). The reaction was allowed to stir for 48 h under nitrogen gas at 20 °C. At the end of this time, the solution was concentrated *in vacuo* on a rotary evaporator (4.0 mbar, 50 °C). The crude product was re-dissolved in PBS buffer (pH 7.40) and purified by membrane dialysis (MWCO = 1 kDa) for 72 h with constant changing of the PBS buffer and lyophilized to yield a fine white powder. ^{1}H NMR (400 MHz, Chloroform-d) δ 5.56 – 5.15 (m, 1H), 3.58 (s, 45H), 1.69 (d, J = 9.4 Hz, 21H), 0.92 – 0.64 (m, 3H). FT-IR (υ in cm-1): 3365, 2924, 1629.2, 1440.9, 1381.4.

7.3.1.6 Synthesis of PGA-Lum conjugate

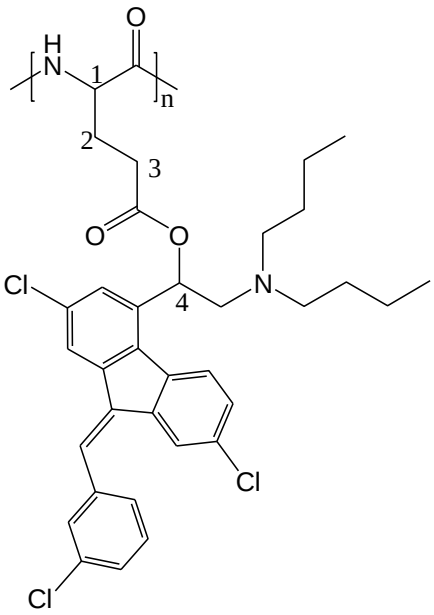

To a stirred solution of the acid, PGA (50 mg, 0.4 mmol, 1.0 mol equiv.) in dry DMF was added EDC (0.33 mg, 1.7 mmol, 3.0 mol equiv.) and NHS (195.65 mg, 1.7 mmol, 3.0 mol equiv.). This solution was allowed to stir for 30 min under nitrogen gas followed by addition of Lum (205 mg, 0.4 mmol, 1.0 mol equiv.). The reaction was allowed to stir at 20 °C for 24 h. At the end of this time, the solution was concentrated *in vacuo* on a rotatory evaporator (4.0 mbar, 50°C) and to the crude product was added PBS buffer (pH 7.40) and purified by membrane dialysis (MWCO, 12 kDa) for 72 h with frequent changing of the PBS buffer. The product was lyophilized to yield a fine yellow powder. **^{1}H NMR (400 MHz, $CDCl_3$)**, δ 7.69 (d, *J* = 2.0 Hz, 1H, Ar-H), 7.68 – 7.64 (m, 1H, Ar-H), 7.60 (d, *J* = 2.0 Hz, 1H, Ar-H), 7.52 – 7.40 (m, 8H, Ar-H), 7.32 (dd, *J* = 8.3, 2.0 Hz, 1H), 6.23 (s, 1H, H-4), 3.47 (s, 8H, H-1), 3.24 – 2.97 (m, 9H), 1.77 (s, 5H), 1.59 (s, 49H, H-3), 1.40 (s, 5H), 1.26 – 0.78 (m, 10H, H-2). **FT-IR (υ in cm^{-1}):** 3253.1, 1617.4, 1555.9, 1522.2, 1403.9, 1226.8, 1026.6.

7.3.1.7 Synthesis of PGA-PQ conjugate

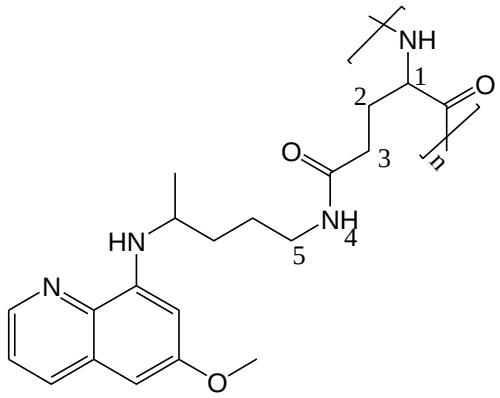

To a stirred solution of sodium salt, PGA (50 mg, 0.33 mmol, 1.0 mol equiv.) in PBS buffer (pH 7.40, 5.0 mL), was added EDC (24.92 mg, 0.13 mmol, 2.0 mol equiv.) and sulfo-NHS (28.23 mg, 0.13 mmol, 2.0 mol equiv.). This was followed immediately by the addition of the PQ (15 mg, 0.059 mmol, 0.20 mol equiv.). The reaction was allowed to proceed in the dark for 2 h at 20 °C. At the end of this time, the solution was transferred to a Vivaspin™ ultrafiltration tube (MWCO = 3 kDa) and centrifuged at 12000 rpm and 6 °C. The pure product was lyophilized to yield a yellow solid of PGA-PQ. **^{1}H NMR (400 MHz, D_2O)**, δ 8.58 (d, *J* = 4.4 Hz, 1H, Ar-H), 8.19 (d, *J* = 8.4 Hz, 1H, Ar-H), 7.49 (d, *J* = 4.5 Hz, 1H, Ar-H), 6.64 (d, *J* = 55.1 Hz, 1H, Ar-H), 4.32 (dd, *J* = 8.8, 5.6 Hz, 69H, H-1), 2.28 (h, *J* = 8.7 Hz, 160H, H-2), 2.13 – 1.86 (m, 166H, H-2). **FT-IR (υ in cm^{-1}):** 3283.0, 1644.8, 1544.0, 1398.0.

7.4 Preparation of chapter five conjugates

7.4.1.1 Synthesis of Fmoc-gly-Cl

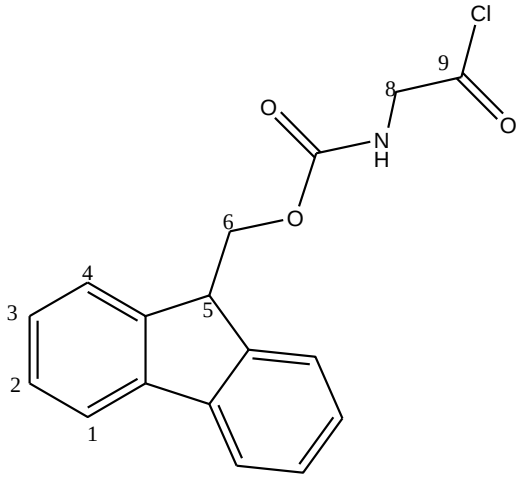

To a stirred solution of Fmoc amino acid (1.0 g, 3.36 mmol, 1.0 mol equiv.) in CH_2Cl_2 (25 mL) was added $SOCl_2$ (18 mL, 15 mmol) and the reaction was allowed to stir for 2 h at 20 °C. The reaction was followed to completion by TLC. Cold hexane (30 mL) was added to precipitate the product which was recovered by gravity filtration and dried at room temperature (20 °C) for 48 h. R_f = 0.12 (hexane: EtOAc , 1:3). The product was obtained as a fine powder (yield = 62.27%).

^{1}H NMR (300 MHz, DMSO-d$_6$) δ 7.92 – 7.87 (m, 2H, H-4), 7.74 – 7.68 (m, 2H, H-2), 7.64 (t, *J* = 6.2 Hz, 1H), 7.42 (td, *J* = 7.5, 1.2 Hz, 2H, H-3), 7.33 (td, *J* = 7.4, 1.3 Hz, 2H, H-1), 4.32 – 4.27 (m, 2H, H-6), 4.23 (dd, *J* = 8.3, 5.3 Hz, 2H, H-8), 3.66 (d, *J* = 6.1 Hz, 1H, H-5).
^{13}C NMR (75 MHz, DMSO-d$_6$) δ 172.06 (C-8), 156.97 (C-9), 127.83 (C-4), 125.69 (C-2), 120.59 (C-1), 66.16 (C-7), 47.09 (C-5).

7.4.1.2 Synthesis of Fmoc-gly-Lum

To a stirred solution of Fmoc amino acid chloride (100 mg, 0.39 mmol, 1.0 mol equiv.) in anhydrous DCM (5.0 mL) was added trimethylamine (1.0 mL) or DMAP (0.01 mol equiv.) and Lum (412.6 mg, 0.78 mmol, 2.0 mol equiv.). The reaction was allowed to proceed at 20

°C for 24 h under argon gas. The reaction was followed to completion with TLC and quenched by removing the solvent *in vacuo* on a rotary evaporator (396 mbar, 40 °C) to obtain a slurry of the crude product. The undesired product was obtained as a yellow oil by flash silica column chromatography eluting with hexane: EtOAc (5:1) R_f = 0.33.

7.4.1.3 Synthesis of Fmoc-gly-Lum using EDC/Sulfo-NHS

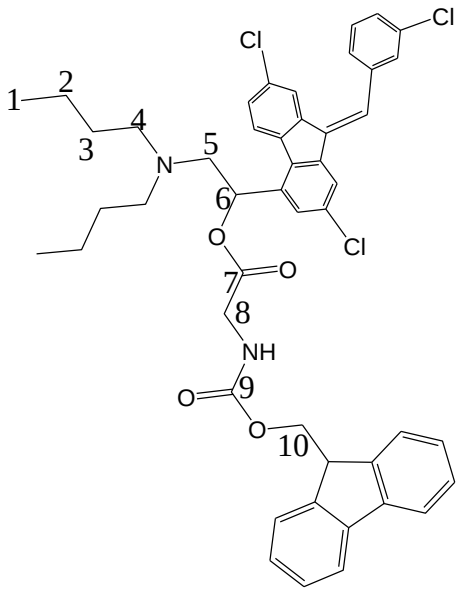

To a stirred solution of the acid, Fmoc amino acid (337 mg, 1.13 mmol, 3.0 mol equiv.) in anhydrous DMF (4 mL) was added, EDC (0.36 g, 1.9 mmol, 5.0 mol equiv.) and Sulfo-NHS (0.41 g, 1.9 mmol, 5.0 mol equiv.). The reaction was allowed to proceed for 30 min under inert condition using argon gas at 20°C. After this period, Lum (200 mg, 0.38 mmol, 1.0 mol equiv.) was added to the stirred solution and reaction was allowed to continue in the dark for 24 h under argon gas at 20°C. The reaction was monitored using TLC and quenched by removing solvent *in vacuo* with a rotary evaporator (4.0 mbar, 50 °C)

7.4.1.4 Column purification

The crude product was purified using flash basified (3 drops of trimethylamine) silica column chromatography eluting with hexane:EtOAc (5:1) R_f = 0.45. This gave an oily yellow undesired product

7.4.1.5 Liquid-Liquid extraction

Liquid-liquid extraction with a hexane-DMF (10 mL each) binary solvent system using separating funnel. The system was shaked several times, allowed to stand for 30 minutes to allow separation of the solvents. The DMF fraction was collected, concentrated *in vacuo* and ^{1}H NMR analysis was done.

7.4.1.6 Precipitation

On the crude product PBS buffer (pH 7.40) was added. A precipitate was formed and filtered through vacuum filtration. The product was purified by washing 5 times with PBS buffer. The final product was left to dry for 48h at ambient temperature, forming a yellow powder (yield = 90.2%, R_f = 0.45 using hexane: EtOAc (5:1) as an eluent.

^{1}H NMR (300 MHz, DMSO-d$_6$) δ 7.78 – 7.68 (m, 2H, Ar-H), 7.67 – 7.62 (m, 2H, Ar-H), 7.61 – 7.54 (m, 3H, Ar-H), 7.48 – 7.41 (m, 1H, Ar-H), 7.35 (ddd, *J* = 7.6, 5.5, 3.1 Hz, 2H, Ar-H), 7.28 (d, *J* = 1.2 Hz, 1H, Ar-H), 7.25 (d, *J* = 1.2 Hz, 1H, Ar-H), 6.10 (d, *J* = 10.4 Hz, 1H, H-10), 4.33 (d, *J* = 7.2 Hz, 2H, H-6), 4.18 (t, *J* = 7.4 Hz, 1H, H-5), 3.94 (d, *J* = 4.8 Hz, 1H, H-8), 3.30 – 2.89 (m, 4H,H-12), 1.78 – 1.55 (m, 4H,H-12, H-14), 1.35 (dq, *J* = 14.0, 7.2 Hz, 2H), 0.94 (dt, *J* = 10.0, 7.3 Hz, 6H, H-15). **^{13}C NMR (101 MHz, DMSO-d$_6$)** δ 170.06 (C-7) 162.77 (C-9), 157.29, 156.95, 141.19, 139.88, 137.88, 134.89, 134.03, 132.92, 131.28, 129.42, 129.36, 128.08, 127.73, 127.50, 125.57, 121.82, 120.57, 120.46, 110.15, 66.28 (C-6), 54.31 (C-5), 47.03 (C-4), 41.14, 36.23, 31.21 (C-3), 23.74, 20.31 (C-2), 14.36 (C-1). **FT-IR (υ in cm^{-1}):** 2959.4, 1713.0, 1448.0, 1401.2, 1215.2, 758.5.

7.4.1.7 Cleaving of Fmoc protection group

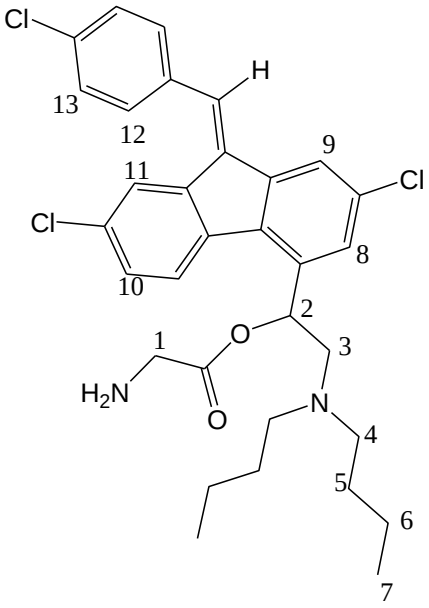

A solution of the Fmoc-N-protected peptide ester, Lum-Fmoc-gly (80 mg) was treated with 20 % piperidine in DMF or 50 % morpholine in DCM at ambient temperature. The reaction was monitored with TLC for 45 minutes and the solvent was removed *in vacuo*. The crude product was purified using flash Column chromatography with hexane:EtOAC (3:1) R_f = 0.29, to yield undesired product.

Appendix

$$DF=\frac{\text{integral of repeating unit}}{\text{number of protons of repeating units}} \times \frac{\text{number of proton of the end group}}{\text{integration of the end group}}$$

$$\frac{37}{4} \times \frac{1}{1} = 9.25$$

Approx 9.

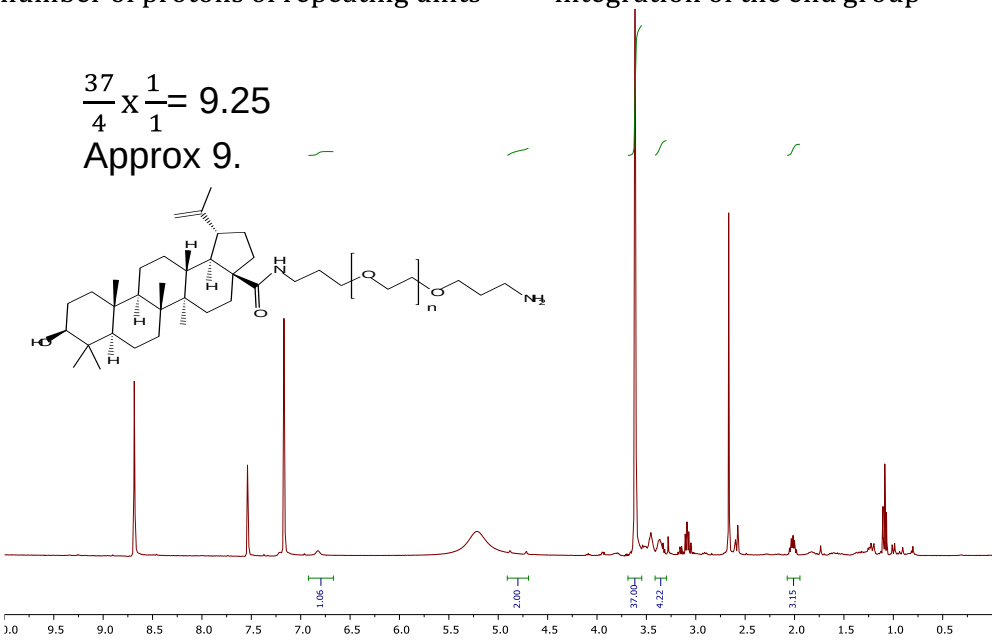

Figure 1A: ^{1}H-NMR spectrum (400 MHz in pyridine-d_5) of PEG-BA conjugate (integrated) showing drug- functionalization calculations.

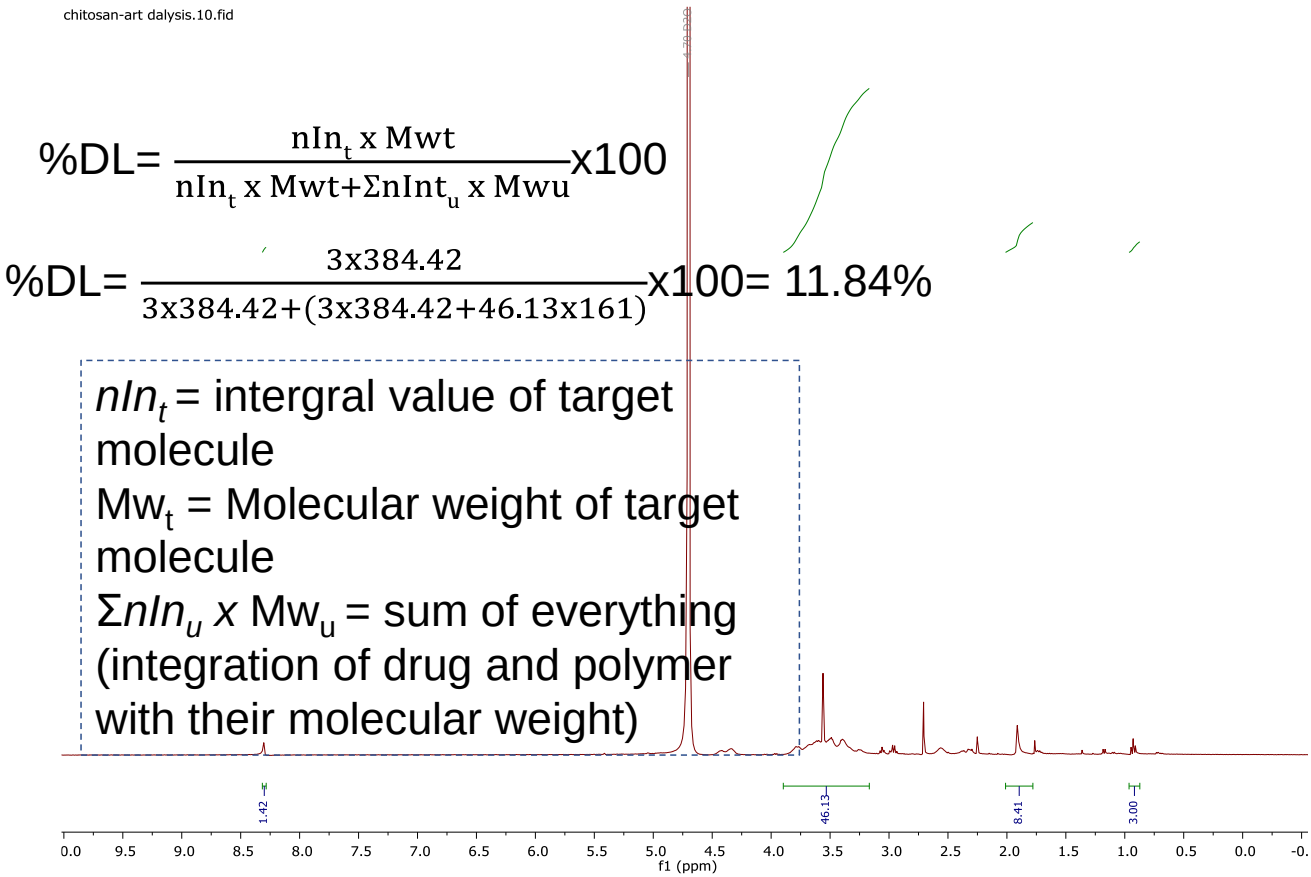

Figure 1B: ^{1}H-NMR spectrum (400 MHz in D_2O) of Chitosan-suc-DHA conjugate (integrated) showing percentage drug-loading calculations.

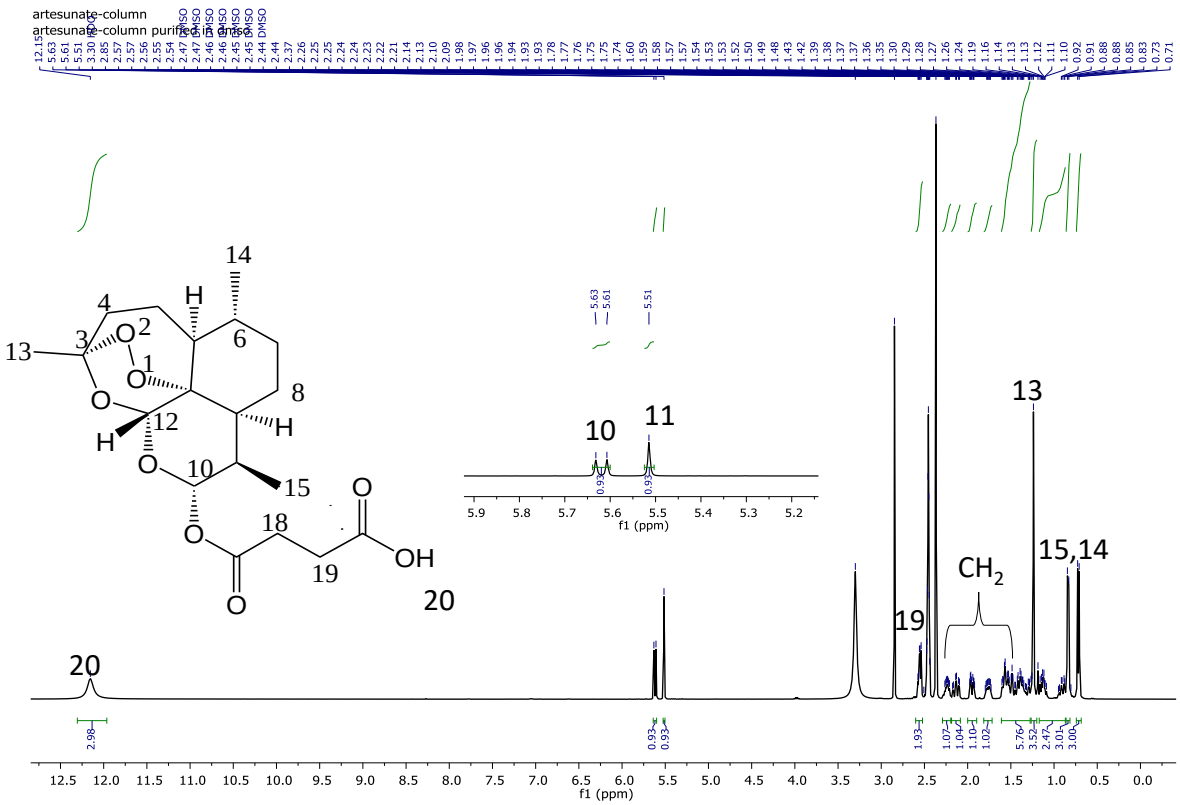

Figure 1C: ^{1}H-NMR (300 MHz) spectrum of DHA-Suc (integrated) in DMSO-d_6.

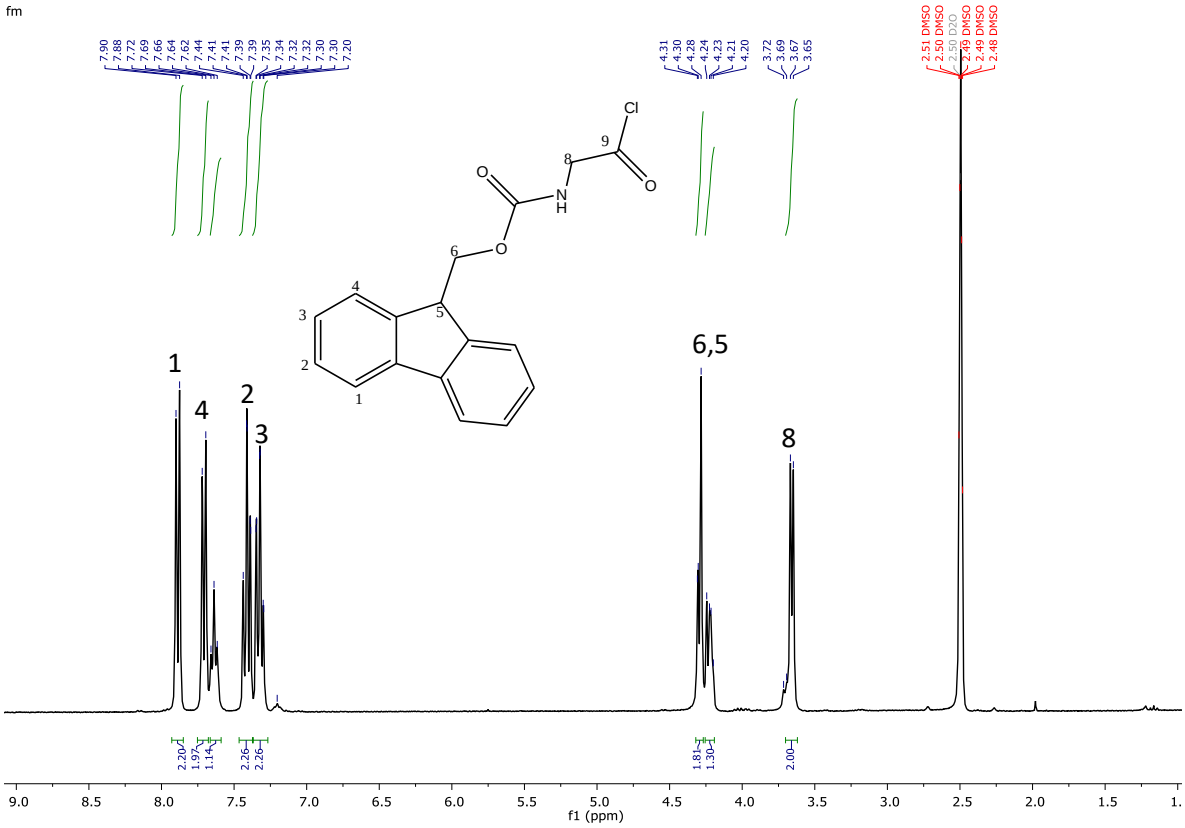

Figure 1D: ^{1}H-NMR (300 MHz) spectrum of FMOC-gly-Cl (integrated) in DMSO-d_6.

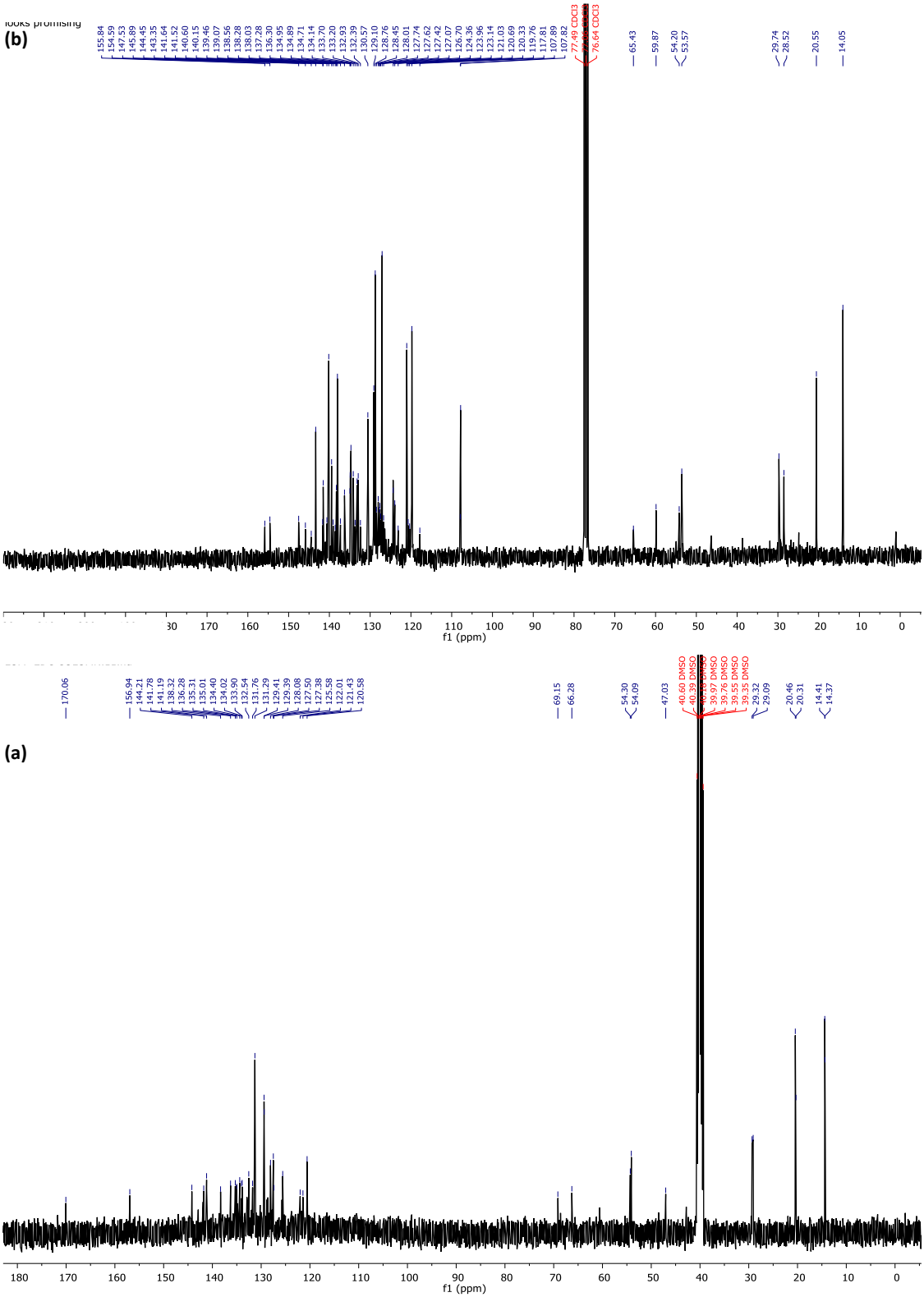

Figure 1E: ^{13}C-NMR spectra (300 MHz) of FMOC-gly-Lum in (a) DMSO-d_6 and (b) $CDCl_3$.

References

Aderibigbe, B. A. Mhlwatika, Z., Nwamadi, M., Balogun, M. O., Matshe, W. M.R., (2019) 'Synthesis, characterization and in vitro analysis of polymer-based conjugates containing dihydrofolate reductase inhibitors', *Journal of Drug Delivery Science and Technology*. Elsevier, 50(February), pp. 388–401. doi: 10.1016/j.jddst.2019.01.038.

Aditya, N. P. Vathsala, P. G. Vieira, V., Murthy, R. S.R., Souto, E. B., (2013) 'Advances in nanomedicines for malaria treatment', *Advances in Colloid and Interface Science*. Elsevier B.V., 201–202, pp. 1–17. doi: 10.1016/j.cis.2013.10.014.

Agtmael, V., (1999) 'Clinical and pharmacological ' studies on artemether in the treatment of malaria', PhD thesis, University of Amsterdam.

Ahmad, M.B., Tay, M.Y., Shameli, K., Hussein, M.Z. and Lim, J.J., (2011) 'Green synthesis and characterization of silver/chitosan/polyethylene glycol nanocomposites without any reducing agent' *International journal of molecular sciences, 12*(8), pp.4872-4884.

Al-Badr, A. A., (2005) 'Primaquine Diphosphate: Comprehensive Profile', *Profiles of Drug Substances, Excipients and Related Methodology*, 32(05), pp. 153–208. doi: 10.1016/S0099-5428(05)32007-7.

Anastasaki, A. Haddleton, Alice J., Zhang, Q., Simula, A., Droesbeke, M., Wilson, P., Haddleton, D. M., (2014) 'Aqueous Copper-Mediated Living Radical Polymerisation of N -Acryloylmorpholine , SET-LRP in Water', *Macromolecular Rapid Communications*, 35, pp. 965–970.

Ansari, M. T., Iqbal, I. and Sunderland, V. B., (2009) 'Dihydroartemisinin-cyclodextrin complexation: Solubility and stability', *Archives of Pharmacal Research*, 32(1), pp. 155–165. doi: 10.1007/s12272-009-1130-4.

Anthony, M. P., Burrows, J. N., Duparc, S., Jmoehrle. J. Wells, Timothy N. C., (2012) 'The global pipeline of new medicines for the control and elimination of malaria', *Malaria Journal*, 316 (11), pp 1-25.

Arenas-Guerrero, P. Delgado, Á.V., Donovan, K. J., Scott, K., Bellini, T., Mantegazza, F., Jiménez, M. L., (2018) 'Determination of the size distribution of non-spherical nanoparticles by electric birefringence-based methods', *Scientific Reports*, 8(1), pp. 1–10. doi: 10.1038/s41598-018-27840-0.

Arrow, K. J., Panosian, C. and Gelband, H., (2004) *Saving Lives, Buying Time: Economics of Malaria Drugs in an Age of Resistance Library of Congress Cataloging-in-Publication Data*. United States of America: National Academy of Science. Available at:

http://www.nap.edu/catalog/11017.html.

Ashley, E.A., Dhorda, M., Fairhurst, R.M., Amaratunga, C., Lim, P., Suon, S., Sreng, S., Anderson, J.M., Mao, S., Sam, B. and Sopha, C., (2014) 'Spread of Artemisinin Resistance in *Plasmodium falciparum* Malaria', *New England Journal of Medicine*. *371*(5), pp.411-423. doi: 10.1056/NEJMoa1314981.

Assanhou, A. G. Li, W., Zhang, L., Xue, L., Kong, L., Sun, H., Mo, R., Zhang, C., (2015) 'Reversal of multidrug resistance by co-delivery of paclitaxel and lonidamine using a TPGS and hyaluronic acid dual-functionalized liposome for cancer treatment', *Biomaterials*. Elsevier Ltd, 73, pp. 284–295. doi: 10.1016/j.biomaterials.2015.09.022.

Atanasov, A. G., Waltenberger, B. and Pferschy-wenzig, E., (2016) 'Discovery and resupply of pharmacologically active plant- derived natural products : A review', *Biotechnology Advances*, 33(8), pp. 1582–1614. doi: 10.1016/j.biotechadv.2015.08.001.Discovery.

Awab, G.R., Imwong, M., Bancone, G., Jeeyapant, A., Day, N.P., White, N.J. and Woodrow, C.J., (2017) 'Chloroquine-primaquine versus chloroquine alone to treat vivax malaria in Afghanistan: An open randomized superiority trial', *American Journal of Tropical Medicine and Hygiene*, 97(6), pp. 1782–1787. doi: 10.4269/ajtmh.17-0290.

Ayers, P.W., Anderson, J.S., Rodriguez, J.I. and Jawed, Z., (2005) 'Indices for predicting the quality of leaving groups', *Physical Chemistry Chemical Physics*, 7(9), pp. 1918–1925. doi: 10.1039/b500996k.

Azad, C.S., Saxena, M., Siddiqui, A.J., Bhardwaj, J., Puri, S.K., Dutta, G.P., Anand, N. and Saxena, A.K., (2017) 'Synthesis of primaquine glyco-conjugates as potential tissue schizontocidal antimalarial agents', *Chemical Biology and Drug Design*, 90(2), pp. 254–261. doi: 10.1111/cbdd.12944.

Azmeera, V., Adhikary, P., and Krishnamoorthi, S. (2012) 'Synthesis and characterization of graft copolymer of dextran and 2-acrylamido-2- methylpropane sulphonic acid' *International Journal of Carbohydrate Chemistry* 2012:209085. doi: 10.1155/2012/209085

Baird, J. K. and Hoffman, S. L. (2004) 'Primaquine Therapy for Malaria', *Clinical Infectious Diseases*, *39*(9), pp.1336-1345 doi: 10.1086/424663.

Bajaj, I. and Singhal, R. (2011) 'Poly (glutamic acid) - An emerging biopolymer of commercial interest', *Bioresource Technology*. Elsevier Ltd, 102(10), pp. 5551–5561. doi: 10.1016/j.biortech.2011.02.047.

Baker, D. A. (2010) 'Molecular & Biochemical Parasitology Malaria gametocytogenesis', *Molecular & Biochemical Parasitology*. Elsevier B.V., 172(2), pp. 57–65. doi: 10.1016/j.molbiopara.2010.03.019.

Bakhmutov, V. I. (2004) 'How to Measure NMR Relaxation Times', in *Practical NMR Relaxation for Chemists*.

Bancone, G., Chowwiwat, N., Somsakchaicharoen, R., Poodpanya, L., Moo, P.K., Gornsawun, G., Kajeechiwa, L., Thwin, M.M., Rakthinthong, S., Nosten, S. and Thinraow,

S., (2016) 'Single low dose primaquine (0.25mg/kg) does not cause clinically significant haemolysis in G6PD deficient subjects', *PLoS ONE*, 11(3), pp. 1–12. doi: 10.1371/journal.pone.0151898.

Banerjee, S.S., Aher, N., Patil, R. and Khandare, J., (2012) 'Poly(ethylene glycol)-Prodrug Conjugates: Concept, Design, and Applications', *Journal of Drug Delivery*, 2012, pp. 1–17. doi: 10.1155/2012/103973.

Barber, B.E., Rajahram, G.S., Grigg, M.J., William, T. and Anstey, N.M., 'World Malaria Report: time to acknowledge Plasmodium knowlesi malaria', *Malaria Journal*. BioMed Central, 16(1), pp. 13–15. doi: 10.1186/s12936-017-1787-y.

Barnett, D. S. and Guy, R. K. (2014) 'Antimalarials in development in 2014', *Chemical Reviews*, 114(22), pp. 11221–11241. doi: 10.1021/cr500543f.

Battle, K.E., Cameron, E., Guerra, C.A., Golding, N., Duda, K.A., Howes, R.E., Elyazar, I.R., Price, R.N., Baird, J.K., Reiner, R.C. and Smith, D.L., (2015) 'Defining the relationship between Plasmodium vivax parasite rate and clinical disease', *Malaria Journal*, 14(1), pp. 1–14. doi: 10.1186/s12936-015-0706-3.

Baumeister, S., Winterberg, M., Duranton, C., Huber, S.M., Lang, F., Kirk, K. and Lingelbach, K., (2006) 'Evidence for the involvement of Plasmodium falciparum proteins in the formation of new permeability pathways in the erythrocyte membrane'. *Molecular microbiology*, *60*(2), pp.493-504. doi: 10.1111/j.1365-2958.2006.05112.x.

Bélanger, Jacqueline MR, JR Jocelyn Paré, and M. S. (1997) 'High Performance Liquid Chromatography (HPLC): Principles and Applications', *Elsevier*. Edited by J.R.J. Pare and J.M.R. Be1anger. Elsevier Science B.V, 18, pp. 37–59.

Berardi, A. and Baldelli Bombelli, F., (2019) 'Oral delivery of nanoparticles-let's not forget about the protein corona' *Expert opinion on drug delivery*, *16*(6), pp.563-566.

Bernaczek, K., Mielańczyk, A., Mielańczyk, Ł., Neugebauer, D. and Grzywna, Z.J., (2019) 'Self-assembling water-soluble polymethacrylate–MTX conjugates: The significance of macromolecules architecture on drug conjugation efficiency, the final shape of particles, and drug release', *Journal of Biomedical Materials Research - Part B Applied Biomaterials*, 107(8), pp. 2476–2487. doi: 10.1002/jbm.b.34338.

Bhatt, S., Weiss, D.J., Cameron, E., Bisanzio, D., Mappin, B., Dalrymple, U., Battle, K.E., Moyes, C.L., Henry, A., Eckhoff, P.A. and Wenger, E.A., (2015) 'The effect of malaria control on Plasmodium falciparum in Africa between 2000 and 2015', *Nature*, 526(7572), pp. 207–211. doi: 10.1038/nature15535.

Bhattacharjee, A. K. and Karle, J. M. (1999) 'Stereoelectronic properties of antimalarial artemisinin analogues in relation to neurotoxicity', *Chemical Research in Toxicology*, 12(5), pp. 422–428. doi: 10.1021/tx9802116.

Biagini, G. A., Ward, S. A. and Bray, P. G. (2005) 'Malaria parasite transporters as a drug-delivery strategy', *Trends in parasitology*, *21*(7), pp.299-301.

Bloland, P. B. (2001) 'Drug resistance in malaria', *World Health*, 41, pp. 45–53. doi:

10.1007/978-1-4613-1267-3.

Bosman, A. and Mendis, K. N. (2007) 'A major transition in malaria treatment: The adoption and deployment of artemisinin-based combination therapies', *American Journal of Tropical Medicine and Hygiene*, 77(SUPPL. 6), pp. 193–197. doi: 10.4269/ajtmh.2007.77.193.

Braslau, R., Axon, J. R. and Lee, B. (2000) 'Synthesis of N-hydroxy peptides: Chemical ligation of O-acyl hydroxamic acids', *Organic Letters*, 2(10), pp. 1399–1401. doi: 10.1021/ol005722+.

Brewer, T.G., Grate, S.J., Peggins, J.O., Weina, P.J., Petras, J.M., Levine, B.S., Heiffer, M.H. and Schuster, B.G., (1994) 'Fatal neurotoxicity of arteether and artemether', *The American journal of tropical medicine and hygiene*, 51(3), p. 251—259.

Burns, W. R. (2008) 'East meets West: how China almost cured malaria', *Endeavour*, pp. 101–106. doi: 10.1016/j.endeavour.2008.07.001.

Butler, A. R., Khan, S. and Ferguson, E. (2010) 'A brief history of malaria chemotherapy', *Journal of the Royal College of Physicians of Edinburgh*, 40(2), pp. 172–177. doi: 10.4997/JRCPE.2010.216.

Cabri, W., D'Acquarica, I., Simone, P., Iorio, M.D., Mattia, M.D., Gasparrini, F., Giorgi, F., Mazzanti, A., Pierini, M., Quaglia, M. and Villani, C., (2011) 'Stereolability of dihydroartemisinin, an antimalarial drug: A comprehensive kinetic investigation. Part 2', *Journal of Organic Chemistry*, 76(12), pp. 4831–4840. doi: 10.1021/jo102392p.

Candela, T. and Fouet, A. (2006) 'Poly-gamma-glutamate in bacteria', *Molecular Microbiology*, 60(5), pp. 1091–1098. doi: 10.1111/j.1365-2958.2006.05179.x.

Cao, M., Geng, W., Zhang, W., Sun, J., Wang, S., Feng, J., Zheng, P., Jiang, A. and Song, C., (2013) 'Engineering of recombinant Escherichia coli cells co-expressing poly- γ -glutamic acid (γ -PGA) synthetase and glutamate racemase for differential yielding of γ -PGA', *Microbial biotechnology*, *6*(6), pp.675-684. doi: 10.1111/1751-7915.12075.

Cesar, A.L., Abrantes, F.A., Farah, L., Castilho, R.O., Cardoso, V., Fernandes, S.O., Araújo, I.D. and Faraco, A.A. (2018) 'New mesalamine polymeric conjugate for controlled release: Preparation, characterization and biodistribution study', *European Journal of Pharmaceutical Sciences*., pp. 57–64. doi: 10.1016/j.ejps.2017.09.037.

Chairat, K., Jittamala, P., Hanboonkunupakarn, B., Pukrittayakamee, S., Hanpithakpong, W., Blessborn, D., White, N.J., Day, N.P. and Tarning, J., (2018) 'Enantiospecific pharmacokinetics and drug–drug interactions of primaquine and blood-stage antimalarial drugs', *Journal of Antimicrobial Chemotherapy*, *73*(11), pp.3102-3113.

Chamignon, C., Duret, D., Charreyre, M.T. and Favier, A., (2016) ^{1}H DOSY NMR Determination of the Molecular Weight and the Solution Properties of Poly- (N -acryloylmorpholine) in Various Solvents', *Macromolecular chemistry and physics*, 217, pp. 2286–2293.

Chang, M., Zhang, F., Wei, T., Zuo, T., Guan, Y., Lin, G. and Shao, W., (2015) 'Smart linkers in polymer – drug conjugates for tumor-targeted delivery', *Journal of drug targeting*, *24*(6),

pp.475-491. doi: 10.3109/1061186X.2015.1108324.

Chang, M. *et al.* (2016) 'Smart linkers in polymer-drug conjugates for tumor-targeted delivery', *Journal of Drug Targeting*, 24(6), pp. 475–491. doi: 10.3109/1061186X.2015.1108324.

Chanphai, P., Konka, V. and Tajmir-Riahi, H. A. (2017) 'Folic acid–chitosan conjugation: A new drug delivery tool', *Journal of Molecular Liquids*. Elsevier B.V, 238, pp. 155–159. doi: 10.1016/j.molliq.2017.04.132.

Charman, S.A., Arbe-Barnes, S., Bathurst, I.C., Brun, R., Campbell, M., Charman, W.N., Chiu, F.C., Chollet, J., Craft, J.C., Creek, D.J. and Dong, Y., (2011) 'Synthetic ozonide drug candidate OZ439 offers new hope for a single-dose cure of uncomplicated malaria', *Proceedings of the National Academy of Sciences of the United States of America*, 108(11), pp. 4400–4405. doi: 10.1073/pnas.1015762108/-/DCSupplemental.www.pnas.org/cgi/doi/10.1073/pnas.1015762108.

Chaturvedi, D., Goswami, A., Saikia, P.P., Barua, N.C. and Rao, P.G., (2010) 'Artemisinin and its derivatives: a novel class of anti-malarial and anti-cancer agents.', *Chemical Society reviews*, 39(2), pp. 435–54. doi: 10.1039/b816679j.

Chen, K., Liao, S., Guo, S., Zhang, H., Cai, H., Gong, Q., Gu, Z. and Luo, K., (2018) 'Enzyme/pH-sensitive dendritic polymer-DOX conjugate for cancer treatment', *Science China Materials*, 61(11), pp. 1462–1474. doi: 10.1007/s40843-018-9277-8..

Chenette, E. J. (2017) 'Recent buzz in malaria research', *FEBS Journal*, pp. 2556–2559. doi: 10.1111/febs.14160.

Chettri, R., Bhutia, M. O. and Tamang, J. P. (2016) 'Poly- γ -Glutamic Acid (PGA) -Producing Bacillus Species Isolated from Kinema , Indian Fermented Soybean Food', *Frontiers in microbiology*, *7*, p.971. doi: 10.3389/fmicb.2016.00971.

Clark, A.E., Kaleta, E.J., Arora, A. and Wolk, D.M., (2013) 'Matrix-Assisted laser desorption ionization-time of flight mass spectrometry: A fundamental shift in the routine practice of clinical microbiology', *Clinical Microbiology Reviews*, 26(3), pp. 547–603. doi: 10.1128/CMR.00072-12.

Clark, R.L., Edwards, T.L., Longo, M., Kinney, J., Walker, D.K., Rhodes, J., Clode, S.A., Rückle, T., Wells, T., Andenmatten, N. and Huber, A.C., (2017) 'Improved safety margin for embryotoxicity in rats for the new endoperoxide artefenomel (OZ439) as compared to artesunate', *Birth defects research, 110*(7), pp.553-578. doi: 10.1002/bdr2.1170.

Collins, W. E. and Jeffery, G. M. (2005) 'Plasmodium ovale: Parasite and disease', *Clinical Microbiology Reviews*, pp. 570–581. doi: 10.1128/CMR.18.3.570-581.2005.

Collins, W. E. and Jeffery, G. M. (2007) 'Plasmodium malariae: Parasite and disease', *Clinical Microbiology Reviews*, 20(4), pp. 579–592. doi: 10.1128/CMR.00027-07.

Constantino, L., Paixao, P., Moreira, R., Portela, M.J., Do Rosario, V.E. and Iley, J., (1999) 'Metabolism of primaquine by liver homogenate fractions', *Experimental and Toxicologic Pathology*, 51(4–5), pp. 299–303. doi: 10.1016/S0940-2993(99)80010-4.

Coskun, O. (2016) 'Separation Tecniques: CHROMATOGRAPHY', *Northern Clinics of Istanbul*, 3(2), pp. 156–160. doi: 10.14744/nci.2016.32757.

Dabbagh, A., Mahmoodian, R., Abdullah, B.J.J., Abdullah, H., Hamdi, M. and Abu Kasim, N.H., (2015) 'Low-melting-point polymeric nanoshells for thermal-triggered drug release under hyperthermia condition' *International Journal of Hyperthermia*, *31*(8), pp.920-929.

Dai, L., Wang, L., Deng, L., Liu, J., Lei, J., Li, D. and He, J., (2014) 'Novel multiarm polyethylene glycol-dihydroartemisinin conjugates enhancing therapeutic efficacy in non-small-cell lung cancer', *Scientific Reports*, 4(1), pp. 1–10. doi: 10.1038/srep05871.

Dai, L., Cao, X., Liu, K.F., Li, C.X., Zhang, G.F., Deng, L.H., Si, C.L., He, J. and Lei, J.D., (2015) 'Self-assembled targeted folate-conjugated eight-arm-polyethylene glycol–betulinic acid nanoparticles for co-delivery of anticancer drugs', *Journal of Materials Chemistry B*, *3*(18), pp.3754-3766.

Danaei, M., Dehghankhold, M., Ataei, S., Hasanzadeh Davarani, F., Javanmard, R., Dokhani, A., Khorasani, S. and Mozafari, M.R., (2018) 'Impact of particle size and polydispersity index on the clinical applications of lipidic nanocarrier systems', *Pharmaceutics*, 10(2), pp. 1–17. doi: 10.3390/pharmaceutics10020057.

Das, A. K. (2015) 'Anticancer Effect of AntiMalarial Artemisinin Compounds Methods of Literature Search Artemisinins Anti-cancer activity of artemisinins : The different pathways', *Annals of medical and health sciences research*, 5(2), pp. 93–102. doi: 10.4103/2141-9248.153609.

Dash, M., Chiellini, F., Ottenbrite, R.M. and Chiellini, E., (2011) 'Chitosan - A versatile semi-synthetic polymer in biomedical applications', *Progress in Polymer Science (Oxford)*. doi: 10.1016/j.progpolymsci.2011.02.001.

Devi, V. K., Jain, N. and Valli, K. S. (2010) 'Importance of novel drug delivery systems in herbal medicines', *Pharmacognosy Review*, 4(7), pp. 27–31. doi: 10.4103/0973-7847.65322.

Djimdé, A. and Lefèvre, G. (2009) 'Understanding the pharmacokinetics of Coartem.', *Malaria journal*, 8 Suppl 1(SUPPL. 1), p. S4. doi: 10.1186/1475-2875-8-S1-S4.

Dondorp, A.M., Nosten, F., Yi, P., Das, D., Phyo, A.P., Tarning, J., Lwin, K.M., Ariey, F., Hanpithakpong, W., Lee, S.J. and Ringwald, P., (2009) 'Artemisinin Resistance in *Plasmodium falciparum* Malaria', *New England Journal of Medicine*, *361*(5), pp.455-467. doi: 10.1056/NEJMoa0808859.

Dong, Y., Wang, X., Kamaraj, S., Bulbule, V.J., Chiu, F.C., Chollet, J., Dhanasekaran, M., Hein, C.D., Papastogiannidis, P., Morizzi, J. and Shackleford, D.M., (2017) 'Structure-Activity Relationship of the Antimalarial Ozonide Artefenomel (OZ439)', *Journal of Medicinal Chemistry*, 60(7), pp. 2654–2668. doi: 10.1021/acs.jmedchem.6b01586.

Dong, Y. Da and Boyd, B. J. (2011) 'Applications of X-ray scattering in pharmaceutical science', *International Journal of Pharmaceutics*, 417(1–2), pp. 101–111. doi: 10.1016/j.ijpharm.2011.01.022.

Doronina, S.O., Mendelsohn, B.A., Bovee, T.D., Cerveny, C.G., Alley, S.C., Meyer, D.L.,

Oflazoglu, E., Toki, B.E., Sanderson, R.J., Zabinski, R.F. and Wahl, A.F., (2006) 'Enhanced activity of monomethylauristatin F through monoclonal antibody delivery: Effects of linker technology on efficacy and toxicity', *Bioconjugate Chemistry*, 17(1), pp. 114–124. doi: 10.1021/bc0502917.

Drelish, J., (2013) 'Nanoparticles in a liquid: New state of liquid', *Journal of Nanomaterials & Molecular Nanotechnology*, *2*(1), pp.1-2.

Dube, A., Lemmer, Y., Hayeshi, R., Balogun, M., Labuschagne, P., Swai, H. and Kalombo, L., (2013) 'State of the art and future directions in nanomedicine for tuberculosis', *Expert Opinion on Drug Delivery*, 10(12), pp. 1725–1734. doi: 10.1517/17425247.2014.846905.

Dube, A. and Ebrahim, N. (2017) 'The nanomedicine landscape of South Africa', *Nanotechnology Reviews*, 6(4), pp. 339–34. doi: 10.1515/ntrev-2016-0108.

Duncan, R., Seymour, L.C., Scarlett, L., Lloyd, J.B., Rejmanová, P. and Kopeček, J., (1986) 'Fate of N-(2-hydroxypropyl)methacrylamide copolymers with pendent galactosamine residues after intravenous administration to rats', - *Biochimica et Biophysica Acta (BBA)-General Subjects, 880(1), pp.62-71.* doi: 10.1016/0304-4165(86)90120-0.

Duncan, R., Kopečková-Rejmanová, P., Strohalm, J., Hume, I., Cable, H.C., Pohl, J., Lloyd, J.B. and Kopeček, J., (1987) 'Anticancer agents coupled to N-(2-hydroxypropyl)methacrylamide copolymers. I. evaluation of daunomycin and puromycin conjugates in vitro', *British Journal of Cancer*, 55(2), pp. 165–174. doi: 10.1038/bjc.1987.33.

Duncan, R. (2003) 'The dawning era of polymer therapeutics', *Nature Reviews Drug Discovery*, 2(5), pp. 347–360. doi: 10.1038/nrd1088.

Duncan, R. (2006) 'Polymer conjugates as anticancer nanomedicines', *Nature Reviews Cancer*, 6(9), pp. 688–701. doi: 10.1038/nrc1958.

Duncan, R. and Vicent, M. J. (2013) 'Polymer therapeutics-prospects for 21st century : The end of the beginning', *Advanced Drug Delivery Reviews*, 65(1), pp. 60–70. doi: 10.1016/j.addr.2012.08.012.

Dutta, P.K., Dutta, J. and Tripathi, V.S., (2004) 'Chitin and chitosan: Chemistry, properties and applications', *Journal of Scientific and Industrial Research* , 63, pp. 20-31.

Ebewele, R. O. (2000) 'Chapter 1: Introdction', *Polymer Science and Technology*, pp. 1–23.

Eldar-Boock, A., Miller, K., Sanchis, J., Lupu, R., Vicent, M.J. and Satchi-Fainaro, R., (2011) 'Integrin-assisted drug delivery of nano-scaled polymer therapeutics bearing paclitaxel', *Biomaterials*, 32(15), pp. 3862–3874. doi: 10.1016/j.biomaterials.2011.01.073.

Erez, R., Segal, E., Miller, K., Satchi-Fainaro, R. and Shabat, D., (2009) 'Enhanced cytotoxicity of a polymer-drug conjugate with triple payload of paclitaxel', *Bioorganic and Medicinal Chemistry*, 17(13), pp. 4327–4335. doi: 10.1016/j.bmc.2009.05.028.

Erickson, H.K., Park, P.U., Widdison, W.C., Kovtun, Y.V., Garrett, L.M., Hoffman, K., Lutz, R.J., Goldmacher, V.S. and Blättler, W.A., (2006) 'Antibody-Maytansinoid Conjugates Are

Activated in Targeted Cancer Cells by Lysosomal Degradation and Linker-Dependent Intracellular Processing Intracellular Processing', *Cancer research*, *66*(8), pp.4426-4433. doi: 10.1158/0008-5472.CAN-05-4489.

Erickson, H.K., Phillips, G.D.L., Leipold, D.D., Provenzano, C.A., Mai, E., Johnson, H.A., Gunter, B., Audette, C.A., Gupta, M., Pinkas, J. and Tibbitts, J., (2012) 'The Effect of Different Linkers on Target Cell Catabolism and Pharmacokinetics / Pharmacodynamics of Trastuzumab Maytansinoid Conjugates', *Molecular cancer therapeutics*, *11*(5), pp.1133-1142. doi: 10.1158/1535-7163.MCT-11-0727.

Everaerts, F., Torrianni, M., Hendriks, M. and Feijen, J., (2008) 'Biomechanical properties of carbodiimide crosslinked collagen: Influence of the formation of ester crosslinks', *Journal of Biomedical Materials Research - Part A*, 85(2), pp. 547–555. doi: 10.1002/jbm.a.31524.

Feist, M. (2015) 'Thermal analysis : basics , applications , and benefit', *ChemTexts*, 1, pp. 1–12. doi: 10.1007/s40828-015-0008-y.

Feng, Q. and Tong, R. (2016) 'Anticancer nanoparticulate polymer-drug conjugate', *Bioengineering & Translational Medicine*, *1*(3), pp.277-296. pp. 277–296. doi: 10.1002/btm2.10033.

Fernandes, D., de Mesquita, L.S.S., do Amaral, F.M.M., de Sousa Ribeiro, M.N. and Malik, S (2017) 'Anticancer Drugs from Plants', *In Biotechnology and Production of anti-Cancer compounds*. Brazil: Springer International Publishing, pp. 121–142. doi: 10.1007/978-3-319-53880-8.

Fields, G. B. (2014) *Chapter 2 Methods for Removing the Fmoc Group*. doi: 10.1385/0-89603-273-6.

Flannery, E. L., Chatterjee, A. K. and Winzeler, E. A. (2014) 'Antimalarial drug discovery—approaches and progress towards new medicines', *Nature Reviews Microbiology*, *11*(12), pp.849-862.

Fontanay, S., Kedzierewicz, F., Duval, R.E. and Clarot, I., (2012) 'Physicochemical and thermodynamic characterization of hydroxy pentacyclic triterpenoic acid/γ-cyclodextrin inclusion complexes' *Journal of Inclusion Phenomena and Macrocyclic Chemistry*, *73*(1-4), pp.341-347.

Forest, V. and Pourchez, J., (2017) 'Preferential binding of positive nanoparticles on cell membranes is due to electrostatic interactions: A too simplistic explanation that does not take into account the nanoparticle protein corona' *Materials Science and Engineering: C*, *70*, pp.889-896.

Forte, G., Chiarotto, I., Giannicchi, I., Loreto, M.A., Martinelli, A., Micci, R., Pepi, F., Rossi, S., Salvitti, C., Stringaro, A. and Tortora, L., (2016) 'Characterization of naproxen-polymer conjugates for drug-delivery', *Journal of Biomaterials Science, Polymer Edition*, 27(1), pp. 69–85. doi: 10.1080/09205063.2015.1108637.

Fortuin, L., Leshabane, M., Pfukwa, R., Coertzen, D., Birkholtz, L.M. and Klumperman, B., (2020) 'Facile route to targeted, biodegradable polymeric prodrugs for the delivery of

combination therapy for malaria', *ACS Biomaterials Science & Engineering*, *6*(11), pp.6217-6227.

Freeman, R. (2014) 'High - Resolution NMR Study of Relaxation Mechanisms in a Two - Spin System High-Resolution NMR Study of Relaxation Mechanisms in a Two-Spin System', *The Journal of Chemical Physics*, *52*(3), pp.1529-1544. doi: 10.1063/1.1673164.

Freeman, R., Hill, H. D. W. and Tomlinsont, B. L. (2014) 'Dipolar Contribution to NMR Spin-Lattice Relaxation of Protons Dipolar contribution to NMR spin-lattice relaxation of protons', *The Journal of Chemical Physics*, *61*(11), pp.4466-4473.. doi: 10.1063/1.1681764.

Gandhi, K. J., Deshmane, S. V. and Biyani, K. R. (2012) 'Polymers in pharmaceutical drug delivery system: A review', *International Journal of Pharmaceutical Sciences Review and Research*, 14(2), pp. 57–66.

Gaspar, R. and Duncan, R. (2009) 'Polymeric carriers : Preclinical safety and the regulatory implications for design and development of polymer therapeutics ☆', *Advanced Drug Delivery Reviews*. Elsevier B.V., 61(13), pp. 1220–1231. doi: 10.1016/j.addr.2009.06.003.

Gavin, W. (2016) 'GPC - Gel Permeation Chromatography', pp. 1–18.

Gawande, M. B. and Branco, P. S. (2011) 'An efficient and expeditious Fmoc protection of amines and amino acids in aqueous media', *Green chemistry*, *13*(12), pp.3355-3359

Gerasimov, A.V., Ziganshin, M.A., Gorbatchuk, V.V. and Usmanova, L.S., (2014) 'Low molecular weight polyethylene glycols as matrix to obtain solid dispersions of sulfanilamide' *International Journal of Pharmacuetical and Pharmacological Science*, *6*, pp.372-7.

Godman, B., McCabe, H., D Leong, T., Mueller, D., Martin, A.P., Hoxha, I., Mwita, J.C., Rwegerera, G.M., Massele, A., Costa, J.D.O. and Do Nascimento, R.C.R.M., (2020) 'Fixed dose drug combinations – are they pharmacoeconomically sound ? Findings and implications especially for lower- and middle- income countries', *Expert review of pharmacoeconomics & outcomes research*, *20*(1), pp.1-26. doi: 10.1080/14737167.2020.1734456.

Golenser, J., Waknine, J.H., Krugliak, M., Hunt, N.H. and Grau, G.E., (2006) 'Current perspectives on the mechanism of action of artemisinins', *International Journal for Parasitology*, 36(14), pp. 1427–1441. doi: 10.1016/j.ijpara.2006.07.011.

Gonzalez-Ceron, L., Rodriguez, M.H., Sandoval, M.A., Santillan, F., Galindo-Virgen, S., Betanzos, A.F., Rosales, A.F. and Palomeque, O.L., (2016) 'Effectiveness of combined chloroquine and primaquine treatment in 14 days versus intermittent single dose regimen, in an open, non-randomized, clinical trial, to eliminate Plasmodium vivax in southern Mexico', *Malaria Journal*, 14(1), pp.1-16 doi: 10.1186/s12936-015-0938-2.

Goodhew, Peter J., and J. H. (2000) *Electron microscopy and analysis*. CRC Press. doi: 10.1017/CBO9781107415324.004.

Goodyer, I.D., Pouvelle, B., Schneider, T.G., Trelka, D.P. and Taraschi, T.F. (1997) 'Characterization of macromolecular transport pathways in malaria-infected erythrocytes.',

Molecular and biochemical parasitology, 87(1), pp. 13–28. doi: 10.1016/S0166-6851(97)00039-X.

Gopalakrishnan, A. M. and Kumar, N. (2015) 'Antimalarial action of artesunate involves DNA damage mediated by reactive oxygen species', *Antimicrobial Agents and Chemotherapy*, 59(1), pp. 317–325. doi: 10.1128/AAC.03663-14.

Gopi, H. N. (2014) 'Biomolecular Chemistry conjugate addition : synthesis and stereochemical γ -amino acids and hybrid peptides', *Royal Society of Chemistry*, pp. 8462–8472. doi: 10.1039/c4ob01548g.

Greco, F. and Vicent, M. J. (2009) 'Combination therapy: Opportunities and challenges for polymer-drug conjugates as anticancer nanomedicines', *Advanced Drug Delivery Reviews*. Elsevier B.V., 61(13), pp. 1203–1213. doi: 10.1016/j.addr.2009.05.006.

Griffin, J. T., Ferguson, N. M. and Ghani, A. C. (2014) 'Estimates of the changing age-burden of Plasmodium falciparum malaria disease in sub-Saharan Africa', *Nature Communications*. Nature Publishing Group, 5, pp. 1–10. doi: 10.1038/ncomms4136.

Gu, K., Onorato, J., Xiao, S.S., Luscombe, C.K. and Loo, Y.L., 2018. Determination of the molecular weight of conjugated polymers with diffusion-ordered NMR spectroscopy. *Chemistry of Materials*, 30(3), pp.570-576.

Hanton, S. D. and Liu, X. M. (2000) 'GPC separation of polymer samples for MALDI analysis', *Analytical Chemistry*, 72(19), pp. 4550–4554. doi: 10.1021/ac000095n.

Harwansh, R. K., Mukherjee, P. K. and Biswas, S. (2017) 'Nanoemulsion as a novel carrier system for improvement of betulinic acid oral bioavailability and hepatoprotective activity', *Journal of Molecular Liquids*. 237, pp. 361–371. doi: 10.1016/j.molliq.2017.04.051.

Haydar, M. A. L. (2011) 'Degradation of Artesunate in Aqueous Solution', (Doctoral dissertation, Curtin University).

Haynes, R.K., Fugmann, B., Stetter, J., Rieckmann, K., Heilmann, H.D., Chan, H.W., Cheung, M.K., Lam, W.L., Wong, H.N., Croft, S.L. and Vivas, L., (2006) 'Artemisone - A highly active antimalarial drug of the artemisinin class', *Angewandte Chemie - International Edition*, 45(13), pp. 2082–2088. doi: 10.1002/anie.200503071.

Hermanson, G. T. (2008) *Bioconjugate Techniques*. 2nd edn. Academic Press. doi: 10.1007/s13398-014-0173-7.2.

Hill, J., Lines, J. and Rowland, M., (2006) 'Insecticide-Treated Nets', *Advances in Parasitology*, 61(05), pp. 77–128. doi: 10.1016/S0065-308X(05)61003-2.

Hosseini, Samira, and S. O. M.-C., (2016) 'Principles and Mechanism of MALDI-ToF-MS Analysis applications in Bio-diagnosis, Tissue Engineering and Drug Delivery', in *Springer*. Springer, pp. 1–19. doi: 10.1007/978-981-10-2356-9.

Hossain, M.A., (2020) 'New Drug Approvals' *Bangladesh Pharmaceutical Journal*, *23*(2), pp.201-202.

Huh, A. J. and Kwon, Y. J., (2011) '"Nanoantibiotics": A new paradigm for treating infectious diseases using nanomaterials in the antibiotics resistant era', *Journal of Controlled Release*. Elsevier B.V., 156(2), pp. 128–145. doi: 10.1016/j.jconrel.2011.07.002.

Hussein-Al-Ali, S.H., Arulselvan, P., Fakurazi, S. and Hussein, M.Z, (2014) 'The in vitro therapeutic activity of betulinic acid nanocomposite on breast cancer cells (MCF-7) and normal fibroblast cell (3T3)', *Journal of Materials Science*, 49(23), pp. 8171–8182. doi: 10.1007/s10853-014-8526-3.

Illum, L., Jabbal-Gill, I., Hinchcliffe, M., Fisher, A.N. and Davis, S.S., (2001) 'Chitosan as a novel nasal delivery system for vaccines', *Advanced drug delivery reviews*, *51*(1-3), pp.81-96.

Islan, G.A., Durán, M., Cacicedo, M.L., Nakazato, G., Kobayashi, R.K., Martinez, D.S., Castro, G.R. and Durán, N., (2017) 'Nanopharmaceuticals as a solution to neglected diseases: Is it possible?', *Acta Tropica*, 170, pp. 16–42. doi: 10.1016/j.actatropica.2017.02.019.

Ivanova, G., Simeonova, M., Cabrita, E.J. and Rangel, M., (2011) 'NMR insight into the supramolecular structure of daunorubicin loaded polymer nanoparticles', *Journal of Physical Chemistry B*, 115(5), pp. 902–909. doi: 10.1021/jp109738e.

Jeon, S., Clavadetscher, J., Lee, D.K., Chankeshwara, S.V., Bradley, M. and Cho, W.S., (2018) 'Surface charge-dependent cellular uptake of polystyrene nanoparticles' *Nanomaterials*, *8*(12), p.1028.

Jo, Y.S., Van Der Vlies, A.J., Gantz, J., Antonijevic, S., Demurtas, D., Velluto, D. and Hubbell, J.A., (2008) 'RAFT homo- and copolymerization of N-acryloyl-morpholine, piperidine, and azocane and their self-assembled structures', *Macromolecules*, 41(4), pp. 1140–1150. doi: 10.1021/ma071710t.

Kang, Y., Zhang, X.M., Zhang, S., Ding, L.S. and Li, B.J., (2015) 'pH-responsive dendritic polyrotaxane drug-polymer conjugates forming nanoparticles as efficient drug delivery system for cancer therapy', *Polymer Chemistry*, 6(11), pp. 2098–2107. doi: 10.1039/c4py01431f.

Kean, T. and Thanou, M., (2010) 'Biodegradation , biodistribution and toxicity of chitosan', *Advanced Drug Delivery Reviews*, 62(1), pp. 3–11. doi: 10.1016/j.addr.2009.09.004.

Kerb, R., Fux, R., Mörike, K., Kremsner, P.G., Gil, J.P., Gleiter, C.H. and Schwab, M., (2009) 'Pharmacogenetics of antimalarial drugs: effect on metabolism and transport', *The Lancet Infectious Diseases*. 9(12), pp. 760–774. doi: 10.1016/S1473-3099(09)70320-2.

Khan, S.A., Khan, S.B., Khan, L.U., Farooq, A., Akhtar, K. and Asiri, A.M., (2018) 'Fourier transform infrared spectroscopy: fundamentals and application in functional groups and nanomaterials characterization', in *Handbook of Materials Characterization*, Springer International Publishing, pp. 317–344.

Kilz, P. and Pasch, H., (2006) 'Coupled Liquid Chromatographic Techniques in Molecular Characterization', *Encyclopedia of Analytical Chemistry*, pp. 7495–7543. doi: 10.1002/9780470027318.a2018.

Knop, K., Hoogenboom, R., Fischer, D. and Schubert, U.S., (2010) 'Poly (ethylene glycol) in drug delivery: pros and cons as well as potential alternatives', *Angewandte chemie international edition*, *49*(36), pp.6288-6308.

Knapik-Kowalczuk, J., Chmiel, K., Pacułt, J., Bialek, K., Tajber, L. and Paluch, M., (2020) 'Enhancement of the physical stability of amorphous sildenafil in a binary mixture, with either a plasticizing or antiplasticizing compound' *Pharmaceutics*, *12*(5), p.460.

Kolaczinski, K., Durrani, N., Rahim, S. and Rowland, M., (2007) 'Sulfadoxine-pyrimethamine plus artesunate compared with chloroquine for the treatment of vivax malaria in areas co-endemic for Plasmodium falciparum and P. vivax: a randomised non-inferiority trial in eastern Afghanistan', *Transactions of the Royal Society of Tropical Medicine and Hygiene*, 101(11), pp. 1081–1087. doi: 10.1016/j.trstmh.2007.06.015.

Kolate, A., Baradia, D., Patil, S., Vhora, I., Kore, G. and Misra, A., (2014) 'PEG - A versatile conjugating ligand for drugs and drug delivery systems', *Journal of controlled release*, *192*, pp.67-81. doi: 10.1016/j.jconrel.2014.06.046.

Kramer, J. R. and Deming, T. J., (2010) 'General Method for Purification of r -Amino acid-*N*-carboxyanhydrides Using Flash Chromatography', pp. 3668–3672. doi: 10.1021/bm101123k.

Krishna, S., Uhlemann, A. C. and Haynes, R. K., (2004) 'Artemisinins: Mechanisms of action and potential for resistance', *Drug Resistance Updates*, 7(4–5), pp. 233–244. doi: 10.1016/j.drup.2004.07.001.

Kumar, S., Koh, J., Kim, H., Gupta, M.K. and Dutta, P.K., (2012) 'A new chitosan-thymine conjugate: Synthesis, characterization and biological activity', *International Journal of Biological Macromolecules*, 50(3), pp. 493–502. doi: 10.1016/j.ijbiomac.2012.01.015.

Kumar, S., Singh, R.K., Sharma, R., Murthy, R.S.R. and Bhardwaj, T.R., (2015) 'Synthesis and evaluation of antimalarial potential of polyphosphazene linked combination therapy of primaquine and dihydroartemisinin', *European Journal of Pharmaceutical Sciences*, 66, pp. 123–137. doi: 10.1016/j.ejps.2014.09.023.

Kwon, S.K. and Kim, D.H., 2006. Effect of process parameters of UV-assisted gas-phase cleaning on the removal of PEG (polyethyleneglycol) from a Si substrate. *Journal-korean physical society*, *49*(4), p.1421.

Lai, J. and Huang, Y., (2015) 'Fibril aggregates of the poly(glutamic acid)–drug conjugate', *Rsc Advances*. Royal Society of Chemistry, pp. 48856–48860. doi: 10.1039/c5ra06755c.

Lanners, H. N., (1991) 'Effect of the 8-aminoquinoline primaquine on culture-derived gametocytes of the malaria parasite Plasmodium falciparum', *Parasitology Research*, 77(6), pp. 478–481. doi: 10.1007/BF00928413.

Larson, N. and Ghandehari, H., (2012) 'Polymeric Conjugates for Drug Delivery', *Chemistry of Materials*, *24*(5), pp.840-853.

Lavignac, N., Nicholls, J.L., Ferruti, P. and Duncan, R., (2009) 'Poly(amidoamine) conjugates containing doxorubicin bound via an acid-sensitive linker', *Macromolecular*

Bioscience, 9(5), pp. 480–487. doi: 10.1002/mabi.200800163.

Le, T. N. and Neralla, V. R. (2020) 'Evaluation of the best pH-sensitive linker using norbornene-derived polymers', *Journal of Macromolecular Science, Part A*. pp. 1–7. doi: 10.1080/10601325.2020.1858717.

Lee, C.C., Cramer, A.T., Szoka, F.C. and Fréchet, J.M., (2006) 'An Intramolecular Cyclization Reaction Is Responsible for the in Vivo Inefficacy and Apparent pH Insensitive Hydrolysis Kinetics of Hydrazone Carboxylate Derivatives of Doxorubicin', *Bioconjugate chemistry*, *17*(5), pp.1364-1368.

Lee, E., Kim, H., Lee, I.H. and Jon, S., (2009) 'In vivo antitumor effects of chitosan-conjugated docetaxel after oral administration', *Journal of Controlled Release*. 140(2), pp. 79–85. doi: 10.1016/j.jconrel.2009.08.014.

Lee, E., Lee, J. and Jon, S. (2010) 'A novel approach to oral delivery of insulin by conjugating with low molecular weight chitosan', *Bioconjugate Chemistry*, 21(10), pp. 1720–1723. doi: 10.1021/bc100093v.

Lee, G.Y., Qian, W.P., Wang, L., Wang, Y.A., Staley, C.A., Satpathy, M., Nie, S., Mao, H. and Yang, L., (2013) 'Theranostic nanoparticles with controlled release of gemcitabine for targeted therapy and MRI of pancreatic cancer', *ACS Nano*, 7(3), pp. 2078–2089. doi: 10.1021/nn3043463.

Lee, I.-S. and Hufford, C. D., (1990) 'Metabolism of antimalarial sesquiterpene lactones', *Pharmacology & Therapeutics*, 48(3), pp. 345–355. doi: https://doi.org/10.1016/0163-7258(90)90053-5.

Leriche, G., Chisholm, L. and Wagner, A. (2012) 'Bioorganic & Medicinal Chemistry Cleavable linkers in chemical biology', *Bioorganic & Medicinal Chemistry*. Elsevier Ltd, 20(2), pp. 571–582. doi: 10.1016/j.bmc.2011.07.048.

Li, W., Zhan, P., De Clercq, E., Lou, H. and Liu, X., (2013) 'Current drug research on PEGylation with small molecular agents', *Progress in Polymer Science*, 38(3–4), pp. 421–444. doi: 10.1016/j.progpolymsci.2012.07.006.

Lisewski, A.M., Quiros, J.P., Ng, C.L., Adikesavan, A.K., Miura, K., Putluri, N., Eastman, R.T., Scanfeld, D., Regenbogen, S.J., Altenhofen, L. and Llinás, M., (2014) 'Supergenomic network compression and the discovery of exp1 as a glutathione transferase inhibited by artesunate', *Cell*, *158*(4), pp.916-928. doi: 10.1016/j.cell.2014.07.011.

Liu, K., Dai, L., Li, C., Liu, J., Wang, L. and Lei, J., (2016) 'Self-assembled targeted nanoparticles based on transferrin-modified eight-arm-polyethylene glycol-dihydroartemisinin conjugate', *Scientific Reports*, 6(1), pp. 1–12. doi: 10.1038/srep29461.

Liu, T., Du, F., Wan, Y., Zhu, F. and Xing, J., (2011) 'Rapid identification of phase I and II metabolites of artemisinin antimalarials using LTQ-Orbitrap hybrid mass spectrometer in combination with online hydrogen/deuterium exchange technique', *Journal of Mass Spectrometry*, 46(8), pp. 725–733. doi: 10.1002/jms.1943.

Liu, X., Patsavas, M. C. and Byrne, R. H. (2011) 'Purification and characterization of meta-

cresol purple for spectrophotometric seawater ph measurements', *Environmental Science and Technology*, 45(11), pp. 4862–4868. doi: 10.1021/es200665d.

Lo, C. I., Fall, B. and Samb-ba, B. (2017) 'Value of matrix assisted laser desorption ionization- time of flight (MALDI-TOF) mass spectrometry in clinical microbiology and infectious diseases in Africa and tropical areas', *African Journal of Microbiology Research*, 11, pp. 1360–1370. doi: 10.5897/AJMR2016.8181.

Lu, J., Jiang, F., Lu, A. and Zhang, G., (2016) 'Linkers having a crucial role in antibody–drug conjugates', *International Journal of Molecular Sciences*, 17(4). p.561. doi: 10.3390/ijms17040561.

Lukas, K. and LeMaire, P. K. (2009) 'Differential Scanning Calorimetry: Fundamental overview', *Resonance*, 14(8), pp. 807–817. doi: 10.1007/s12045-009-0076-7.

Lundqvist, M., Augustsson, C., Lilja, M., Lundkvist, K., Dahlbäck, B., Linse, S. and Cedervall, T., (2017) 'The nanoparticle protein corona formed in human blood or human blood fractions' *PloS one*, *12*(4), p.e0175871.

Luo, Z., Guo, Y., Liu, J., Qiu, H., Zhao, M., Zou, W. and Li, S., (2016) 'Microbial synthesis of poly-γ-glutamic acid: Current progress, challenges, and future perspectives', *Biotechnology for Biofuels*, 9(1), pp. 1–12. doi: 10.1186/s13068-016-0537-7.

Maguire, C.M., Rösslein, M., Wick, P. and Prina-Mello, A., (2018) 'Characterisation of particles in solution–a perspective on light scattering and comparative technologies', *Science and Technology of Advanced Materials*. Taylor & Francis, 19(1), pp. 732–745. doi: 10.1080/14686996.2018.1517587.

Mahesh, S., Tang, K.C. and Raj, M., (2018) 'Molecules Bond Activation Activation of Amide'. *Molecules*, *23*(10), p.2615. doi: 10.3390/molecules23102615.

Mainardes, R. M., Gremião, M. P. D. and Evangelista, R. C. (2006) 'Thermoanalytical study of praziquantel-loaded PLGA nanoparticles', *Revista Brasileira de Ciencias Farmaceuticas/Brazilian Journal of Pharmaceutical Sciences*, 42(4), pp. 523–530. doi: 10.1590/S1516-93322006000400007.

Mallamace, F., Corsaro, C., Mallamace, D., Vasi, S., Vasi, C. and Dugo, G., (2015) 'The role of water in protein's behavior: The two dynamical crossovers studied by NMR and FTIR techniques', *Computational and Structural Biotechnology Journal*, 13, pp. 33–37. doi: 10.1016/j.csbj.2014.11.007.

Malik, N.S., Ahmad, M., Minhas, M.U., Tulain, R., Barkat, K., Khalid, I. and Khalid, Q., (2020), 'Chitosan/xanthan gum based hydrogels as potential carrier for an antiviral drug: fabrication, characterization, and safety evaluation' *Frontiers in chemistry*, *8*, p.50.

Manaia, E.B., Abuçafy, M.P., Chiari-Andréo, B.G., Silva, B.L., Junior, J.A.O. and Chiavacci, L.A., (2017) 'Physicochemical characterization of drug nanocarriers', *International Journal of Nanomedicine*, 12, pp. 4991–5011. doi: 10.2147/IJN.S133832.

Marasini, N., Haque, S. and Kaminskas, L. M. (2017) 'Polymer-drug conjugates as inhalable drug delivery systems: A review ', *Current Opinion in Colloid & Interface Science*, *31*,

pp.18-29. doi: 10.1016/j.cocis.2017.06.003.

Margaritis, A. and Manocha, B. (2010) 'Controlled release of doxorubicin from doxorubicin/γ-polyglutamic acid ionic complex', *Journal of Nanomaterials, 161*(2), pp.446-460.doi: 10.1155/2010/780171.

Mathiyalagan, R., Kim, Y.J., Wang, C., Jin, Y., Subramaniyam, S., Singh, P., Wang, D. and Yang, D.C., (2016). 'Protopanaxadiol aglycone ginsenoside-polyethylene glycol conjugates: synthesis, physicochemical characterizations, and in vitro studies' *Artificial cells, nanomedicine, and biotechnology*, *44*(8), pp.1803-1809.

Markovsky, E., Baabur-Cohen, H., Eldar-Boock, A., Omer, L., Tiram, G., Ferber, S., Ofek, P., Polyak, D., Scomparin, A. and Satchi-Fainaro, R., (2012) 'Administration , distribution , metabolism and elimination of polymer therapeutics', *Journal of Controlled Release*, 161(2), pp. 446–460. doi: 10.1016/j.jconrel.2011.12.021.

McCarron, P.A., Olwill, S.A., Marouf, W.M., Buick, R.J., Walker, B. and Scott, C.J., (2005) 'Antibody conjugates and therapeutic strategies.', *Molecular interventions*, 5(6), pp. 368–380. doi: 10.1124/mi.5.6.9.

McCarthy, J.S., Lotharius, J., Rückle, T., Chalon, S., Phillips, M.A., Elliott, S., Sekuloski, S., Griffin, P., Ng, C.L., Fidock, D.A. and Marquart, L., (2017) 'Safety , tolerability , pharmacokinetics , and activity of the novel long-acting antimalarial DSM265 : a two-part first-in-human phase 1a / 1b randomised study', T*he Lancet Infectious Diseases*, 17(6), pp.626-635. doi: 10.1016/S1473-3099(17)30171-8.

Mccarthy, J. S. and Price, R. N. (2018) 'Tafenoquine for the radical cure and prevention of malaria: the importance of testing for G6PD deficiency', pp. 152–154. doi: 10.5694/mja2.50474.

Medhi, B., Patyar, S., Rao, R.S., Ds, P.B. and Prakash, A., (2009) 'Pharmacokinetic and toxicological profile of artemisinin compounds: An update', *Pharmacology*, 84(6), pp. 323–332. doi: 10.1159/000252658.

Medicine for Malaria Venture (2020) 'Jan_2020_MMV_portfolio_slides'. https://www.mmv.org/research-development/mmv-supported-projects.

Mensah, M.L., Komlaga, G., Forkuo, A.D., Firempong, C., Anning, A.K. and Dickson, R.A., (2019) 'Toxicity and Safety Implications of Herbal Medicines Used in Africa', *Herbal medicine*, *63*, pp.1992-0849

Merckx, P. (2014) Synthesis, Physicochemical Characterisation and Cytotoxicity Evaluation of Different Pga-Ptx Conjugates. *Ghent University*. Available at: http://lib.ugent.be/fulltxt/RUG01/002/166/891/RUG01-002166891_2015_0001_AC.pdf.

Meshnick, S. R. (2002) 'Artemisinin: Mechanisms of action, resistance and toxicity', *International Journal for Parasitology*, 32(13), pp. 1655–1660. doi: 10.1016/S0020-7519(02)00194-7.

Meshnick, S. R., Taylor, T. E. and Kamchonwongpaisan, S. (1996) 'Artemisinin and the antimalarial endoperoxides: From herbal remedy to targeted chemotherapy', *Microbiological*

Reviews, 60(2), pp. 301–315. doi: 10.1128/mmbr.60.2.301-315.1996.

Mihaly, G.W., Ward, S.A., Edwards, G., Nicholl, D.D., Orme, M.L. and Breckenridge, A.M., (1985) 'Pharmacokinetics of primaquine in man . I . Studies of the absolute bioavailability and effects of dose size', *British journal of clinical pharmacology*, *19*(6), pp.745-750.

Mike Sargent (2013) 'Guide to achieving reliable quantitative LC-MS measurements'. Edited by M. Sargent. *RSC Analytical Methods Committee*, pp. 3–61.

Mishra, M., Mishra, V.K., Kashaw, V., Iyer, A.K. and Kashaw, S.K., (2017) 'Comprehensive review on various strategies for antimalarial drug discovery', *European journal of medicinal chemistry*, *125*, pp.1300-1320. doi: 10.1016/j.ejmech.2016.11.025.

Mokhtari, R.B., Homayouni, T.S., Baluch, N., Morgatskaya, E., Kumar, S., Das, B. and Yeger, H., (2017) 'Combination therapy in combating cancer systematic review: combination therapy in combating cancer background', *Oncotarget*, 8(23), pp. 38022–38043.

Monajjemzadeh, F. and Ghaderi, F., (2015) 'Thermal analysis methods in pharmaceutical quality control' *Journal of Molecular Pharmacuetics Organic Process*, *3*(1), p.e121.

Morales-serna, J. A. (2011) 'ChemInform Abstract: Using Benzotriazole Esters as a Strategy in the Esterification of Tertiary Alcohols.' *Synthesis*, *2010*(24), pp.4261-4267. doi: 10.1002/chin.201115053.

Moreira, D.D.L., Teixeira, S.S., Monteiro, M.H.D., De-Oliveira, A.C.A. and Paumgartten, F.J., (2014) 'Original article Traditional use and safety of herbal medicines', *Revista Brasileira de Farmacognosia*, *24*(2), pp.248-257. doi: 10.1016/j.bjp.2014.03.006.

Mvango S, Matshe WM, Balogun AO, Pilcher LA, Balogun MO., (2018) 'Nanomedicines for Malaria Chemotherapy: Encapsulation vs. Polymer Therapeutics', *Pharmaceutical Research*. Pharmaceutical Research, 35(12). doi: 10.1007/s11095-018-2517-z.

Nagarajan, S., Nagarajan, R., Bruno, F., Samuelson, L.A. and Kumar, J., (2009) 'A stable biomimetic redox catalyst obtained by the enzyme catalyzed amidation of iron porphyrin', *Green Chemistry*, 11(3), pp. 334–33. doi: 10.1039/b813823k.

Nakajima, N. and Ikada, Y., (1995) 'Mechanism of Amide Formation by Carbodiimide for Bioconjugation in Aqueous Media', *Bioconjugate chemistry*, *6*(1), pp.123-130.

Nan, A., Nanayakkara, N.D., Walker, L.A., Yardley, V., Croft, S.L. and Ghandehari, H., (2001) 'N-(2-hydroxypropyl)methacrylamide (HPMA) copolymers for targeted delivery of 8-aminoquinoline antileishmanial drugs', *Journal of Controlled Release*, 77(3), pp. 233–243. doi: 10.1016/S0168-3659(01)00514-4.

Nan, A., Croft, S.L., Yardley, V. and Ghandehari, H., (2004) 'Targetable water-soluble polymer-drug conjugates for the treatment of visceral leishmaniasis', *Journal of Controlled Release*, 94(1), pp. 115–127. doi: 10.1016/j.jconrel.2003.09.012.

Navaratnam, V., Mansor, S.M., Sit, N.W., Grace, J., Li, Q. and Olliaro, P., (2000) 'Pharmacokinetics of Artemisinin-Type Compounds', *Clinical Pharmacokinetics*, 39(4), pp. 255–270.

Nicoletti, S., Seifert, K. and Gilbert, I. H. (2009) 'N-(2-hydroxypropyl)methacrylamide-amphotericin B (HPMA-AmB) copolymer conjugates as antileishmanial agents', *International Journal of Antimicrobial Agents*. Elsevier B.V. and the International Society of Chemotherapy, 33(5), pp. 441–448. doi: 10.1016/j.ijantimicag.2008.10.013.

Nino-Pariente, A., J. Nebot, V. and J. Vicent, M. (2016) 'Relevant Physicochemical Descriptors of "Soft Nanomedicines" to Bypass Biological Barriers', *Current Pharmaceutical Design*, 22(9), pp. 1274–1291. doi: 10.2174/1381612822666151216152143.

Nosten, F. and Brasseur, P. (2002) 'Combination Therapy for Malaria The Way Forward ?' *Drugs*, *62*(9), pp.1315-1329.

Ntuku, H.M., Ferrari, G., Burri, C., Tshefu, A.K., Kalemwa, D.M. and Lengeler, C., (2016) 'Feasibility and acceptability of injectable artesunate for the treatment of severe malaria in the Democratic Republic of Congo', *Malaria Journal*, 15(1) pp. 1–10. doi: 10.1186/s12936-015-1072-x.

Ogunleye, A., Bhat, A., Irorere, V.U., Hill, D., Williams, C. and Radecka, I., (2015) 'Poly-γ-glutamic acid: Production, properties and applications', *Microbiology*, 161(1), pp. 1–17. doi: 10.1099/mic.0.081448-0.

Oledzka, E., Sawicka, A., Sobczak, M., Nalecz-Jawecki, G., Skrzypczak, A. and Kolodziejski, W., (2015) 'Prazosin-conjugated matrices based on biodegradable polymers and α-amino acids - Synthesis, characterization, and in vitro release study', *Molecules*, 20(8), pp. 14533–14551. doi: 10.3390/molecules200814533.

Olliaro, P. (2001) 'Mode of action and mechanisms of resistance for antimalarial drugs', *Pharmacology and Therapeutics*, 89(2), pp. 207–219. doi: 10.1016/S0163-7258(00)00115-7.

Pandey, A.V., Tekwani, B.L., Singh, R.L. and Chauhan, V.S., (1999) 'Artemisinin, an endoperoxide antimalarial, disrupts the hemoglobin catabolism and heme detoxification systems in malarial parasite', *Journal of Biological Chemistry*, 274(27), pp. 19383–19388. doi: 10.1074/jbc.274.27.19383.

Pang, X., Du, H.L., Zhang, H.Q., Zhai, Y.J. and Zhai, G.X., (2013) 'Polymer-drug conjugates: Present state of play and future perspectives', *Drug Discovery Today*, 18(23–24), pp. 1316–1322. doi: 10.1016/j.drudis.2013.09.007.

Pang, X., Jiang, Y., Xiao, Q., Leung, A.W., Hua, H. and Xu, C., (2016) 'pH-responsive polymer – drug conjugates : Design and progress', *Journal of Controlled Release*, 222, pp. 116–129. doi: 10.1016/j.jconrel.2015.12.024.

Paquet, T., Le Manach, C., Cabrera, D.G., Younis, Y., Henrich, P.P., Abraham, T.S., Lee, M.C., Basak, R., Ghidelli-Disse, S., Lafuente-Monasterio, M.J. and Bantscheff, M., (2017) 'Antimalarial efficacy of MMV390048, an inhibitor of Plasmodium phosphatidylinositol 4-kinase', *Science Translational Medicine*, 9(387). doi: 10.1126/scitranslmed.aad9735.

Parapini, S., Olliaro, P., Navaratnam, V., Taramelli, D. and Basilico, N., (2015) 'Stability of

the antimalarial drug dihydroartemisinin under physiologically relevant conditions: Implications for clinical treatment and pharmacokinetic and in vitro assays', *Antimicrobial Agents and Chemotherapy*, 59(7), pp. 4046–4052. doi: 10.1128/AAC.00183-15.

Patsavas, M. C., Byrne, R. H. and Liu, X. (2013) 'Puri fi cation of meta-cresol purple and cresol red by fl ash chromatography : Procedures for ensuring accurate spectrophotometric seawater pH measurements', *Marine Chemistry*, 150, pp. 19–24. doi: 10.1016/j.marchem.2013.01.004.

Petras, J.M., Kyle, D.E., Gettayacamin, M., Young, G.D., Bauman, R.A., Webster, H.K., Corcoran, K.D., Peggins, J.O., Vane, M.A. and Brewer, T.G., (1997) 'Arteether: Risks of two-week administration in Macaca mulatta', *American Journal of Tropical Medicine and Hygiene*, 56(4), pp. 390–396. doi: 10.4269/ajtmh.1997.56.390.

Phillips, M. A., (2017) 'Malaria', *Nature Reviews Disease Primers*, 3. doi: 10.1038/nrdp.2017.50.

Pillai, C. K.S., Paul, W. and Sharma, C. P. (2009) 'Chitin and chitosan polymers: Chemistry, solubility and fiber formation', *Progress in Polymer Science*, *34*(7), pp.641-678. doi: 10.1016/j.progpolymsci.2009.04.001.

Ping-Chang Lin, Stephen Lin, Paul C. Wang, and R. S. (2014) 'Techniques for physicochemical characterization of nanomaterials Ping-Chang', *Biotechnology Advances*, 32(4), pp. 711–726. doi: 10.1038/jid.2014.371.

Pirson, P., Steiger, R. and Trouet, A. (1982) 'The disposition of free and liposomally encapsulated antimalarial primaquine in mice', *Biochemical Pharmacology*, 31(21), pp. 3501–3507. doi: 10.1016/0006-2952(82)90633-5.

Pitt, J. J. (2009) 'Principles and Applications of Liquid Chromatography- Mass Spectrometry in Clinical Biochemistry', *The Clinical Biochemist Reviews*, 30(February), pp. 19–34.

Portilla-Arias, J.A., García-Alvarez, M., de Ilarduya, A.M. and Muñoz-Guerra, S., (2007) 'Thermal decomposition of microbial poly(γ-glutamic acid) and poly(γ-glutamate)'s, *Polymer Degradation and Stability*, 92(10), pp. 1916–1924. doi: 10.1016/j.polymdegradstab.2007.06.011.

Presser, A., Feichtinger, A. and Buzzi, S. (2017) 'A simplified and scalable synthesis of artesunate', *Monatshefte fur Chemie*. Springer Vienna, 148(1), pp. 63–68. doi: 10.1007/s00706-016-1865-9.

Price, R.N., Uhlemann, A.C., van Vugt, M., Brockman, A., Hutagalung, R., Nair, S., Nash, D., Singhasivanon, P., Anderson, T.J., Krishna, S. and White, N.J., (2006) 'Molecular and Pharmacological Determinants of the Therapeutic Response to Artemether-Lumefantrine in Multidrug-Resistant Plasmodium falciparum Malaria', *Clinical Infectious Diseases*, 42(11), pp. 1570–1577. doi: 10.1086/503423.

Priya, V.S.V., Roy, H.K., Jyothi, N. and Prasanthi, N.L., (2016) 'Polymers in Drug Delivery Technology, Types of Polymers and Applications', *Scholars Academic Journal of Pharmacy*, 5(7), pp. 305–308. doi: 10.21276/sajp.2016.5.7.7.

Qian, Z., Galuska, L., McNutt, W.W., Ocheje, M.U., He, Y., Cao, Z., Zhang, S., Xu, J., Hong, K., Goodman, R.B. and Rondeau-Gagné, S., (2019) 'Challenge and Solution of Characterizing Glass Transition Temperature for Conjugated Polymers by Differential Scanning Calorimetry', *Journal of Polymer Science, Part B: Polymer Physics*, 57(23), pp. 1635–1644. doi: 10.1002/polb.24889.

Quan, L., Zhang, Y., Crielaard, B.J., Dusad, A., Lele, S.M., Rijcken, C.J., Metselaar, J.M., Kostková, H., Etrych, T., Ulbrich, K. and Kiessling, F., (2013) 'Nanomedicines for In fl ammatory Arthritis : Head-to-Head Comparison of Glucocorticoid-Containing', *ACS Nano*, 8(1), pp. 458–466.

Quiliano, M., Mendoza, A., Fong, K.Y., Pabón, A., Goldfarb, N.E., Fabing, I., Vettorazzi, A., de Cerain, A.L., Dunn, B.M., Garavito, G. and Wright, D.W., (2016) 'Exploring the scope of new arylamino alcohol derivatives: Synthesis, antimalarial evaluation, toxicological studies, and target exploration', *International Journal for Parasitology: Drugs and Drug Resistance*, 6(3), pp. 184–198. doi: 10.1016/j.ijpddr.2016.09.004.

Rinaudo, M. (2006) 'Chitin and chitosan : Properties and applications', *Progress in polymer science*, *31*(7), pp.603-632. doi: 10.1016/j.progpolymsci.2006.06.001.

Ringsdorf, H. (1975) 'Structure and properties of pharmacologically active polymers', *Journal of Polymer Science: Polymer Symposia*, 51(1), pp. 135–153. doi: 10.1002/polc.5070510111.

Roberts, M. J., Bentley, M. D. and Harris, J. M. (2002) 'Chemistry for peptide and protein PEGylation', *Advanced drug delivery reviews*, *54*(4), pp.459-476.

Ross, P. L. and Wolfe, J. (2016) 'Antibody-Drug Conjugates: An Overview of the CMC and Characterization Process', *Antibody-Drug Conjugates*, pp. 59–83. doi: 10.1002/9781119060727.ch3.

S. Murdande, M. Pikal, R. Shanker, R. B. (2009) 'Aqueous Solubility of Crystalline and Amorphous Drugs: Challenges in Measurement', *Pharmaceutical Development and technology*, 16(3), pp. 187–200.

Sagita, E., Syahdi, R. R. and Arrahman, A. (2018) 'Synthesis of Polymer-Drug Conjugates Using Natural Polymer : What , Why and How ?', *Pharmaceutical Sciences & Research*, *5*(3), p.1.

Saneja, A., Sharma, L., Dubey, R.D., Mintoo, M.J., Singh, A., Kumar, A., Sangwan, P.L., Tasaduq, S.A., Singh, G., Mondhe, D.M. and Gupta, P.N., (2017) 'Synthesis , characterization and augmented anticancer potential of PEG-betulinic acid conjugate', *Materials Science and Engineering: C*, *73*, pp.616-626.

Santos-magalhães, N. S., Carla, V. and Mosqueira, F. (2010) 'Nanotechnology applied to the treatment of malaria ', *Advanced Drug Delivery Reviews*. Elsevier B.V., 62(4–5), pp. 560–575. doi: 10.1016/j.addr.2009.11.024.

Santos-Magalhães, N. S. and Mosqueira, V. C. F. (2010) 'Nanotechnology applied to the treatment of malaria', *Advanced Drug Delivery Reviews*, pp. 560–575. doi:

10.1016/j.addr.2009.11.024.

Sartore, L., Vic, M. and Ranucci, E. (1997) 'United States Patent 19'.

Saucier-Sawyer, J.K., Deng, Y., Seo, Y.E., Cheng, C.J., Zhang, J., Quijano, E. and Saltzman, W.M., (2015) 'Systemic delivery of blood–brain barrier-targeted polymeric nanoparticles enhances delivery to brain tissue' *Journal of drug targeting*, *23*(7-8), pp.736-749.

Schiavon, O., Caliceti, P., Ferruti, P. and Veronese, F.M., (2000) 'Therapeutic proteins: A comparison of chemical and biological properties of uricase conjugated to linear or branched poly(ethylene glycol) and poly(N- acryloylmorpholine)', *Farmaco*, 55(4), pp. 264–269. doi: 10.1016/S0014-827X(00)00031-8.

Schittny, A., Huwyler, J. and Puchkov, M. (2020) 'Mechanisms of increased bioavailability through amorphous solid dispersions: a review', *Drug Delivery*. Taylor & Francis, 27(1), pp. 110–127. doi: 10.1080/10717544.2019.1704940.

Schellekens, H., Hennink, W.E. and Brinks, V., (2013) 'The immunogenicity of polyethylene glycol: facts and fiction', *Pharmaceutical research*, *30*(7), pp.1729-1734.

Scintag, I. (1999) 'Chapter 7 : Basics of X-ray Diffraction', in *Providing Solution To Your Diffraction Needs*, pp. 7–1.

Scriven, E. F. V. and Murugan, R. (2005) 'Pyridine and Pyridine Derivatives', *Kirk-Othmer Encyclopedia of Chemical Technology*. doi: 10.1002/0471238961.1625180919031809.a01.pub2.

Seymour, L.W., Ulbrich, K., Wedge, S.R., Hume, I.C., Strohalm, J. and Duncan, R., (1991) 'N-(2-hydroxypropyi)methacrylamide copolymers targeted to the hepatocyte galactose-receptor: Pharmacokinetics in DBA2mice', *British Journal of Cancer*, 63(6), pp. 859–866. doi: 10.1038/bjc.1991.190.

Seymour, L.W., Ferry, D.R., Anderson, D., Hesslewood, S., Julyan, P.J., Poyner, R., Doran, J., Young, A.M., Burtles, S. and Kerr, D.J., (2002) 'Hepatic drug targeting: Phase I evaluation of polymer-bound doxorubicin', *Journal of Clinical Oncology*, 20(6), pp. 1668–1676. doi: 10.1200/JCO.20.6.1668.

Shenfield, G. M. (1984) 'Fixed Combination Drug Therapy', 480, pp. 462–480.

Sherman, M.R., Williams, L.D., Sobczyk, M.A., Michaels, S.J. and Saifer, M.G., (2012), 'Role of the methoxy group in immune responses to mPEG-protein conjugates', *Bioconjugate chemistry*, *23*(3), pp.485-499.

Sherman Hsu, C.P., (1998) 'Handbook of instrumental techniques for analytical chemistry: Chapter 15, infrared spectroscopy' *IEEE Electrical Insulation Magazine*, *14*(6), pp.247-283. https://mmrc.caltech.edu/FTIR/Literature/General/IR%20spectroscopy%20Hsu.pdf

Siengalewicz, P., Mulzer, J. and Rinner, U. (2014) '6.09 Synthesis of Esters and Lactones', in Knochel, P. B. T.-C. O. S. I. I. (Second E. (ed.). Amsterdam: Elsevier, pp. 355–410. doi: https://doi.org/10.1016/B978-0-08-097742-3.00612-1.

Park, Y.J., Liang, J., Yang, Z. and Yang, V.C., (2001) 'Water-soluble poly-(L-glutamic acid)-Gly-camptothecin conjugates enhance camptothecin stability and efficacy in vivo', *Journal of Controlled Release*, 74(1–3), pp. 243–247. doi: 10.1016/S0168-3659(01)00323-6.

Singer, J. W., De Vries, P., Bhatt, R., Tulinsky, J., Klein, P., Li, C., Milas, L., Lewis, R.A. and Wallace, S., (2006) 'Conjugation of Camptothecins to Poly- (L -Glutamic Acid)', *Annals of the New York Academy of Science*, 922(1), pp. 136–150.

Singh, K. K. Andreani, T., de Souza, A.L.R., Silva, A.M. and Souto, E.B., 2012. 'Sol–Gel Carrier System: A Novel Controlled Drug Delivery' In *Patenting Nanomedicines* (pp. 151-166). Springer, Berlin, Heidelberg.

Slade, D., Galal, A.M., Gul, W., Radwan, M.M., Ahmed, S.A., Khan, S.I., Tekwani, B.L., Jacob, M.R., Ross, S.A. and ElSohly, M.A., (2009) 'Antiprotozoal, anticancer and antimicrobial activities of dihydroartemisinin acetal dimers and monomers', *Bioorganic and Medicinal Chemistry*. Elsevier Ltd, 17(23), pp. 7949–7957. doi: 10.1016/j.bmc.2009.10.019.

Slor, G. and Amir, R. J. (2021) 'Using High Molecular Precision to Study Enzymatically Induced Disassembly of Polymeric Nanocarriers: Direct Enzymatic Activation or Equilibrium-Based Degradation?', *Macromolecules*, *54*(4), pp.1577-1588.doi: 10.1021/acs.macromol.0c02263.

Smith, G. L. C. and A. F. (1986) 'X-Ray Diffraction studies of chitin, chitosan, and derivatives'', *The journal of physical chemistry*, 40(7), pp. 863–879.

Şoica, C. M. *et al.* (2012) 'Physico-chemical comparison of betulinic acid, betulin and birch bark extract and in vitro investigation of their cytotoxic effects towards skin epidermoid carcinoma (A431), breast carcinoma (MCF7) and cervix adenocarcinoma (HeLa) cell lines', *Natural Product Research*, 26(10), pp. 968–974. doi: 10.1080/14786419.2010.545352.

Spillman, N. J. and Kirk, K. (2015) 'The malaria parasite cation ATPase PfATP4 and its role in the mechanism of action of a new arsenal of antimalarial drugs', *International Journal for Parasitology: Drugs and Drug Resistance*, *5*(3), pp.149-162. doi: 10.1016/j.ijpddr.2015.07.001.

Stegemann, S., Leveiller, F., Franchi, D., De Jong, H. and Lindén, H., (2007) 'Conference report: When poor solubiliyy becomes an issue: From early stage to proof of concept, *European journal of pharmaceutical sciences*, *31*(5), pp.249-261.

Subramani Parasuraman , Anish R, Subramani Balamurugan , Selvadurai Muralidharan, K. J. K. and V. V. (2014) 'An Overview of Liquid Chromatography-Mass Spectroscopy Instrumentation', *Pharmaceutical methods*, 5, pp. 47–55. doi: 10.5530/phm.2014.2.2.

Soulard, V., Bosson-Vanga, H., Lorthiois, A., Roucher, C., Franetich, J.F., Zanghi, G., Bordessoulles, M., Tefit, M., Thellier, M., Morosan, S. and Le Naour, G., (2015) 'Plasmodium falciparum full life cycle and Plasmodium ovale liver stages in humanized mice' *Nature communications*, *6*(1), pp.1-9. doi: 10.1038/ncomms8690.

Sun, Y., Zhang, J., Han, J., Tian, B., Shi, Y., Ding, Y., Wang, L. and Han, J., (2017) 'Galactose-Containing Polymer-DOX Conjugates for Targeting Drug Delivery', *AAPS*

PharmSciTech, 18(3), pp. 749–758. doi: 10.1208/s12249-016-0557-4.

Takahashi, D., Inomata, T. and Fukui, T. (2017) 'Peptide Synthesis AJIPHASE : A Highly Efficient Synthetic Method for One-Pot Peptide Elongation in the Solution Phase by an Fmoc Strategy Angewandte', *Angewandte Chemie*, *129*(27), pp.7911-7915., doi: 10.1002/anie.201702931.

Tang, F., Cen, S.Y., He, H., Liu, Y., Yuan, B.F. and Feng, Y.Q., (2016) 'Peptidylation for the determination of low-molecular-weight compounds by matrix-assisted laser desorption/ionization time-of-flight mass spectrometry' *Analyst*, *141*(11), pp.3259-3265.

Tchaparian, E., Sambol, N.C., Arinaitwe, E., McCormack, S.A., Bigira, V., Wanzira, H., Muhindo, M., Creek, D.J., Sukumar, N., Blessborn, D. and Tappero, J.W., (2016). 'Population pharmacokinetics and pharmacodynamics of lumefantrine in young Ugandan children treated with artemether-lumefantrine for uncomplicated malaria'. *The Journal of infectious diseases*, 214(8), pp.1243-1251

Teicher, B. A. and Chari, R. V. J. (2011) 'Antibody conjugate therapeutics: Challenges and potential', *Clinical Cancer Research*, 17(20), pp. 6389–6397. doi: 10.1158/1078-0432.CCR-11-1417.

Teng, C., Chai, Z., Yuan, Z., Ren, L., Lin, C., Yan, Z., He, W., Qin, C., Yang, L., Han, X. and Yin, L., (2020) 'Desirable PEGylation for improving tumor selectivity of hyaluronic acid-based nanoparticles via low hepatic captured , long circulation times and CD44 receptor-mediated tumor targeting', *Nanotechnology, Biology and Medicine*, *24*, p.102105. doi: 10.1016/j.nano.2019.102105.

Thomas, D., Tazerouni, H., Sundararaj, K.G.S. and Cooper, J.C., (2016) 'Therapeutic failure of primaquine and need for new medicines in radical cure of Plasmodium vivax', *Acta Tropica*. Elsevier B.V., 160, pp. 35–38. doi: 10.1016/j.actatropica.2016.04.009.

Thompson, C.J., Hansford, D., Munday, D.L., Higgins, S., Rostron, C. and Hutcheon, G.A., (2008) 'Synthesis and evaluation of novel polyester-ibuprofen conjugates for modified drug release', *Drug Development and Industrial Pharmacy*, 34(8), pp. 877–884. doi: 10.1080/03639040801929075.

Tilley, L., Dixon, M. W. A. and Kirk, K. (2011) 'The Plasmodium falciparum-infected red blood cell', *International Journal of Biochemistry and Cell Biology*, 43(6), pp. 839–842. doi: 10.1016/j.biocel.2011.03.012.

Tomiya, N., Jardim, J.G., Hou, J., Pastrana-Mena, R., Dinglasan, R.R. and Lee, Y.C., (2013) 'Liver-targeting of primaquine-(poly-γ-glutamic acid) and its degradation in rat hepatocytes', *Bioorganic and Medicinal Chemistry*, *21*(17), pp.5275-5281. doi: 10.1016/j.bmc.2013.06.028.

Tripathy, S., Das, S., Chakraborty, S.P., Sahu, S.K., Pramanik, P. and Roy, S., (2012) 'Synthesis , characterization of chitosan – tripolyphosphate conjugated chloroquine nanoparticle and its in vivo anti-malarial efficacy against rodent parasite : A dose and duration dependent approach', *International Journal of Pharmaceutics*. Elsevier B.V., 434(1–2), pp. 292–305. doi: 10.1016/j.ijpharm.2012.05.064.

Tsakos, M., Schaffert, E.S., Clement, L.L., Villadsen, N.L. and Poulsen, T.B., (2015) 'Ester coupling reactions – an enduring challenge in the chemical synthesis of bioactive natural products †', *Natural product reports*, *32*(4), pp.605-632. doi: 10.1039/C4NP00106K.

Tun, K.M., Imwong, M., Lwin, K.M., Win, A.A., Hlaing, T.M., Hlaing, T., Lin, K., Kyaw, M.P., Plewes, K., Faiz, M.A. and Dhorda, M., (2015) 'Spread of artemisinin-resistant Plasmodium falciparum in Myanmar: A cross-sectional survey of the K13 molecular marker', *The Lancet Infectious Diseases*, 15(4), pp. 415–421. doi: 10.1016/S1473-3099(15)70032-0.

Tuteja, R. (2007) 'Malaria-an overview', *FEBS Journal*, 274, pp. 4670–4679. doi: 10.1111/j.1742-4658.2007.05997.x.

Tzitzios, V., Basina, G., Gjoka, M., Alexandrakis, V., Georgakilas, V., Niarchos, D., Boukos, N. and Petridis, D., (2006) 'Chemical synthesis and characterization of hcp Ni nanoparticles' *Nanotechnology*, *17*(15), p.3750.

Uliyanchenko, E., van der Wal, S. and Schoenmakers, P.J., (2012) 'Challenges in polymer analysis by liquid chromatography' *Polymer Chemistry*, *3*(9), pp.2313-2335.

Umeyor, C.E., Kenechukwu, F.C., Uronnachi, E.M., Chime, S.A., Reginald-Opara, J. and Attama, A.A., (2013) 'Recent advances in particulate anti-malarial drug delivery systems : A review', *International Journal of Drug Delivery*, *5*(1), p.01.

Urbán, P. *et al.* (2014) 'Use of poly(amidoamine) drug conjugates for the delivery of antimalarials to Plasmodium', *Journal of Controlled Release*, 177, pp. 84–95. doi: //doi.org/10.1016/j.jconrel.2013.12.032.

van Kampen, J.J., Burgers, P.C., de Groot, R., Gruters, R.A. and Luider, T.M., (2011) 'Biomedical application of MALDI mass spectrometry for small-molecule analysis' *Mass spectrometry reviews*, *30*(1), pp.101-120.

Vauthier, C. and Bouchemal, K. (2009) 'Expert Review Methods for the Preparation and Manufacture of Polymeric Nanoparticles', *Pharmaceutical research*, *26*(5), pp.1025-1058. doi: 10.1007/s11095-008-9800-3.

Venditto, V. J. and Jr., F. C. S. (2014) 'Cancer Nanomedicines: So Many Papers and So Few Drugs!', *Advanced drug delivery reviews*, *65*(1), pp.80-88. doi: 10.1016/j.addr.2012.09.038.Cancer.

Ventola, C.L., (2012). 'The nanomedicine revolution: part 2: current and future clinical applications', *Pharmacy and Therapeutics*, *37*(10), p.582.

Verhoef, J. J. F. and Anchordoquy, T. J. (2013) 'Questioning the use of PEGylation for drug delivery', *Drug Delivery and Translational Research*. doi: 10.1007/s13346-013-0176-5.

Veronese, F. M. and Pasut, G. (2005) 'PEGylation, successful approach to drug delivery', *Drug Discovery Today*. doi: 10.1016/S1359-6446(05)03575-0.

Vicent, M. J. and Duncan, R. (2006) 'Polymer conjugates: Nanosized medicines for treating cancer', *Trends in Biotechnology*. doi: 10.1016/j.tibtech.2005.11.006.

Vishwakarma, R.A., Mehrotra, R., Tripathi, R. and Dutta, G.P., (1992) 'Stereoselective synthesis and antimalarial activity of alpha-artelinic acid from artemisinin', *Journal of Natural Products*, 55(8), pp. 1142–1144. doi: Doi 10.1021/Np50086a018.

Vranic, E. (2004) 'Amorphous Pharmaceutical Solids', *Bosnian Journal of Basic Medical Science*, 4(3), pp. 35–39. doi: 10.1016/j.addr.2016.04.011.

Vugt, M.V., Wilairatana, P., Gemperli, B., Gathmann, I., Phaipun, L., Brockman, A., Luxemburger, C., White, N.J., Nosten, F. and Looareesuwan, S., (1999) 'Efficacy of six doses of artemether-lumefantrine (benflumetol) in multidrug-resistant Plasmodium falciparum malaria', *American Journal of Tropical Medicine and Hygiene*, 60(6), pp. 936–942.

Walker, N. F., Nadjm, B. and Whitty, C. J. M. (2010) 'Malaria', *Medicine*, pp. 41–46. doi: 10.1016/j.mpmed.2009.09.017.

Wang, D., Li, H., Gu, J., Guo, T., Yang, S., Guo, Z., Zhang, X., Zhu, W. and Zhang, J., (2013) 'Ternary system of dihydroartemisinin with hydroxypropyl-β-cyclodextrin and lecithin: Simultaneous enhancement of drug solubility and stability in aqueous solutions', *Journal of Pharmaceutical and Biomedical Analysis*. Elsevier B.V., 83, pp. 141–148. doi: 10.1016/j.jpba.2013.05.001.

Wang, J., Zhang, C.J., Chia, W.N., Loh, C.C., Li, Z., Lee, Y.M., He, Y., Yuan, L.X., Lim, T.K., Liu, M. and Liew, C.X., (2015) 'Haem-activated promiscuous targeting of artemisinin in Plasmodium falciparum', *Nature Communications*. Nature Publishing Group, 6, pp. 1–11. doi: 10.1038/ncomms10111.

Wannachaiyasit, S., Chanvorachote, P. and Nimmannit, U. (2008) 'Research Article A Novel Anti-HIV Dextrin – Zidovudine Conjugate Improving the Pharmacokinetics of Zidovudine in Rats', *Aaps Pharmscitech*, 9(3), pp. 840–850. doi: 10.1208/s12249-008-9122-0.

Warhurst, DC, Adagu, IS, Beck, HP, Duraisingh, MT, Kirby, GC, von Seidlein, L, Wright, C. (2001) 'Mode of action of artemether lumefantrine (COARTEM): The sole, fixid, oral ADCC and its role in combatting multidrug resistance', *The Southeast Asian journal of tropical medicine and public health*, 32(January), pp. 4–8.

Watkins, R., Wu, L., Zhang, C., Davis, R.M. and Xu, B., (2015) 'Natural product-based nanomedicine : recent advances and issues', *International Journal of nanomedicine*, 10, pp. 6055–6074.

Welling, D. A. and Atherton, E. (1997) 'Standard Fmoc removal', in *Methods in Enzymology*, pp. 44–67.

Wells, T. N. C., Van Huijsduijnen, R. H. and Van Voorhis, W. C. (2015a) 'Malaria medicines: A glass half full?', *Nature Reviews Drug Discovery*, pp. 424–442. doi: 10.1038/nrd4573.

Wells, T. N. C., Van Huijsduijnen, R. H. and Van Voorhis, W. C. (2015b) 'Malaria medicines: A glass half full?', *Nature Reviews Drug Discovery*. Nature Publishing Group, 14(6), pp. 424–442. doi: 10.1038/nrd4573.

Wen-hsuan Tsai, Kun-hua, Yu Yi-cheng huang, cheng-I. lee (2018) 'EGFR-targeted photodynamic therapy by curcumin-encapsulated chitosan / TPP nanoparticles', *Internationa Journal of nanomedicine*, 13, pp. 903–916.

White, N.J., (2011) 'Determinants of relapse periodicity in Plasmodium vivax malaria' *Malaria journal*, *10*(1), pp.1-36.

World Health Organization, (2001) 'Antimalarial drug combination therapy. Report of a WHO technical consultation' *Geneva: World Health Organization*, *33*.

Williams, D.B. and Carter, C.B., (2009) 'Scattering and diffraction." Transmission Electron Microscopy', in *Polymer-Solvent Molecular Compounds*. Boston, MA: Springer, pp. 23–38. doi: 10.1016/b978-008045144-2.50006-4.

Windridge, G. and Jorgensen, E. C. (1973) '1-Hydroxybenzotriazole as a racemization-suppressing reagent for the incorporation of im-benzyl-L-histidine into peptides', *Journal of the American Chemical Society*, *93*(23), pp. 6318–6319. doi: 10.1021/ja00752a081.

Wong, R.P., Salman, S., Ilett, K.F., Siba, P.M., Mueller, I. and Davis, T.M., (2011) 'Desbutyl-Lumefantrine Is a Metabolite of Lumefantrine with Potent In Vitro Antimalarial Activity That May Influence Artemether-Lumefantrine Treatment Outcome', *Antimicrobial agents and chemotherapy* 55(3), pp. 1194–1198. doi: 10.1128/AAC.01312-10.

Wongsrichanalai, C., Pickard, A.L., Wernsdorfer, W.H. and Meshnick, S.R., (2002) 'Reviews Epidemiology of drug-resistant malaria', *The Lancet infectious diseases*, *2*(4), pp.209-218.

World Health Organization (2015) *Guidelines for the treatment of Malaria*, *Guidelines For The Treatment of Malaria*. doi: 10.1016/0035-9203(91)90261-V.

World Health Organization (2017) *World Malaria Report 2017*, *ECOS*. doi: 10.1071/EC12504.

World Health Organization (WHO) (2012) 'Updated WHO Policy Recommendation (October 2012) Single dose Primaquine as a gametocytocide in Plasmodium falciparum malaria', *Who 2012*, (October), p. 2012.

World Health Organization (WHO) (2013) 'Summary of Product Characteristics', *Guilin Pharmaceuticals Co., Ltd.*, (June).

World Health Organization (WHO) (2015) 'Policy brief on single-dose primaquine as a gametocytocide in Plasmodium falciparum malaria January 2015', (January), pp. 1–8.

World Health Organization (WHO) (2016) *Overview of malaria treatment*, *WHO*. World Health Organization. Available at: https://www.who.int/malaria/areas/treatment/overview/en/#.X48HJZIN6CU. (Accessed: 20 October 2020).

World Health Organization (WHO) (2019) *World malaria report 2019*.

World Health Organization (WHO) (2020) *World Malaria Report 2020*, *WHO*. doi:

10.1002/(SICI)1096-8628(19971128)73:1<1::AID-AJMG1>3.0.CO;2-Y.

Xiao, D., Yang, B., Yang, X.M., Yi, D., Liao, X.L., Yang, J. and Gao, C.Z., (2013) 'Synthesis of Water Soluble Chitosan-Artemisinin Conjugate', *Asian Journal of chemistry*, 25(8), pp. 4637–4639.

Xiao, D., Yang, B., Chen, Y.J., Liao, X.L., Yang, X.M., Qin, Q.X. and Yi, D., (2013) 'Synthesis of Water Soluble C-10-Phenoxy Artemisinin-Chitosan Conjugate', *Asian Journal of chemistry*, 25(8), pp. 4654–4656.

Xu, W., Li, S., Whitely, N. and Pan, W.P., (2005) 'Fundamentals of TGA and SDT' pp. 1–7.

Xu, R., Han, T., Shen, L., Zhao, J. and Lu, X.A., (2019) 'Solubility determination and modeling for artesunate in binary solvent mixtures of methanol, ethanol, isopropanol, and propylene glycol+ water' *Journal of Chemical & Engineering Data*, *64*(2), pp.755-762.

Yang, X. (2011) 'Preparation and characterization of γ-poly(glutamic acid) copolymer with glycol diglycidyl ether', *Procedia Environmental Sciences*, 8(November), pp. 11–15. doi: 10.1016/j.proenv.2011.10.004.

Yang, Y. (2016) 'Chapter 5 - Side Reactions Upon Amino Acid/Peptide Carboxyl Activation', in Yang, Y. B. T.-S. R. in P. S. (ed.). Oxford: Academic Press, pp. 95–118. doi: https://doi.org/10.1016/B978-0-12-801009-9.00005-7.

Yang, Y., Zhu, W., Cheng, L., Cai, R., Yi, X., He, J., Pan, X., Yang, L., Yang, K., Liu, Z. and Tan, W., (2020) 'Tumor microenvironment (TME)-activatable circular aptamer-PEG as an effective hierarchical-targeting molecular medicine for photodynamic therapy' *Biomaterials*, *246*, p.119971.doi: 10.1016/j.biomaterials.2020.119971.

Yap, T. A., Omlin, A. and De Bono, J. S. (2013) 'Development of therapeutic combinations targeting major cancer signaling pathways', *Journal of Clinical Oncology*, 31(12), pp. 1592–1605. doi: 10.1200/JCO.2011.37.6418.

Younis, Y., Douelle, F., Feng, T.S., Cabrera, D.G., Manach, C.L., Nchinda, A.T., Duffy, S., White, K.L., Shackleford, D.M., Morizzi, J. and Mannila, J., (2012) '3,5-Diaryl-2-Aminopyridines As a Novel Class of Orally Active Antimalarials Demonstrating Single Dose Cure in Mice and Clinical Candidate Potential', *Journal of Medicinal Chemistry*, 55(7), pp. 3479–3487. doi: 10.1021/jm3001373.

Yu, Y., Chen, C.K., Law, W.C., Mok, J., Zou, J., Prasad, P.N. and Cheng, C., (2013) 'Well-defined degradable brush polymer-drug conjugates for sustained delivery of paclitaxel', *Molecular Pharmaceutics*, 10(3), pp. 867–874. doi: 10.1021/mp3004868.

Zhang, S., Chen, Y., Xiong, S., Wang, G., Chen, J. and Yang, G., (2010) 'A novel strategy for MALDI-TOF MS analysis of small molecules' *Journal of the American Society for Mass Spectrometry*, *21*(1), pp.154-160.

Zhong, Y. J., Shao, L. H. and Li, Y. (2013) 'Cathepsin B-cleavable doxorubicin prodrugs for targeted cancer therapy (Review)', I*nternational journal of oncology*, *42*(2), pp.373-383. doi: 10.3892/ijo.2012.1754.

Zhou, M., Zhang, R.H., Wang, M., Xu, G.B. and Liao, S.G., (2017) 'Prodrugs of triterpenoids and their derivatives', *European journal of medicinal chemistry*, *131*, pp.222-236.doi: 10.1016/j.ejmech.2017.03.005.

Zhou, Y., Zhou, C., Zou, Y., Jin, Y., Han, S., Liu, Q., Hu, X., Wang, L., Ma, Y. and Liu, Y., (2020) 'Multi pH-sensitive polymer-drug conjugate mixed micelles for efficient co-delivery of doxorubicin and curcumin to synergistically suppress tumor metastasis', *Biomaterials Science*, 8(18), pp. 5029–5046. doi: 10.1039/d0bm00840k.

Zucker, J. R. (1996) 'Changing Patterns of Autochthonous Malaria Transmission in the United States: A Review of Recent Outbreaks', *Emerging Infectious Diseases*, 2(1), pp. 37–43. doi: 10.3201/eid0201.960104